AD-A058 127 ARMY ELECTRONICS RESEARCH AND DEVELOPMENT COMMAND WS--ETC F/G 4/2
VERTICAL STRUCTURE IN ATMOSPHERIC FOG AND HAZE AND ITS EFFECTS --ETC(U)
JUL 78 R G PINNICK, D L HOIHJELLE

UNCLASSIFIED ERADCOM/ASL-TR-0010 NL

1 OF 2
ADA
058127

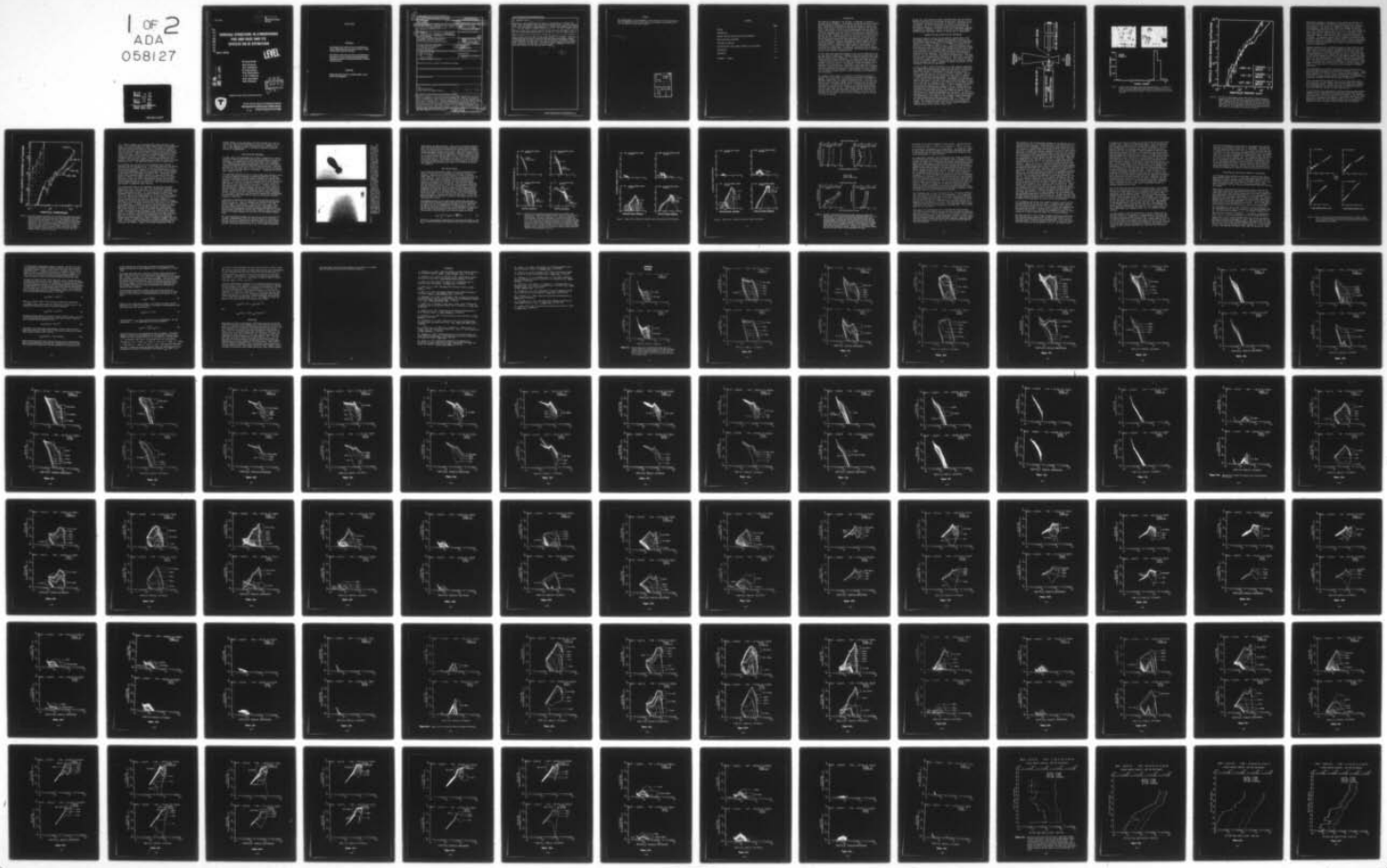

ASL-TR-0010

AD
Reports Control Symbol
OSD-1366

ADA058127

VERTICAL STRUCTURE IN ATMOSPHERIC FOG AND HAZE AND ITS EFFECTS ON IR EXTINCTION

JULY 1978

LEVEL II

Prepared By

R.G. Pinnick
D.L. Hoihjelle
G. Fernandez
E.B. Stenmark
J. D. Lindberg
S.G. Jennings
G.B. Hoidale

AD No. _____
DDC FILE COPY

DDC
RECEIVED
AUG 29 1978
A

Approved for public release; distribution unlimited.

US Army Electronics Research and Development Command
Atmospheric Sciences Laboratory
White Sands Missile Range, N.M. 88002

78 08 28 014

NOTICES

Disclaimers

The findings in this report are not to be construed as an official Department of the Army position, unless so designated by other authorized documents.

The citation of trade names and names of manufacturers in this report is not to be construed as official Government indorsement or approval of commercial products or services referenced herein.

Disposition

Destroy this report when it is no longer needed. Do not return it to the originator.

SECURITY CLASSIFICATION OF THIS PAGE (When Data Entered)

ERADCOM

REPORT DOCUMENTATION PAGE

READ INSTRUCTIONS BEFORE COMPLETING FORM

1. REPORT NUMBER: ASL-TR-0010
2. GOVT ACCESSION NO.
3. RECIPIENT'S CATALOG NUMBER
4. TITLE (and Subtitle): VERTICAL STRUCTURE IN ATMOSPHERIC FOG AND HAZE AND ITS EFFECTS ON IR EXTINCTION.
5. TYPE OF REPORT & PERIOD COVERED: Technical Report.
6. PERFORMING ORG. REPORT NUMBER
7. AUTHOR(s): R. G. Pinnick, D. L. Hoihjelle, G. Fernandez, E. B. Stenmark, J. D. Lindberg, S. G. Jennings, and G. B. Hoidale
8. CONTRACT OR GRANT NUMBER(s)
9. PERFORMING ORGANIZATION NAME AND ADDRESS: Atmospheric Sciences Laboratory, White Sands Missile Range, NM 88002
10. PROGRAM ELEMENT, PROJECT, TASK AREA & WORK UNIT NUMBERS: DA Task 1L161102D53A SA3
11. CONTROLLING OFFICE NAME AND ADDRESS: US Army Electronics Research and Development Command, Adelphi, MD 20783
12. REPORT DATE: Jul 1978
13. NUMBER OF PAGES: 139
14. MONITORING AGENCY NAME & ADDRESS (if different from Controlling Office): 135 p.
15. SECURITY CLASS. (of this report): UNCLASSIFIED
15a. DECLASSIFICATION/DOWNGRADING SCHEDULE

16. DISTRIBUTION STATEMENT (of this Report)

Approved for public release; distribution unlimited.

17. DISTRIBUTION STATEMENT (of the abstract entered in Block 20, if different from Report)

18. SUPPLEMENTARY NOTES

19. KEY WORDS (Continue on reverse side if necessary and identify by block number)

Fog
Infrared extinction
Light scattering aerosol counter

20. ABSTRACT (Continue on reverse side if necessary and identify by block number)

Vertical structure of the size distribution and number concentration of particulates in atmospheric fog and haze near Grafenwöhr, West Germany, was measured with a balloon-borne light-scattering aerosol counter for periods spanning parts of 8 days in February 1976. The work was done as part of the Atmospheric Sciences Laboratory's contribution to a US Army field exercise conducted by the Night Vision Laboratory for the purpose of determining the effect of atmospheric constituents on various night vision systems. For haze (5 km visibility) conditions, little vertical variation is seen; but for low visibility (< 1 km) fog,

DD FORM 1 JAN 73 1473 EDITION OF 1 NOV 65 IS OBSOLETE

410 663

SECURITY CLASSIFICATION OF THIS PAGE (When Data Entered)

78 08 28 034

20. ABSTRACT (cont)

conditions, significant vertical increases in concentration of droplets with radii larger than 4μm are seen over the first 150 m altitude. For haze, the particle size distribution is approximated by a lognormal with geometric mean radius $r_g \approx 0.2\mu m$ and geometric standard deviation $\sigma_g \approx 1.9$. For fog, a bimodal distribution is found with a relative maximum for the larger particle mode at radii of 4μm to 6μm and corresponding values $r_g \approx 5\mu m$ and $\sigma_g \approx 1.6$; the smaller particle mode has values of $r_g \approx 0.3\mu m$ to $r_g \approx 0.6\mu m$ and $\sigma_g \approx 1.8$ to $\sigma_g \approx 2.5$. Liquid water content values for haze and fog range from 10^{-4} to 0.45 g/m^3. Extinction calculated from the particle size distributions shows an approximate $1/\lambda$ wavelength dependence for haze conditions, but nearly neutral (wavelength independent) extinction for heavy fog. A correlation exists between calculated particulate extinction and calculated liquid water content, independent of particle size distribution, for the fogs and hazes studied.

micrometers

0.0001

cm/m

PREFACE

We acknowledge Mr. Lucien Biberman of the Institute for Defense Analysis for his suggestion that we look into the correlation of extinction in the infrared and liquid water content.

→ lamba

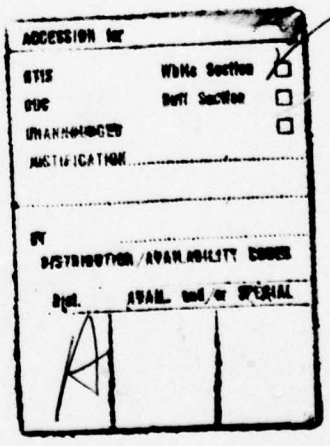

CONTENTS

	Page
PREFACE	1
INTRODUCTION	3
AEROSOL DETECTOR DESCRIPTION AND CALIBRATION	4
DATA COLLECTION PROCEDURES	11
HAZE AND FOG RESULTS	13
EXTINCTION AND LIQUID WATER CONTENT OF FOG AND HAZE	21
CONCLUSIONS	25
REFERENCES	27
APPENDIX. FIGURES	A-1

INTRODUCTION

The presence of atmospheric fog and haze is important to radiative transfer in the atmosphere. For example, fog and haze particles degrade the performance of electro-optical systems and affect the earth's climate. Quantitative estimates of these effects generally require knowledge of the vertical variation of fog and haze particle size distributions. Near-surface size distribution measurements have been made by impaction techniques [1-6] by collection of particles on spiderwebs [7], by a laser hologram camera [8], and by light-scattering single-particle counters [9,10]. However, measurements of the vertical structure of fog and haze particle size distributions are difficult to make and consequently are rather sparce with some exceptions [11,12]. Both Pilié et al. and Goodman used impaction techniques to measure droplet spectra to 150-200 m altitudes. Impaction measurements involve laborious microscope measurement of droplets or droplet replicas which restrict their usefulness, as only a relatively small number of distributions can realistically be determined. Furthermore, corrections must be applied to obtain true droplet size and collection efficiencies must be known to obtain relative particle concentrations.

In this report we present measurements of the size distributions of fog and haze particles made with a tethered balloon-borne light-scattering particle counter, with emphasis on their effect on radiation for visible through middle infrared wavelengths. The primary advantage of using a light-scattering counter over an impactor technique is that the measurement is done in situ in real time, with minimal disturbance to the particles during measurement. Measurement of vertical structure of atmospheric fog and haze under relatively stable conditions is possible with this technique because a statistically significant size distribution measurement can be completed in approximately 1/2 minute, permitting an upleg and downleg profile to 200 m altitude to be completed in 15 to 30 minutes.

The purpose of this report is to present the vertical structure of fog and haze that occurred in a wintertime continental environment in Germany, as measured with a light-scattering counter, in the form of particle number, area, and volume distributions, and in the form of extinction and liquid water content values calculated from the measured distributions. An additional purpose is to investigate the spectral dependence of extinction, and to examine correlations between extinction and liquid water content. Measurements reported here were made during February 1976 near Grafenwöhr, a town located 100 km north of Nürnberg near the eastern border of West Germany. The local terrain consists of rolling hills and is partially forested; some of the land is tilled for farming.

Because the light-scattering counter technique offers only an indirect measure of particle size, and because the particular instrument we used is heretofore untested, we first give in section 2 a discussion of its calibration. The balloon experiment data collection procedures are described in section 3. In section 4 typical haze and fog profiles are presented, together with discussion of their significance regarding propagation of radiation. Finally, in section 5 the relation between extinction and liquid water content of fog and haze is investigated.

AEROSOL DETECTOR DESCRIPTION AND CALIBRATION

The aerosol detector used for the measurements reported here is the Knollenberg (after R. G. Knollenberg, the developer) Classical Scattering Aerosol Spectrometer (CSAS) manufactured by Particle Measurement Systems, Inc. (PMS), of Boulder, CO. A schematic of the optical system of this instrument is shown in Fig. 1. The device works on the principle that as aerosol particles flow through an illuminated volume, light scattered into a particular (near forward scattering) solid angle by a single particle is measured photoelectrically and is used to determine particle size by electronically classifying response pulses according to their magnitude. The response signal can be related to particle size by a calibration supplied by the manufacturer. One problem with using the manufacturer calibration is that it does not consider the refractive index of the particle measured. Particles of the same size but of different composition give significantly different response pulses; therefore, we deem it necessary to address the question of the instrument calibration in some detail.

In order to make a definitive measure of the CSAS response characteristics, monodisperse aerosols with known sizes and indexes of refraction are needed. We generated uniform spherical particles of nigrosin dye (index = 1.67-0.26i, λ = 6328 Å) with a technique described earlier [13] and measured particle sizes using electron microscopy. We also generated uniform particles of polystyrene latex (index = 1.592-0i, λ = 5893 Å) available from Dow Chemical, by atomizing the hydrosol samples (diluted with distilled water). Measurement of uniform aerosol with the CSAS results in a peak in the pulse height spectrum; the position of the peak is a measure of the response of the instrument to aerosol of that size and refractive index. A typical spectrum for monodisperse aerosol of nigrosin dye is shown in Fig. 2, together with a scanning electron microscope micrograph of several of these particles collected onto a Nuclepore filter. The response of the CSAS to solid particles of nigrosin dye and polystyrene latex are shown in Fig. 3. Typical errors in response measurements are also shown. The errors in measurement of particle radii are less than the size of the dots marking the measurements. The squares in Fig. 3 denote response measurements for nearly monodisperse crown glass beads (index = 1.51-0i, λ = 5893 Å) available from Particle Information Services, Inc., Grants Pass, Oregon. The standard deviation in particle size of these beads is shown by the horizontal "error" bars, and the standard deviation in response pulses by the vertical "error" bars.

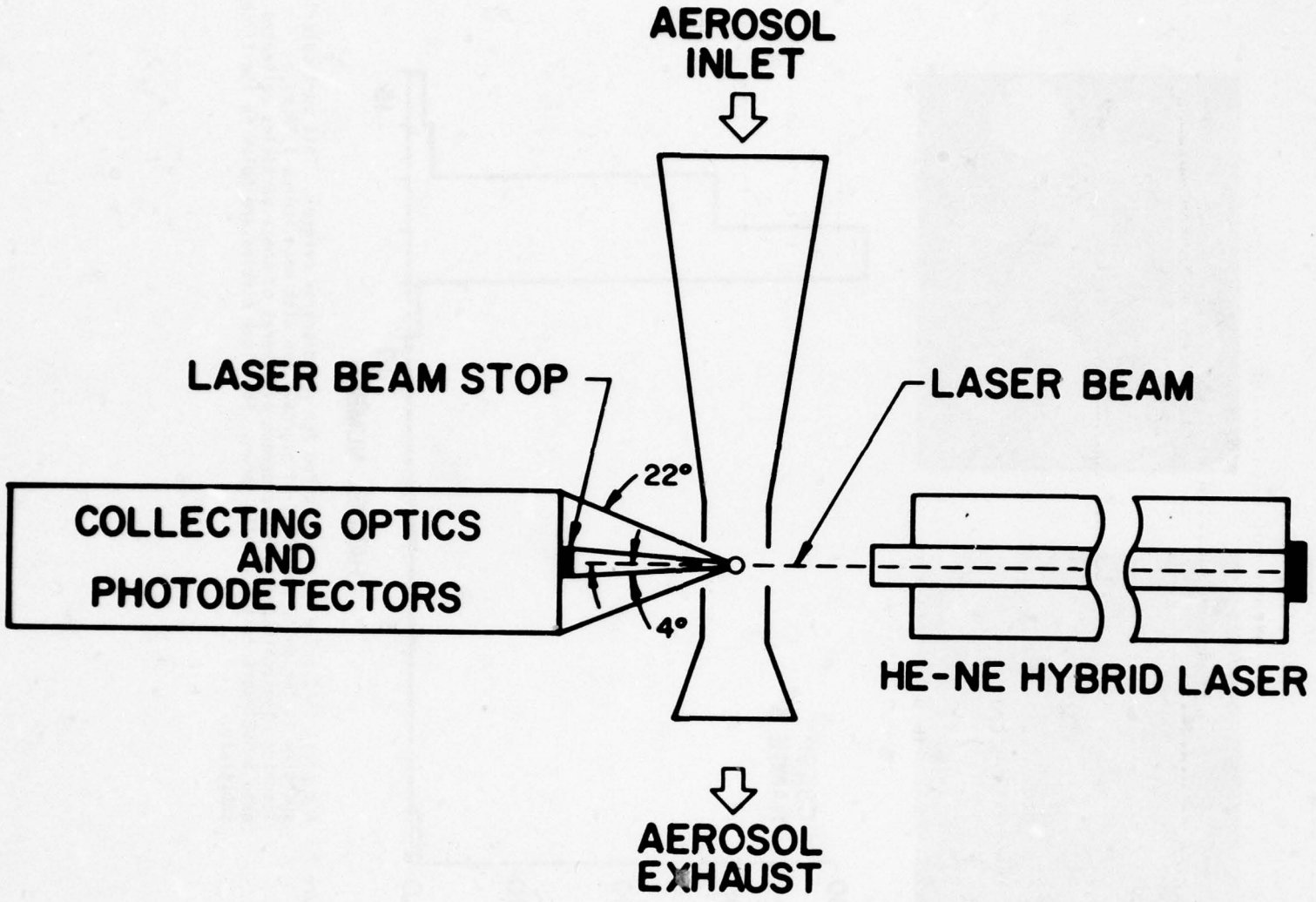

Figure 1. Schematic of the Particle Measurement Systems CSAS light-scattering aerosol counter optical system.

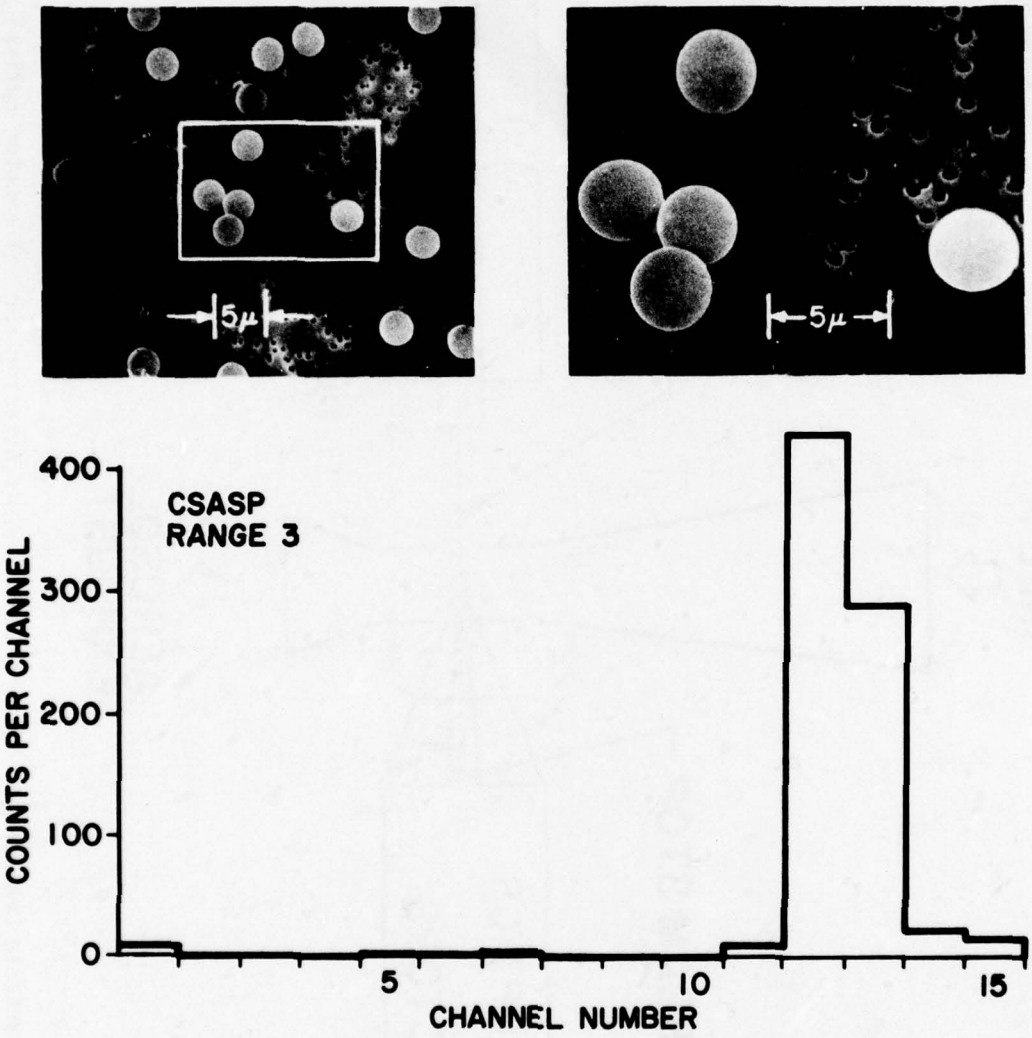

Figure 2. A typical CSAS pulse height spectrum for monodisperse aerosol. This particular spectrum is for solid particles of nigrosin dye with mean radius 1.78μm; a scanning electron microscope micrograph of several of these particles collected onto a Nuclepore filter is also shown. The black circles are holes in the filter substrate.

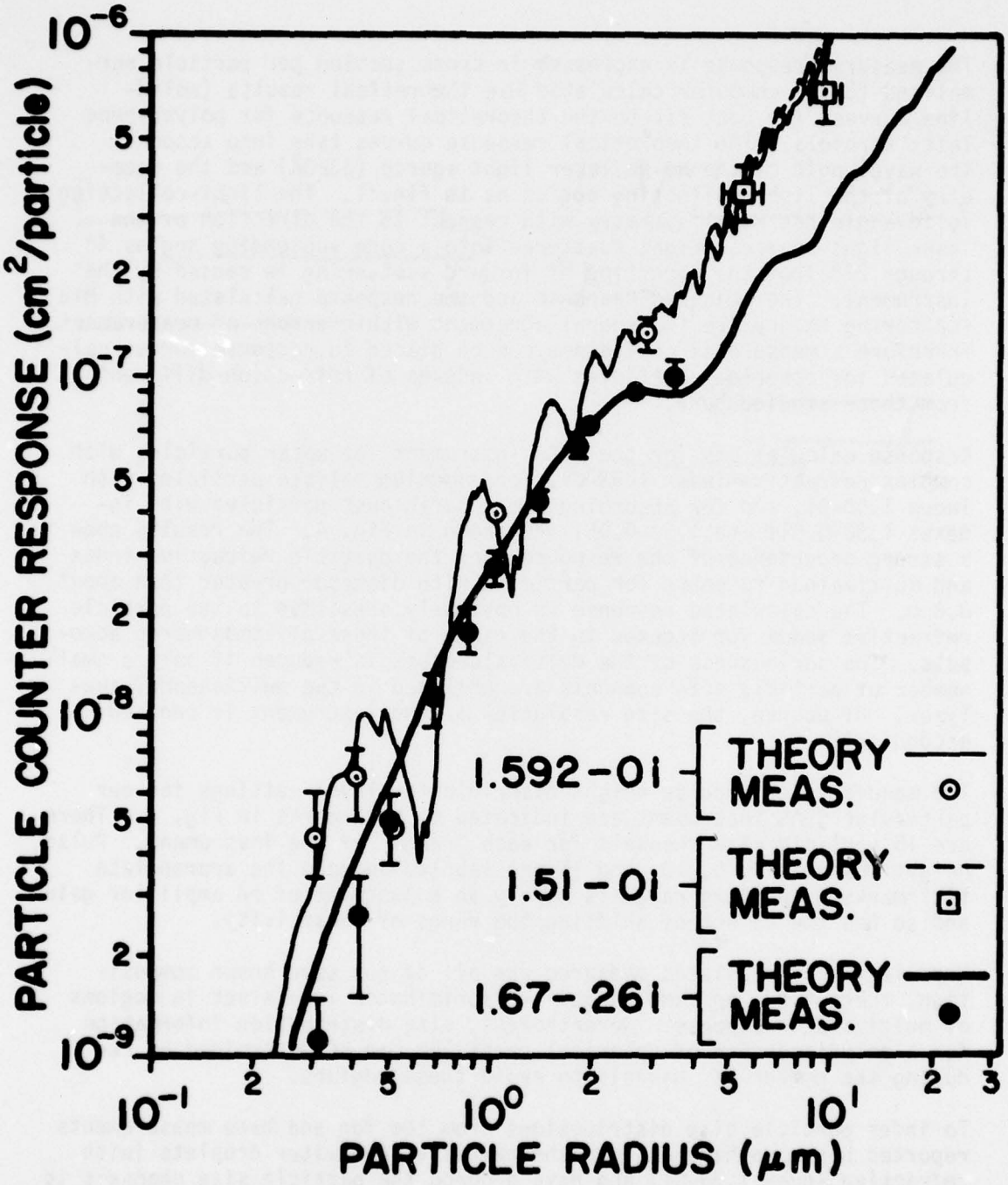

Figure 3. The Particle Measurement Systems CSAS particle counter response; measured (circles and squares) and calculated using Mie scattering theory (smooth curves) for single spherical particles vs particle size. Measured values have been normalized for the best fit to the theoretical values for polystyrene latex particles with refractive index 1.592-0i. The theoretical curve for glass beads with refractive index 1.51-0i extends only to about 4μm radius.

The measured response is expressed in cross section per particle normalized to the computer calculated Mie theoretical results (solid-line curves) for best fit to the theoretical response for polystyrene latex aerosols. The theoretical response curves take into account the wavelength of the He-Ne laser light source (6328Å) and the geometry of the light-collecting optics as in Fig. 1. The light-collecting solid angle has axial symmetry with respect to the direction of the laser light source. Light scattered into a cone subtending angles 4° through 22° from the direction of forward scattering is sensed by the instrument. The measured response and the response calculated with Mie scattering theory are in general agreement within errors of measurement. Therefore a measure of confidence can be placed in response curves calculated for spherical particles with indexes of refraction different from those studied here.

Response calculations for the CSAS instrument for water particles with complex refractive index 1.33-0i, for ammonium sulfate particles with index 1.50-0i, and for absorbing atmospheric dust particles with indexes 1.50-0.01i and 1.50-0.05i are shown in Fig. 4. The results show a strong dependence of the response upon the particle refractive index and multivalued response for particles with diameter greater than about 0.8μm. The calculated response is obviously sensitive to the particle refractive index for indexes in the range of those of atmospheric aerosols. The seriousness of the multivaluedness is reduced if only a small number of particle size channels are utilized in the multichannel analyzer. Of course, the size resolution of the instrument is reduced accordingly.

The manufacturer's pulse height discriminator level settings for our particular CSAS instrument are indicated by tick marks in Fig. 4. There are 15 particle size channels for each "range" of the instrument. Pulse height channels 1, 5, 10, and 15 are labeled between the appropriate tick marks. Changing range is merely an adjustment of an amplifier gain and so has the effect of shifting the range of sensitivity.

Even if the particulates measured are all of the same known composition, there are - on some ranges - discriminator levels set in regions of multivalued response. Nevertheless, size distribution information for a polydispersion of spherical particles can be determined by reducing the number of channels to avoid these regions.

To infer particle size distributions from the fog and haze measurements reported here, we have assumed the particles are water droplets (with refractive index 1.33-0i) and have grouped the particle size channels to avoid regions of multivalued response. This channel grouping for water particles is indicated by the heavy tick marks in Fig. 4. Specific channel size limits for the different ranges of the instrument can be determined from this figure by noting at what radii on the water

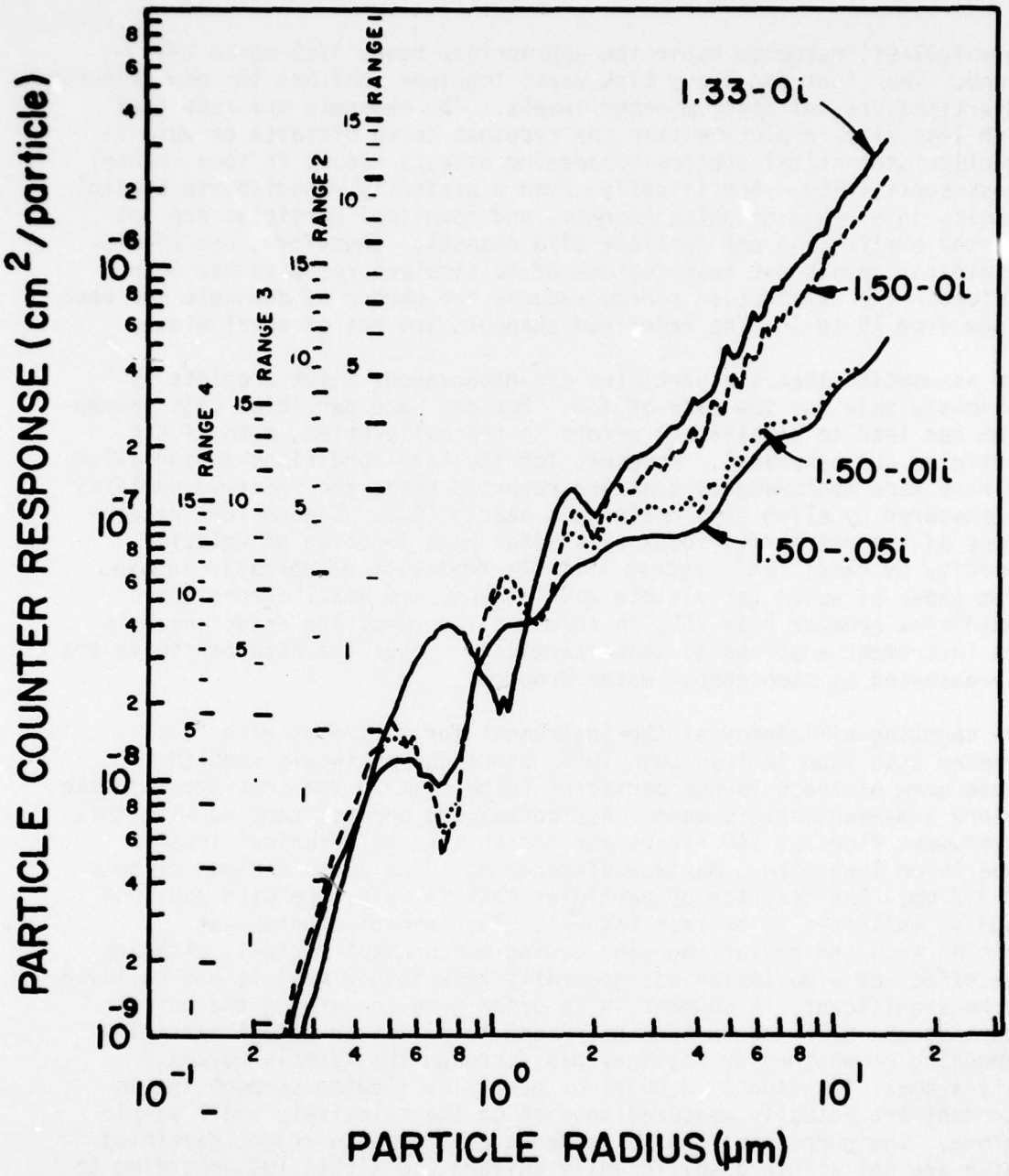

Figure 4. Mie theory response calculations for the Particle Measurement Systems CSAS particle counter for water particles with refractive index 1.33-0i, ammonium sulfate with approximate index 1.50-0i, and atmospheric dust with indexes 1.5-0.01i and 1.50-.05i. The tick marks indicate the pulse height discriminator level settings as set by the manufacturer for the detector. Channels 1, 5, and 15 are labeled between the appropriate tick marks for the different range settings of the instrument. The heavy tick marks indicate the pulse height discriminator level settings used in grouping channels together to avoid regions of multivalued response under the assumption that all particles are water.

(m = 1.33-0i) response curve the appropriate heavy tick marks correspond. The light and heavy tick marks together indicate the manufacturer advertised channel discriminator levels. The channels are redefined with less size resolution than the response curve dictates because in practice statistical spectra broadening effects result in some channel cross sensitivity. Specifically, even a perfectly monodisperse aerosol results in a range of pulse heights, and identical particles are not counted entirely in one particle size channel. Therefore, use of discriminator levels set near regions of multivalued response has been avoided. The calibration scheme reduces the number of channels for each range from 15 to 7. The redefined channels are not of equal width.

Our assumption that the particles are homogeneous water droplets is obviously safe for the case of fog. For dry haze particles this assumption can lead to significant errors in the calibration, even if the particles are spherical. However, for the haze conditions during which we have made measurements that are reported here, the relative humidity as measured by sling psycrometer was nearly 100%. Theoretical predictions of the refractive index of aerosol as a function of relative humidity by Hänel [14] suggest that the deviation of particle indexes from those of water (at visible wavelengths) are small for relative humidities greater than 95%, in terms of the resulting differences in the instrument response to these particles. Thus the haze particles are approximated by homogeneous water droplets.

The counting efficiency of the instrument for particles with radii greater than 15μm is less than 100%, since nonisokinetic samplings cause some of these larger particles to be lost in the instrument intake before a measurement is made. Air containing aerosol sampled with this instrument flows at 340 liters per minute through a conical intake tube 45 cm long with a maximum diameter of 10 cm and a minimum diameter of 3.3 cm. The fraction of particles lost in this tube with radii of 15μm is estimated to be less than 7%. The aerosol counter was pointed into the prevailing wind during measurement periods, although the effect of wind (which was generally less than 3 m/s) is not believed to be significant. A comment is in order here concerning the coincidence scheme utilized in the instrument to reject or accept particles depending on whether or not they pass through the "sample volume." Only a small fraction (~ 0.003%) of particles flowing through the instrument are actually measured because of the relatively small sample volume. The purpose of the coincidence scheme is to reject particles which are not within a sufficiently uniform (to within 10% according to PMS) part of the laser beam by opto-electronically discriminating against out-of-focus particles. There is evidence to suggest that this scheme results in a sample volume that is somewhat dependent on particle sizes. In other words, the instrument flow rate may be different for different size channels. However, simultaneous measurements made on

uniform aerosols in our laboratory with both the CSAS and a particle counter of a special design developed by Rosen [15] suggest this effect is less than 20%, at least for particles with radii less than 1μm. A more complete account of the aerosol detector calibration problem is in preparation.

DATA COLLECTION PROCEDURES

The basic goal of the experiment was to obtain information on vertical profiles of particle size distribution during atmospheric fog and haze conditions. To accomplish this, the CSAS particle counter together with temperature and visible radiation flux sensors was incorporated into a single payload weighing approximately 9 kg and carried aloft to a maximum altitude of 250 m by a 1500 ft^3 tethered balloon. Digitized data was sent via a wire link to a data acquisition unit on the ground; this link also furnished power to the payload. A photograph of the system is shown in Fig. 5.

This experiment was done as part of a much larger field exercise, and as a result considerable constraint on operating schedules was imposed. For example, there was a problem caused by presence of a nearby radar station, so that data could only be collected when the radar was not in operation. In addition, the balloon experiment could not be operated at night because it was not equipped with lights which were required to meet local aircraft hazard warning regulations. Choice of actual operating conditions (ascent and descent rates, and altitude intervals) was determined by a compromise between the need for long counting intervals to produce statistically meaningful aerosol size distribution results, the desire for short counting intervals to obtain reasonable vertical spacial resolution, and the need to complete the ascent/descent in a relatively short time interval because of continually changing atmospheric conditions.

A choice was also made in the field controlling the CSAS counter size range (see Fig. 4). Under the assumption of spherical water droplets the size ranges are: range 1, 0.5-16μm radius; range 2, 0.37-8μm radius; range 3, 0.29-4μm radius; range 4, 0.24-1.6μm radius. Since the range setting could not be changed remotely, measurements made during an upleg and downleg traverse were necessarily made for a single range setting, optimized to cover the most important range of particle size for the widely different fog and haze size distributions encountered.

The usual operational procedure for a particular balloon traverse was to sample intermittently (with the CSAS positioned at a fixed altitude and set on 30- to 60-second accumulation times) at 30 m altitude intervals during the upleg portion, and to sample continuously (with the CSAS continuously moving and set on 20- to 30-second accumulation

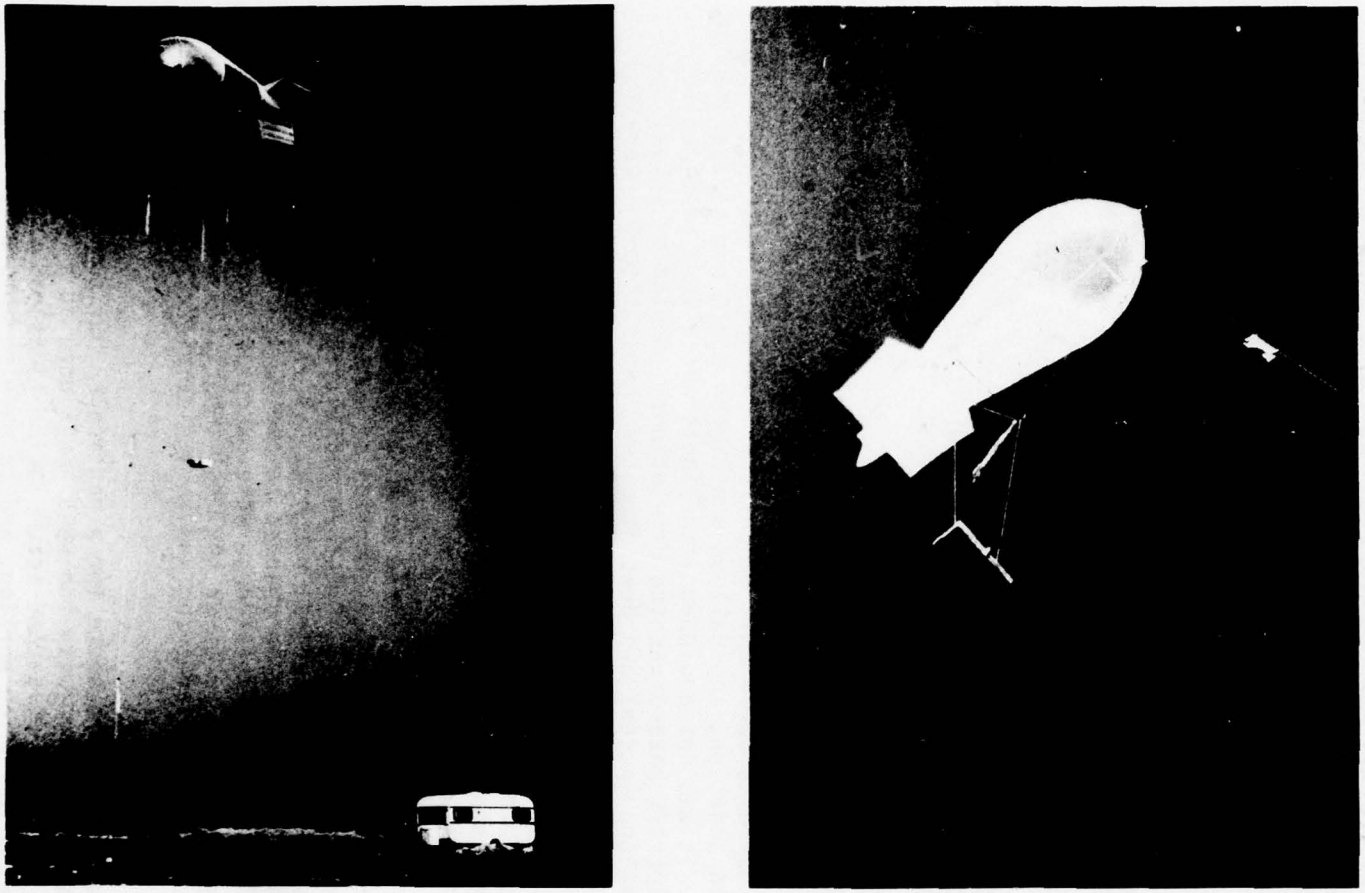

Figure 5. Photographs of the balloon-borne aerosol detector system used for fog and haze measurements near Grafenwöhr, West Germany. The detector (a light-scattering aerosol counter model CSAS manufactured by Particle Measurement Systems of Boulder, CO) is suspended approximately 15 m below the 1500 ft^3 tethered balloon and is rigged so that the detector intake points into the prevailing wind. Temperature and radiation flux sensors are incorporated into the payload.

times) during the downleg portion. Since the size distribution measurements made during upleg and downleg portions of each traverse compared well, and since more vertical resolution was obtained during the downleg portion, we concentrate only on the latter. Thus, particle size distribution measurements reported here have been obtained by integrating over 8 m to 12 m altitude intervals (depending on the CSAS accumulation time), as the payload descent rate was about 0.4 m/s. The altitude identified with a particular size distribution is the lower limit of the corresponding altitude interval. During heavy fog conditions it was not possible to achieve altitudes greater than 150 m, as copious amounts of water and rime condensed onto the balloon and tether line, reducing the balloon lift capability.

HAZE AND FOG RESULTS

Four profiles of haze and fog, typical of 19 profiles measured during 8 days in February 1976 near Grafenwöhr are presented in Figures 6 through 8. These show the vertical structure in terms of particle number (dN/d log r), cross sectional (dS/d log r), and volume (dV/d log r) distributions. Some of the particle counter measurements (solid lines) have been fitted with lognormal size distributions (dashed curves) for the purpose of estimating the effects of extending and smoothing the measured size distributions. The reason for showing the area and volume distributions is that for limiting regimes of particle size the extinction cross section is nearly proportional to either the integrated cross-sectional area (for particles large compared to the wavelength) or volume (for particles small compared to the wavelength, as will be discussed in a following section). These distributions can therefore be used to infer the range of particle sizes that contribute most to extinction. Generally the values for dN/d log r < 10 cm^{-3} are based upon fewer than 10 particle counts per size channel and thus have large statistical errors.

Corresponding profiles of the liquid water content (LWC) and extinction coefficients calculated from the measured and fitted distributions at 0.55μm, 4μm, and 10μm wavelengths are shown in Fig. 9. Note that the abscissa scales are different for the different parts of Fig. 9. The LWC and extinction for the fitted size distributions are calculated only for one or two altitudes for each profile in Fig. 9. The Mie single scatter extinction coefficients were calculated as follows:

$$\beta_{ext} = \int_{-0}^{\infty} \pi r^2 \, Q_{ext}(m, x) \, \frac{dN(r)}{dr} \, dr \qquad (1)$$

Here N(r) is the particle concentration for particles with radius $\geq$ r and Q_{ext} is the Mie efficiency factor defined as the ratio of single particle

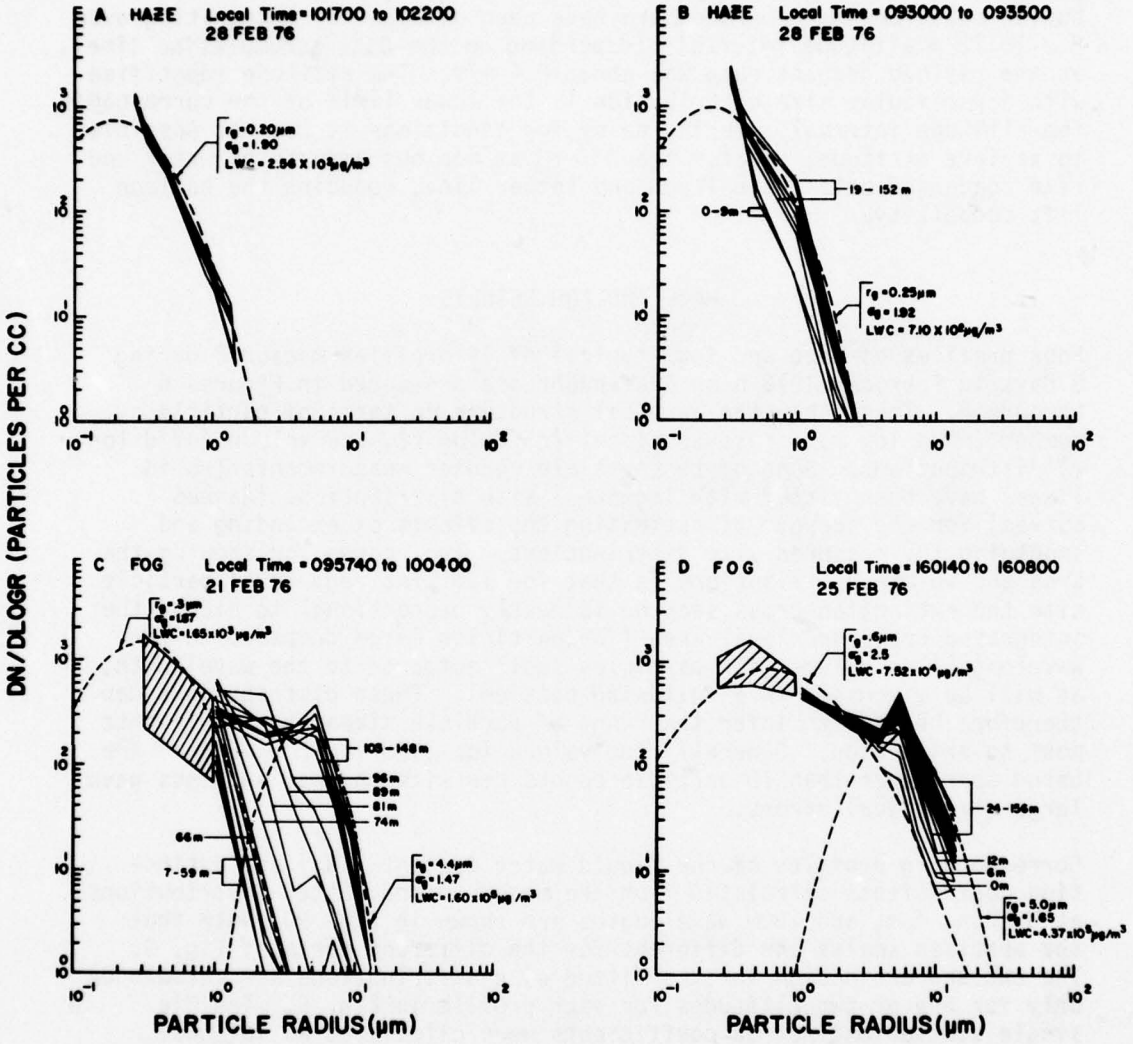

Figure 6. Particulate size distribution measurements made near Grafenwöhr, West Germany, with a tethered balloon-borne aerosol counter for several haze and fog conditions. Each size distribution is for a particular altitude or altitude range as indicated. Measurements at particular altitudes (121 m in Fig. 6A, 95 m in Fig. 6B, 59 m and 126 m in Fig. 6C, and ground level and 135 m in Fig. 6D) have been fitted with lognormal size distributions (dashed curves) for the purpose of estimating the effects of extrapolating the measured distributions. Values of geometric mean radius r_g, geometric standard deviation σ_g, and liquid water content LWC, are shown with the corresponding lognormal curves. The date, local time (hours, minutes, seconds), and time interval for the measurements are given.

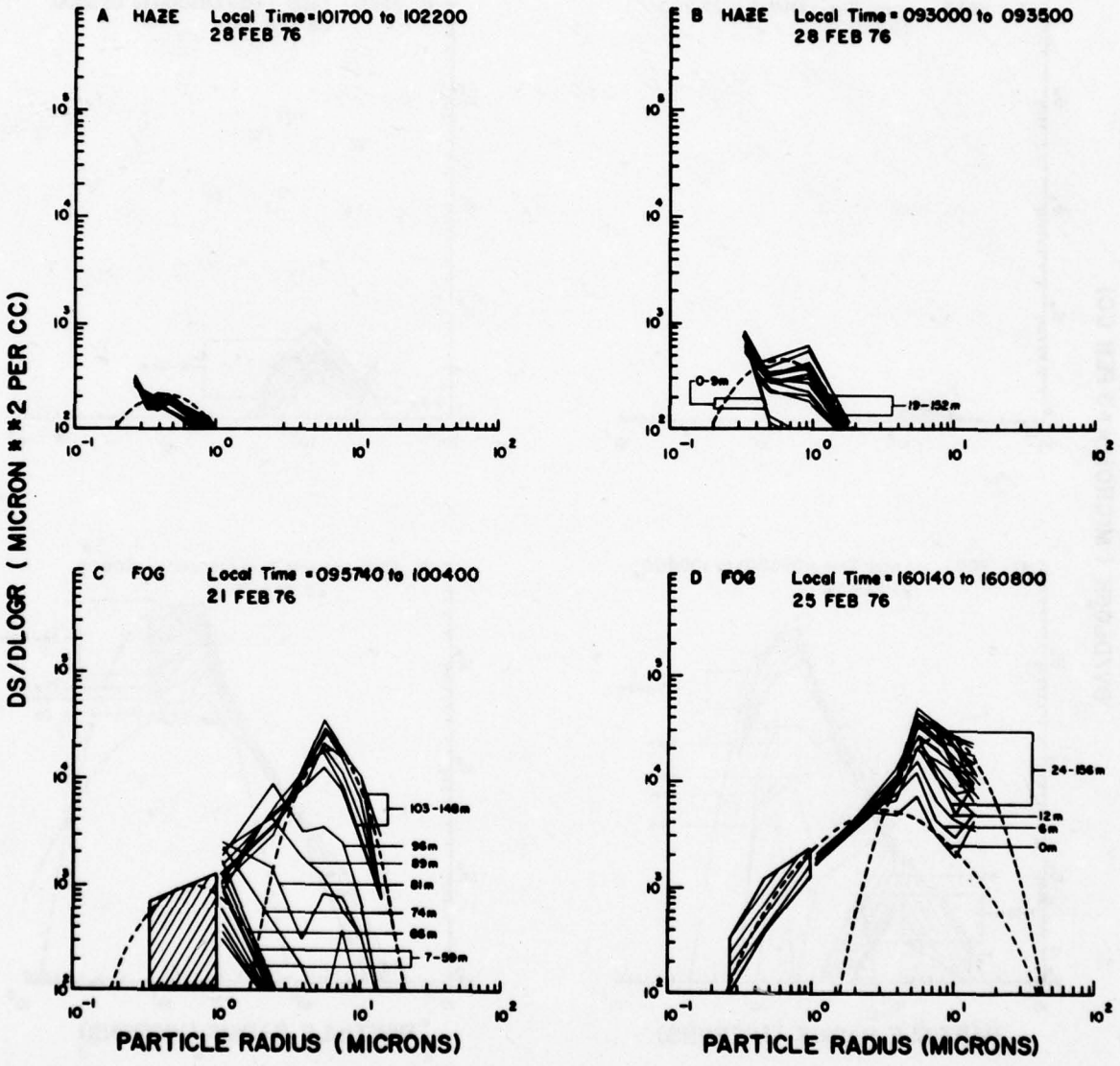

Figure 7. Same as Fig. 6 except for particle area (cross-sectional) distribution.

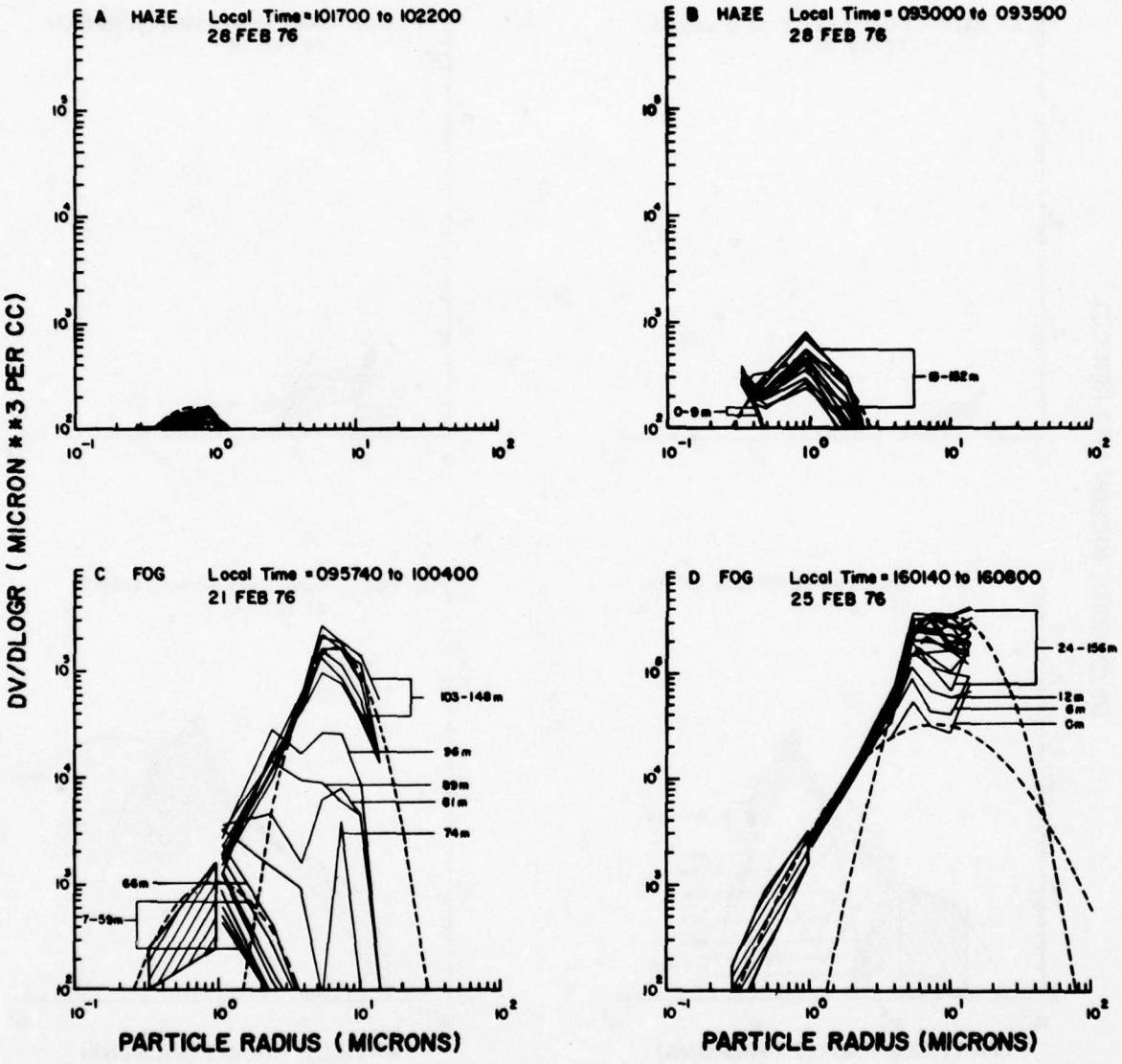

Figure 8. Same as Fig. 6 except for particle volume distribution.

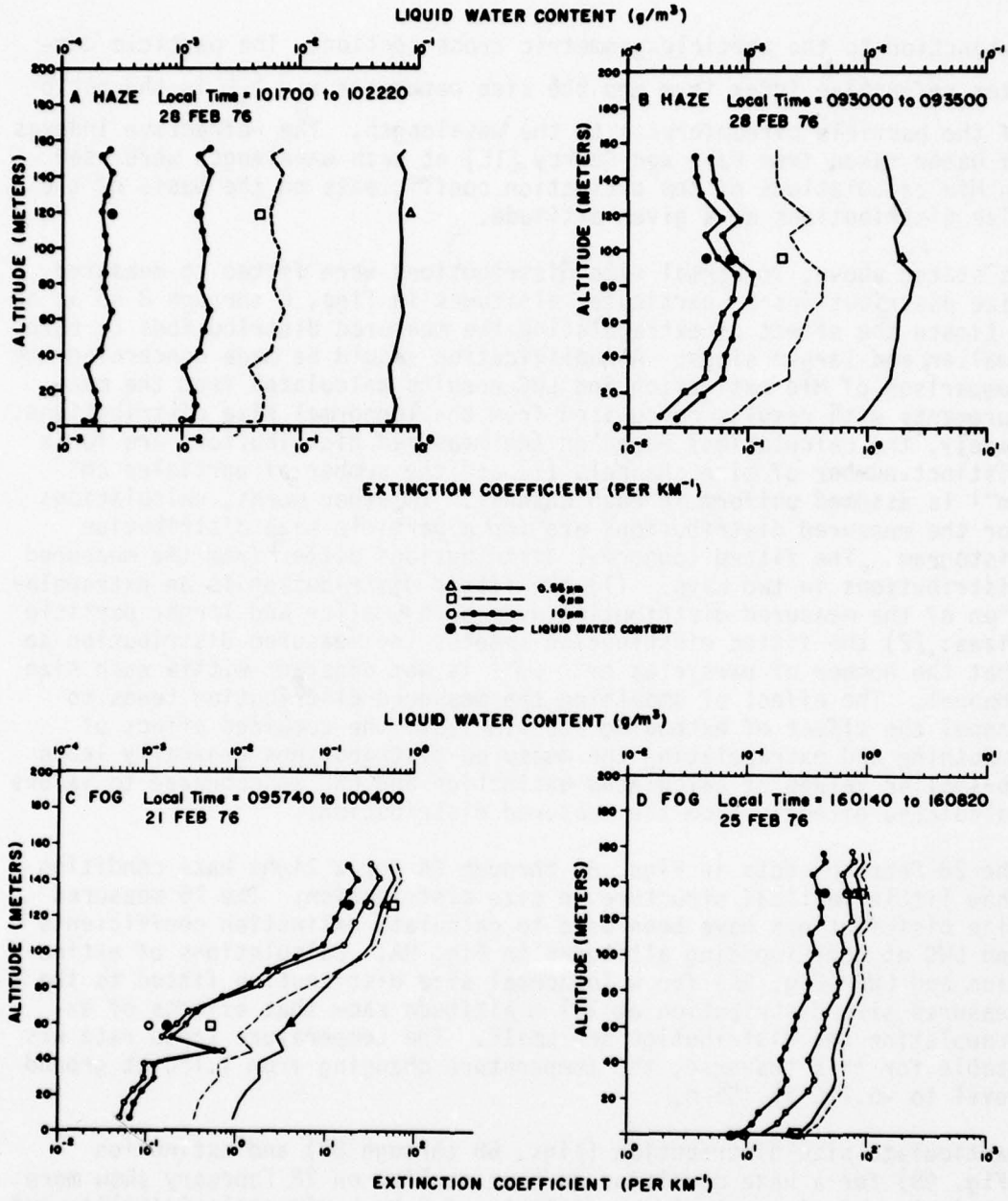

Figure 9. Profiles of particulate extinction and water content calculated from particle size distribution and concentration measurements shown in Fig. 6. The solid-dot curve indicates the liquid water content and the solid, dashed, and open-dot curves indicate the extinction at 0.55μm, 4μm, and 10μm wavelengths. Calculations of the extinction and LWC for particular lognormal distributions fitted to measured distributions (Figs. 6 through 8) are shown at the corresponding altitudes, and are denoted by triangle, square, open-circle, and solid circle symbols for extinction at 0.55μm, 4μm, 10μm, and liquid water content. The date, local time (hours, minutes, seconds), and time interval for the measurements are given.

extinction to the particle geometric cross section. The particle complex refractive index is m and the size parameter $x = \frac{2\pi r}{\lambda}$ is the ratio of the particle circumference to the wavelength. The refractive indexes of water taken from Hale and Querry [16] at each wavelength were used in Mie calculations of the extinction coefficients on the basis of the size distributions at a given altitude.

As stated above, lognormal size distributions were fitted to measured size distributions at particular altitudes in Figs. 6 through 8 so as to estimate the effect of extrapolating the measured distributions to both smaller and larger sizes. A qualification should be made concerning the comparison of Mie extinction and LWC results calculated from the measurements with results calculated from the lognormal size distributions. Namely, the calculations based on the measured distributions are for a distinct number of size channels (7) and the number of particles cm^{-3} μm^{-1} is assumed uniform in each channel. In other words, calculations for the measured distributions are for a particle size distribution histogram. The fitted lognormal distributions differ from the measured distributions in two ways: (1) the fitted distribution is an extrapolation of the measured distribution over both smaller and larger particle sizes; (2) the fitted distribution smooths the measured distribution so that the number of particles cm^{-3} μm^{-1} is not constant within each size channel. The effect of smoothing the measured distribution tends to cancel the effect of extending it. In fact, the combined effect of smoothing and extrapolating the measured distributions generally leads to smaller values of calculated extinction and LWC as compared to values calculated directly from the measured distribution.

The 28 February data in Figs. 6A through 8A for a light haze condition show little vertical structure in size distribution. The 16 measured size distributions have been used to calculate extinction coefficients and LWC at corresponding altitudes in Fig. 9A. Calculations of extinction and LWC (Fig. 9A) for a lognormal size distribution fitted to the measured size distribution at 121 m altitude show that effects of extrapolating the distribution are small. The temperature lapse rate was stable for this traverse, the temperature changing from 1.1°C at ground level to -0.1°C at 155 m.

Particulate size distribution (Figs. 6B through 8B) and extinction (Fig. 9B) for a haze condition an hour earlier on 28 February show more vertical variation. A visual estimate of 2 km horizontal visibility was made during this traverse. Using Koschmieder's formula to relate visibility to extinction for a threshold contrast ratio of 2%, this yields a value of 1.96 km^{-1} extinction for this haze condition, comparing favorably with extinction at 0.55μm (Fig. 9B) calculated from the measured size distributions.

The fog data in Fig. 6C show large increases in concentration of 4μm to 16μm radius particles with altitude and Figs. 7C, 8C, and 9C show the effects of these increases. The cross-hatched areas indicate the altitude variation in measurements made during traverses before and after the traverse in question, with the instrument set so as to sense smaller particles. Assuming that temporal changes are relatively small during these series of traverses (a period of about 2 hours for all traverses was involved here), the cross-hatched areas show the approximate shape of the envelope of the distribution for smaller particles. Generally, the concentration of these smaller particles increased with altitude. The temperature lapse rate for this traverse is again stable with a ground temperature of -3.3°C. The calculated extinction coefficients and LWC in Fig. 9C vary by 2 to 3 orders of magnitude over this 150-m traverse. Comparison of results from the measured and fitted lognormal size distributions suggests that effects of smoothing and extrapolating the measured distribution are significant (as much as a factor 2 in extinction at 10μm, but nearly zero at 0.55μm) for altitudes less than about 70 m. At higher altitudes, the effects of smoothing and extrapolating the size distributions would appear to be relatively small, since at 126 m altitude the differences in extinction and LWC are less than 5%. For the largest particle size channel (centered at 14μm radius) the number of counts for this traverse is not statistically significant. In fact, the point to which six number, area, and volume size distribution curves (at altitudes 111-148 m) converge in Figs. 6C through 8C correspond to only 1 particle count for each curve. Nevertheless, the trend in the size distributions for the next two smaller size channels (centered at 12μm and 9μm) strongly suggests the measured fog distributions can be adequately extrapolated to larger particle sizes with the lognormal. Further, the shape of the distribution for the larger particle sizes is in good agreement with the preceding upleg measurements made about 15 minutes earlier. We point out here that the measured distribution at 126 m altitude was actually fitted by a sum of three lognormal distributions (two of which are shown here) to better accommodate the measurements in the 1μm to 4μm radius interval.

It is noteworthy that during this traverse a visual siting of the balloon payload was lost at 148 m altitude. Integrating the 0.55μm extinction coefficient profile over the first 148 m of this traverse, we find an optical depth of 3.02, a value 23% lower than expected from the Koschmieder relation. Considering the uncertainty in making a visibility estimate and in applying the Koschmieder relation to relate visibility to optical depth, we judge this to be good agreement.

The heavy fog data in Fig. 9D shows increasing extinction coefficient with altitude, again caused by the increased concentration of 4μm to 16μm radius particles shown in Figs. 6D through 8D. The 21 size distribution curves in Figs. 6D through 8D were used to calculate extinction coefficients and LWC presented in Fig. 9D. In contrast to the

21 February fog, vertical increases in extinction and LWC are only about a factor 2 to 4. Again the cross-hatched areas in Figs. 6D through 8D show the shape of distributions for submicrometer particles for a balloon traverse made 1/2 hour after the traverse in question. This traverse is similar to six traverses made during stable fog conditions 25-26 February 1976 in Grafenwöhr. Ground windspeed for each of these traverses was generally less than 2 m/s, suggesting the fog was radiation type rather than advection type. Here it is evident that the log-normal extrapolation to particle sizes larger than those measured may be significantly in error, particularly in calculations of LWC (Fig. 8D) and extinction at 10μm, for which a third mode of larger particles may contribute significantly, even though their relative number may be small. However, although a third mode of larger fog particles cannot be ruled out, a bimodal nature of the distributions is in agreement with measurements of wintertime radiation fogs in England by Garland et al. [1,17] by Roach et al. [18] and some radiation fog measurements by Krasikov and Chikirova [2] near Leningrad. The extinction coefficient is neutral (wavelength independent) within a factor of about 2; the extinction at 4μm being slightly greater than that at .55μm and 10μm. Errors due to size distribution extrapolation and smoothing, assuming no mode of particles with radii greater than 16μm is important, are small. The nearly neutral extinction for low visibility conditions has been found by Patterson [19] for soil-derived aerosols as well, suggesting that a broad range of low (< 1 km) visibility atmospheric conditions result in neutral extinction from visible wavelengths through the middle-infrared (0.5μm to 10μm).

Each of the four haze and fog profiles presented here is for a downleg portion of a balloon traverse. The corresponding upleg values of extinction and liquid water content are generally within 50% of the downleg values, so that temporal changes encountered are usually small compared to the vertical variations. These four profiles are typical of the 19 profiles taken during 8 days at Grafenwöhr. For haze conditions, little vertical variation in the size distribution is observed; but for fog conditions, there are significant increases in the concentration of droplets with radii greater than about 4μm. Measurements of the downward visible radiation flux made with a photodetector attached to the balloon package show that for each of the traverses the flux change with altitude was less than 10%. This suggests that the fog or haze depths were somewhat greater than the maximum altitudes attained.

The trend toward increasing concentration of larger droplets with increasing altitude is in agreement with measurements of advection fogs over San Francisco by Goodman [12], although in direct contradiction to previous measurements of continental fogs, notably those of Pilié et al. [11] for fogs in the Chemung River Valley near Elmira, New York. In view of the paucity of definitive measurements of the vertical structure of fog and haze, similar measurements at different geographical locations and under different meteorological conditions are clearly warranted.

For sake of completeness we have given in the appendix the remaining data for all 19 balloon traverses made in Grafenwöhr. Shown are the upleg and downleg values of dN/d log r vs radius (Fig. A1), dS/d log r vs radius (Fig. A2), dV/d log r (Fig. A3), downleg extinction and LWC vs altitude (Fig. A4), and upleg and downleg values of LWC vs altitude (Fig. A5). The data are presented in chronological order; haze conditions existed during 14 December 1975 and 28 February 1976, fog during 21, 22, 23, 25, and 26 February 1976. The volume distributions for the 25-26 February fog data reveal an increasing contribution of larger (> 10μm radius) particles to LWC and suggest a significant error in LWC resulting from inability of the detector to measure droplets with radius greater than 16μm. Temporal variations during these traverses were generally small and less than vertical variations, as is evidenced by comparison of upleg and downleg LWC profiles in Fig. A5.

EXTINCTION AND LIQUID WATER CONTENT OF FOG AND HAZE

To investigate the correlation of particulate extinction and liquid water content evident in Fig. 9, these data, along with data from the remaining 15 balloon traverses made in Grafenwöhr, appear in Fig. 10. Plotted are values of the Mie calculated extinction for 0.55μm, 1.2μm, 4μm, and 10μm wavelengths versus the liquid water content. Each point corresponds to a size distribution measurement made with the aerosol counter.

These results show approximate relationships between extinction and liquid water content, for 289 measured distributions of fog and haze with liquid water content values ranging over four orders of magnitude. Such relationships have been noted before at visible wavelengths by Eldridge [20,21], Barteneva and Polyakova [6], and Kumai [3]. Recently, Chýlek [22] has shown that in fact a linear relationship should exist between extinction and LWC, independent of particle size distribution, but only for a wavelength determined by the radii of the largest particles present in the polydispersion of droplets. This is a result of the efficiency factor for extinction Q_{ext} being nearly proportional to size parameter x, which leads to extinction being proportional to LWC, providing droplets have size parameters less than a maximum value x_m. The maximum size parameter $x_m \cong 7$, but depends slightly on refractive index and hence on wavelength. If we choose a wavelength of 10μm, then $x_m = 8$ [22] and according to the Chýlek approximation we should find a linear relation between extinction and LWC for polydispersions of droplets having radii $r \leq 12\mu m$. Most of our haze and fog distributions satisfy this condition and, as verified in Fig. 10, there does exist a nearly linear relation between extinction at 10μm and LWC. Even for heavy fog the presence of larger droplets (r > 12μm), insofar as they do not dominate the smaller ones, does not destroy the linear

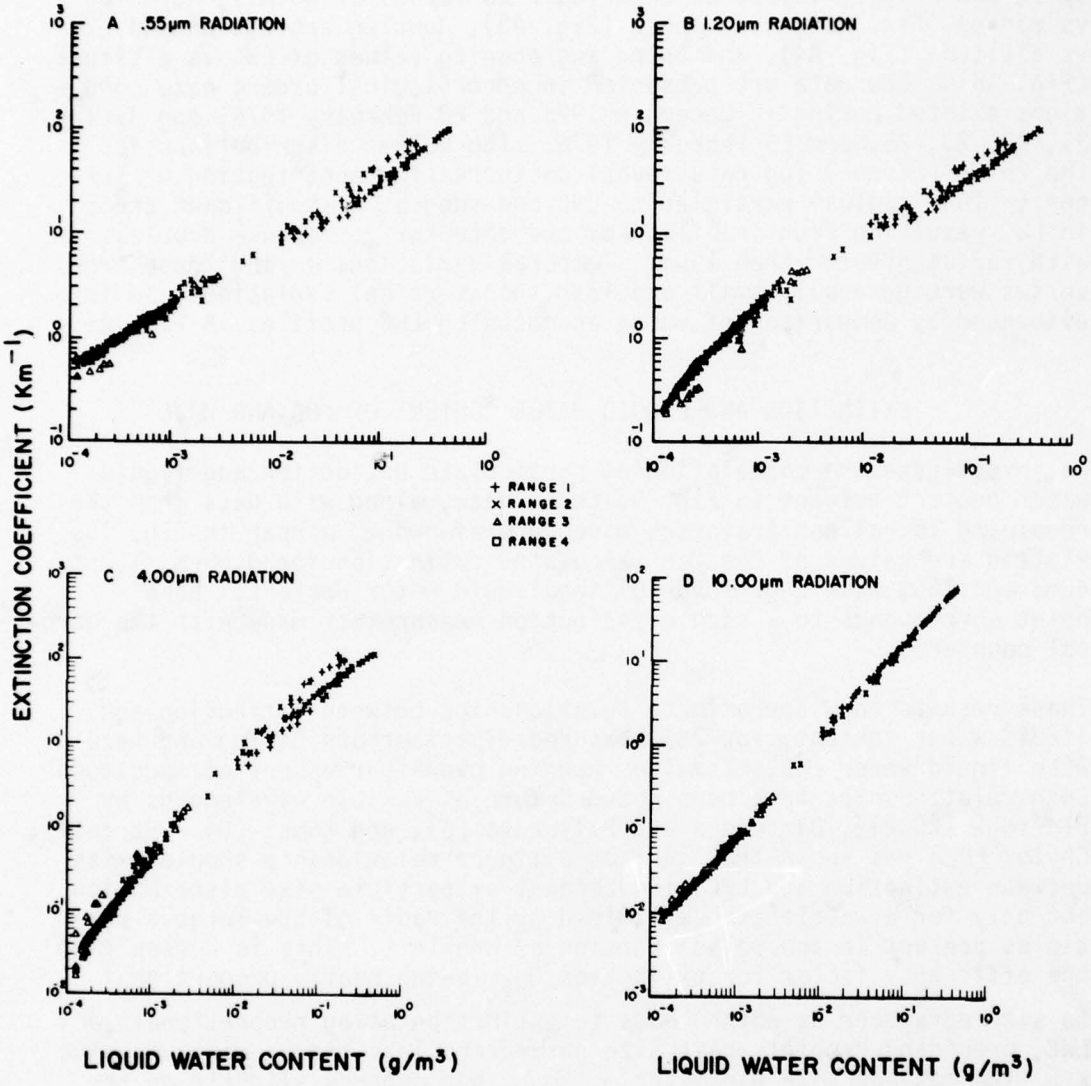

Figure 10. Values of Mie theory calculated particulate extinction at 0.55μm, 1.2μm, 4μm, and 10μm wavelengths vs liquid water content for a variety of particle size distributions of atmospheric fog and haze measured during February 1976 near Grafenwöhr, West Germany.

size distribution independent relation. However, the fact that there are approximate relationships between extinction and LWC for shorter wavelengths (namely 0.55μm, 1.2μm, and 4μm) for heavy fog (for which particles with $x > 7$ dominate extinction) is probably a result of the common form of the measured fog distributions (see for example, Fig. 6D), since for arbitrary distributions and wavelengths there is no reason to expect a unique relationship between extinction and LWC.

To check our contention that there should not exist a unique relation between extinction and LWC in fog, regardless of the form of the droplet size distribution or value of the wavelength, we compare empirical relationships between extinction at visible wavelengths and LWC determined by other workers for fog measurements made under different meteorological conditions and at different geographical locales. For the present work an approximate empirical relation between extinction at 0.55μm and LWC can be derived from the results in Fig. 10A:

$$\beta_{ext}(0.55) \simeq 145\ w^{.63}\ , \tag{2}$$

where β_{ext} (0.55) refers to the particulate extinction coefficient at 0.55μm, in km^{-1}, and w refers to liquid water content in g/m^3. For comparison Eldridge [21] gives the empirical relation

$$\beta_{ext}(0.55) \simeq 160\ w^{.65}\ , \tag{3}$$

for fogs and hazes having liquid water content 0.001-0.2 g/m^3. For fogs in the Tsei gorge near Leningrad with liquid water content 0.0002-0.2 g/m^3, Barteneva and Polyakova [6] find

$$\beta_{ext}(\text{visible}) \simeq 142\ w^{.87}. \tag{4}$$

From Kumai's [3] simultaneous measurements of arctic fog size distribution and prevailing visual range at Point Barrow, Alaska, with liquid water content 0.005-0.1 g/m^3, we find

$$\beta_{ext}(\text{visible}) \simeq (100 \text{ to } 200)\ w. \tag{5}$$

where the extinction has been inferred from the visual range measurements using Koschmieder's relation for a threshold ratio of 2%. Kumai has calculated the extinction from the measured size distributions as

we have done and the visual range calculated from these extinction values at 0.55μm are in good agreement with his measurements of visual range.

Using these four empirical expressions relating visible extinction to LWC, for an LWC of 0.01 g/m^3, we get extinction coefficients of 8.0 km^{-1}, 8.0 km^{-1}, 2.6 km^{-1}, and 1.0-2.0 km^{-1}, respectively, for the present work, Eldridge, Barteneva and Polyakova, and Kumai. These values differ by roughly an order of magnitude. These differences are most likely due to the widely differing fog droplet size distributions measured by the various authors, and thus any size distribution independent relation between extinction (at visible wavelengths) and LWC cannot be applied to fogs in general.

The approximation proposed by Chýlek [20] can also be used to explain the approximate $1/\lambda$ wavelength dependence of extinction for haze evident in Figs. 9A and 9B. The approximation can be written in the form

$$\beta_{ext}(\lambda) \cong \frac{3\pi c}{2\rho\lambda} W \qquad (6)$$

where W is the liquid water content, ρ the density of water, and the coefficient c is equal to the slope of a straight line approximating the efficiency factor for extinction by

$$Q_{ext}(x,\lambda) \cong c(\lambda)x \ . \qquad (7)$$

The coefficient c is a slowly varying function of wavelength. For two wavelengths λ_1, λ_2 the approximation (6) can be rewritten

$$\beta_{ext}(\lambda_1) \cong \frac{c_1\lambda_2}{c_2\lambda_1} \beta_{ext}(\lambda_2) \ , \qquad (8)$$

relating extinction at one wavelength to that at another. This approximation is only valid for polydispersions of droplets having size parameter less than a maximum value x_m, or equivalently, a maximum radius r_m. From Chylek's [22] Table 1 the maximum radii and corresponding c values are: at λ = 0.5μm, r_m = 0.5μm, c = 0.61; at λ = 3.8μm, r_m = 3.6μm, c = 0.68; and at λ = 10μm, r_m = 12μm, c = 0.35. Haze particles have maximum radii of about 2μm (Figs. 6A and 6B); hence the approximation (8) can be applied at 4μm and 10μm wavelengths and we obtain β_{ext} (4μm) ≅ 4.9

$\beta_{ext}(10\mu m)$, in good agreement with the exact Mie results in Figs. 9A and 9B. At the 0.55μm wavelength the Chýlek approximation cannot legitimately be used since particles with radii greater than the maximum value ($r_m \approx$ 0.5μm) contribute a significant part of the extinction for some haze distributions. Nevertheless, if we apply the approximation we obtain $\beta_{ext}(.55\mu m) \cong 6.5\ \beta_{ext}(4\mu m)$, a result that is within a factor 2 of the exact Mie results in Figs. 9A and 9B.

Since the reader may be interested in the radiative effects of fog and haze particles at other wavelengths in the infrared atmospheric windows, we have included in the appendix calculations of extinction vs LWC (for the 289 distributions measured at Grafenwöhr) at λ = 3μm, 5μm, 8μm, 11μm, and 12μm (Fig. A6). These data are replotted in the form of extinction at λ = 0.55μm vs extinction at λ = 1.2μm, 3μm, 4μm, 5μm, 8μm, 10μm, 11μm, and 12μm in Fig. A7. Approximate empirical relationships between extinction at a particular infrared wavelength and extinction at λ = 0.55μm can be derived from Fig. A7. For example, fitting the points in Fig. A7-c and A7-f with straight lines yields:

$$\beta_{ext}(4\mu m) \cong 0.12\ \beta_{ext}(0.55\mu m)^{1.75} ,$$

and

$$\beta_{ext}(10\mu m) \cong 0.036\ \beta_{ext}(0.55\mu m)^{1.72} .$$

CONCLUSIONS

Measurements of haze and fog droplet distributions carried out during 8 days in wintertime in West Germany show little vertical structure for haze, but a general trend toward increasing concentration of 4μm to 16μm radius droplets with altitude for fog conditions with visibilities < 1 km. Particulate extinction calculated from measured distributions at 0.55μm, 4μm, and 10μm wavelengths shows increases by a factor of 2 to 1000 over the first 150 m altitude for fog. Extinction is found to be approximately proportional to $1/\lambda$ over this spectral region for haze conditions, but nearly independent of wavelength for fog. Thus, for fog, from the point of view of extinction of radiation, there is no advantage of an infrared imaging system operating in the 8-12μm atmospheric window over one operating in the 3-5μm window. There exists a size distribution independent linear relationship between particle extinction coefficient and liquid water content at 10μm. However, the approximate relationships found between extinction (from visible through

4μm wavelengths) and liquid water content are attributed to a common form of the fog and haze size distributions measured.

REFERENCES

1. Garland, J. A., 1971, "Some Fog Droplet Size Distributions Obtained by an Impaction Method," Quart. J. Roy. Meteorol. Soc., 97:483-494.

2. Krasikov, P. N., and G. A. Chikirova, 1956, "Microphysical Characteristics of Local Fogs," Trudy Glavnoy Geofiz. Observ., 57:88-100.

3. Kumai, M., 1973, "Arctic Fog Droplet Size Distribution and Its Effect on Light Attenuation," J. Atmos. Sci., 30:635-643.

4. Low, R. D. H., 1975, "Microphysical Evolution of Fog," J. Rech. Atmos., 2:23-32.

5. May, K. R., 1961, "Fog Droplet Sampling Using a Modified Impactor Technique," Quart. J. Roy. Meteorol. Soc., 87:535-548.

6. Barteneva, O. D., and E. A. Polyakova, 1965, "A Study of Attenuation and Scattering of Light in a Natural Fog Due to Its Microphysical Properties," Izv., Atmos. and Oceanic Phys., 1:193-207.

7. Arnulf, A., J. Bricard, E. Cure, and C. Veret, 1957, "Transmission by Haze and Fog in the Spectral Region 0.35 to 10 Microns," J. Opt. Soc., 47:491-498.

8. Kunkel, B. A., 1971, "Fog Drop-Size Distributions Measured With a Laser Hologram Camera," J. Appl. Meteorol., 10:482-486.

9. Eldridge, R. G., 1961, "A Few Fog Drop-Size Distributions," J. Appl. Meteorol., 18:671-676.

10. Laktionov, A. G., 1967, "Variation of the Size and Concentration of Drops During the Scattering of Fog," Izv., Atmos. and Oceanic Phys., 3:566-569.

11. Pilié, R. J., E. J. Mack, W. C. Kocmond, W. J. Eadie, and C. W. Rogers, 1975, "The Life Cycle of Valley Fog. Part II: Fog Microphysics," J. Appl. Meteorol., 14:364-374.

12. Goodman, J., 1977, "The Microstructure of California Coastal Fog Light-Scattering Properties of Individual Aerosol Particles Compared to Mie Scattering Theory," Appl. Opt., 12:37-41.

14. Hanel, G., 1971, "New Results Concerning the Dependence of Visibility on Relative Humidity and Their Significance in a Model for Visibility Forecast," Beitr. Phys. Atmos., 44:137-167.

15. Rosen, J. M., 1968, "Simultaneous Dust and Ozone Soundings over North and Central America," J. Geophys. Res., 73:479-486.

16. Hale, G. M., and M. R. Querry, 1973, "Optical Constants of Water in the 200 nm to 200 μm Wavelength Region," Appl. Opt., 12:555-563.

17. Garland, J. A., J. R. Branson, and I. C. Cox, 1973, "A Study of the Contribution of Polution to Visibility in a Radiation Fog," Atmos. Environ., 7:1079-1092.

18. Roach, W. T., R. Brown, S. J. Caughly, J. A. Garland, and C. J. Readings, 1976, "The Physics of Radiation Fog: I-a Field Study," Quart J. Roy. Meteorol. Soc., 102:313-333.

19. Patterson, E. M., 1977, "Atmospheric Extinction Between 0.55 and 10.6 μm Due to Soil Derived Aerosols," Appl. Opt., 16:2414-2418.

20. Eldridge, R. G., 1966, "Haze and Fog Aerosol Distributions," J. Atmos. Sci., 23:605-613.

21. Eldridge, R. G., 1971, "The Relationship Between Visibility and Liquid Water Content in Fog," J. Atmos. Sci., 28:1183-1186.

22. Chýlek, Petr, 1978, "Extinction and Liquid Water Content of Fogs," J. Atmos. Sci., 35:296-300.

APPENDIX
FIGURES

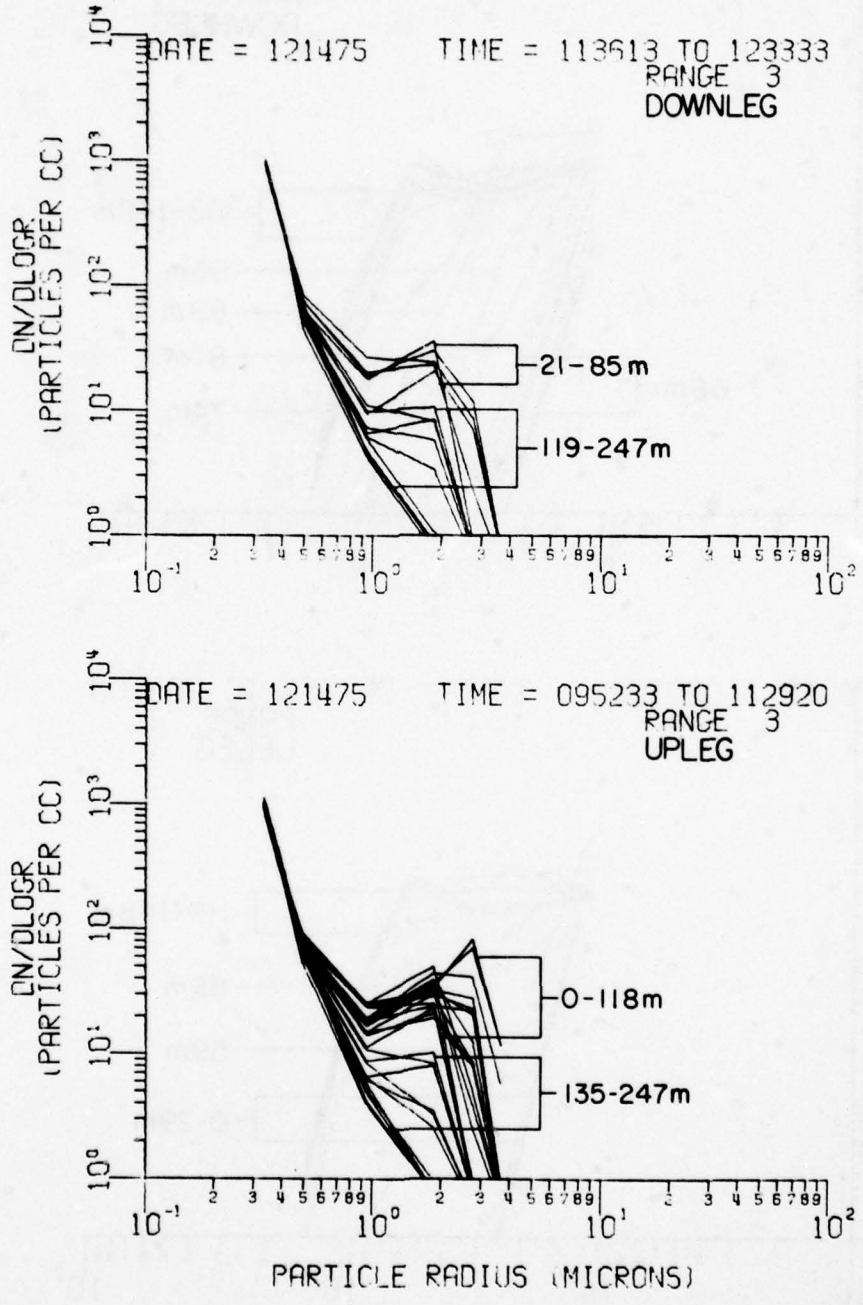

Figure A1-a Particle number size distribution measurements made with a tethered balloon-borne aerosol counter for 20 upleg and downleg profiles during haze and fog conditions. The date, local time (hours, minutes, seconds), and time interval for the measurements are given, as well as the size range setting (see Fig. 4) of the aerosol counter.

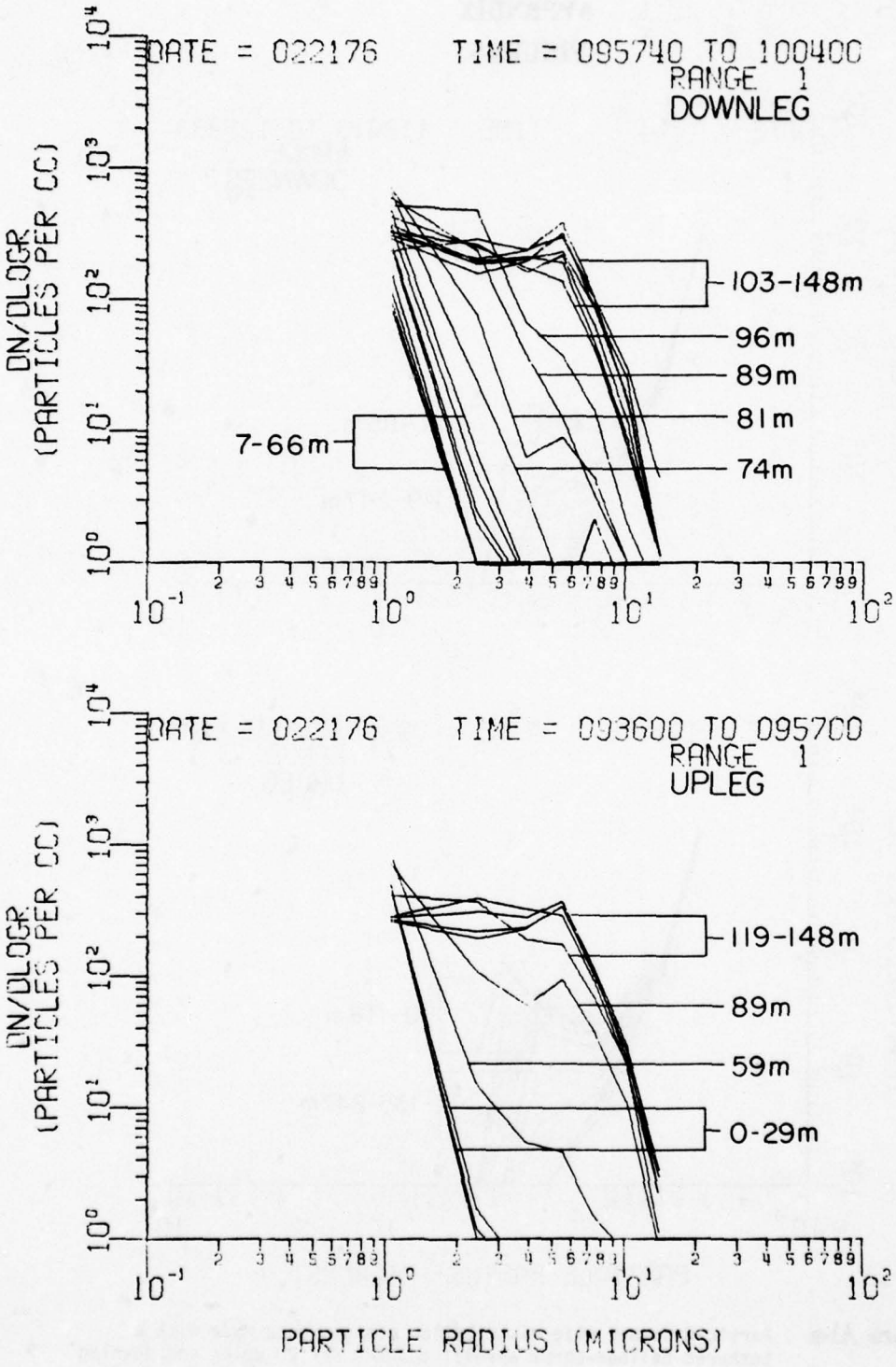
DATE = 022176
TIME = 095740 TO 100400
RANGE 1
DOWNLEG
DN/DLOGR
(PARTICLES PER CC)
103-148m
96m
89m
81m
7-66m
74m
DATE = 022176
TIME = 093600 TO 095700
RANGE 1
UPLEG
DN/DLOGR
(PARTICLES PER CC)
119-148m
89m
59m
0-29m
PARTICLE RADIUS (MICRONS)

Figure Al-b

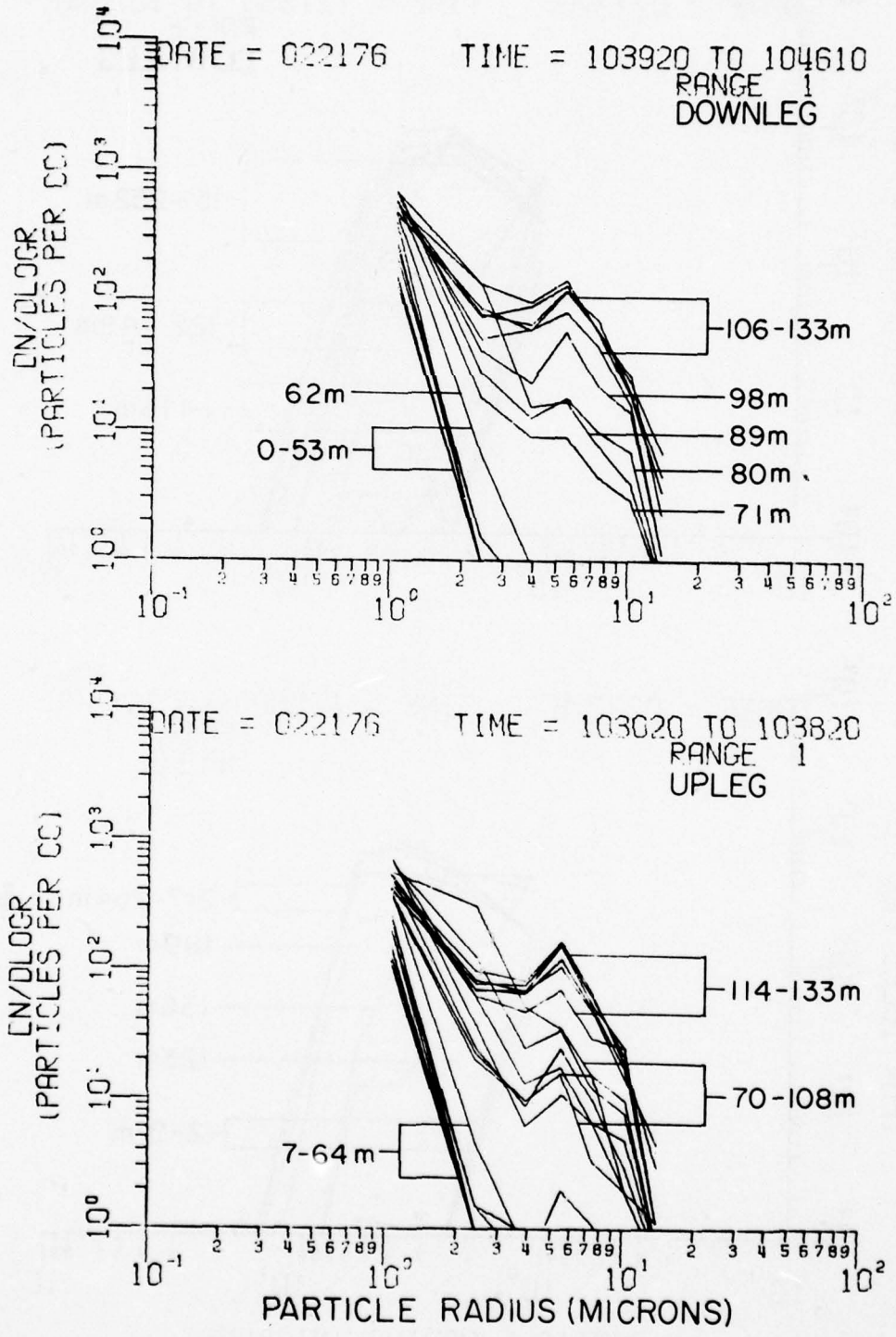
DATE = 022176
TIME = 103920 TO 104610
RANGE 1
DOWNLEG
DN/DLOGR
(PARTICLES PER CC)
106-133m
98m
89m
80m
71m
62m
0-53m
DATE = 022176
TIME = 103020 TO 103820
RANGE 1
UPLEG
114-133m
70-108m
7-64m
PARTICLE RADIUS (MICRONS)

Figure Al-c

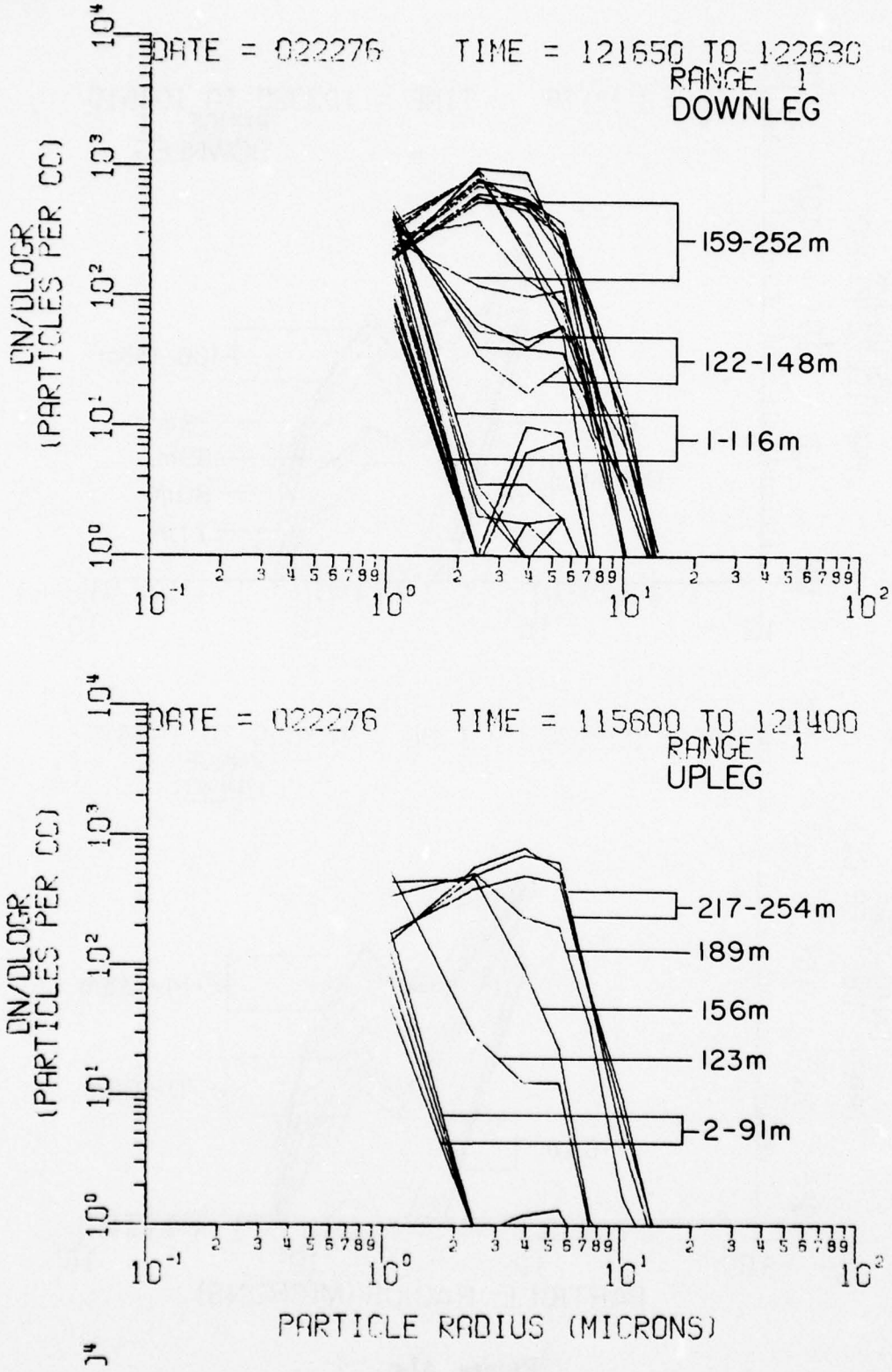
DATE = 022276
TIME = 121650 TO 122630
RANGE 1
DOWNLEG
DN/DLOGR
(PARTICLES PER CC)
159-252 m
122-148m
1-116m
DATE = 022276
TIME = 115600 TO 121400
RANGE 1
UPLEG
217-254m
189m
156m
123m
2-91m
PARTICLE RADIUS (MICRONS)

Figure Al-d

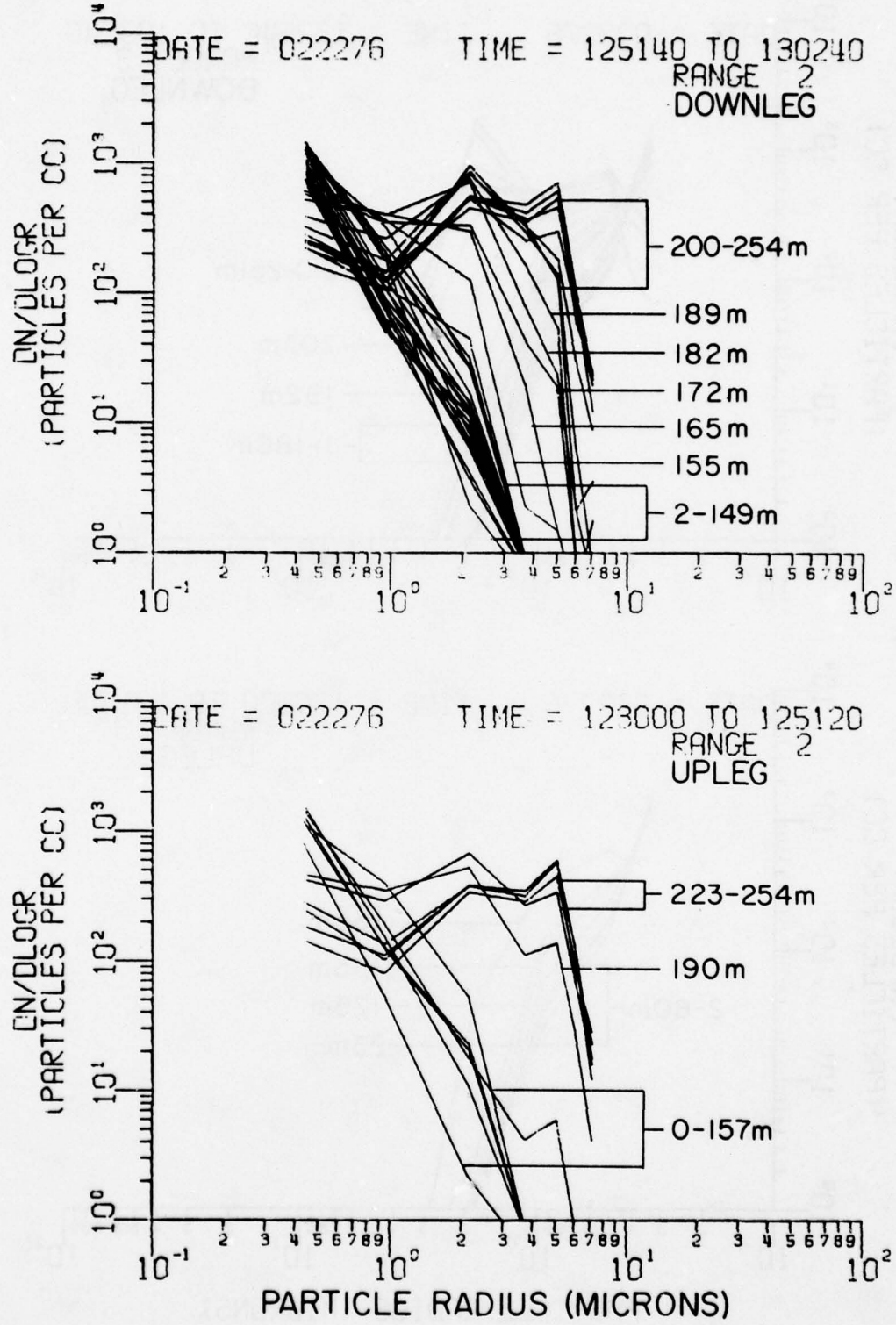
DATE = 022276
TIME = 125140 TO 130240
RANGE 2
DOWNLEG
200-254m
189m
182m
172m
165m
155m
2-149m
DN/DLOGR
(PARTICLES PER CC)
DATE = 022276
TIME = 123000 TO 125120
RANGE 2
UPLEG
223-254m
190m
0-157m
PARTICLE RADIUS (MICRONS)

Figure Al-e

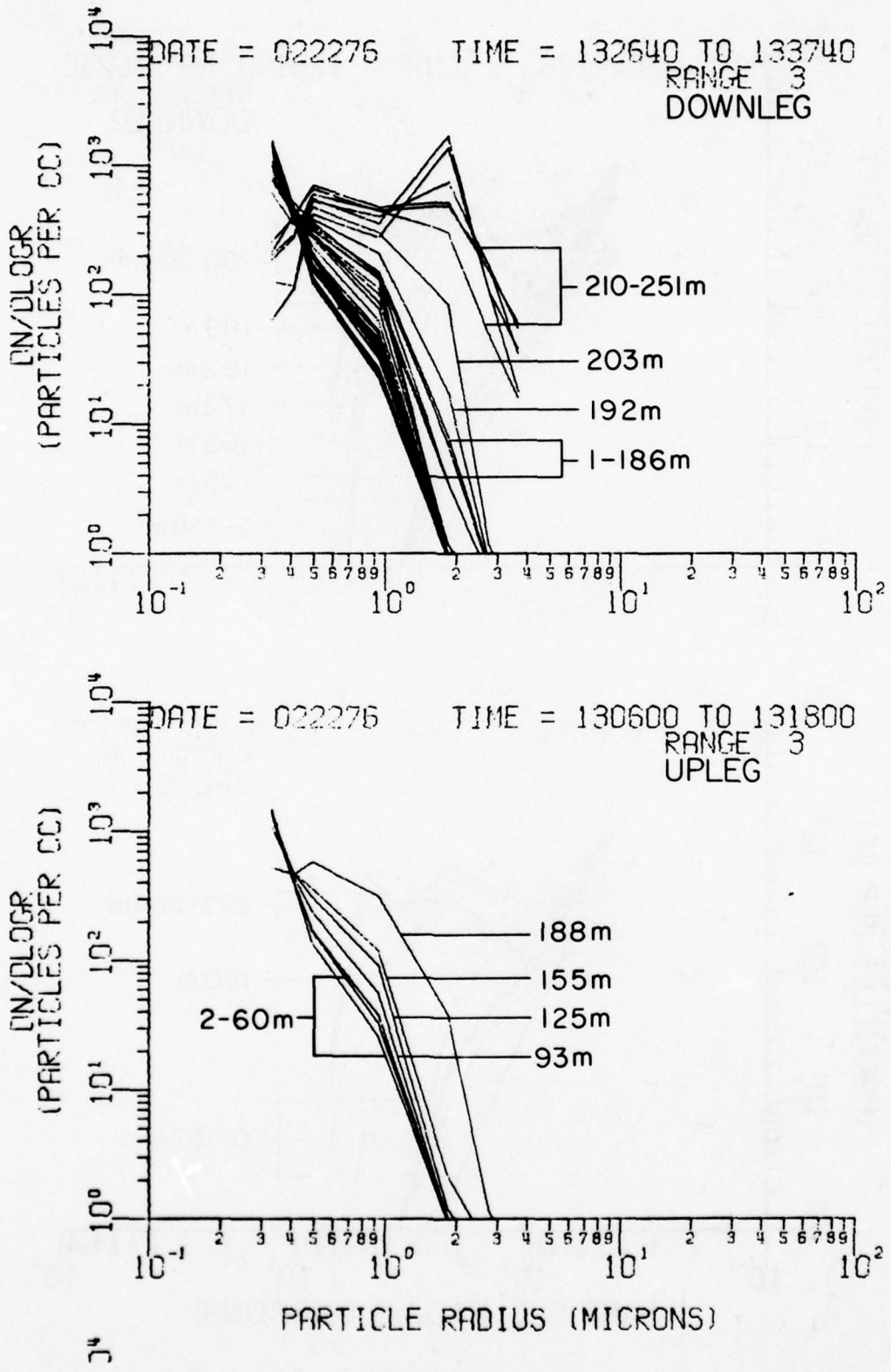
DATE = 022276 TIME = 132640 TO 133740
RANGE 3
DOWNLEG
210-251m
203m
192m
1-186m
DN/DLOGR
(PARTICLES PER CC)
DATE = 022276 TIME = 130600 TO 131800
RANGE 3
UPLEG
188m
155m
2-60m
125m
93m
PARTICLE RADIUS (MICRONS)

Figure A1-f

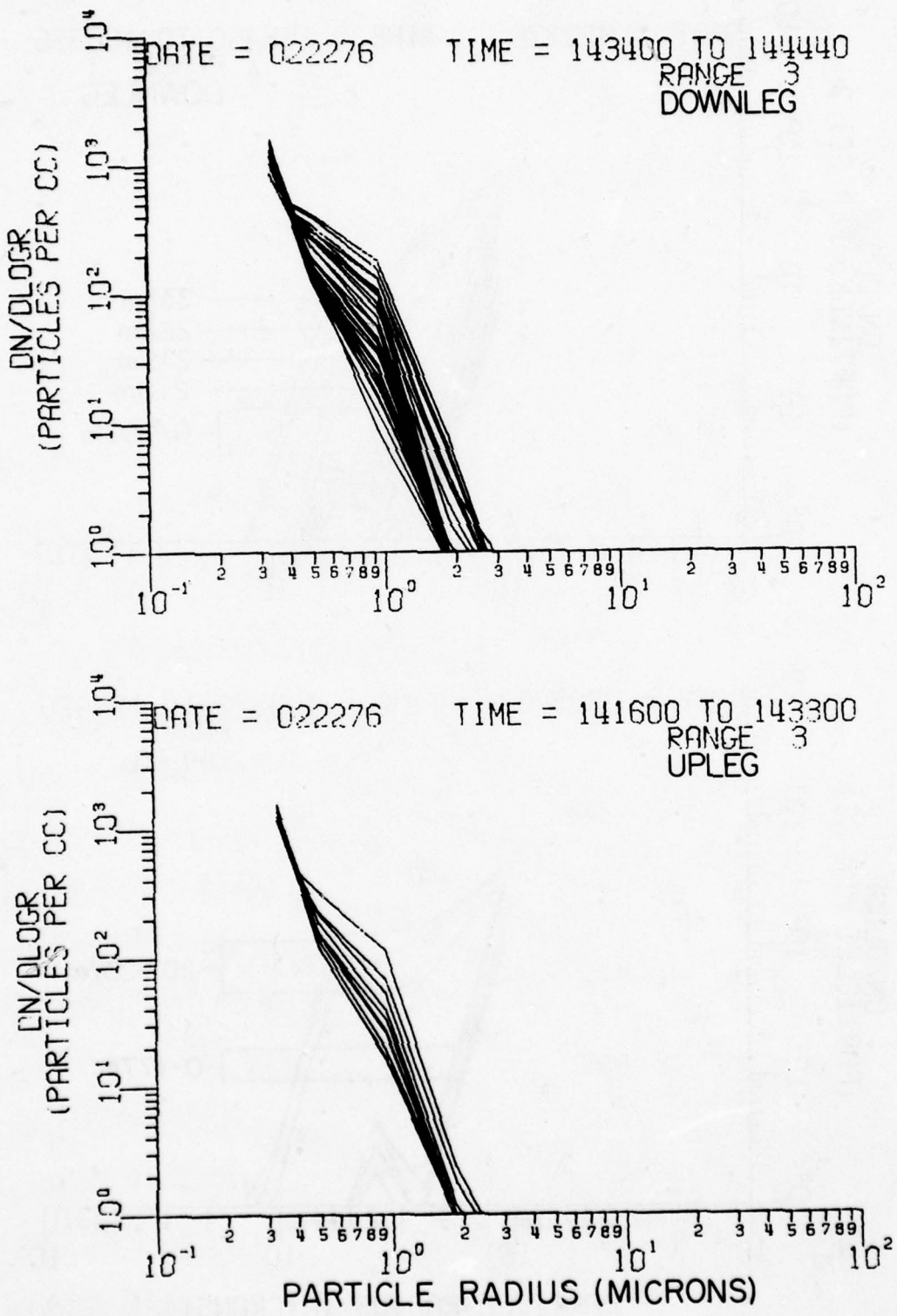
DATE = 022276
TIME = 143400 TO 144440
RANGE 3
DOWNLEG
DN/DLOGR
(PARTICLES PER CC)
DATE = 022276
TIME = 141600 TO 143300
RANGE 3
UPLEG
DN/DLOGR
(PARTICLES PER CC)
PARTICLE RADIUS (MICRONS)

Figure Al-g

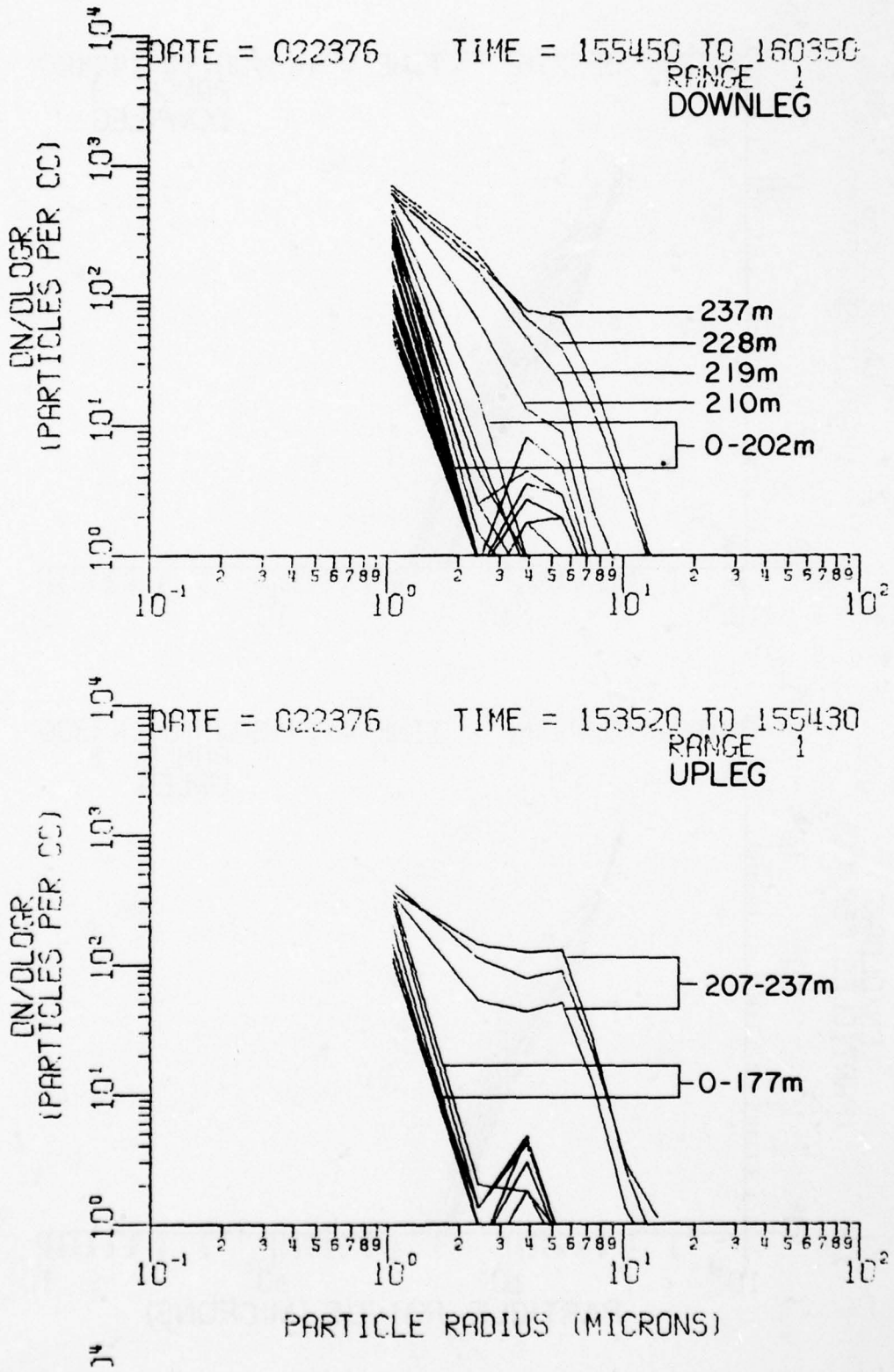
DATE = 022376
TIME = 155450 TO 160350
RANGE 1
DOWNLEG
DN/DLOGR
(PARTICLES PER CC)
237m
228m
219m
210m
0-202m
DATE = 022376
TIME = 153520 TO 155430
RANGE 1
UPLEG
207-237m
0-177m
PARTICLE RADIUS (MICRONS)

Figure Al-h

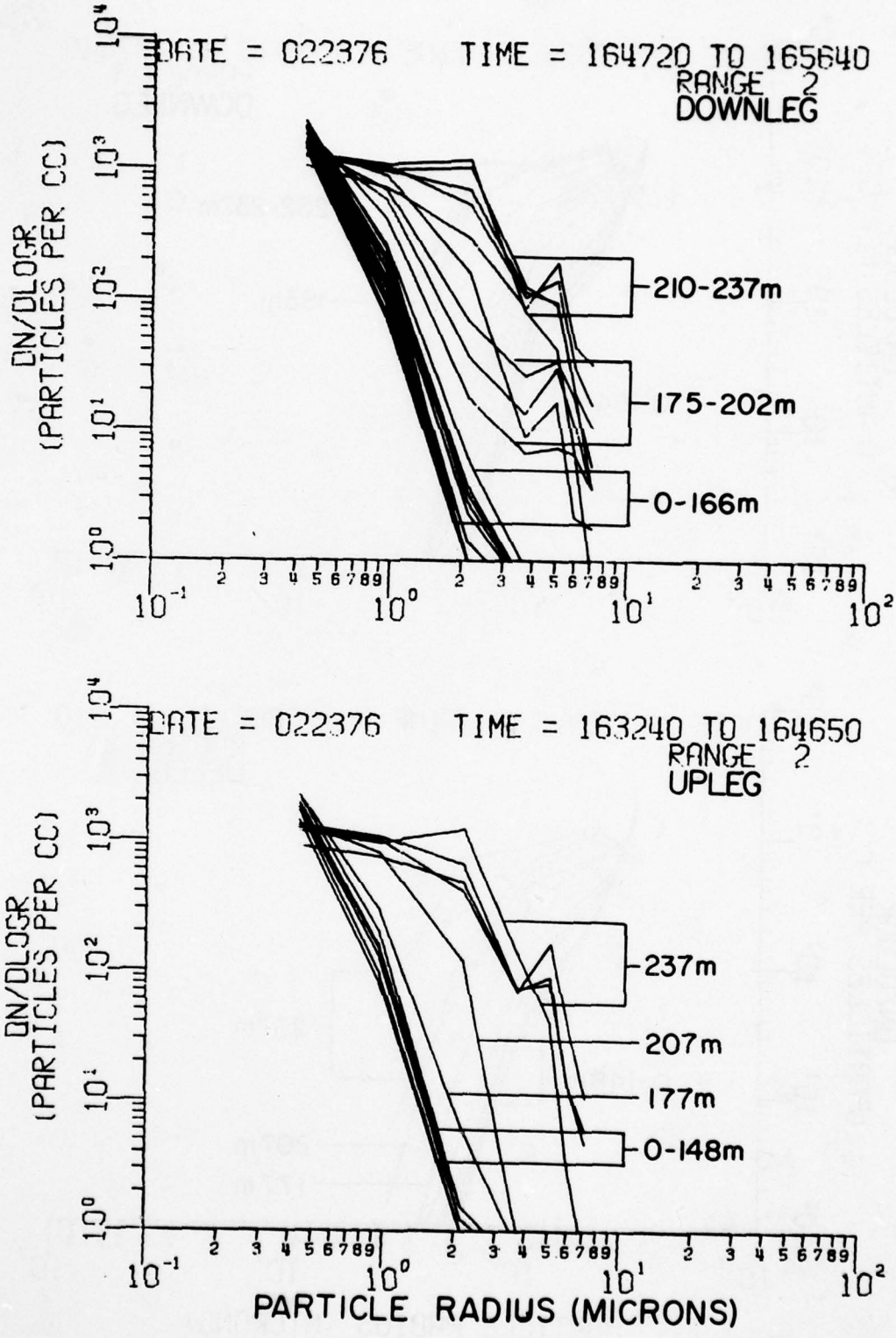
DATE = 022376
TIME = 164720 TO 165640
RANGE 2
DOWNLEG
210-237m
175-202m
0-166m
DN/DLOGR
(PARTICLES PER CC)
DATE = 022376
TIME = 163240 TO 164650
RANGE 2
UPLEG
237m
207m
177m
0-148m
PARTICLE RADIUS (MICRONS)

Figure A1-1

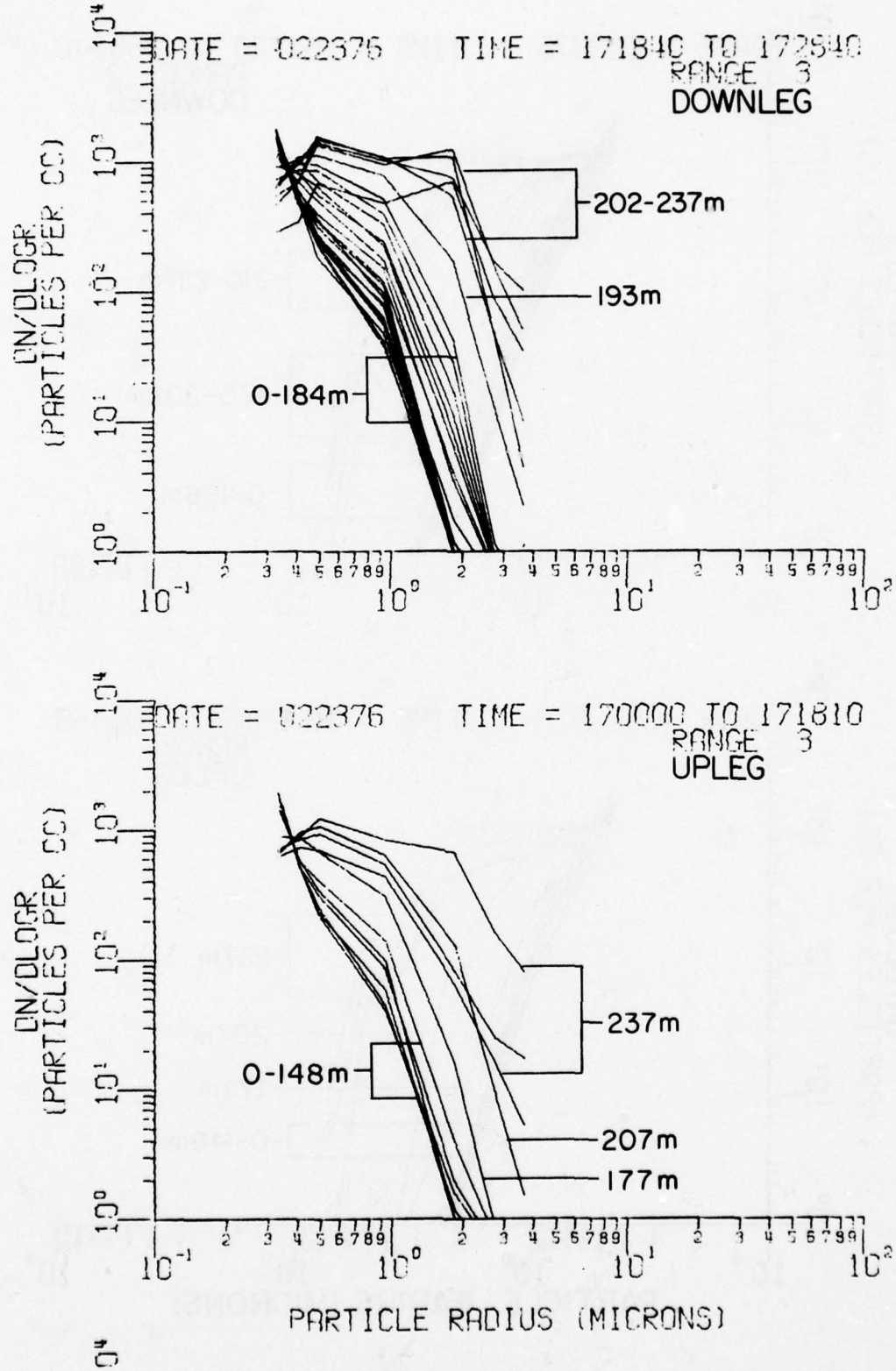
DATE = 022376 TIME = 171840 TO 172840
RANGE 3
DOWNLEG
202-237m
193m
0-184m
DN/DLOGR
(PARTICLES PER CC)
DATE = 022376 TIME = 170000 TO 171810
RANGE 3
UPLEG
237m
0-148m
207m
177m
PARTICLE RADIUS (MICRONS)

Figure Al-j

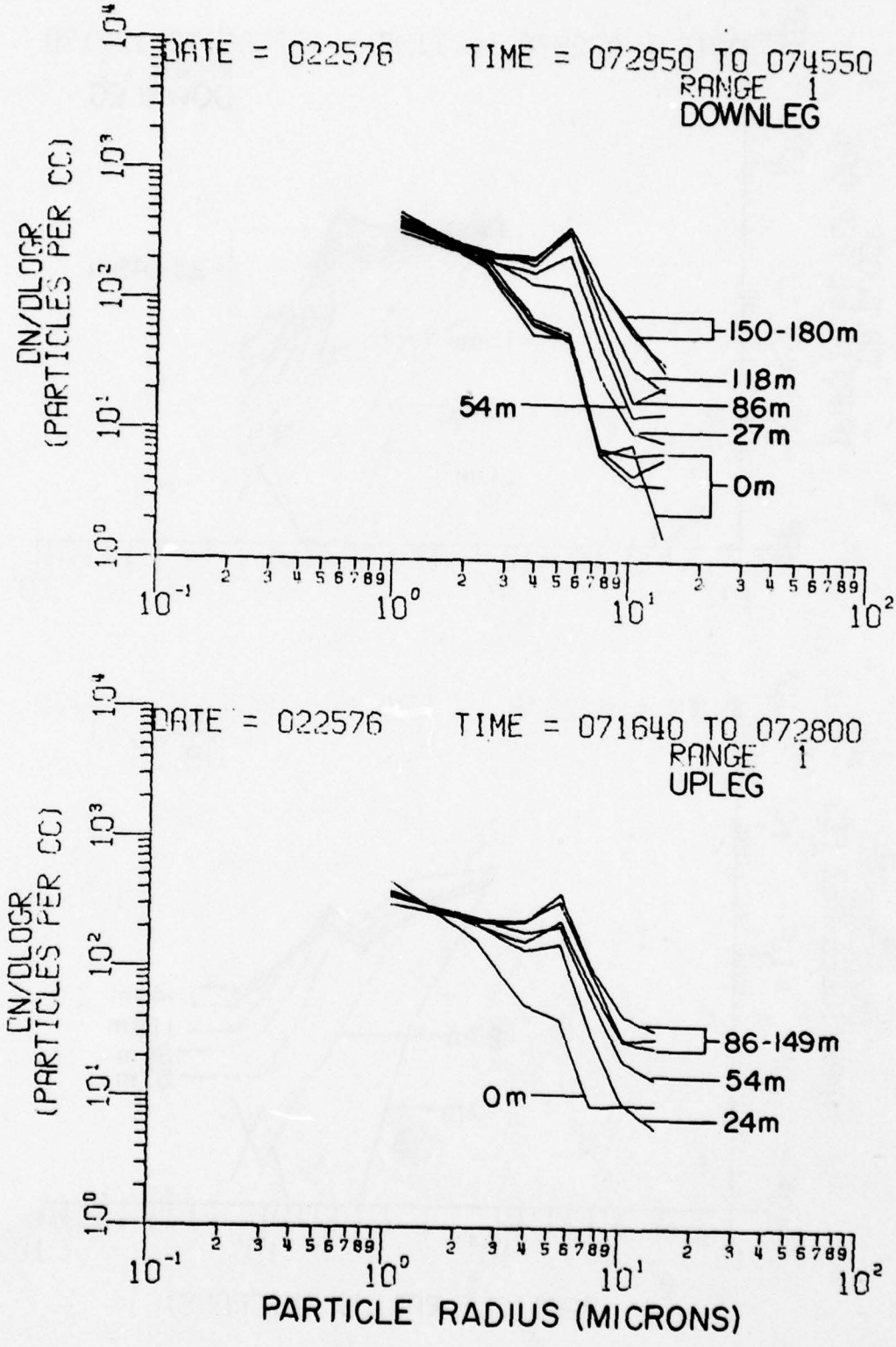
DATE = 022576
TIME = 072950 TO 074550
RANGE 1
DOWNLEG
DN/DLOGR
(PARTICLES PER CC)
150-180m
118m
54m
86m
27m
0m
DATE = 022576
TIME = 071640 TO 072800
RANGE 1
UPLEG
DN/DLOGR
(PARTICLES PER CC)
86-149m
54m
0m
24m
PARTICLE RADIUS (MICRONS)

Figure A1-k

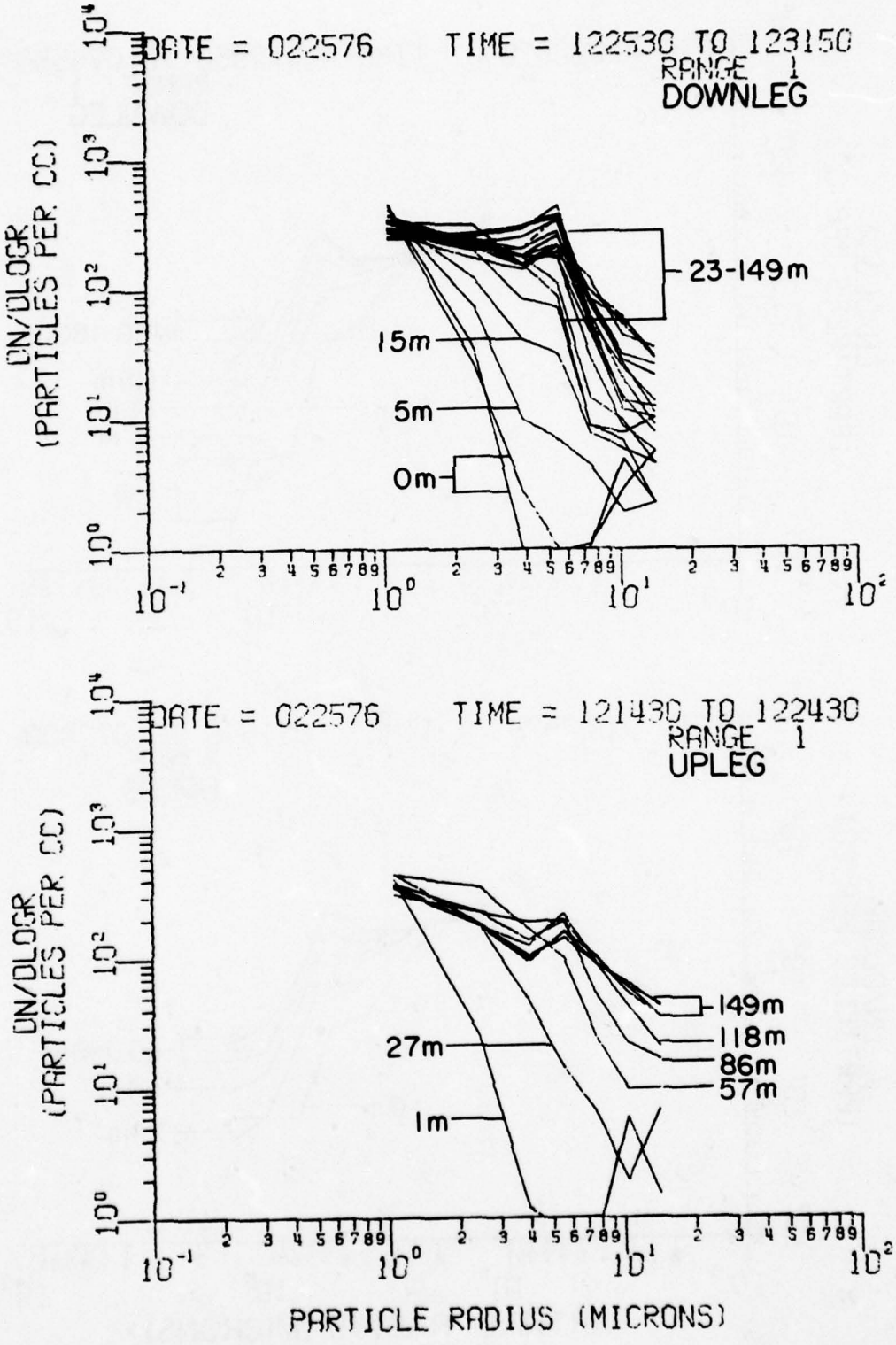
DATE = 022576
TIME = 122530 TO 123150
RANGE 1
DOWNLEG
DN/DLOGR
(PARTICLES PER CC)
23-149m
15m
5m
0m
DATE = 022576
TIME = 121430 TO 122430
RANGE 1
UPLEG
149m
118m
86m
57m
27m
1m
PARTICLE RADIUS (MICRONS)

Figure A1-1

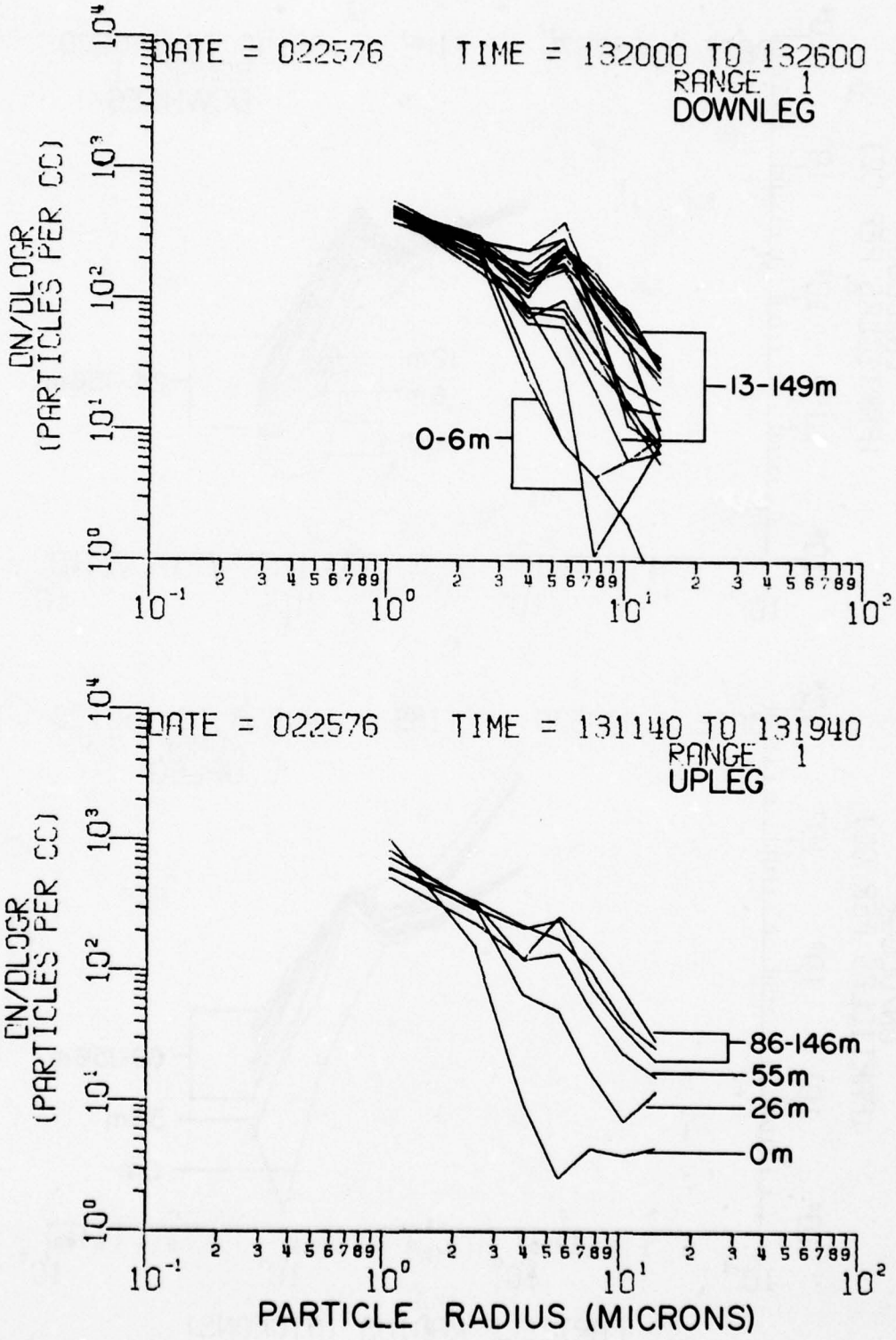
DATE = 022576
TIME = 132000 TO 132600
RANGE 1
DOWNLEG
DN/DLOGR
(PARTICLES PER CC)
13-149m
0-6m
DATE = 022576
TIME = 131140 TO 131940
RANGE 1
UPLEG
86-146m
55m
26m
0m
PARTICLE RADIUS (MICRONS)

Figure Al-m

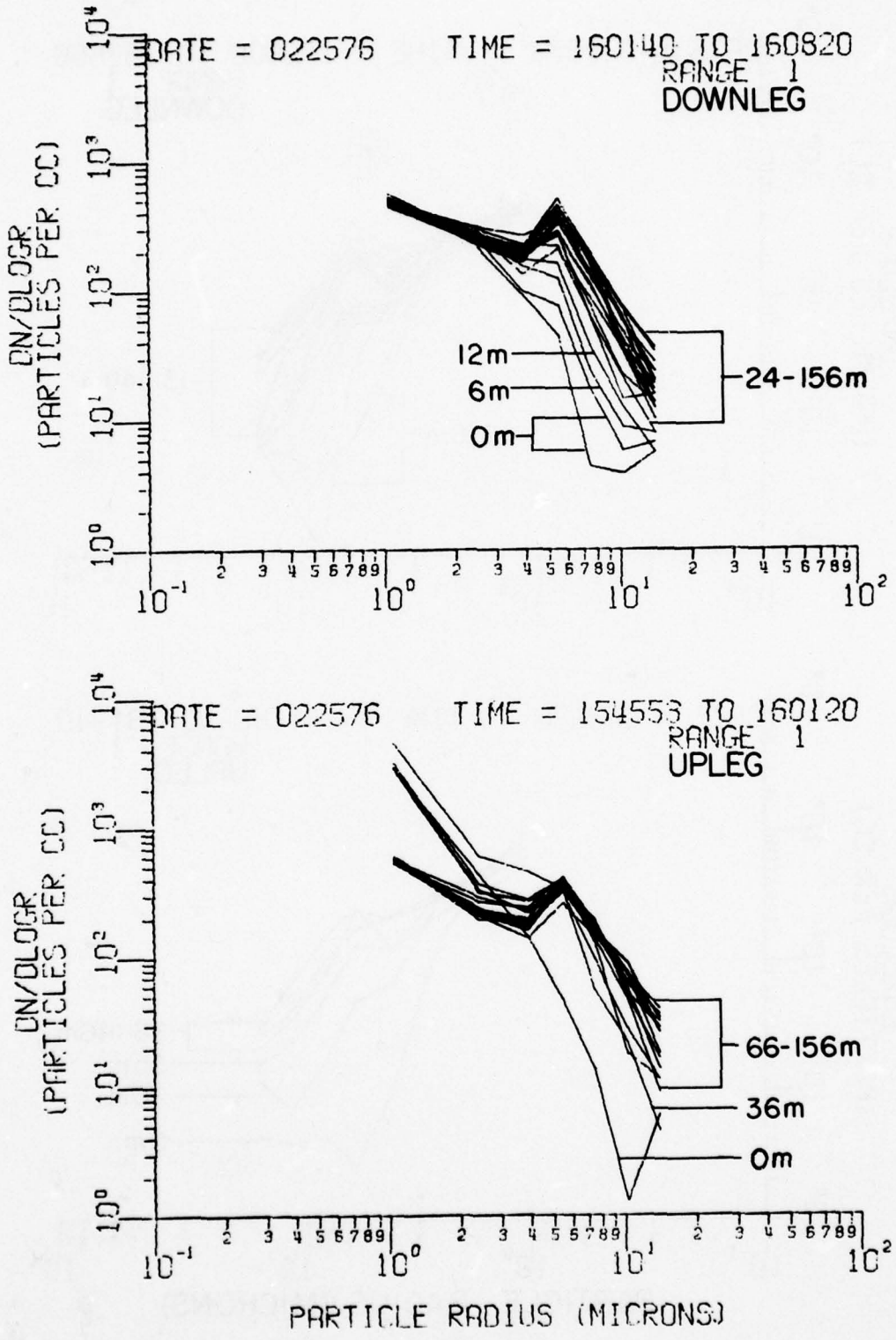
DATE = 022576
TIME = 160140 TO 160820
RANGE 1
DOWNLEG
DN/DLOGR
(PARTICLES PER CC)
12m
6m
0m
24-156m
DATE = 022576
TIME = 154553 TO 160120
RANGE 1
UPLEG
66-156m
36m
0m
PARTICLE RADIUS (MICRONS)

Figure Al-n

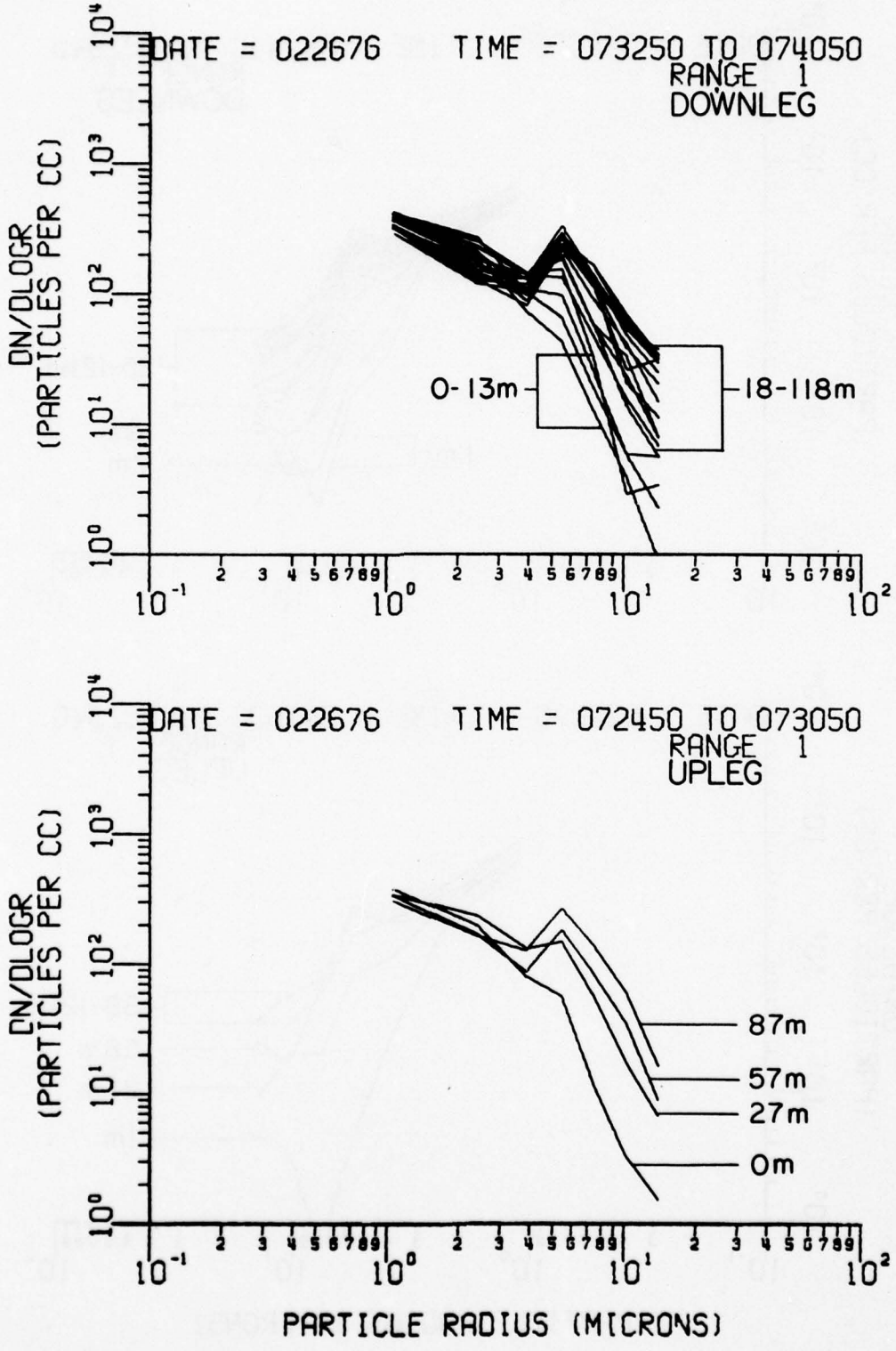
DATE = 022676
TIME = 073250 TO 074050
RANGE 1
DOWNLEG
DN/DLOGR
(PARTICLES PER CC)
0-13m
18-118m
DATE = 022676
TIME = 072450 TO 073050
RANGE 1
UPLEG
87m
57m
27m
0m
PARTICLE RADIUS (MICRONS)

Figure Al-o

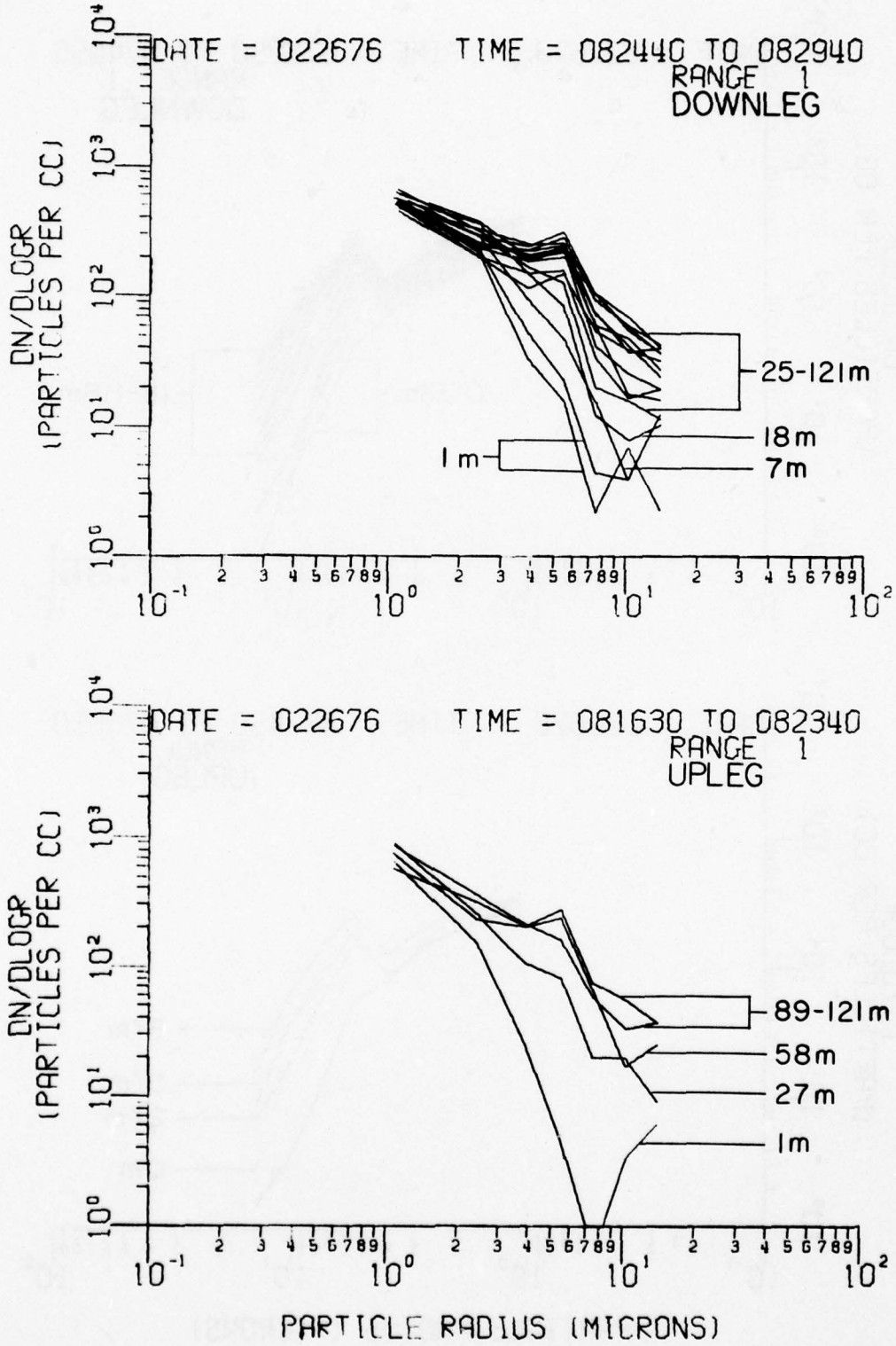
DATE = 022676
TIME = 082440 TO 082940
RANGE 1
DOWNLEG
DN/DLOGR
(PARTICLES PER CC)
25-121m
18m
7m
1m
DATE = 022676
TIME = 081630 TO 082340
RANGE 1
UPLEG
89-121m
58m
27m
1m
PARTICLE RADIUS (MICRONS)

Figure Al-p

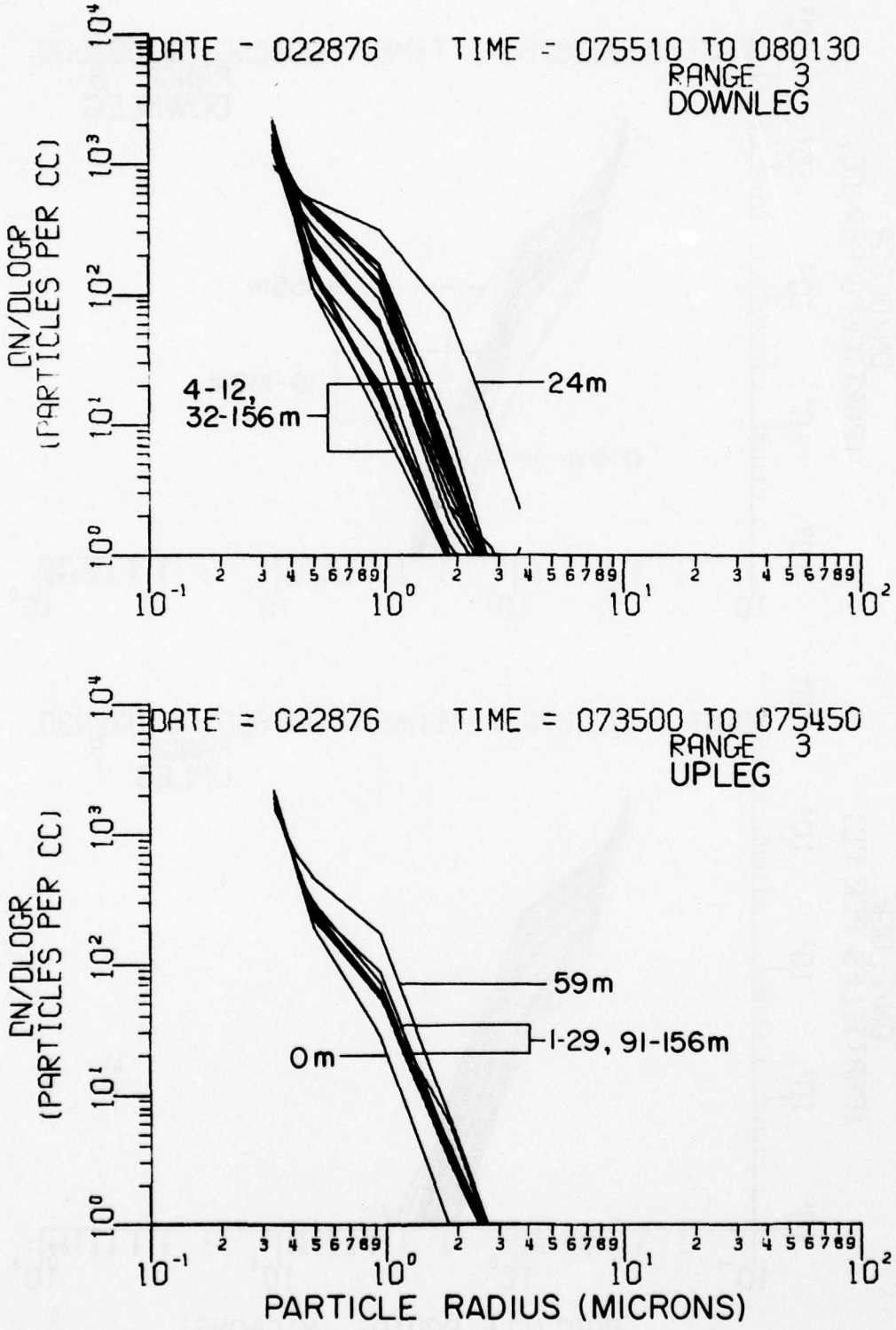
DATE - 022876
TIME - 075510 TO 080130
RANGE 3
DOWNLEG
DN/DLOGR
(PARTICLES PER CC)
4-12,
32-156m
24m
DATE = 022876
TIME = 073500 TO 075450
RANGE 3
UPLEG
59m
1-29, 91-156m
0m
PARTICLE RADIUS (MICRONS)

Figure Al-q

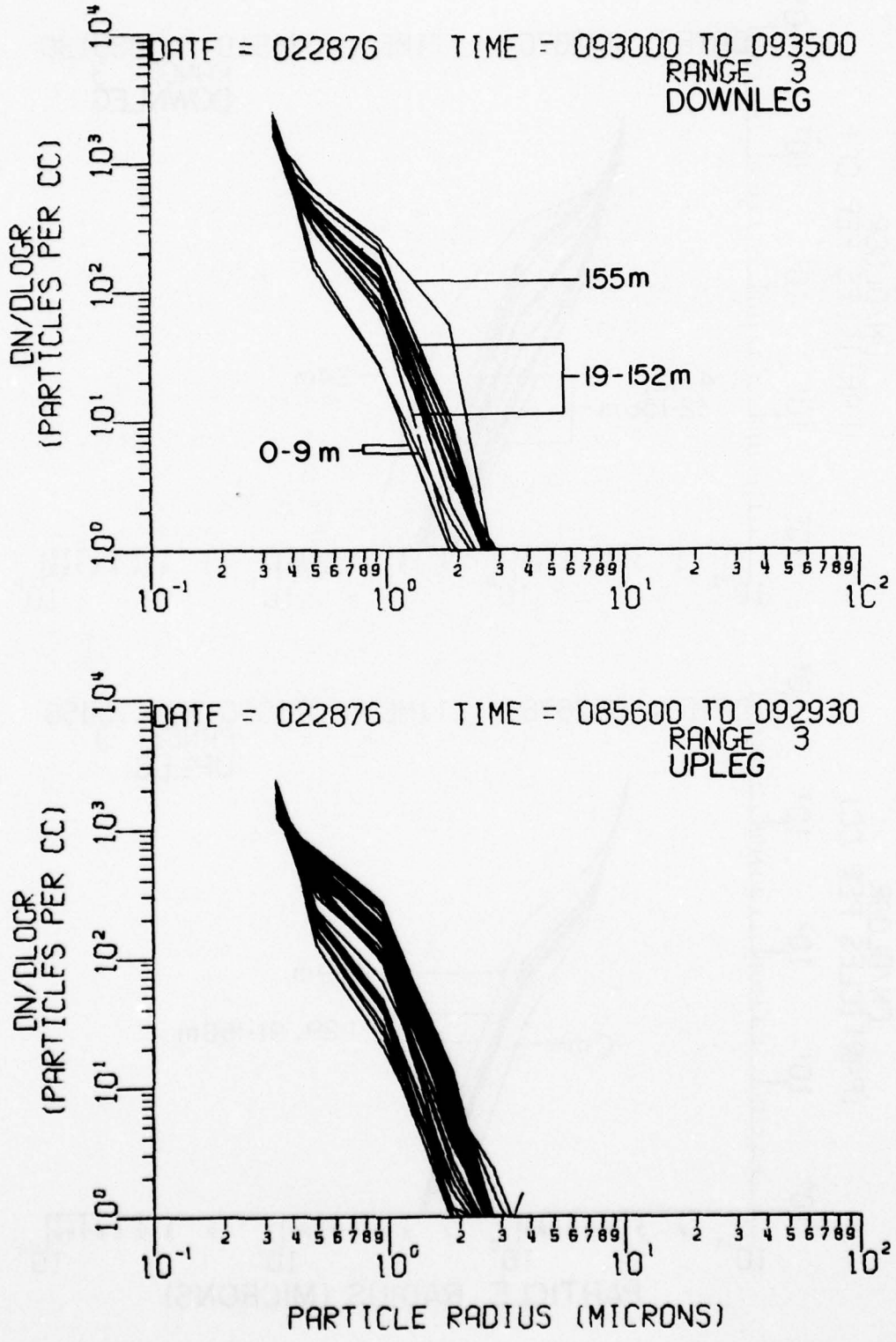
DATE = 022876
TIME = 093000 TO 093500
RANGE 3
DOWNLEG
155m
19-152m
0-9 m
DN/DLOGR
(PARTICLES PER CC)
DATE = 022876
TIME = 085600 TO 092930
RANGE 3
UPLEG
PARTICLE RADIUS (MICRONS)

Figure Al-r

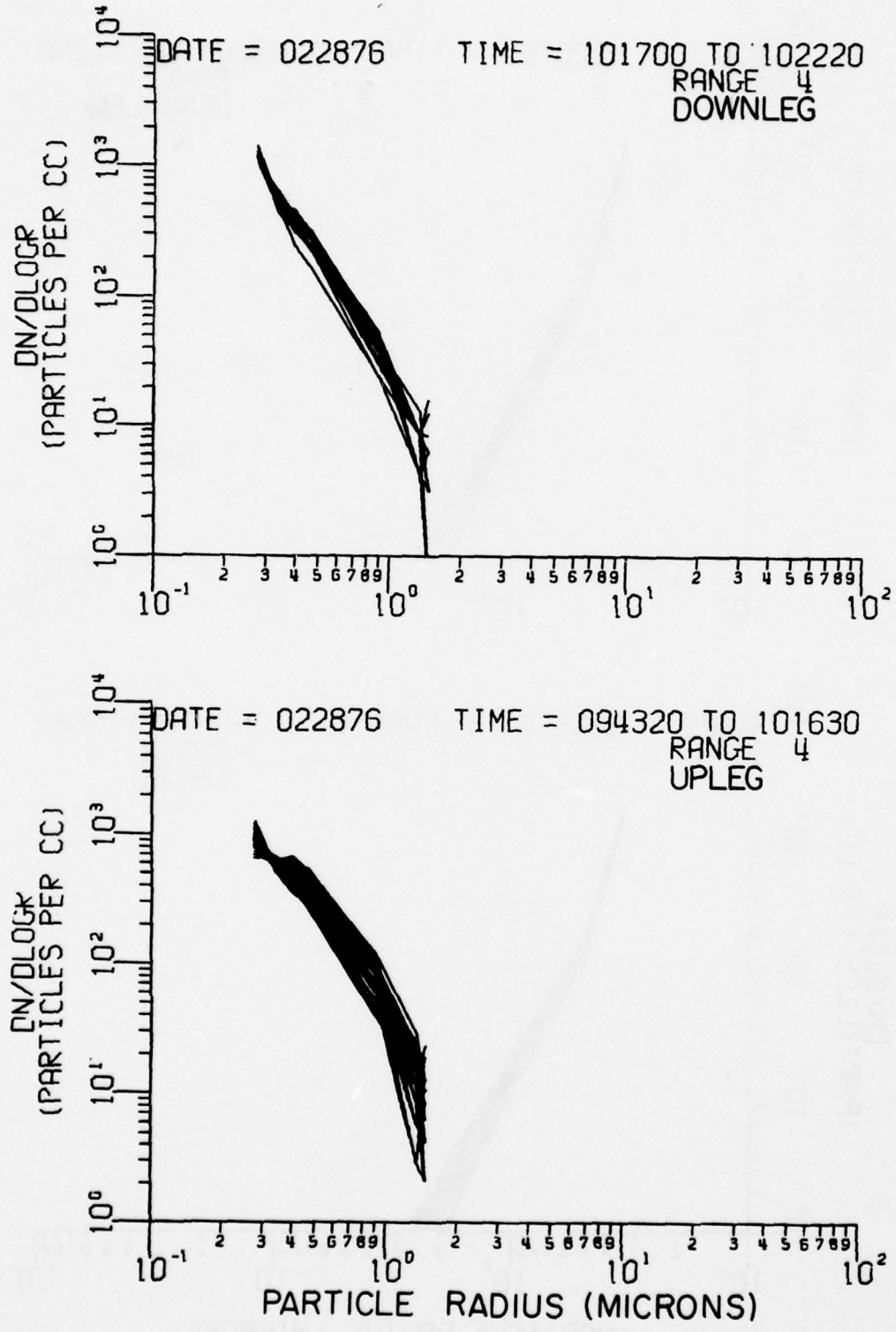
DATE = 022876
TIME = 101700 TO 102220
RANGE 4
DOWNLEG
DN/DLOGR
(PARTICLES PER CC)
DATE = 022876
TIME = 094320 TO 101630
RANGE 4
UPLEG
DN/DLOGR
(PARTICLES PER CC)
PARTICLE RADIUS (MICRONS)

Figure A1-s

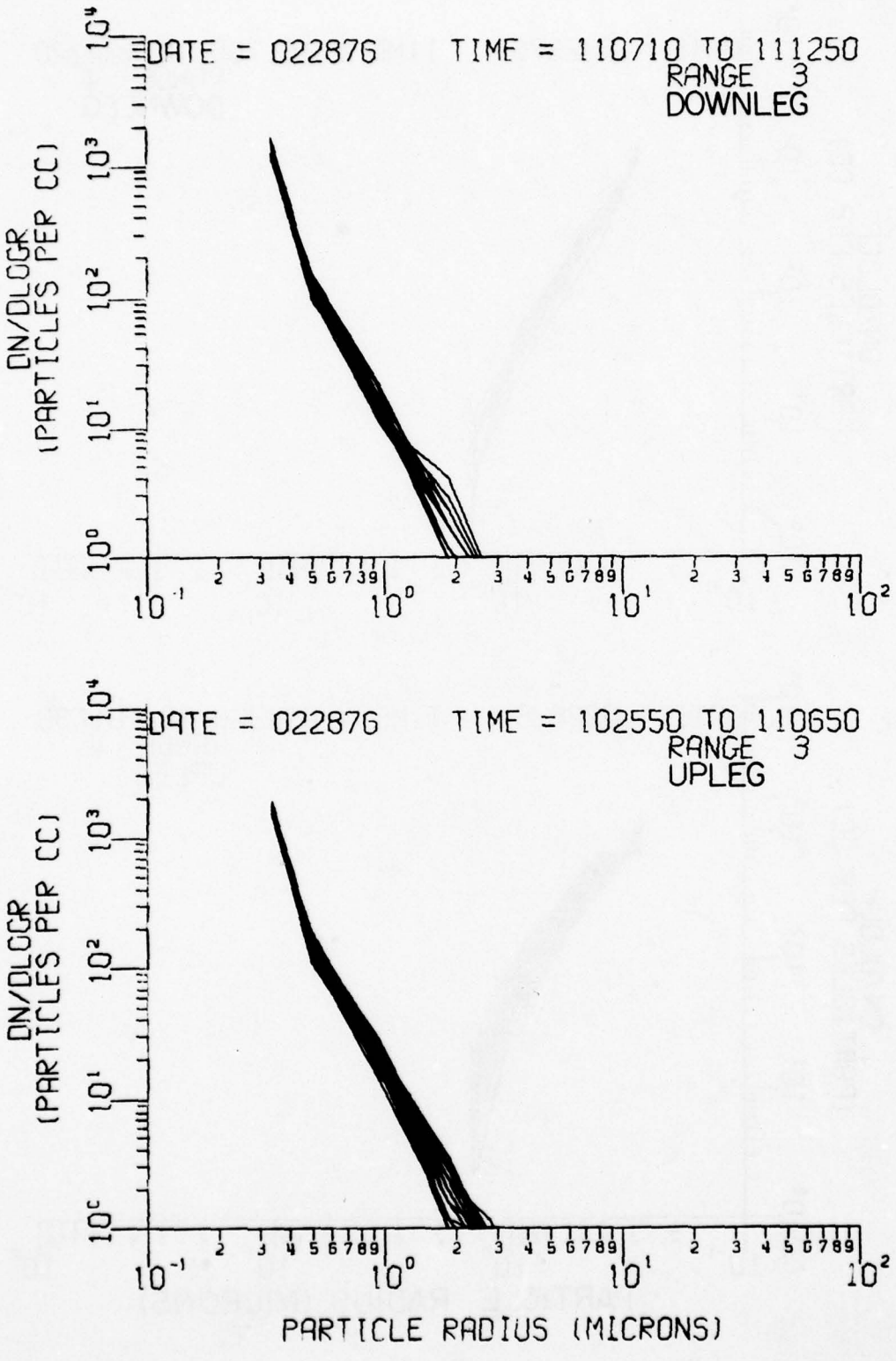
DATE = 022876
TIME = 110710 TO 111250
RANGE 3
DOWNLEG
DN/DLOGR
(PARTICLES PER CC)
DATE = 022876
TIME = 102550 TO 110650
RANGE 3
UPLEG
PARTICLE RADIUS (MICRONS)

Figure Al-t

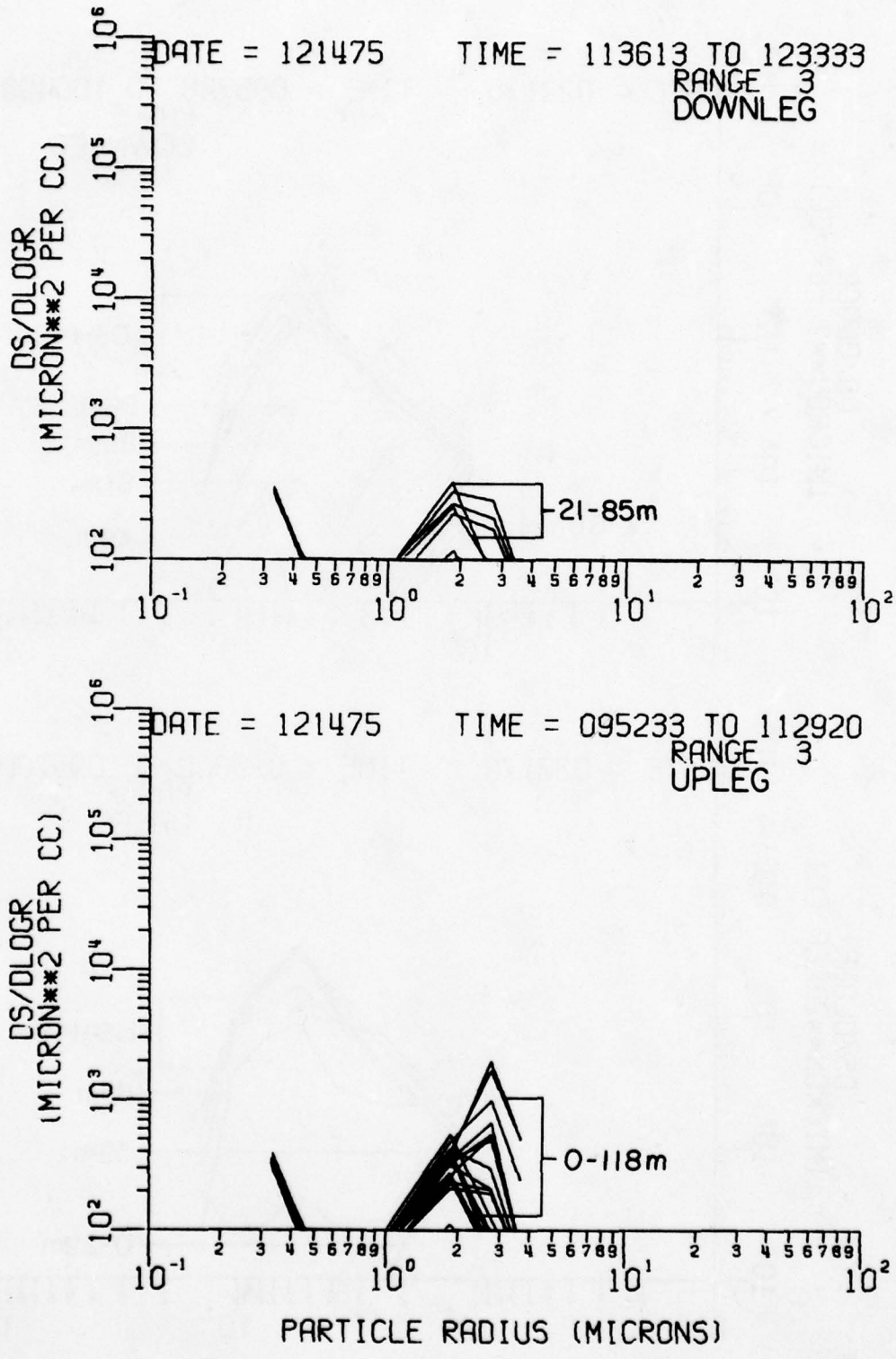

Figure A2-a. Same as Fig. A1 except for particle area (cross-sectional) distribution.

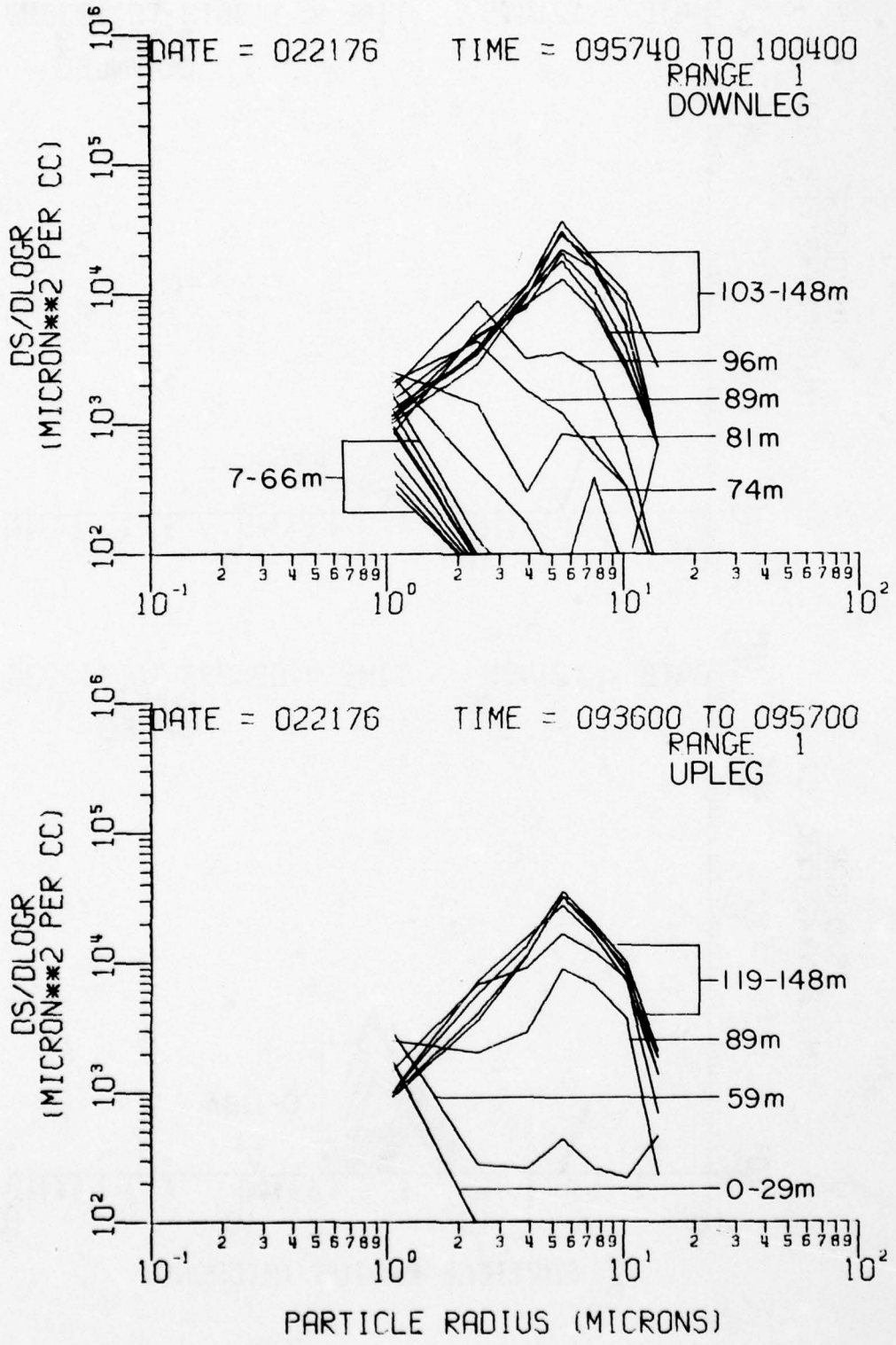
DATE = 022176
TIME = 095740 TO 100400
RANGE 1
DOWNLEG
DS/DLOGR
(MICRON**2 PER CC)
103-148m
96m
89m
81m
7-66m
74m
DATE = 022176
TIME = 093600 TO 095700
RANGE 1
UPLEG
119-148m
89m
59m
0-29m
PARTICLE RADIUS (MICRONS)

Figure A2-b

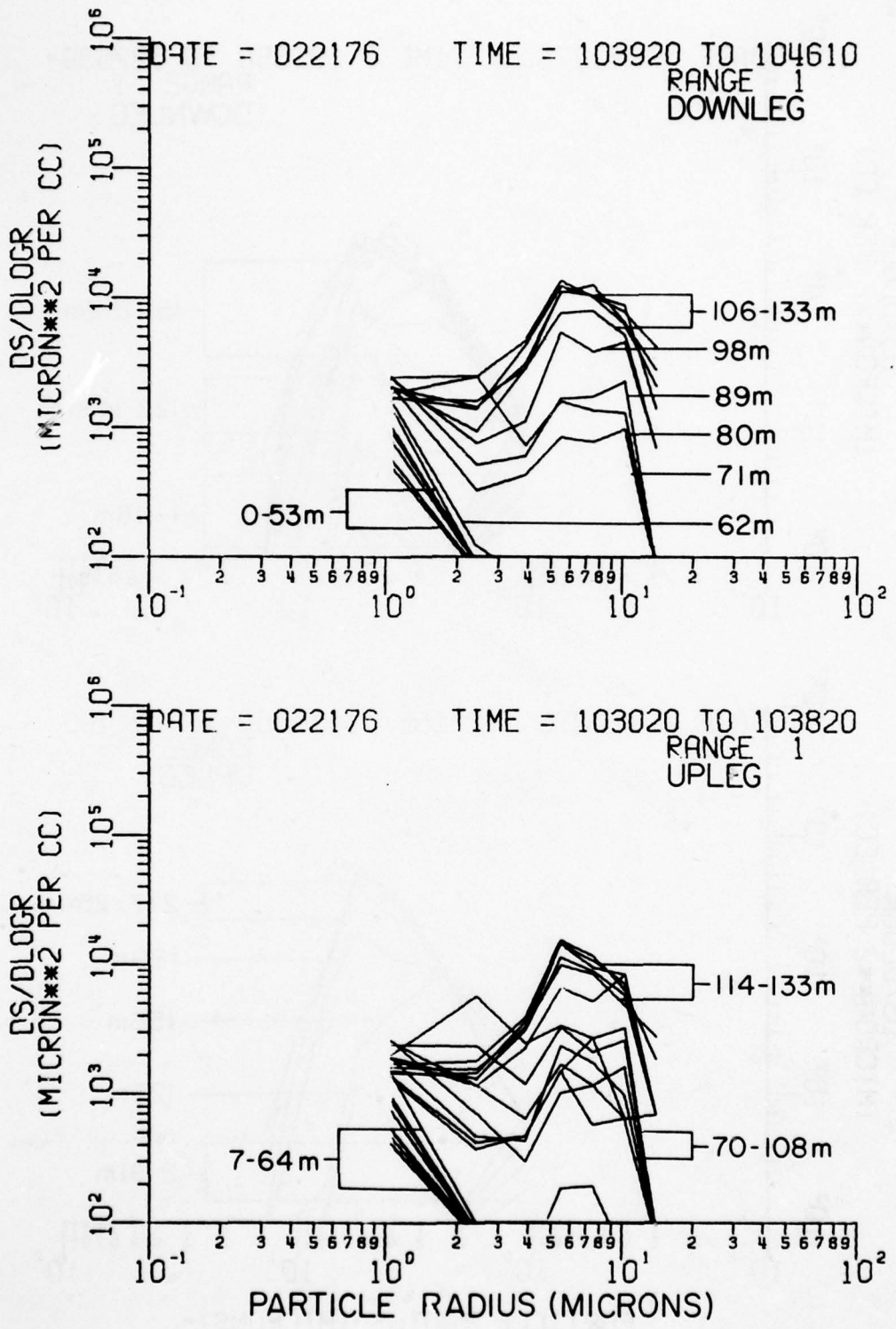
DATE = 022176
TIME = 103920 TO 104610
RANGE 1
DOWNLEG
DS/DLOGR
(MICRON**2 PER CC)
106-133m
98m
89m
80m
71m
62m
0-53m
DATE = 022176
TIME = 103020 TO 103820
RANGE 1
UPLEG
114-133m
70-108m
7-64m
PARTICLE RADIUS (MICRONS)

Figure A2-c

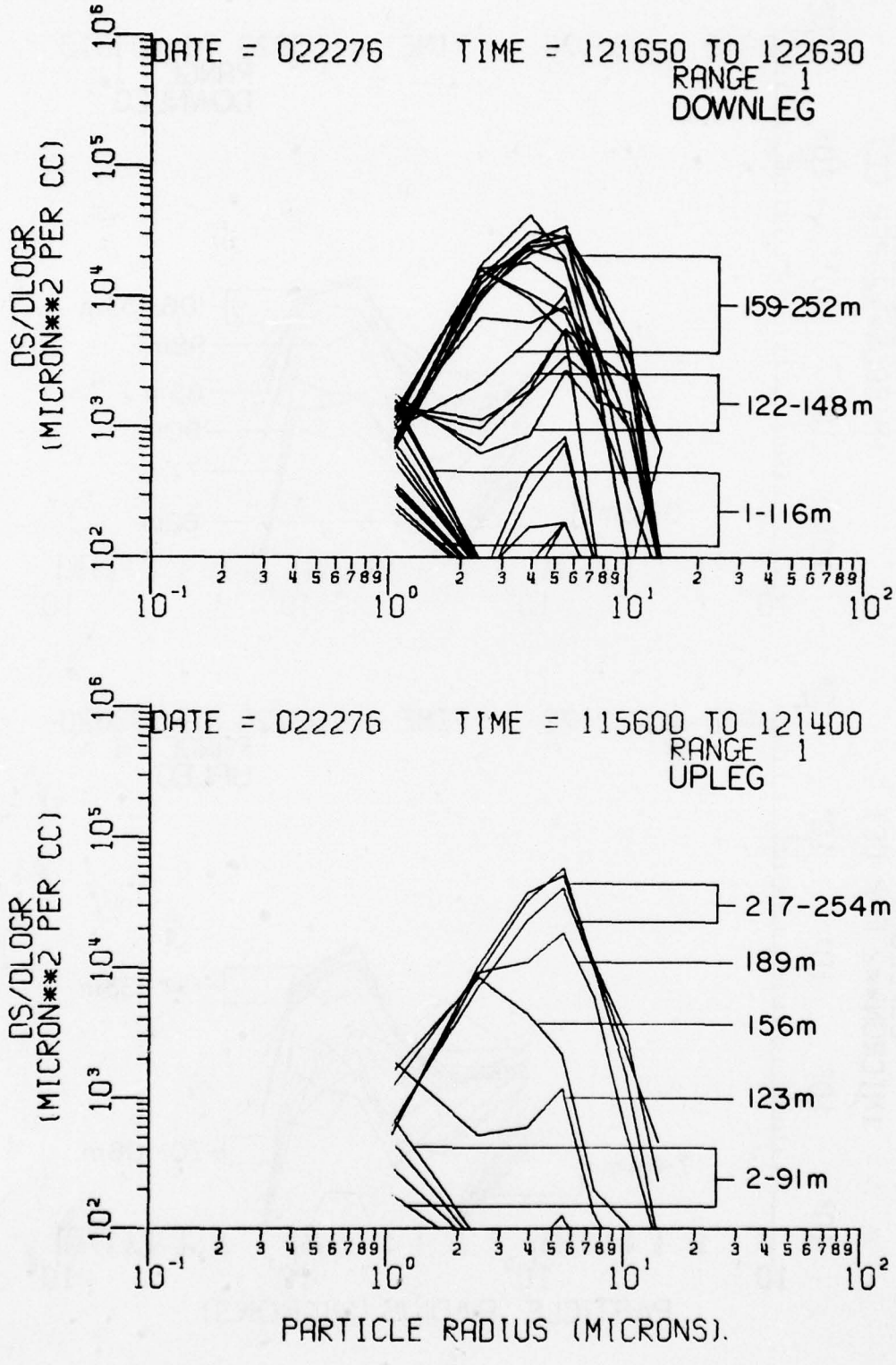
DATE = 022276
TIME = 121650 TO 122630
RANGE 1
DOWNLEG
159-252m
122-148m
1-116m
DS/DLOGR
(MICRON**2 PER CC)
DATE = 022276
TIME = 115600 TO 121400
RANGE 1
UPLEG
217-254m
189m
156m
123m
2-91m
PARTICLE RADIUS (MICRONS).

Figure A2-d

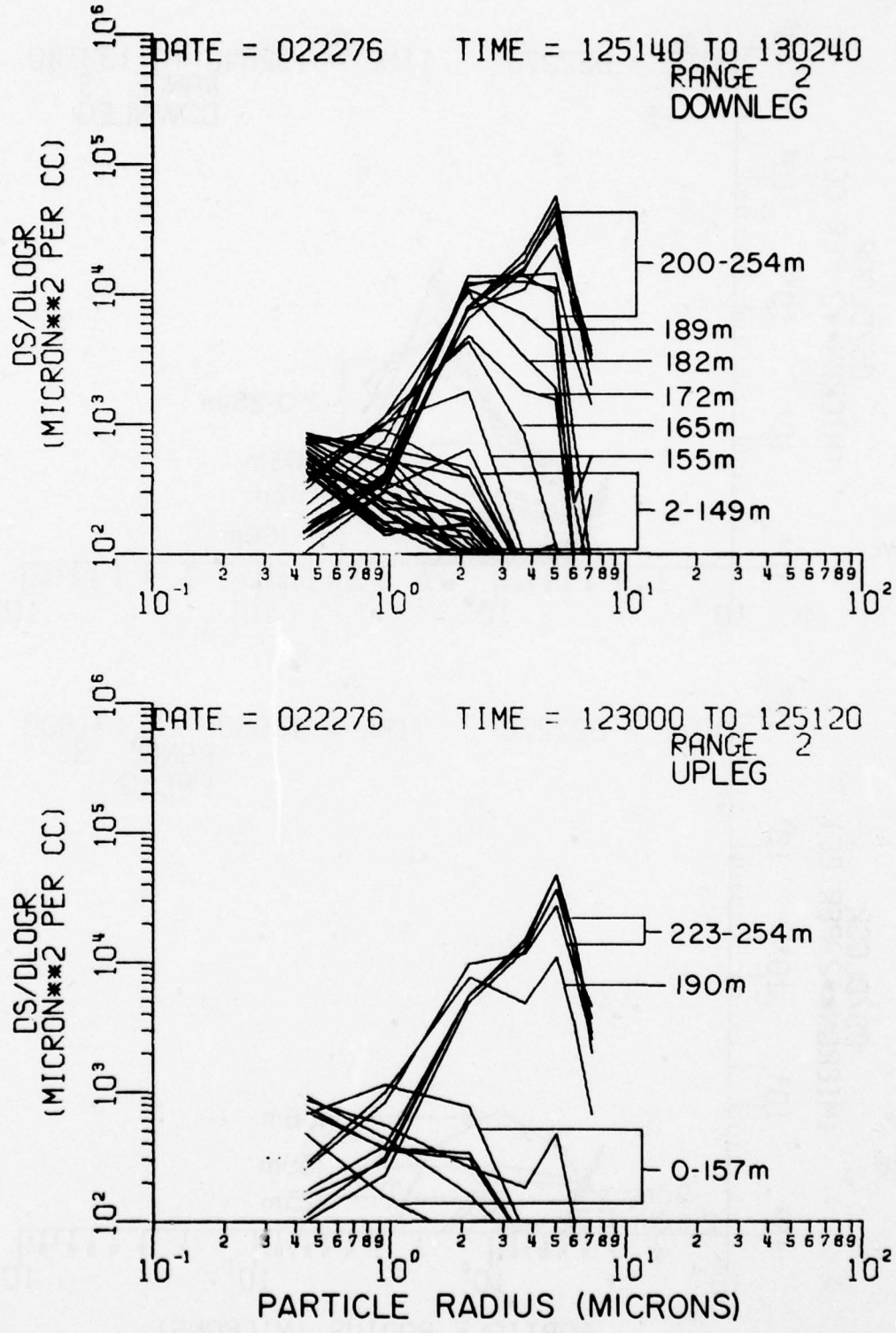
DATE = 022276
TIME = 125140 TO 130240
RANGE 2
DOWNLEG
200-254m
189m
182m
172m
165m
155m
2-149m
DS/DLOGR
(MICRON**2 PER CC)
DATE = 022276
TIME = 123000 TO 125120
RANGE 2
UPLEG
223-254m
190m
0-157m
PARTICLE RADIUS (MICRONS)

Figure A2-e

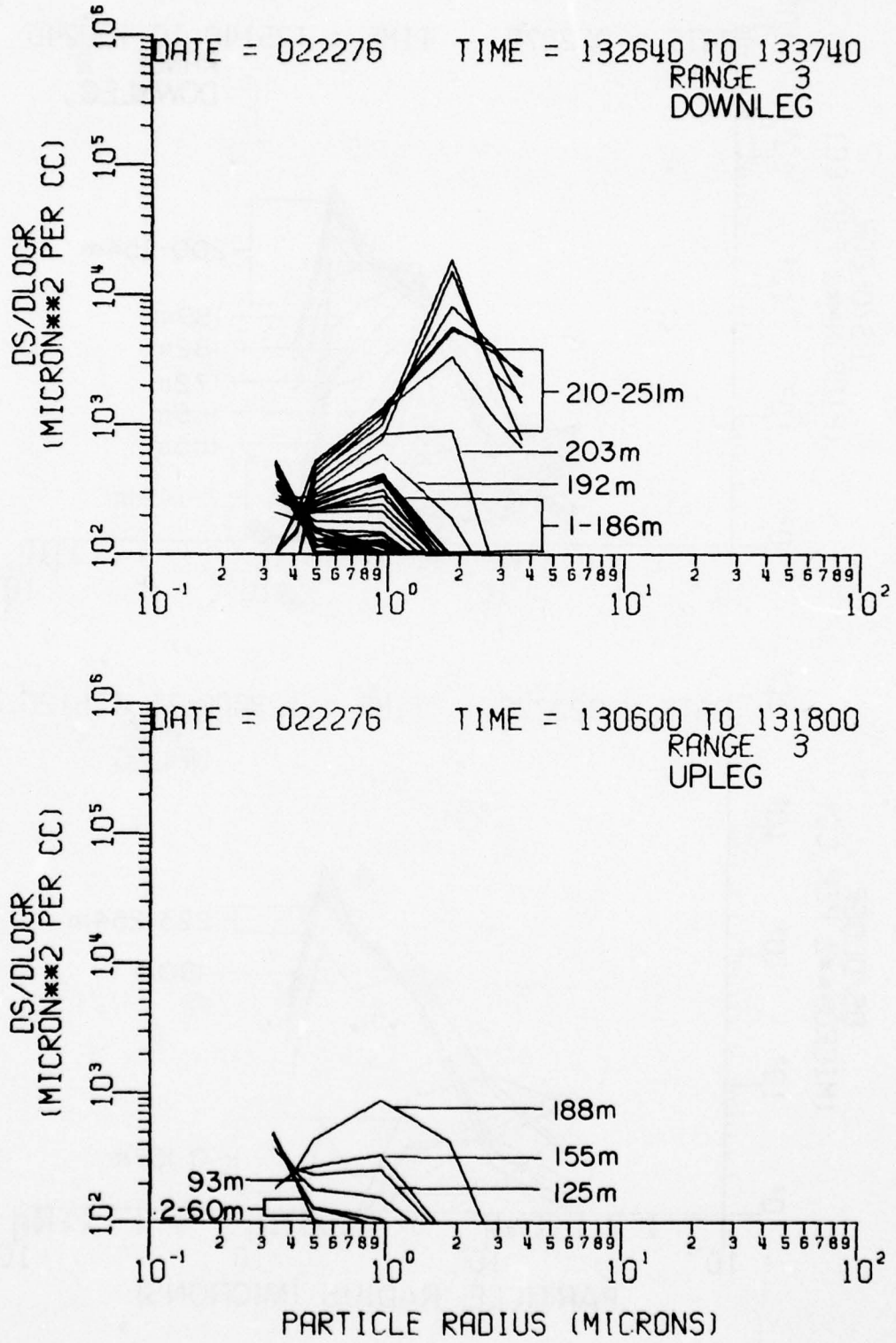
DATE = 022276 TIME = 132640 TO 133740
RANGE 3
DOWNLEG
DS/DLOGR
(MICRON**2 PER CC)
210-251m
203m
192m
1-186m
DATE = 022276 TIME = 130600 TO 131800
RANGE 3
UPLEG
188m
155m
125m
93m
2-60m
PARTICLE RADIUS (MICRONS)

Figure A2-f

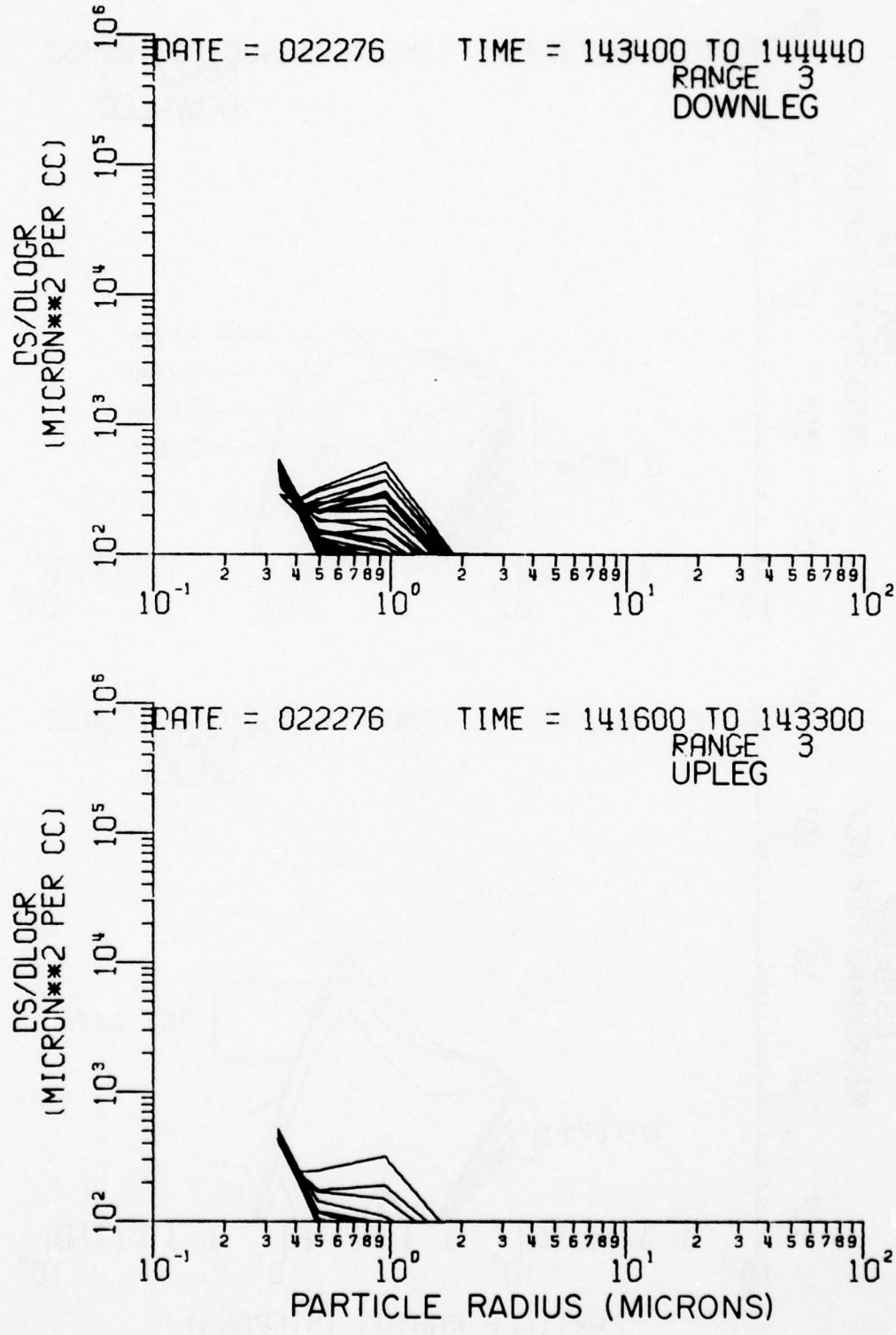
DATE = 022276
TIME = 143400 TO 144440
RANGE 3
DOWNLEG
DS/DLOGR
(MICRON**2 PER CC)
DATE = 022276
TIME = 141600 TO 143300
RANGE 3
UPLEG
DS/DLOGR
(MICRON**2 PER CC)
PARTICLE RADIUS (MICRONS)

Figure A2-g

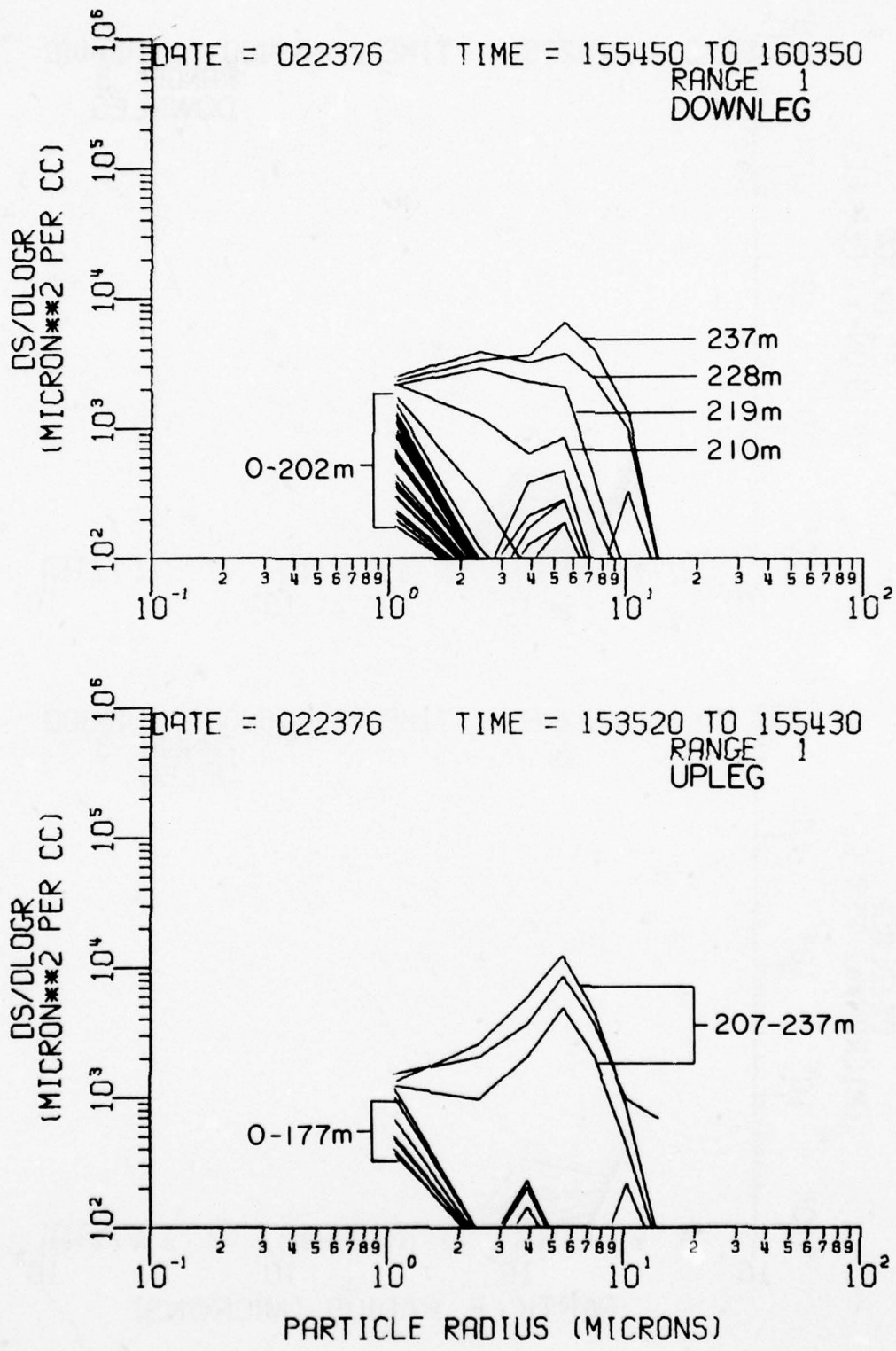
DATE = 022376
TIME = 155450 TO 160350
RANGE 1
DOWNLEG
237m
228m
219m
210m
0-202m
DATE = 022376
TIME = 153520 TO 155430
RANGE 1
UPLEG
207-237m
0-177m
DS/DLOGR
(MICRON**2 PER CC)
PARTICLE RADIUS (MICRONS)

Figure A2-h

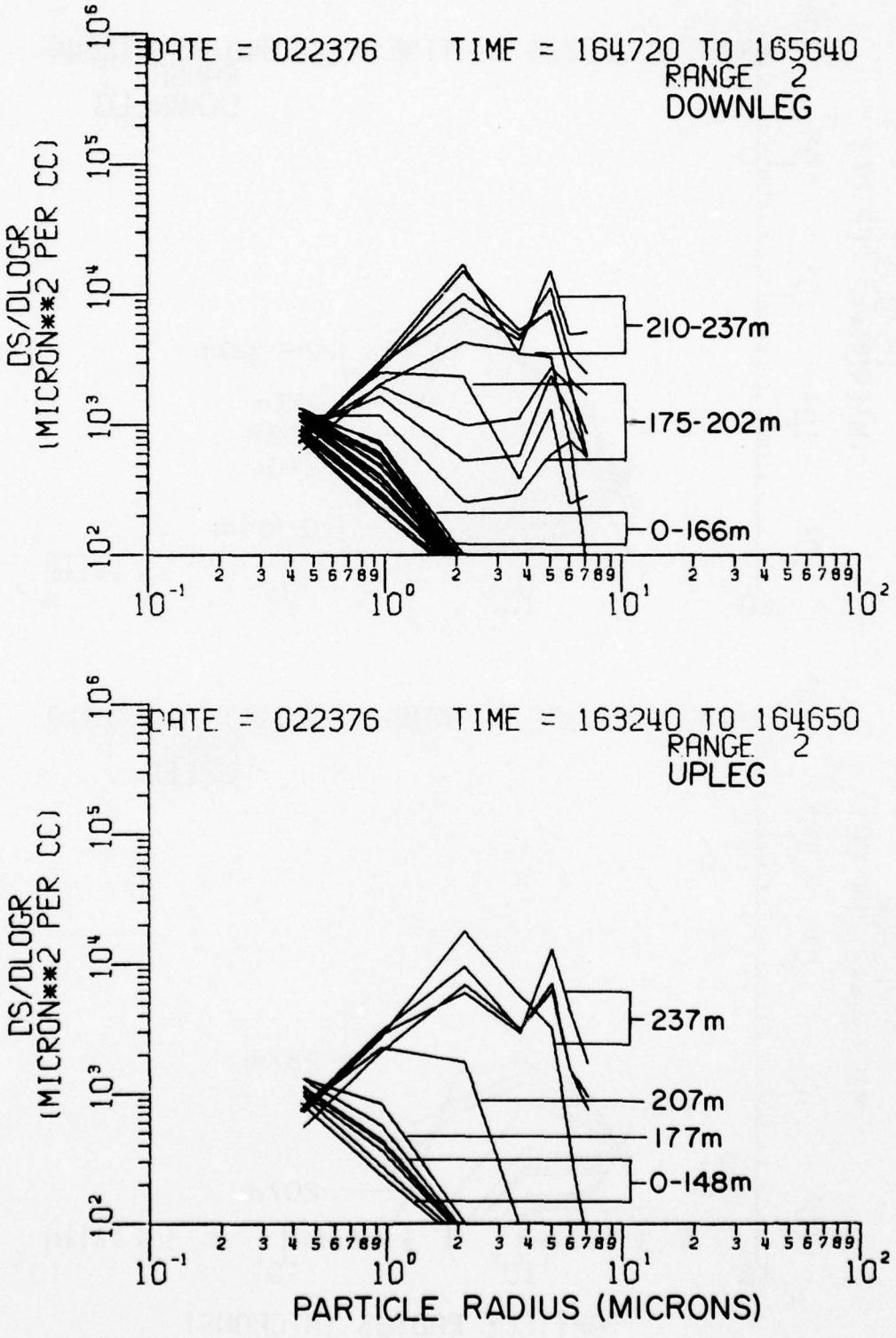
DATE = 022376
TIME = 164720 TO 165640
RANGE 2
DOWNLEG
DS/DLOGR
(MICRON**2 PER CC)
210-237m
175-202m
0-166m
DATE = 022376
TIME = 163240 TO 164650
RANGE 2
UPLEG
237m
207m
177m
0-148m
PARTICLE RADIUS (MICRONS)

Figure A2-i

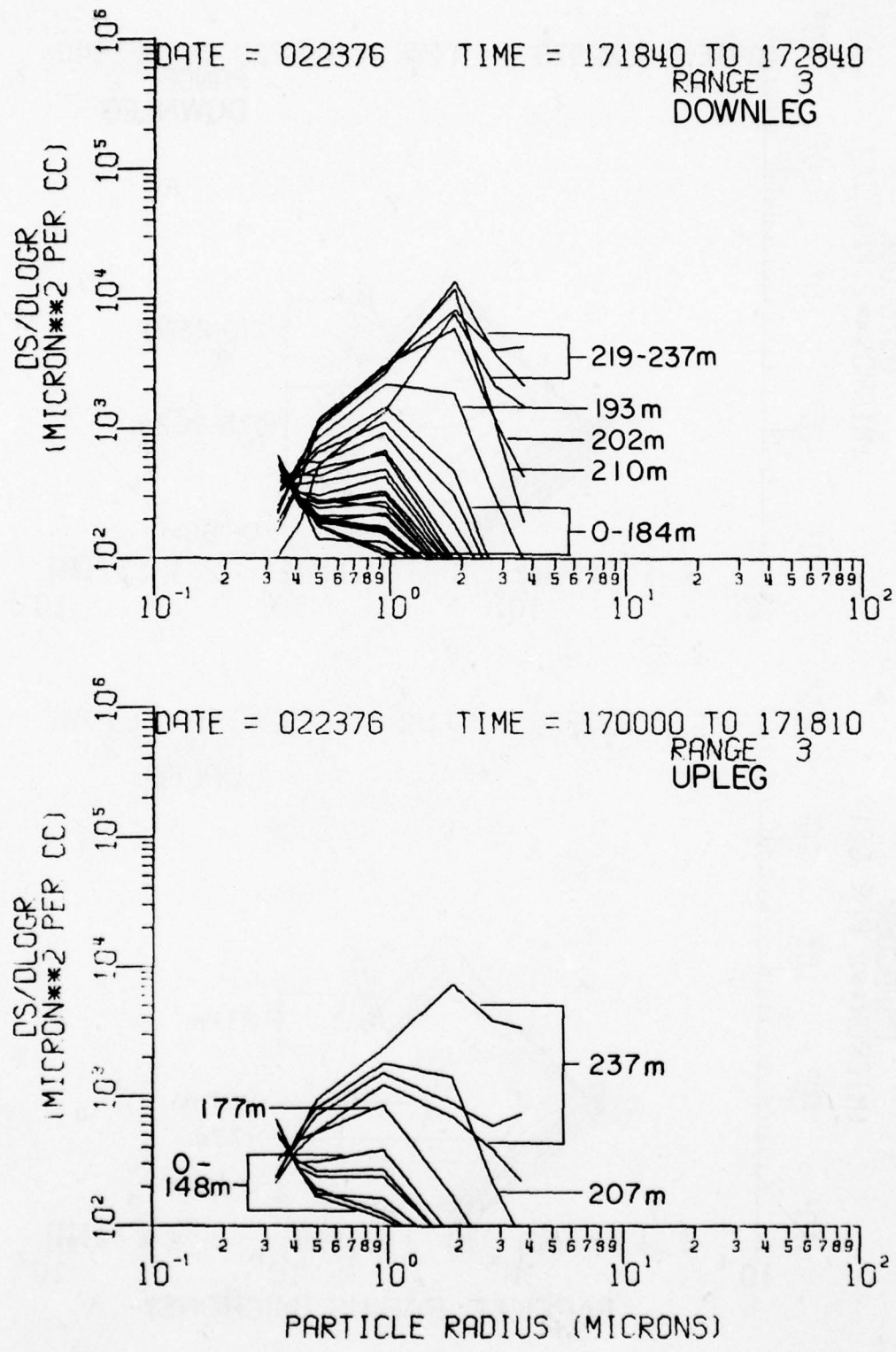
DATE = 022376 TIME = 171840 TO 172840
RANGE 3
DOWNLEG
DS/DLOGR
(MICRON**2 PER CC)
219-237m
193m
202m
210m
0-184m
DATE = 022376 TIME = 170000 TO 171810
RANGE 3
UPLEG
237m
177m
0-
148m
207m
PARTICLE RADIUS (MICRONS)

Figure A2-j

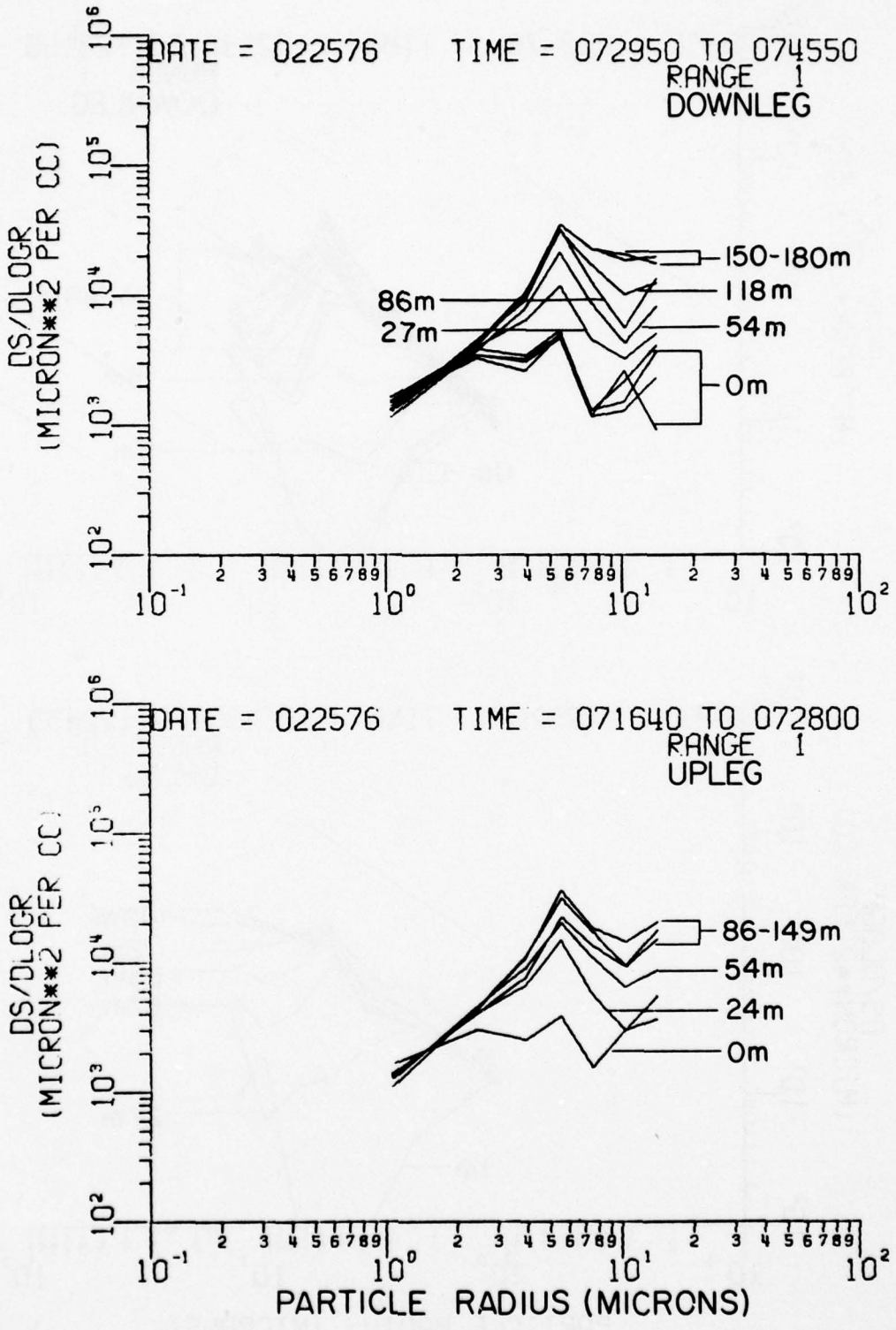
DATE = 022576
TIME = 072950 TO 074550
RANGE 1
DOWNLEG
DS/DLOGR
(MICRON**2 PER CC)
150-180m
118m
86m
54m
27m
0m
DATE = 022576
TIME = 071640 TO 072800
RANGE 1
UPLEG
86-149m
54m
24m
0m
PARTICLE RADIUS (MICRONS)

Figure A2-k

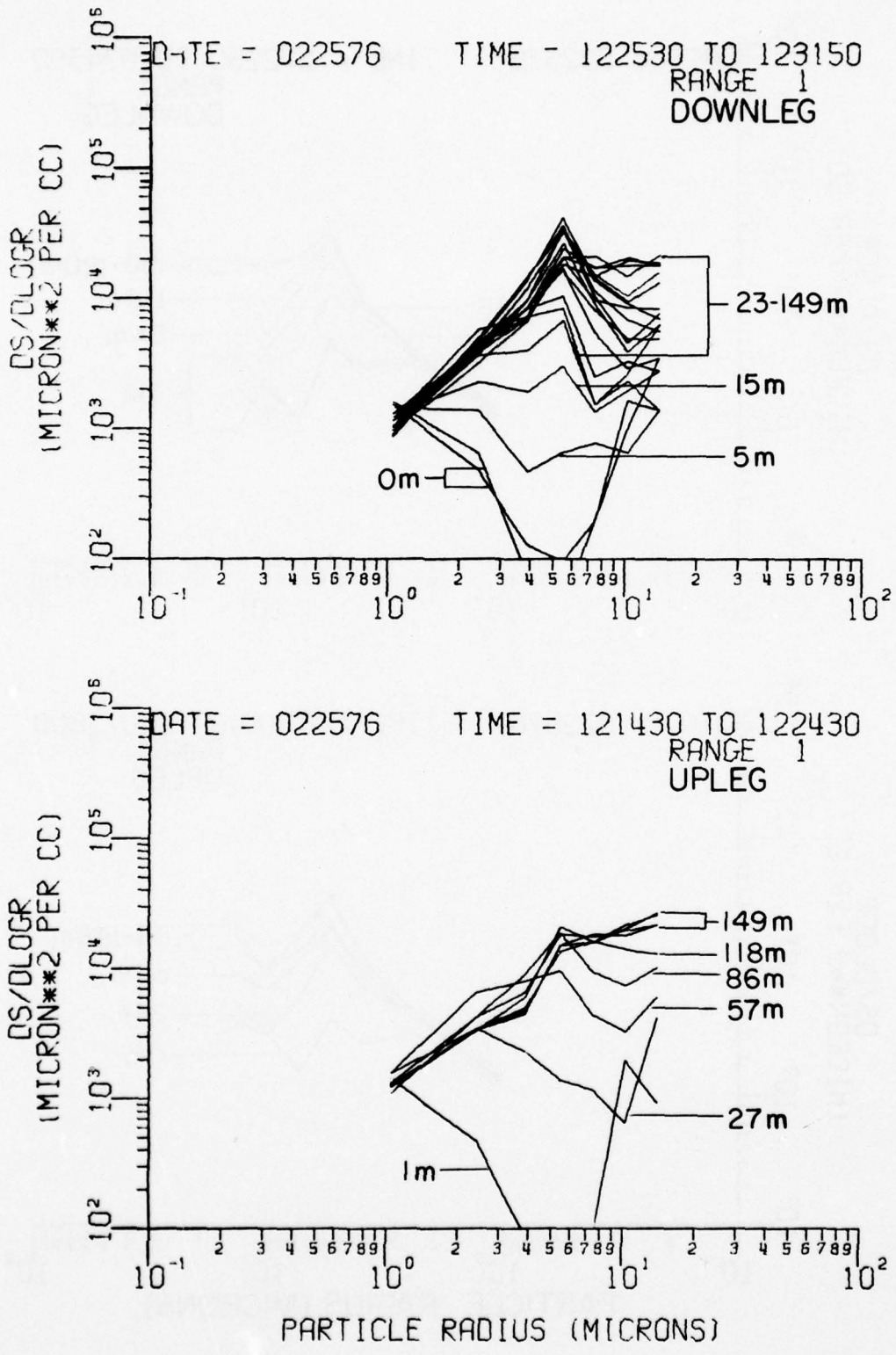
DATE = 022576 TIME = 122530 TO 123150
RANGE 1
DOWNLEG
DS/DLOGR
(MICRON**2 PER CC)
23-149m
15m
5m
0m
DATE = 022576 TIME = 121430 TO 122430
RANGE 1
UPLEG
149m
118m
86m
57m
27m
1m
PARTICLE RADIUS (MICRONS)

Figure A2-1

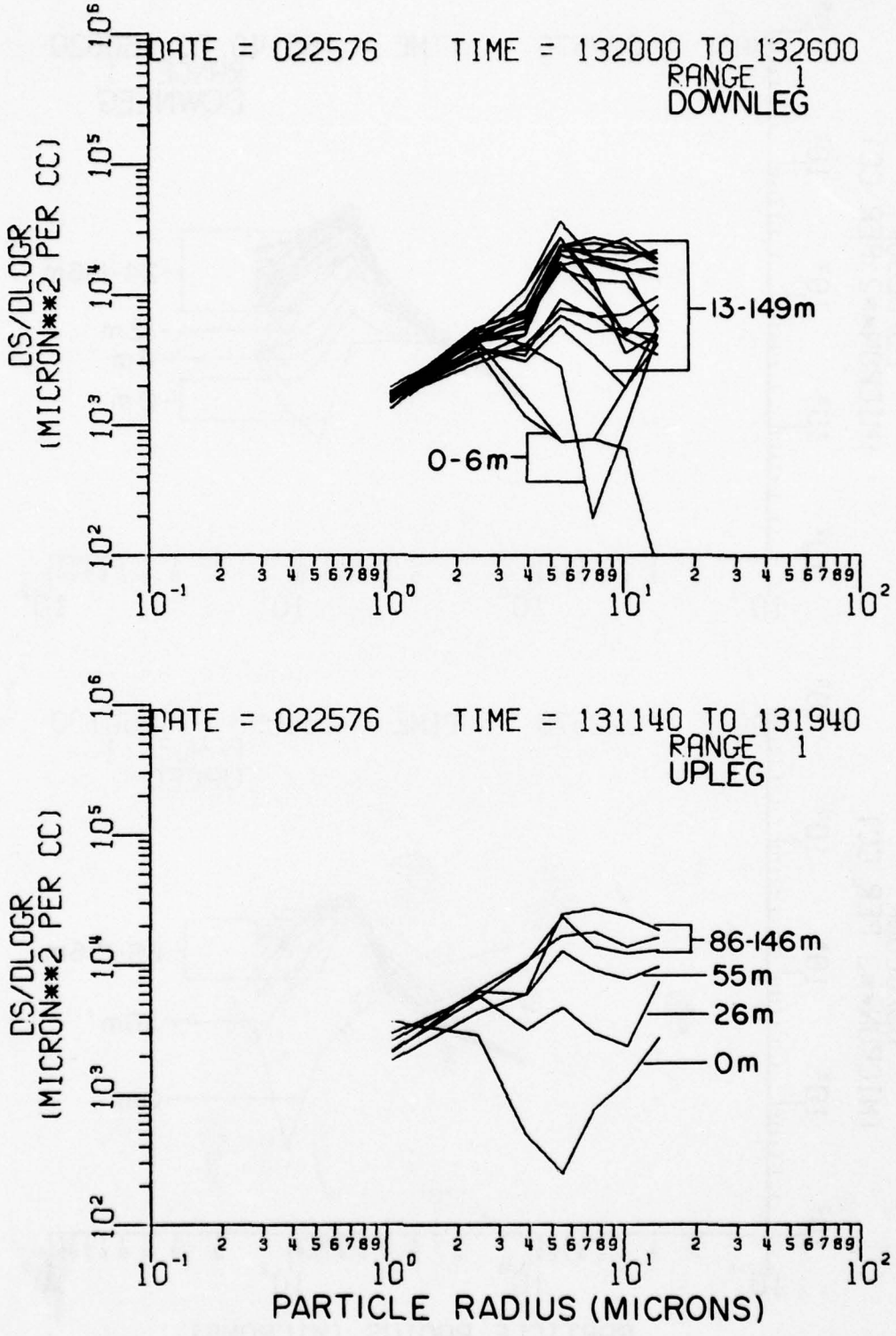
DATE = 022576
TIME = 132000 TO 132600
RANGE 1
DOWNLEG
DS/DLOGR
(MICRON**2 PER CC)
13-149m
0-6m
DATE = 022576
TIME = 131140 TO 131940
RANGE 1
UPLEG
86-146m
55m
26m
0m
PARTICLE RADIUS (MICRONS)

Figure A2-m

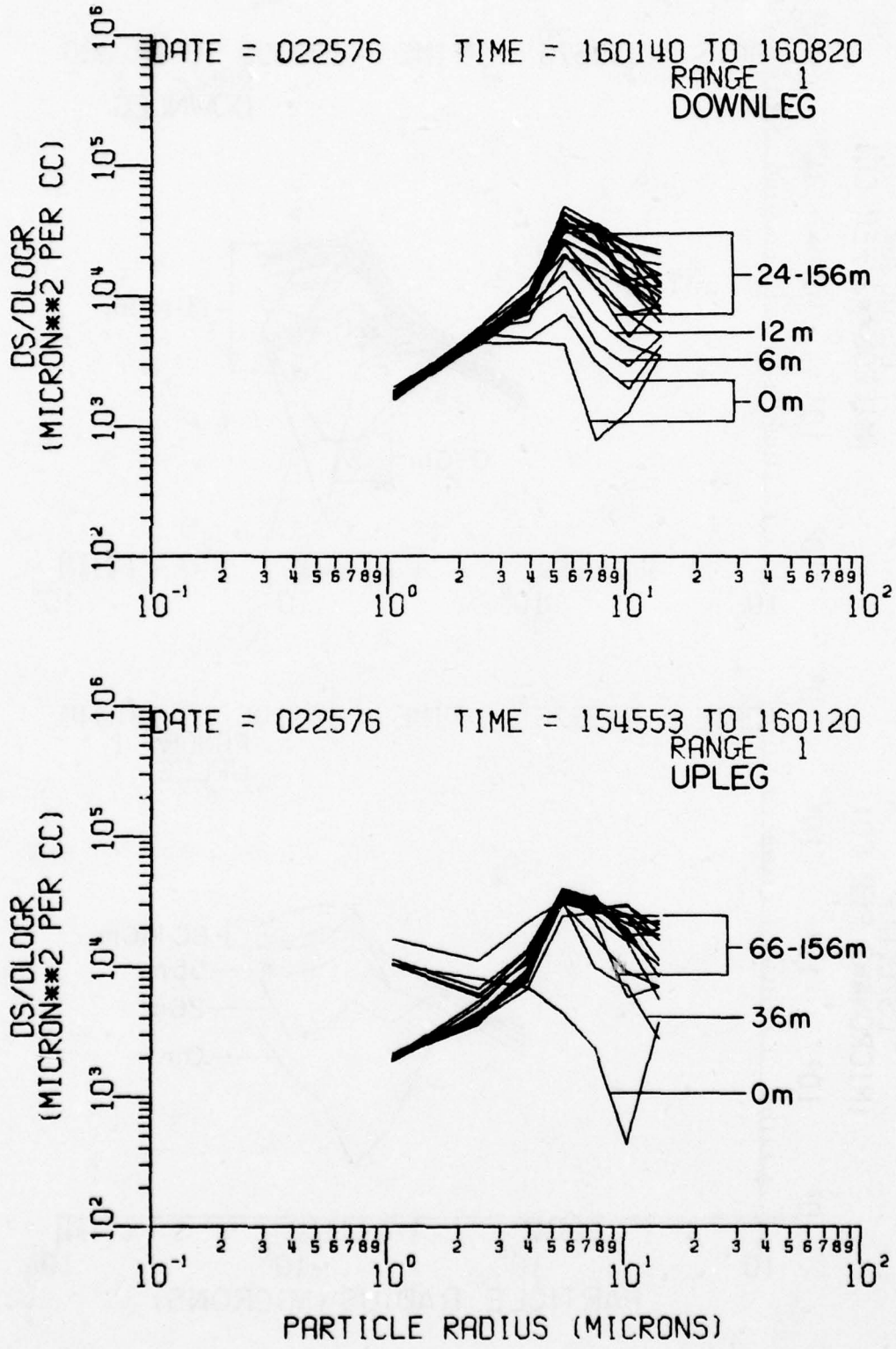
DATE = 022576
TIME = 160140 TO 160820
RANGE 1
DOWNLEG
24-156m
12 m
6m
0m
DS/DLOGR
(MICRON**2 PER CC)
DATE = 022576
TIME = 154553 TO 160120
RANGE 1
UPLEG
66-156m
36m
0m
PARTICLE RADIUS (MICRONS)

Figure A2-n

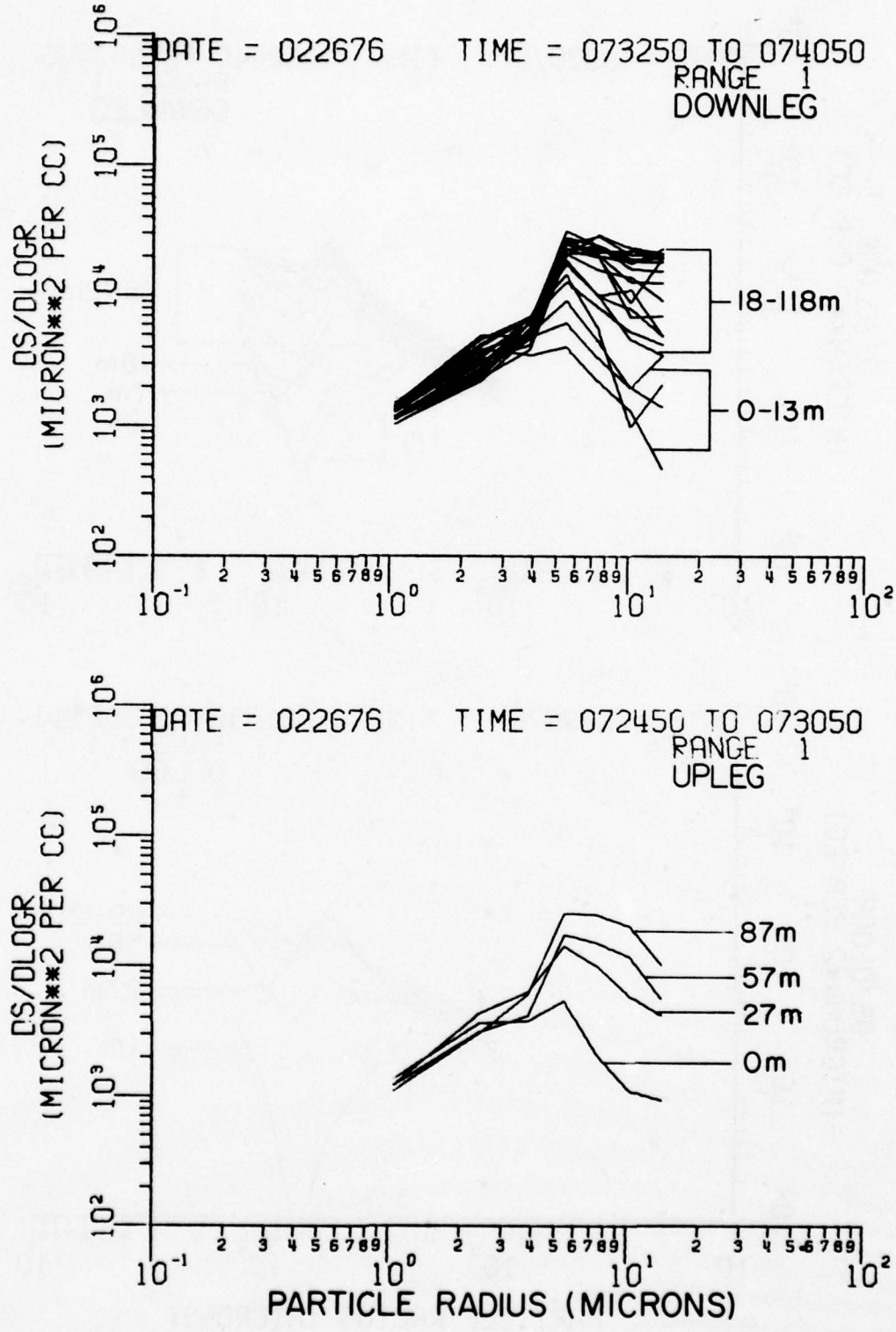
DATE = 022676
TIME = 073250 TO 074050
RANGE 1
DOWNLEG
18-118m
0-13m
DS/DLOGR
(MICRON**2 PER CC)
DATE = 022676
TIME = 072450 TO 073050
RANGE 1
UPLEG
87m
57m
27m
0m
PARTICLE RADIUS (MICRONS)

Figure A2-o

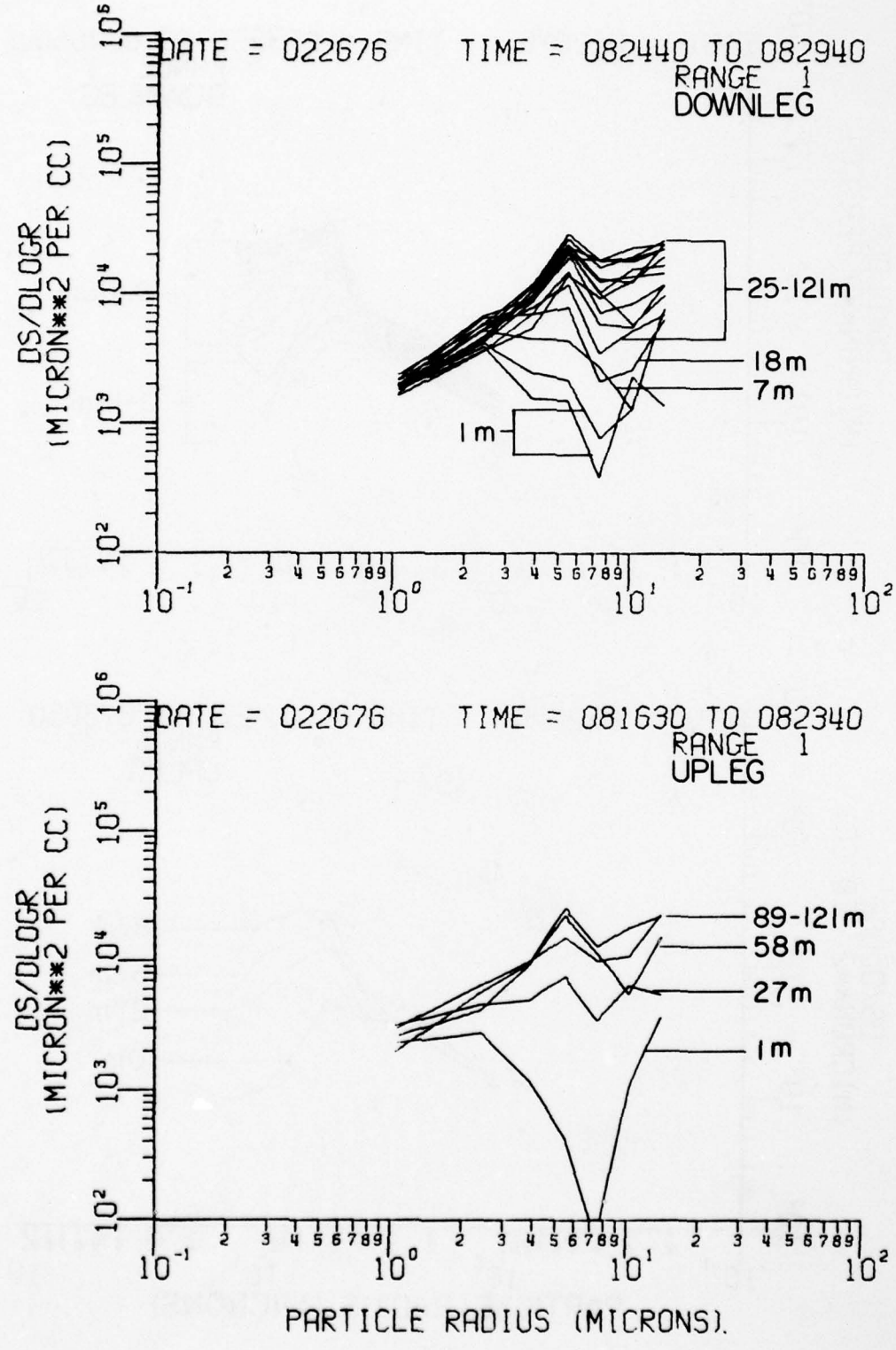
DATE = 022676
TIME = 082440 TO 082940
RANGE 1
DOWNLEG
DS/DLOGR
(MICRON**2 PER CC)
25-121m
18m
7m
1m
DATE = 022676
TIME = 081630 TO 082340
RANGE 1
UPLEG
89-121m
58m
27m
1m
PARTICLE RADIUS (MICRONS)

Figure A2-p

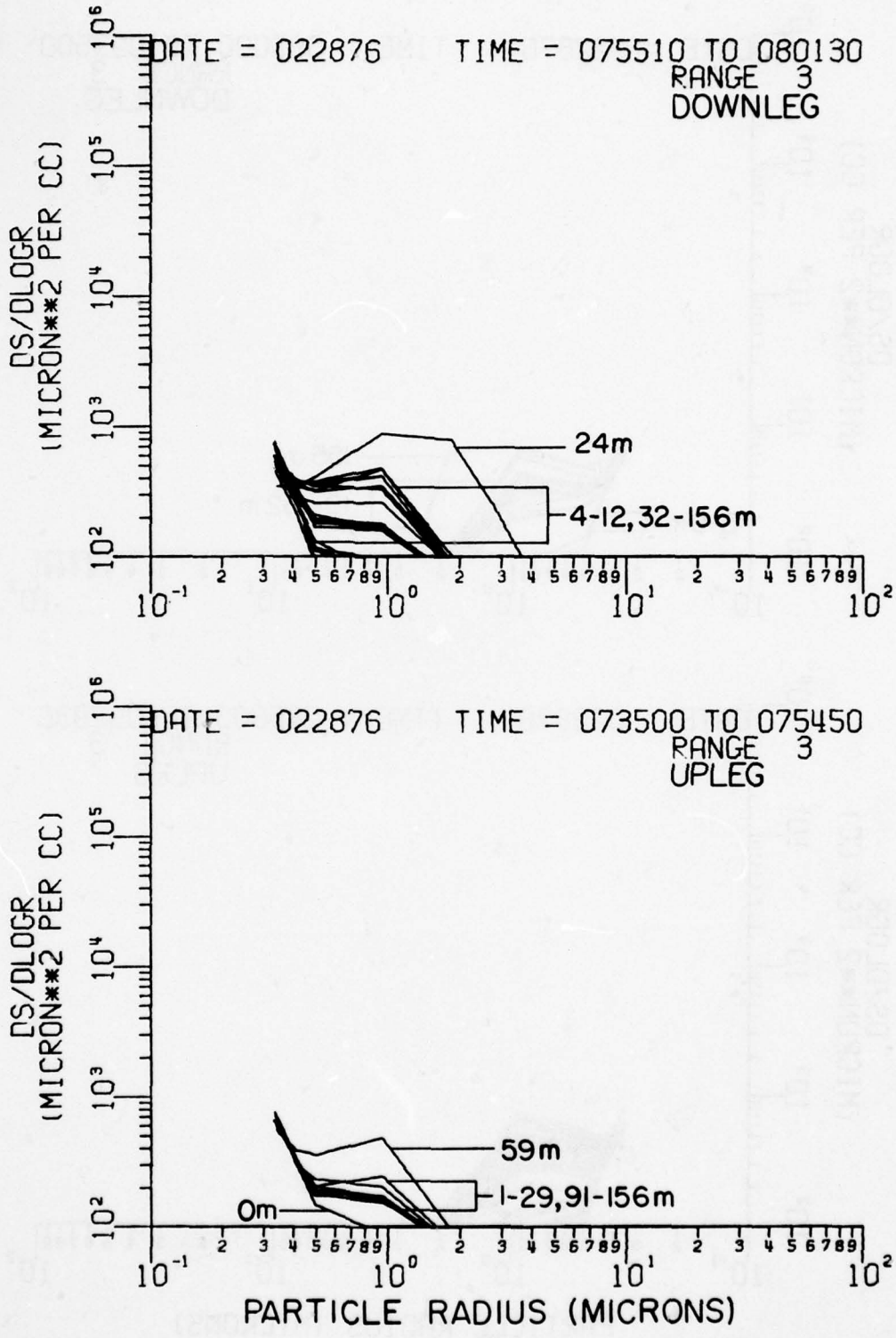
DATE = 022876
TIME = 075510 TO 080130
RANGE 3
DOWNLEG
DS/DLOGR
(MICRON**2 PER CC)
24m
4-12,32-156m
DATE = 022876
TIME = 073500 TO 075450
RANGE 3
UPLEG
59m
1-29,91-156m
0m
PARTICLE RADIUS (MICRONS)

Figure A2-q

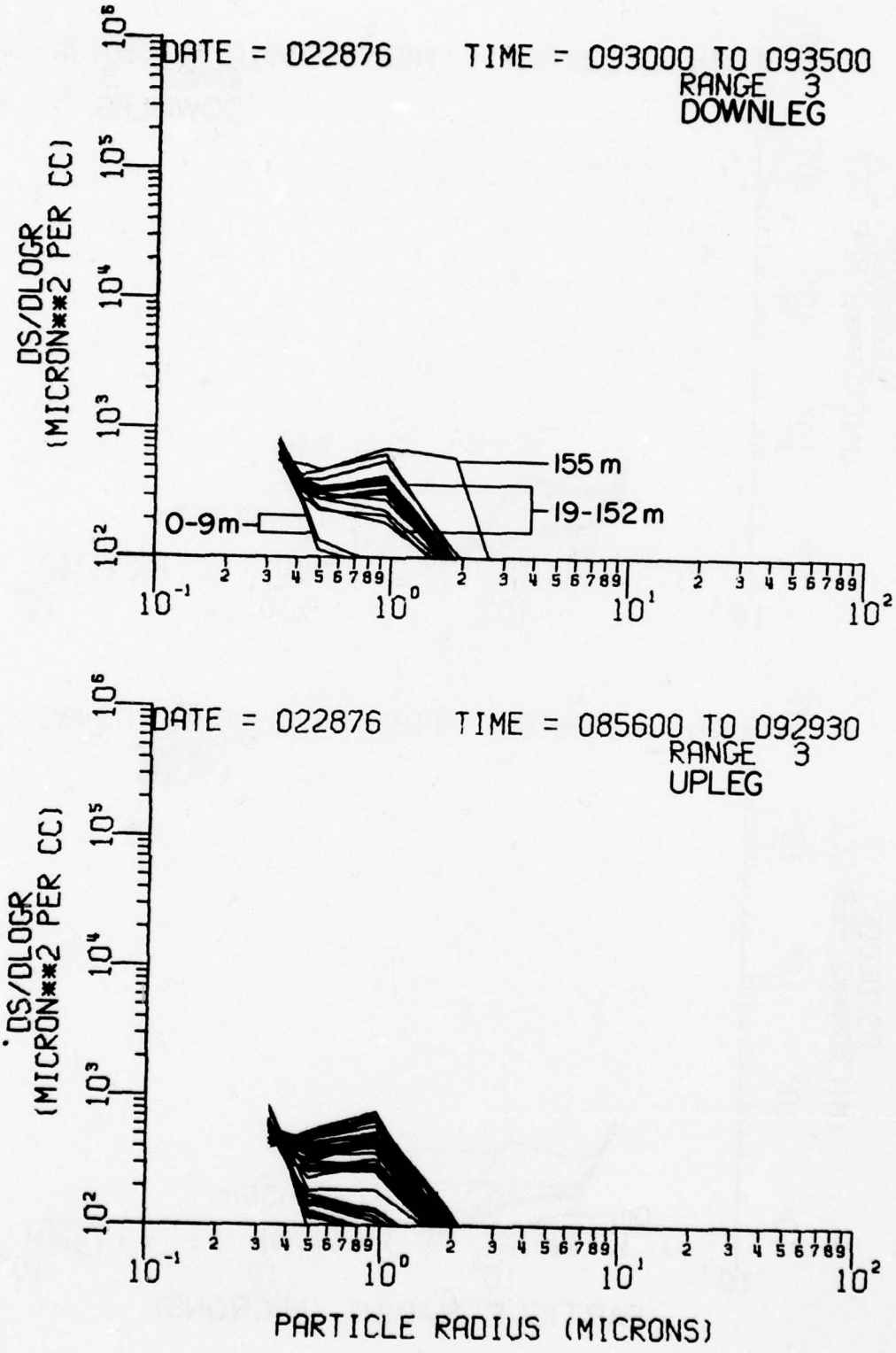
DATE = 022876
TIME = 093000 TO 093500
RANGE 3
DOWNLEG
DS/DLOGR
(MICRON**2 PER CC)
155 m
19-152 m
0-9m
DATE = 022876
TIME = 085600 TO 092930
RANGE 3
UPLEG
PARTICLE RADIUS (MICRONS)

Figure A2-r

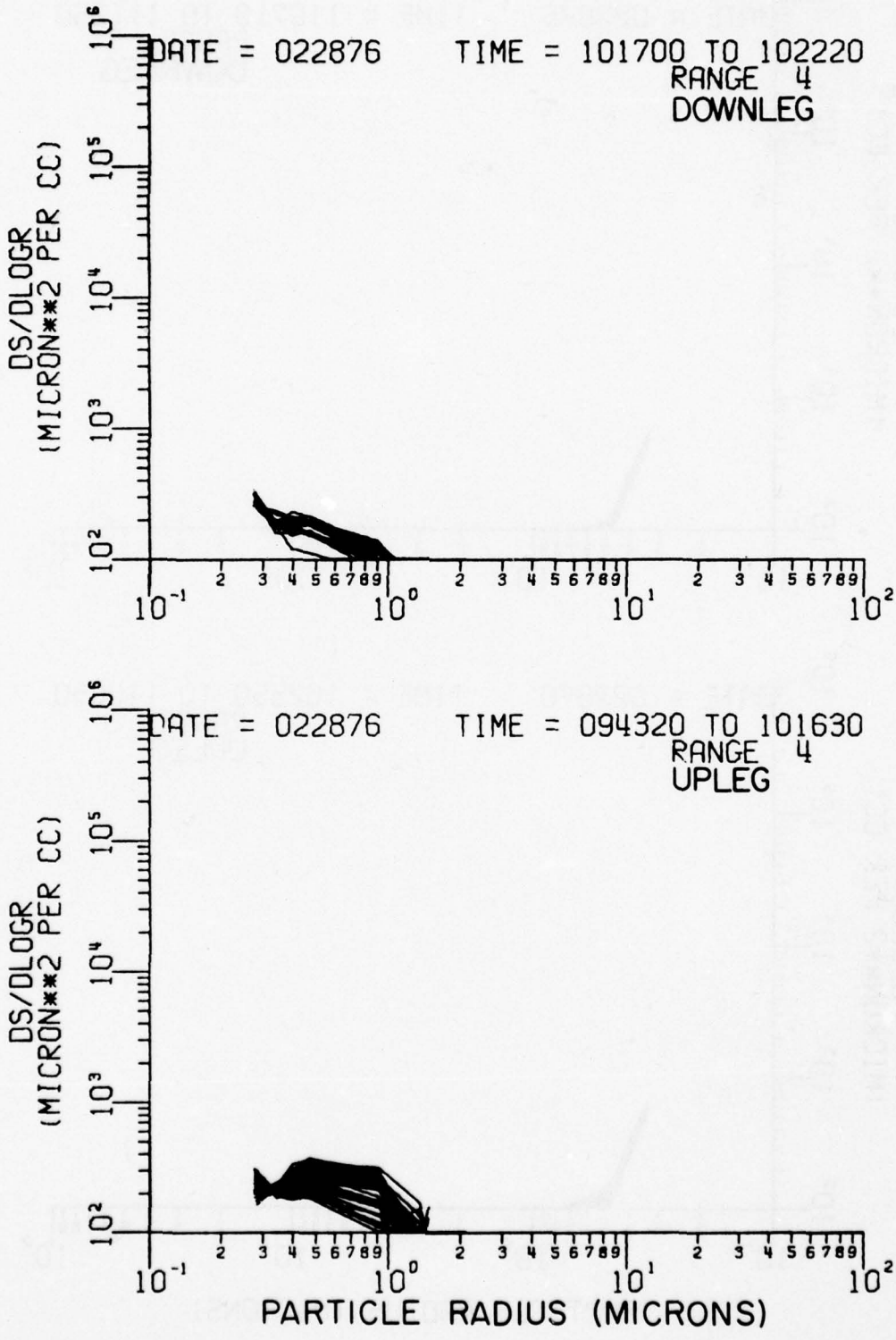
DATE = 022876
TIME = 101700 TO 102220
RANGE 4
DOWNLEG
DS/DLOGR
(MICRON**2 PER CC)
DATE = 022876
TIME = 094320 TO 101630
RANGE 4
UPLEG
DS/DLOGR
(MICRON**2 PER CC)
PARTICLE RADIUS (MICRONS)

Figure A2-s

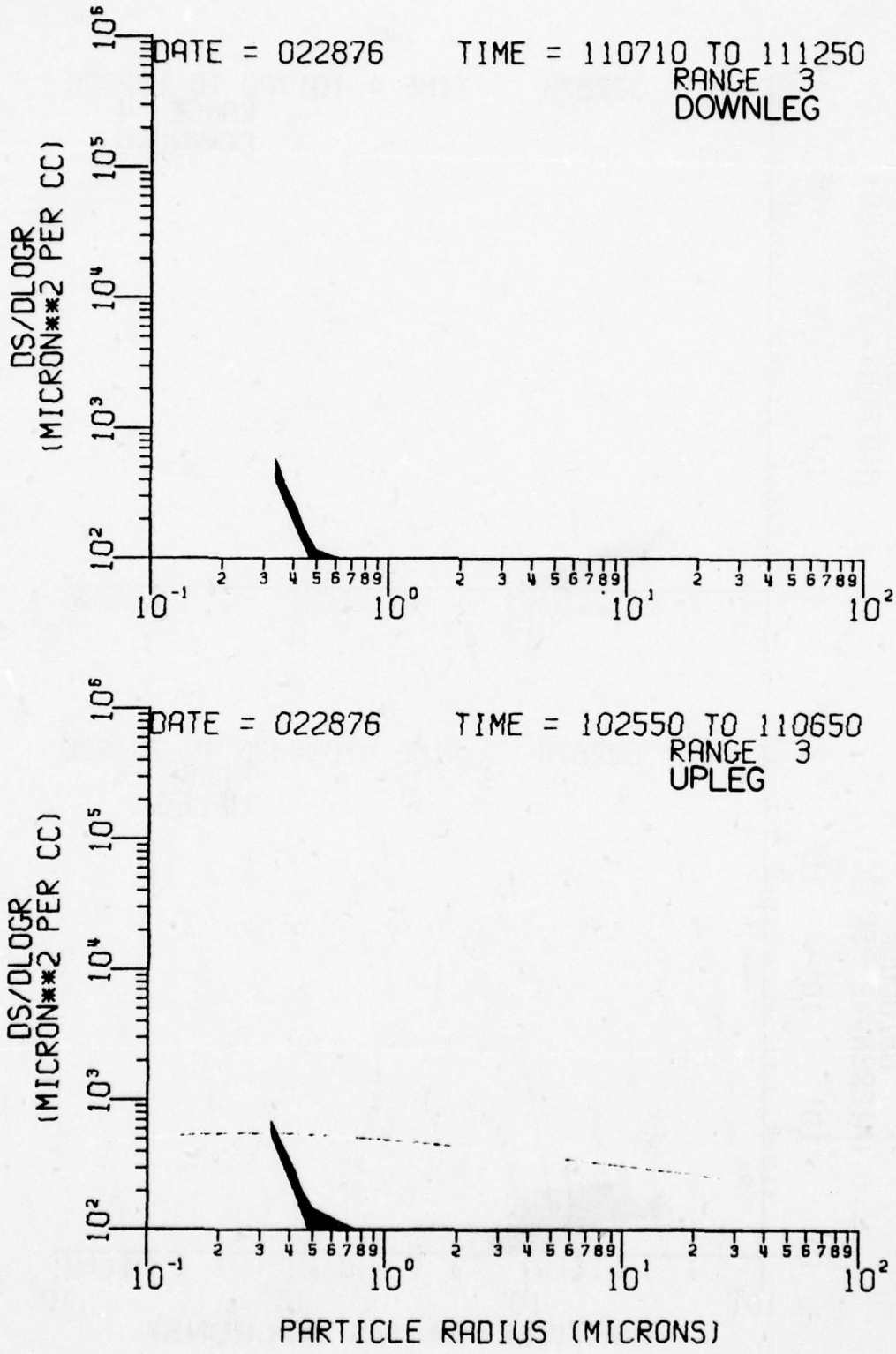
DATE = 022876
TIME = 110710 TO 111250
RANGE 3
DOWNLEG
DS/DLOGR
(MICRON**2 PER CC)
DATE = 022876
TIME = 102550 TO 110650
RANGE 3
UPLEG
DS/DLOGR
(MICRON**2 PER CC)
PARTICLE RADIUS (MICRONS)

Figure A2-t

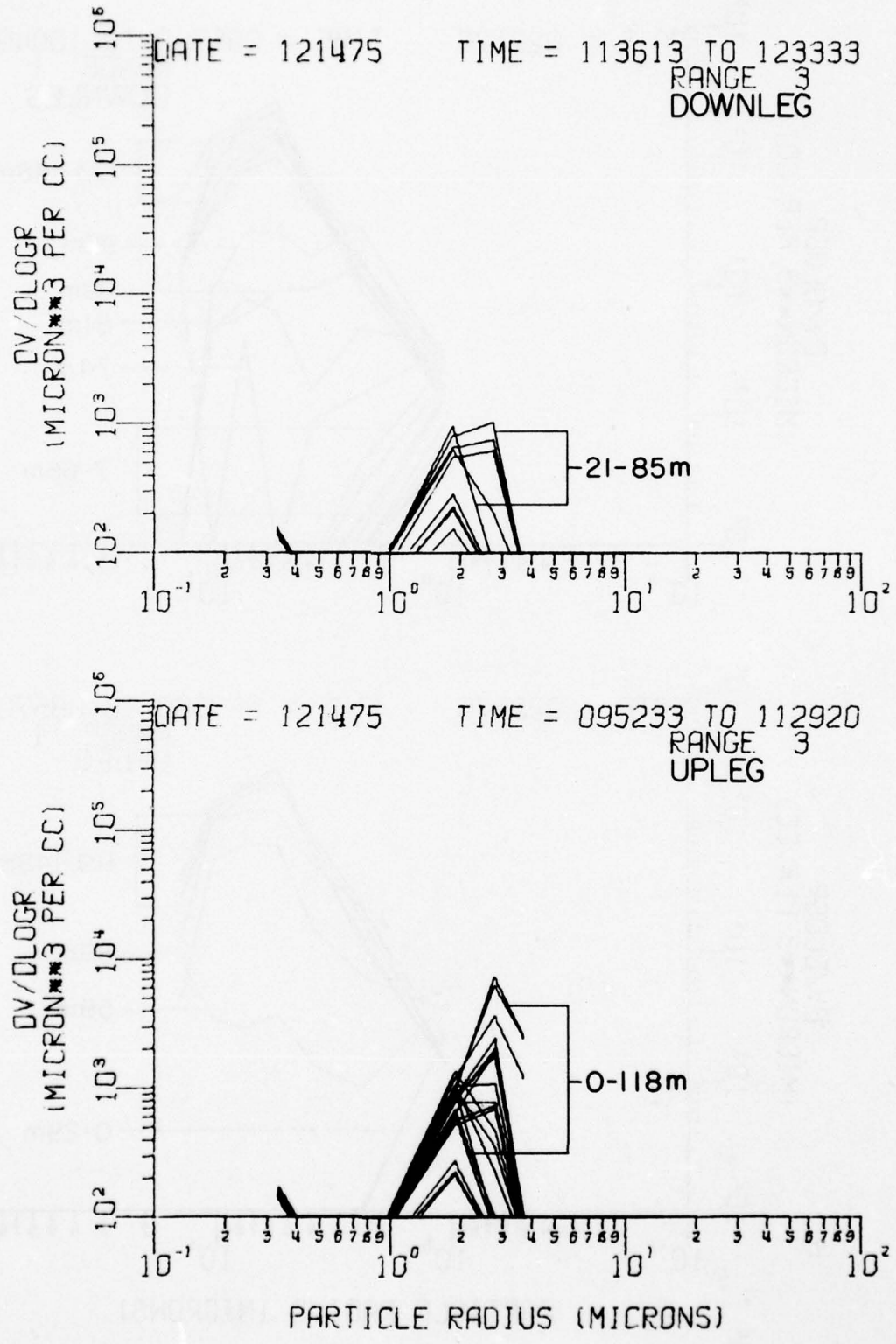

Figure A3-a. Same as Fig. A1 except for particle volume distribution.

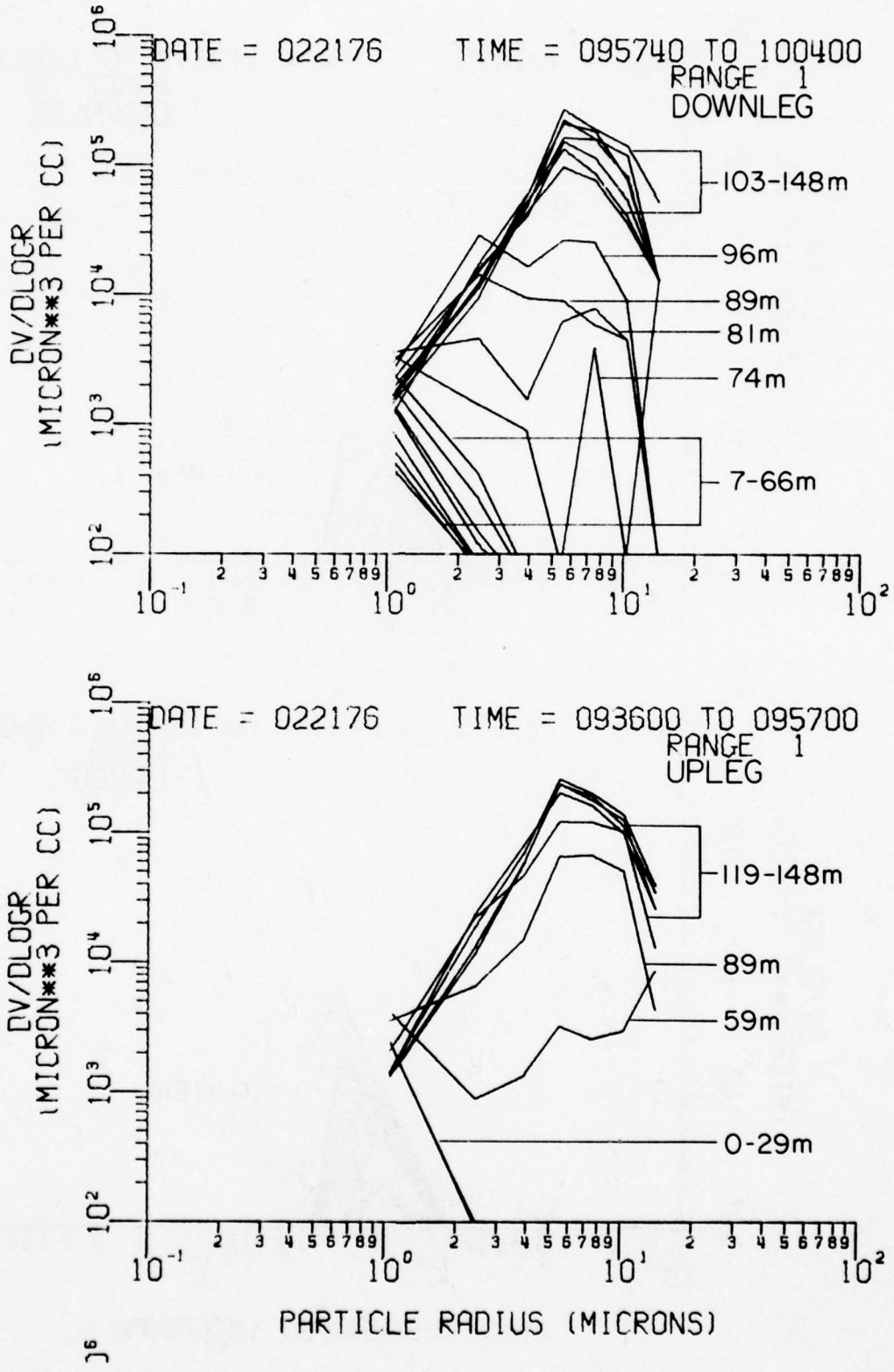
DATE = 022176
TIME = 095740 TO 100400
RANGE 1
DOWNLEG
103-148m
96m
89m
81m
74m
7-66m
DV/DLOGR
(MICRON**3 PER CC)
DATE = 022176
TIME = 093600 TO 095700
RANGE 1
UPLEG
119-148m
89m
59m
0-29m
PARTICLE RADIUS (MICRONS)

Figure A3-b

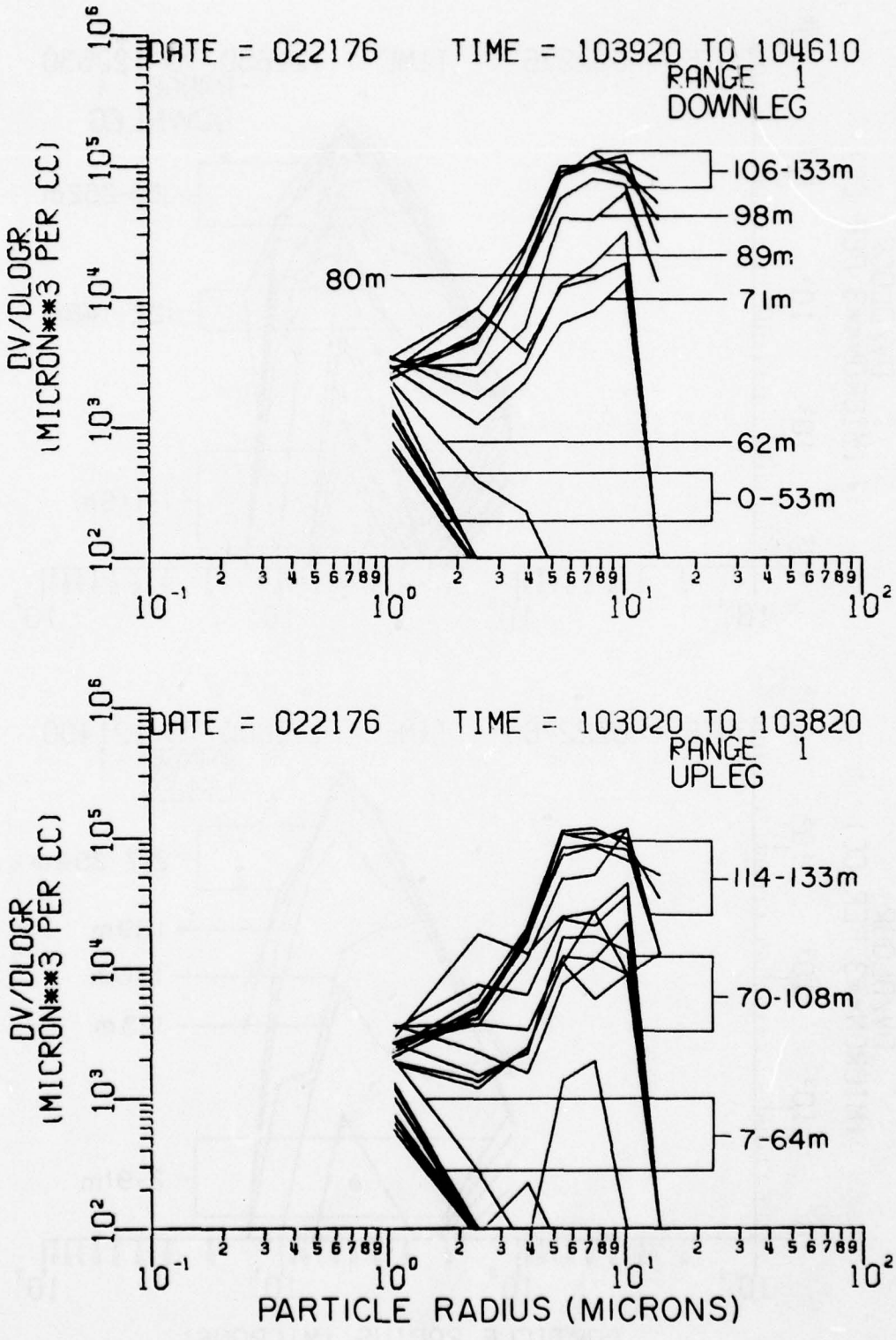
DATE = 022176
TIME = 103920 TO 104610
RANGE 1
DOWNLEG
106-133m
98m
89m
80m
71m
62m
0-53m
DV/DLOGR
(MICRON**3 PER CC)
DATE = 022176
TIME = 103020 TO 103820
RANGE 1
UPLEG
114-133m
70-108m
7-64m
PARTICLE RADIUS (MICRONS)

Figure A3-c

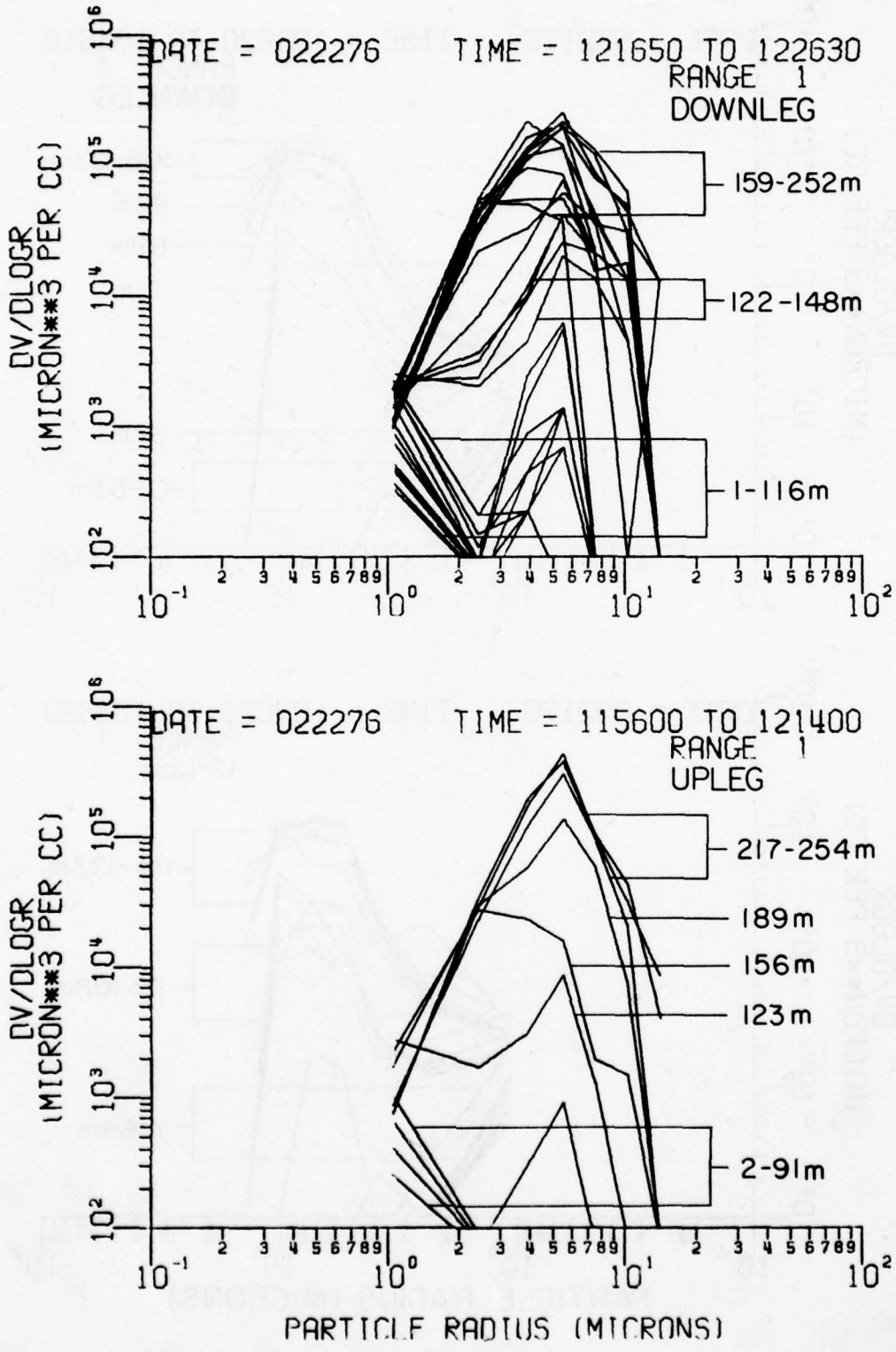
DATE = 022276
TIME = 121650 TO 122630
RANGE 1
DOWNLEG
159-252m
122-148m
1-116m
DV/DLOGR
(MICRON**3 PER CC)
DATE = 022276
TIME = 115600 TO 121400
RANGE 1
UPLEG
217-254m
189m
156m
123m
2-91m
PARTICLE RADIUS (MICRONS)

Figure A3-d

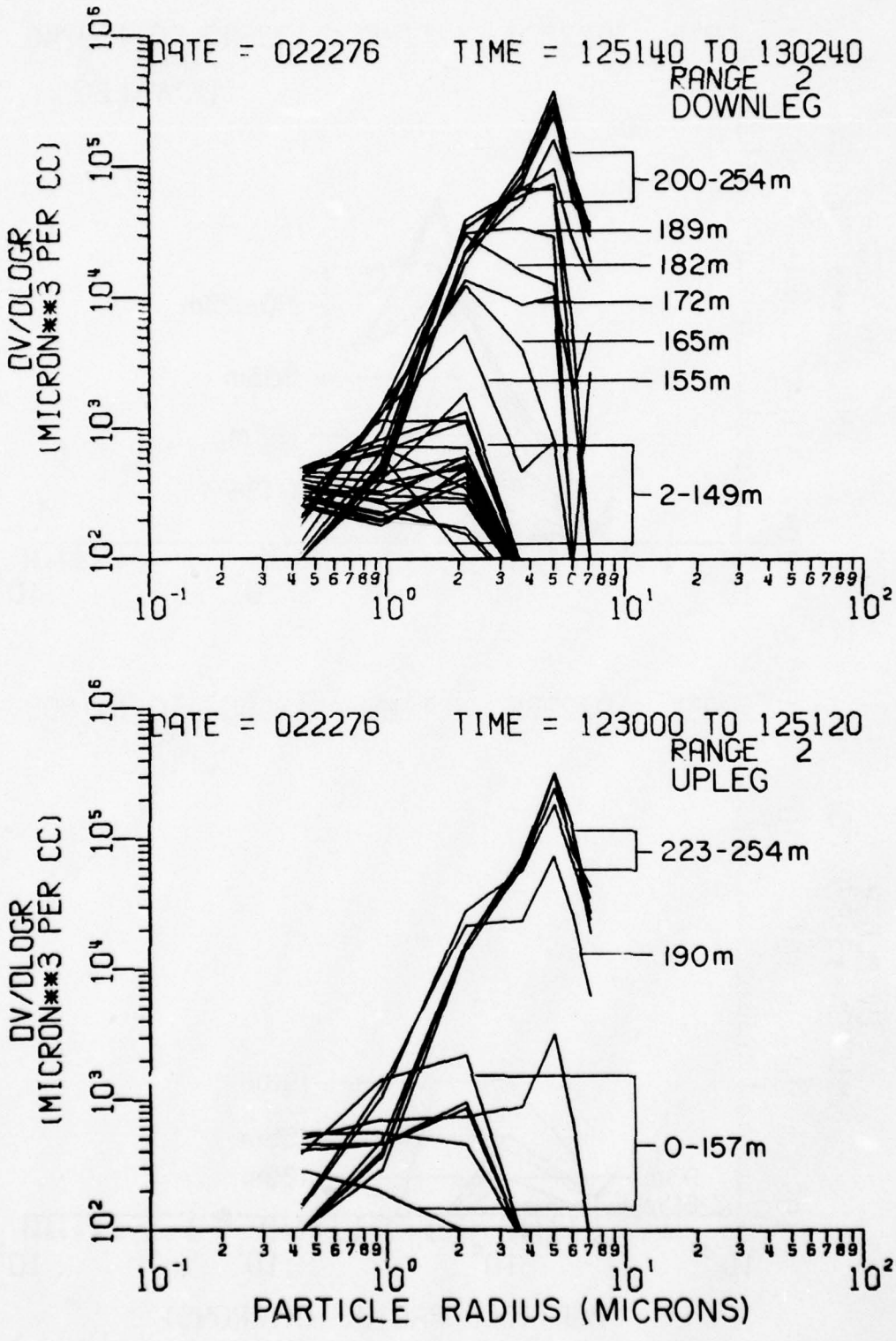
DATE = 022276
TIME = 125140 TO 130240
RANGE 2
DOWNLEG
200-254m
189m
182m
172m
165m
155m
2-149m
DV/DLOGR
(MICRON**3 PER CC)
DATE = 022276
TIME = 123000 TO 125120
RANGE 2
UPLEG
223-254m
190m
0-157m
PARTICLE RADIUS (MICRONS)

Figure A3-e

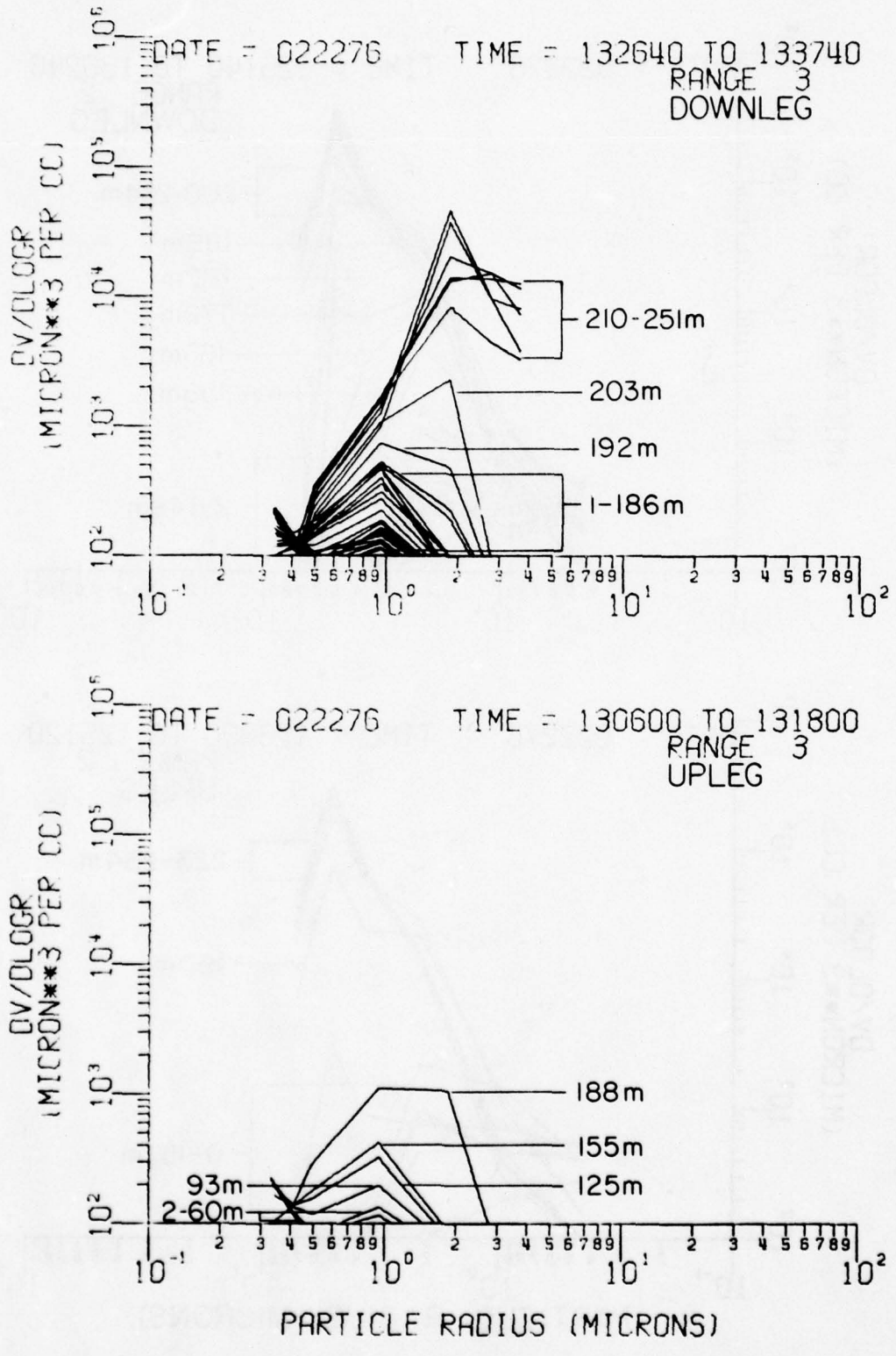
DATE = 022276
TIME = 132640 TO 133740
RANGE 3
DOWNLEG
210-251m
203m
192m
1-186m
DV/DLOGR
(MICRON**3 PER CC)
DATE = 022276
TIME = 130600 TO 131800
RANGE 3
UPLEG
188m
155m
125m
93m
2-60m
PARTICLE RADIUS (MICRONS)

Figure A3-f

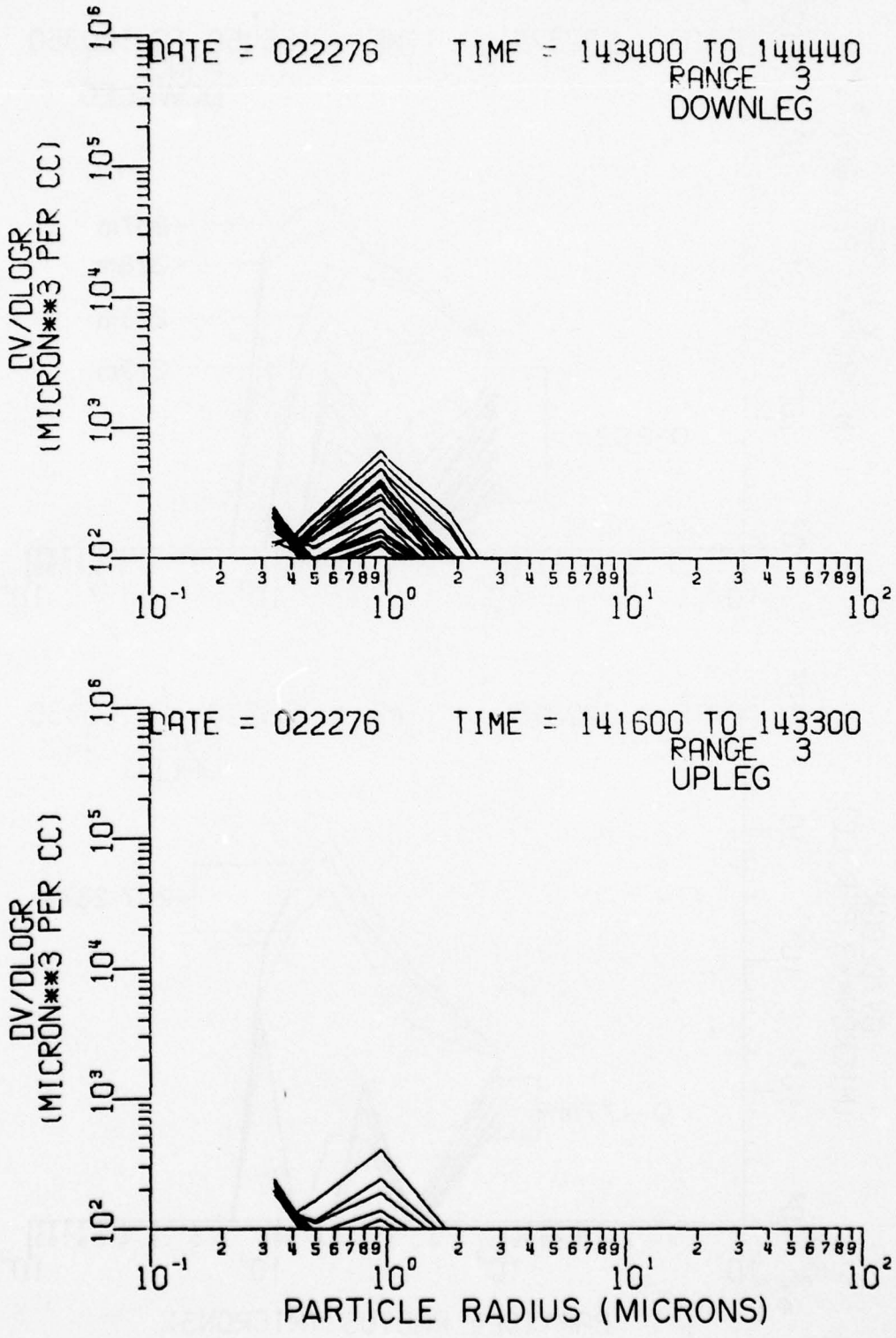
DATE = 022276 TIME = 143400 TO 144440
RANGE 3
DOWNLEG
DV/DLOGR
(MICRON**3 PER CC)
DATE = 022276 TIME = 141600 TO 143300
RANGE 3
UPLEG
PARTICLE RADIUS (MICRONS)

Figure A3-g

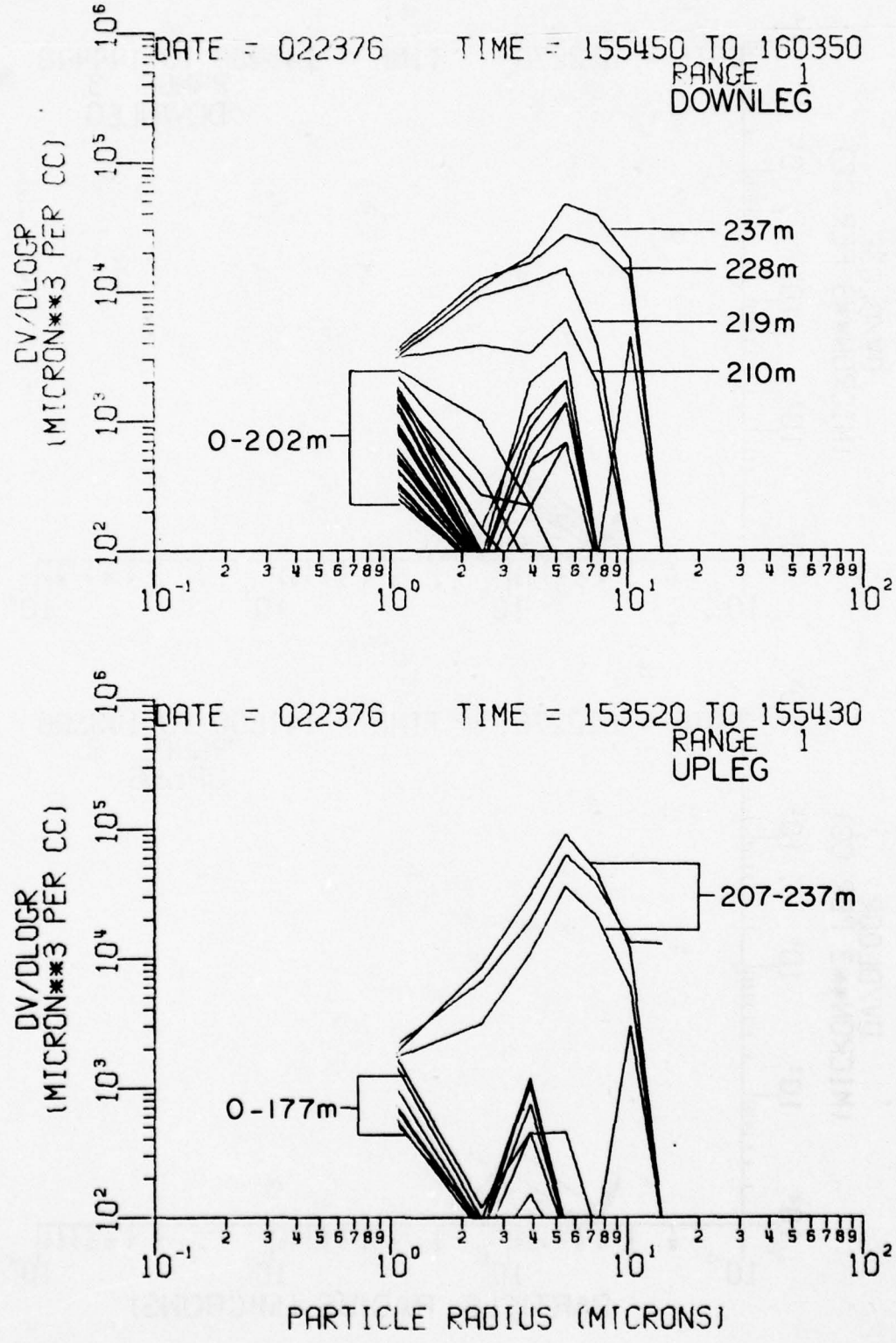
DATE = 022376
TIME = 155450 TO 160350
RANGE 1
DOWNLEG
237m
228m
219m
210m
0-202m
DV/DLOGR
(MICRON**3 PER CC)
DATE = 022376
TIME = 153520 TO 155430
RANGE 1
UPLEG
207-237m
0-177m
PARTICLE RADIUS (MICRONS)

Figure A3-h

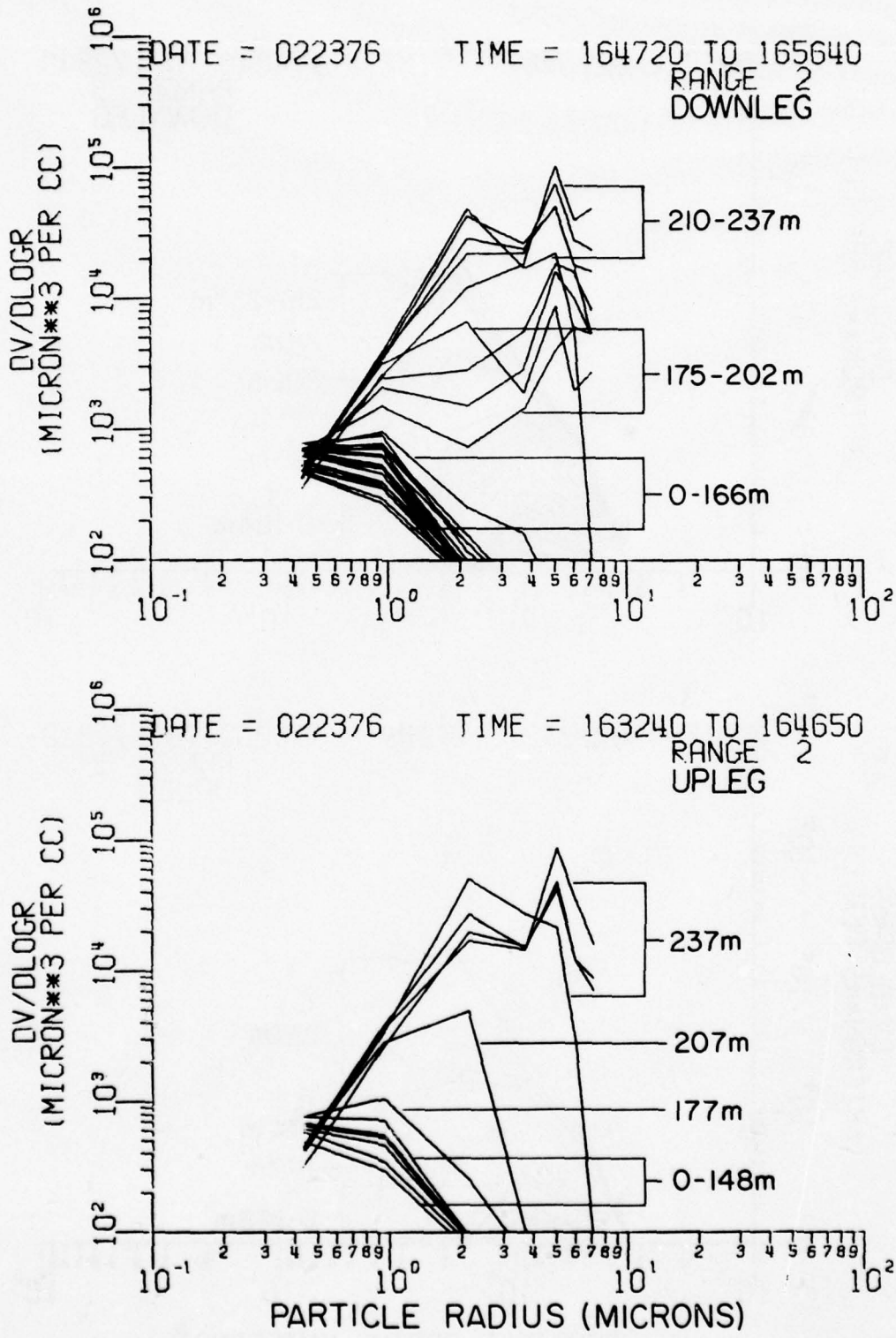
DATE = 022376
TIME = 164720 TO 165640
RANGE 2
DOWNLEG
210-237m
175-202m
0-166m
DV/DLOGR
(MICRON**3 PER CC)
DATE = 022376
TIME = 163240 TO 164650
RANGE 2
UPLEG
237m
207m
177m
0-148m
PARTICLE RADIUS (MICRONS)

Figure A3-i

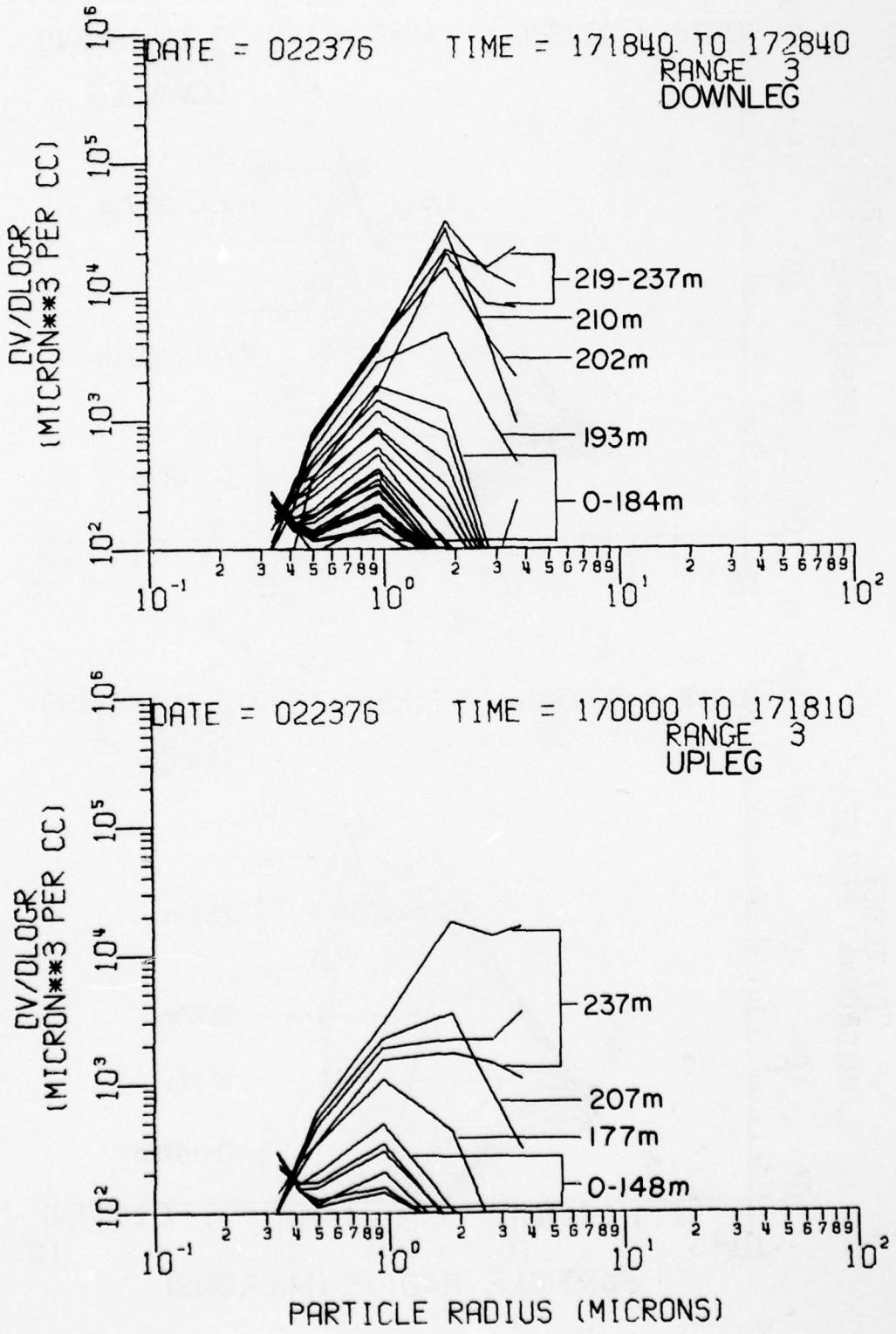
DATE = 022376
TIME = 171840 TO 172840
RANGE 3
DOWNLEG
DV/DLOGR
(MICRON**3 PER CC)
219-237m
210m
202m
193m
0-184m
DATE = 022376
TIME = 170000 TO 171810
RANGE 3
UPLEG
237m
207m
177m
0-148m
PARTICLE RADIUS (MICRONS)

Figure A3-j

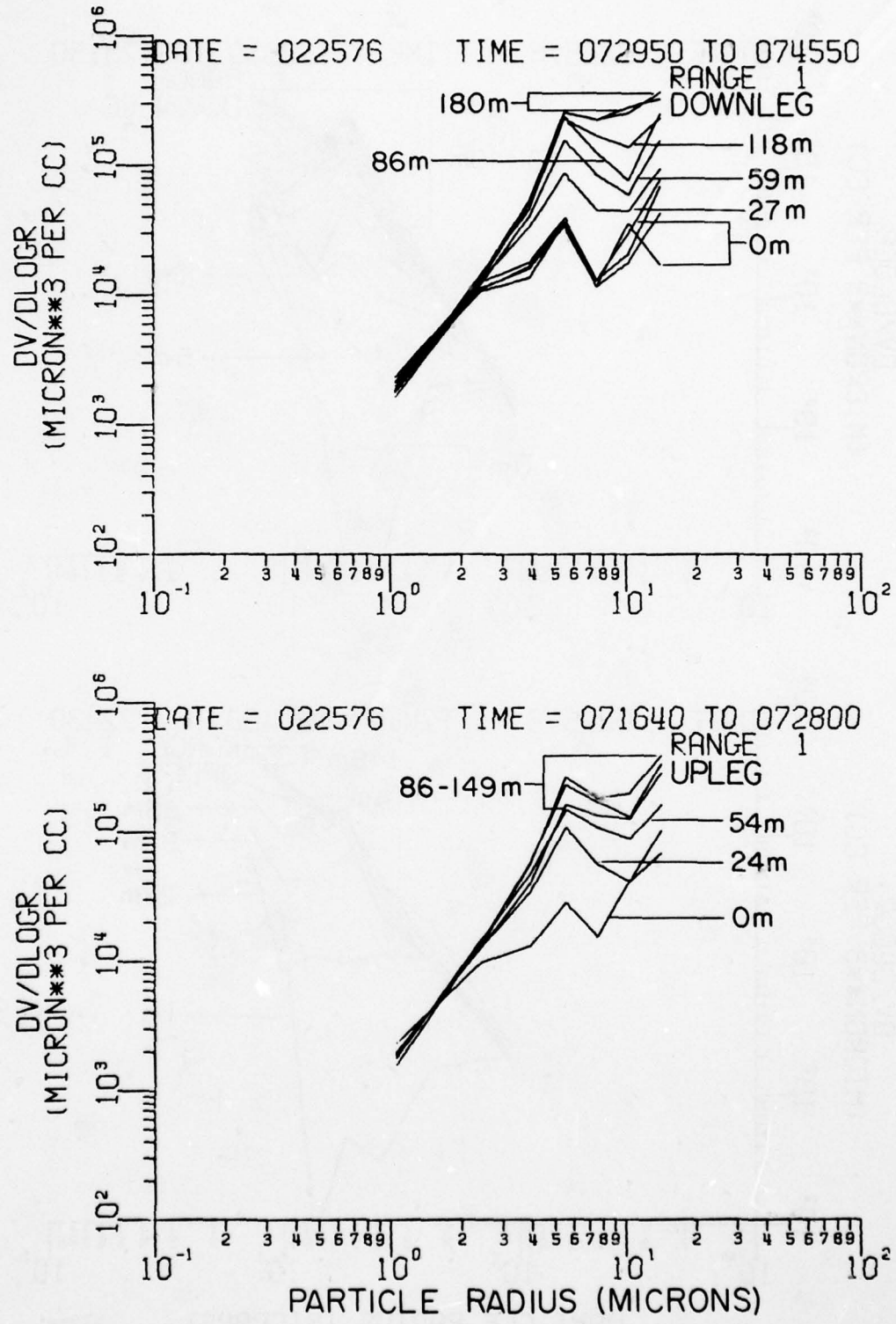
DATE = 022576
TIME = 072950 TO 074550
RANGE 1
DOWNLEG
180m
118m
86m
59m
27m
0m
DV/DLOGR
(MICRON**3 PER CC)
DATE = 022576
TIME = 071640 TO 072800
RANGE 1
UPLEG
86-149m
54m
24m
0m
PARTICLE RADIUS (MICRONS)

Figure A3-k

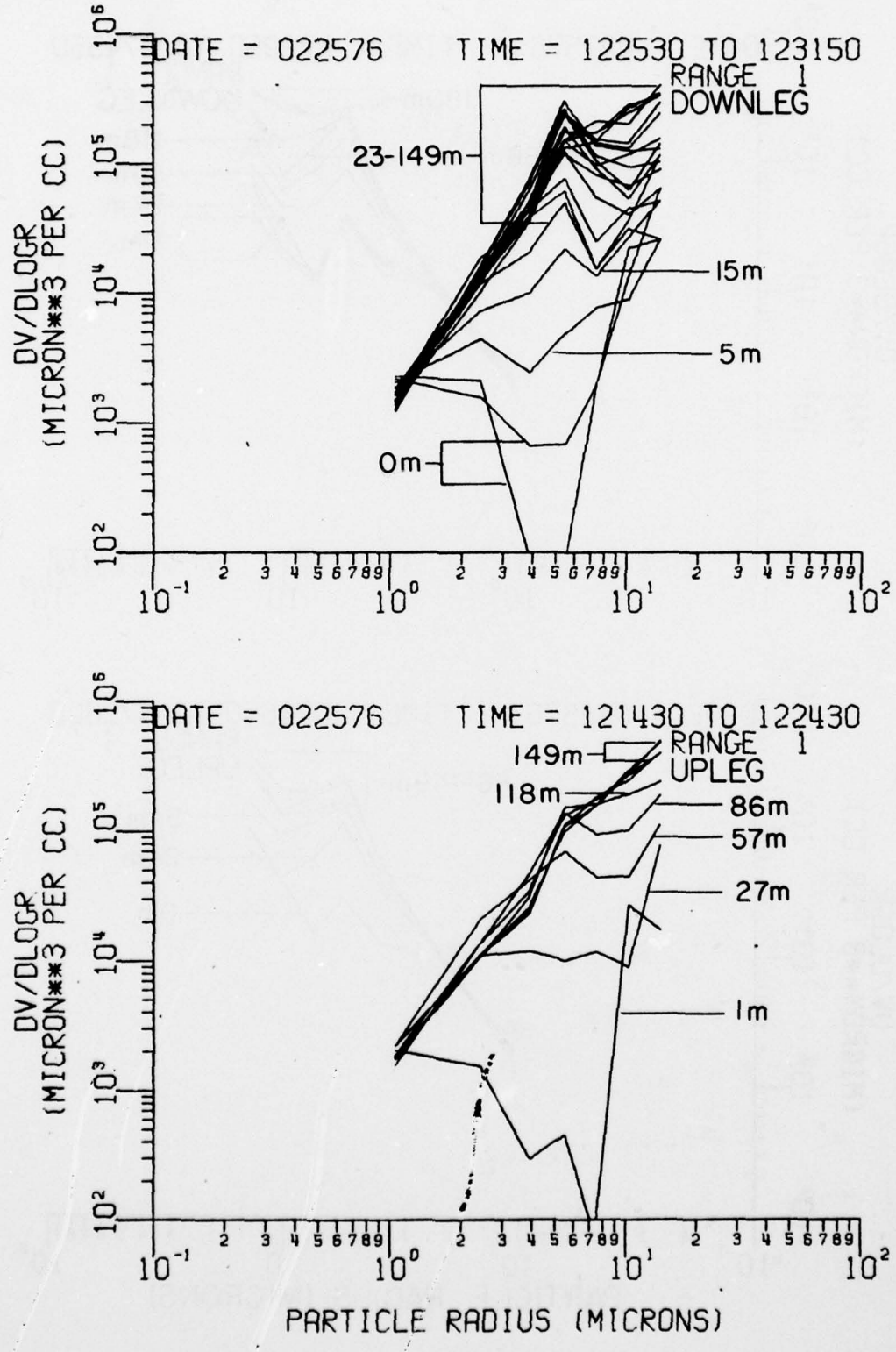
DATE = 022576
TIME = 122530 TO 123150
RANGE 1
DOWNLEG
23-149m
15m
5m
0m
DV/DLOGR
(MICRON**3 PER CC)
DATE = 022576
TIME = 121430 TO 122430
RANGE 1
UPLEG
149m
118m
86m
57m
27m
1m
PARTICLE RADIUS (MICRONS)

Figure A3-1

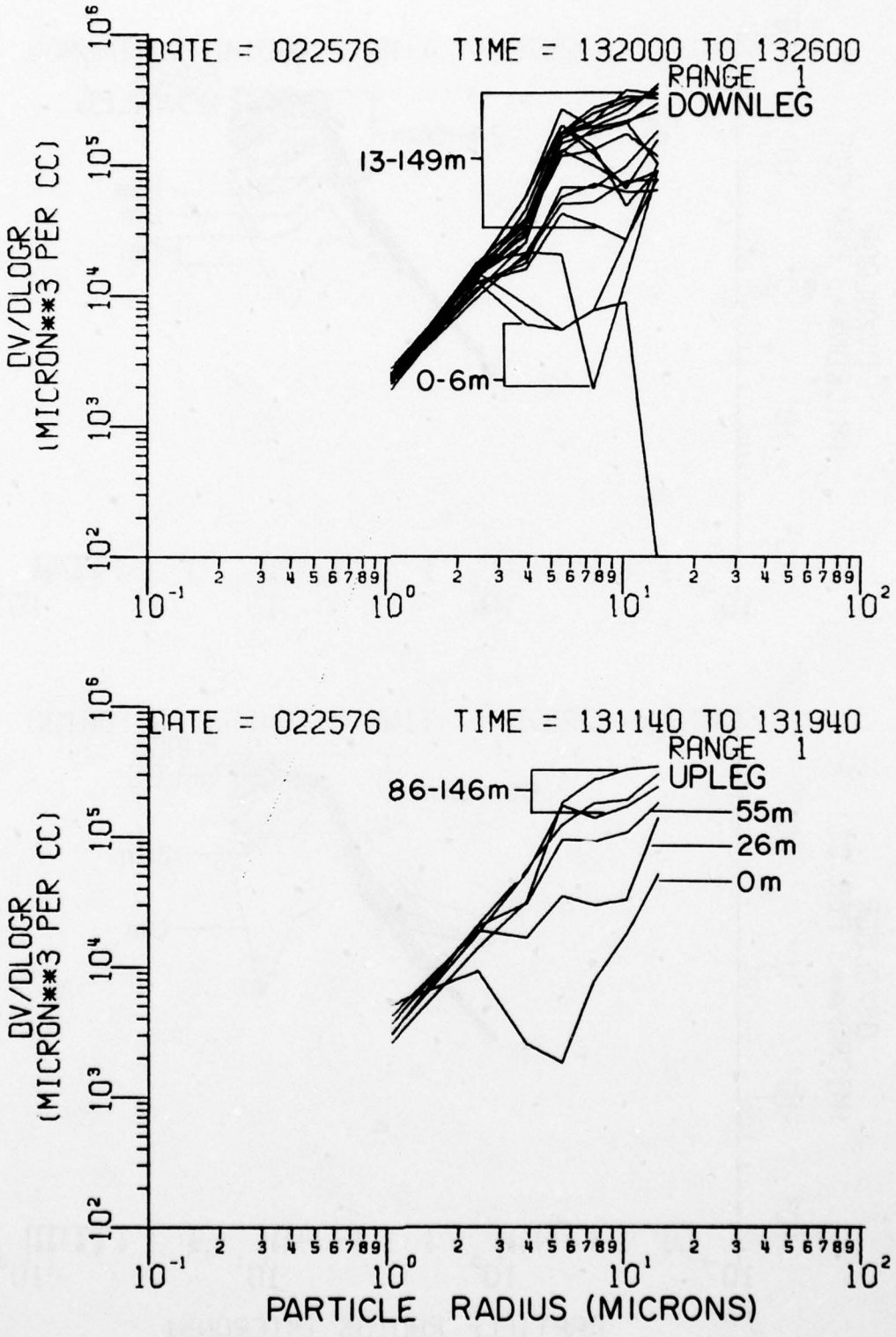
DATE = 022576
TIME = 132000 TO 132600
RANGE 1
DOWNLEG
13-149m
0-6m
DV/DLOGR
(MICRON**3 PER CC)
DATE = 022576
TIME = 131140 TO 131940
RANGE 1
UPLEG
86-146m
55m
26m
0m
PARTICLE RADIUS (MICRONS)

Figure A3-m

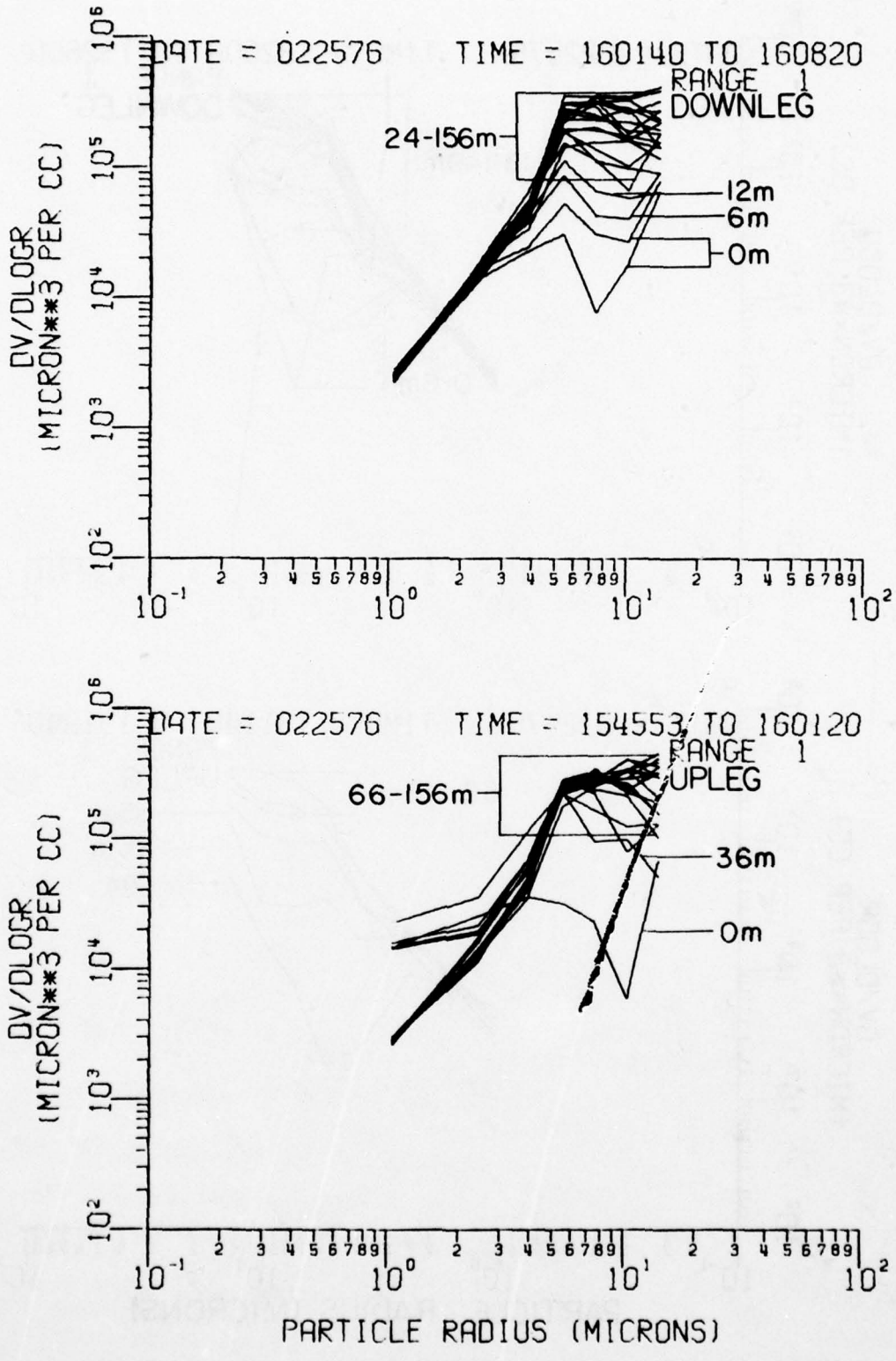
DATE = 022576
TIME = 160140 TO 160820
RANGE 1
DOWNLEG
24-156m
12m
6m
0m
DV/DLOGR
(MICRON**3 PER CC)
DATE = 022576
TIME = 154553 TO 160120
RANGE 1
UPLEG
66-156m
36m
0m
PARTICLE RADIUS (MICRONS)

Figure A3-n

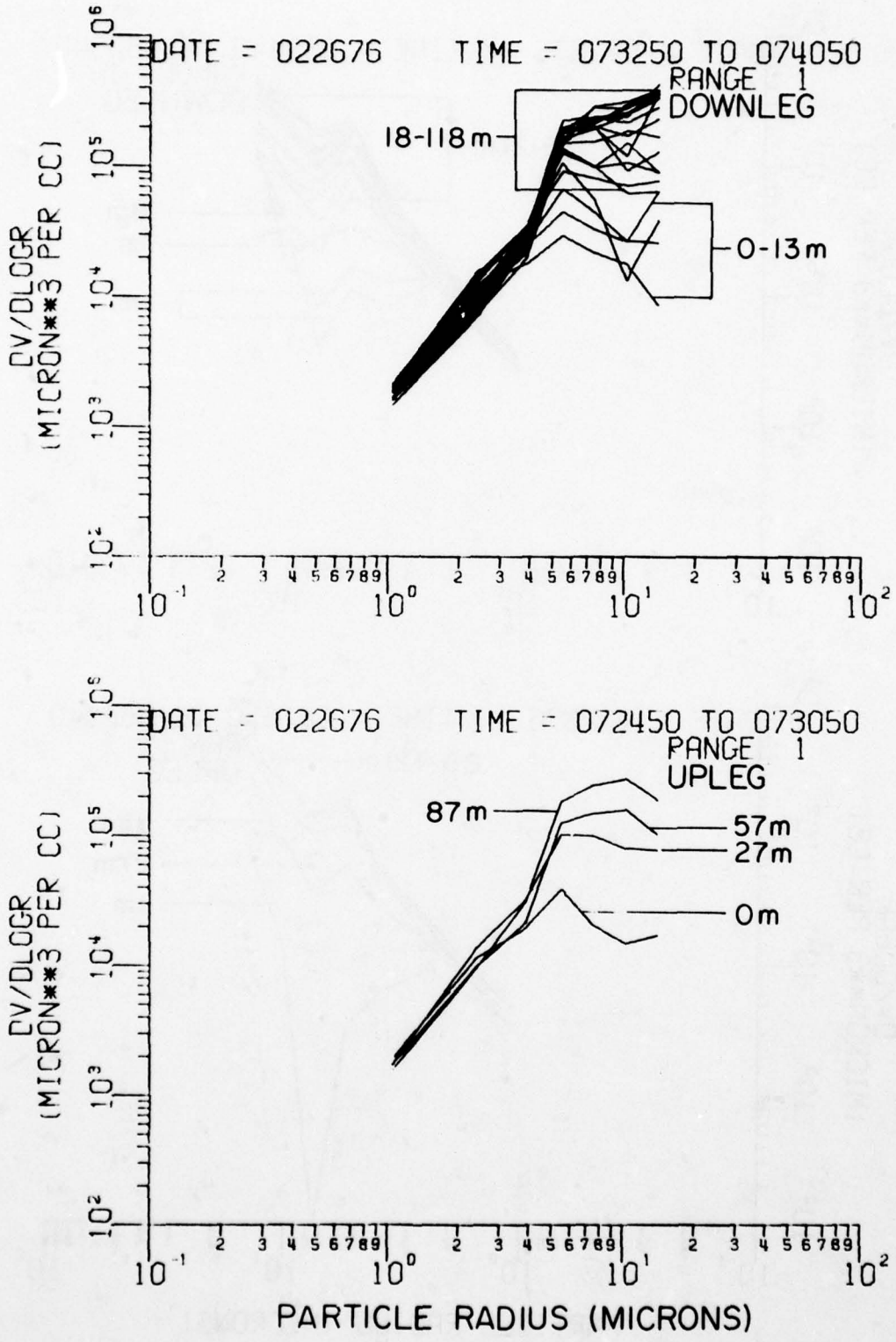
DATE = 022676
TIME = 073250 TO 074050
RANGE 1
DOWNLEG
18-118m
0-13m
DV/DLOGR
(MICRON**3 PER CC)
DATE = 022676
TIME = 072450 TO 073050
RANGE 1
UPLEG
87m
57m
27m
0m
PARTICLE RADIUS (MICRONS)

Figure A3-o

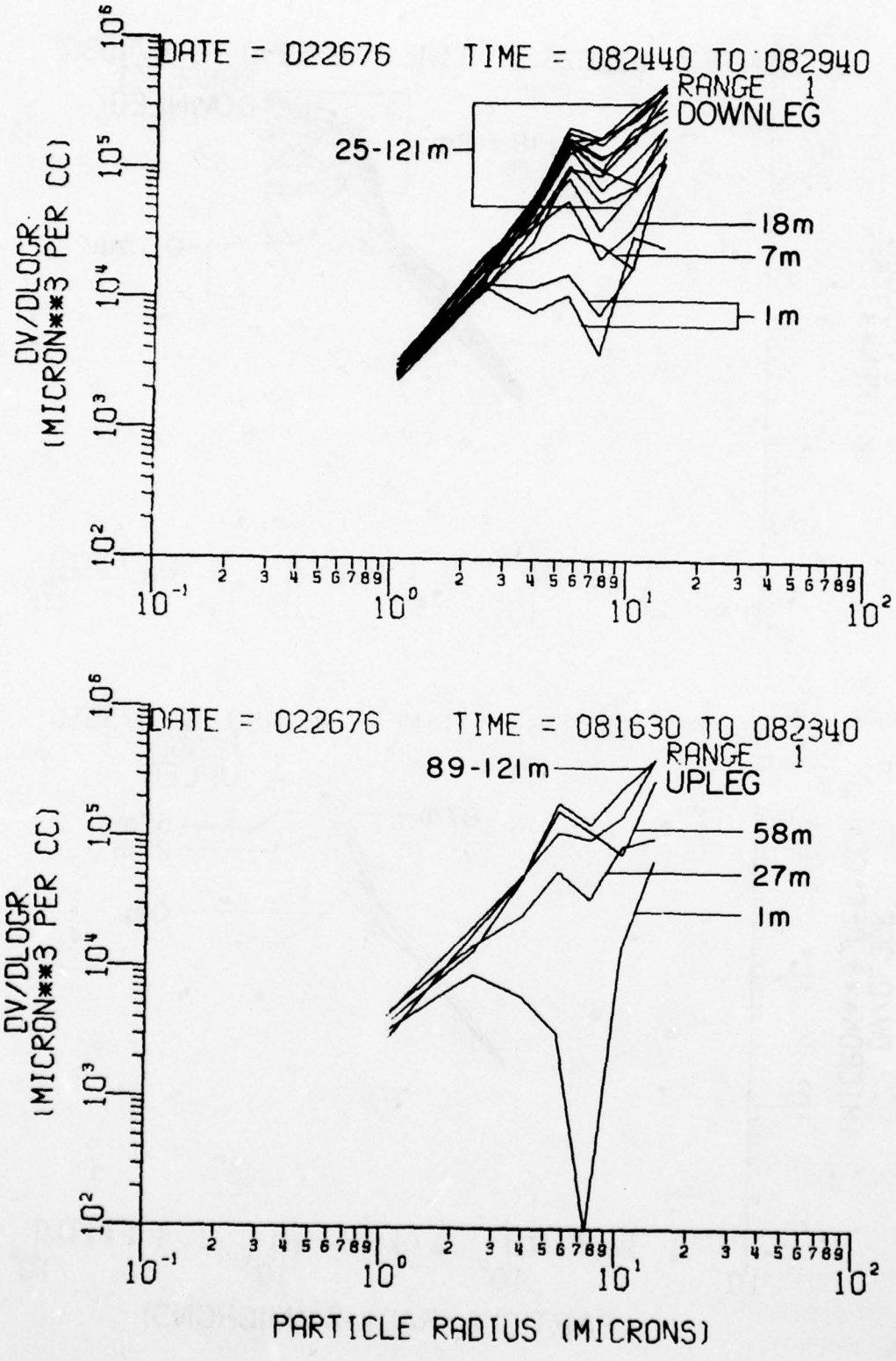
DATE = 022676
TIME = 082440 TO 082940
RANGE 1
DOWNLEG
25-121m
18m
7m
1m
DV/DLOGR
(MICRON**3 PER CC)
DATE = 022676
TIME = 081630 TO 082340
RANGE 1
UPLEG
89-121m
58m
27m
1m
PARTICLE RADIUS (MICRONS)

Figure A3-p

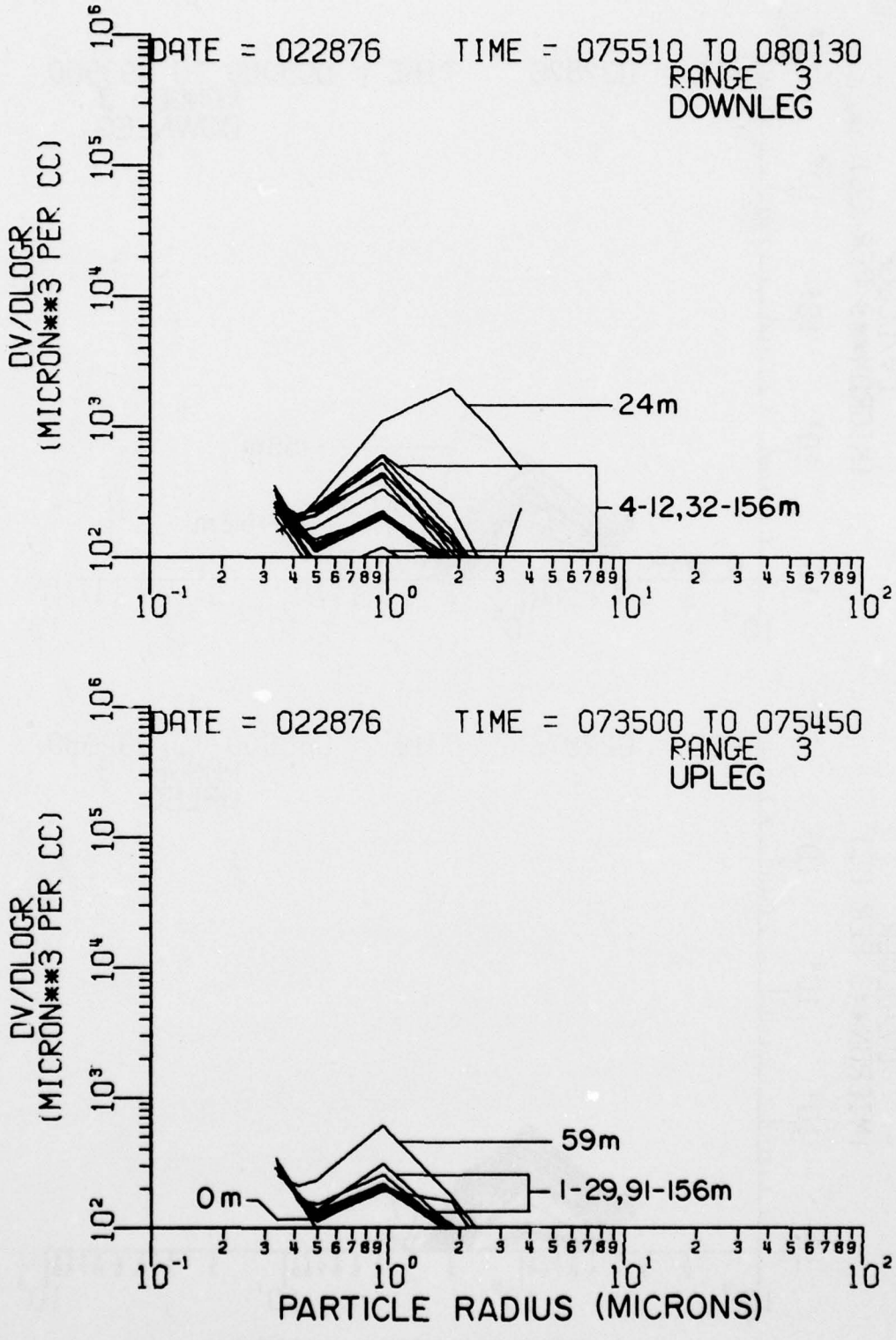
DATE = 022876
TIME = 075510 TO 080130
RANGE 3
DOWNLEG
DV/DLOGR
(MICRON**3 PER CC)
24m
4-12,32-156m
DATE = 022876
TIME = 073500 TO 075450
RANGE 3
UPLEG
59m
0m
1-29,91-156m
PARTICLE RADIUS (MICRONS)

Figure A3-q

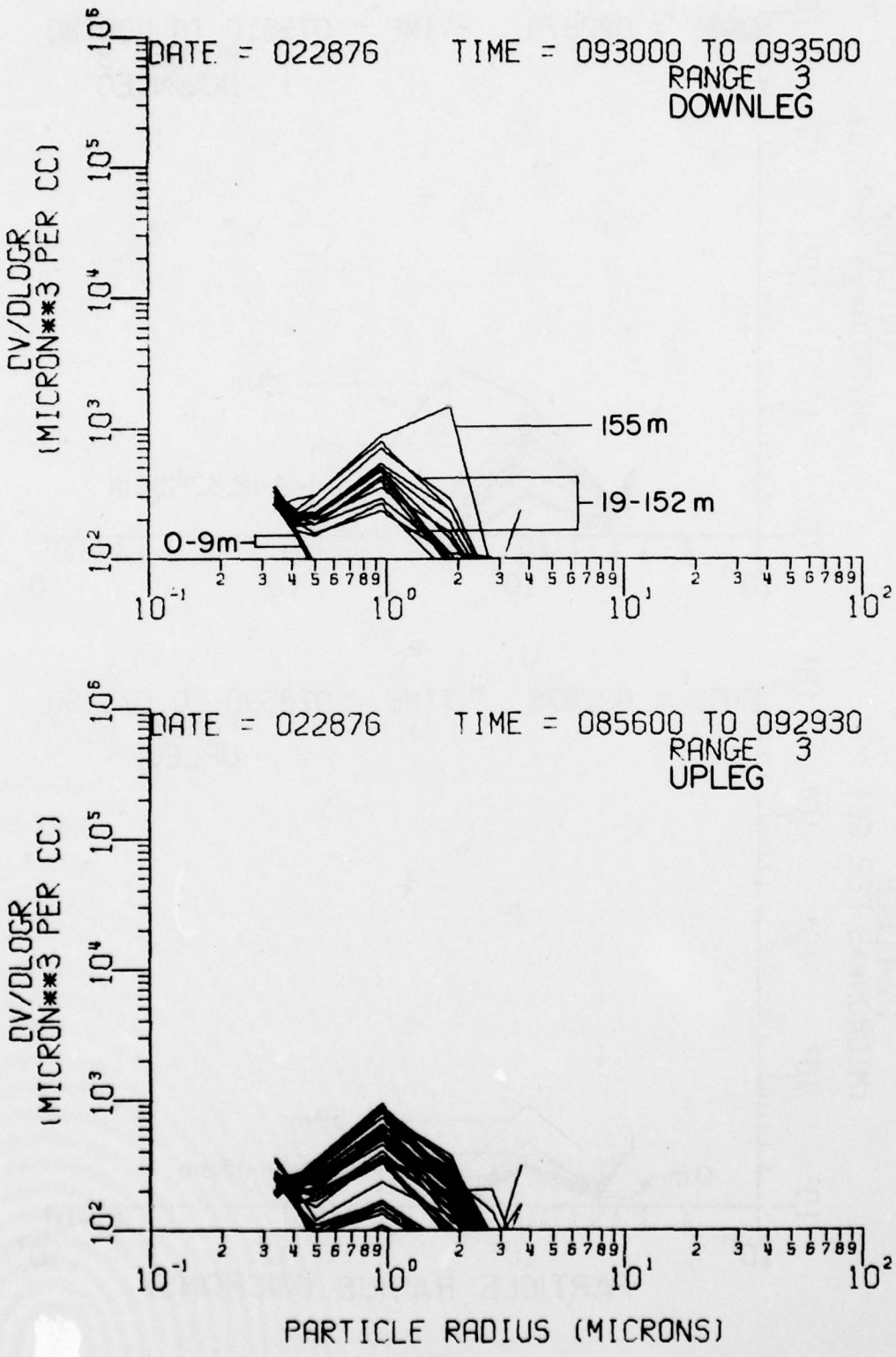
DATE = 022876
TIME = 093000 TO 093500
RANGE 3
DOWNLEG
DV/DLOGR
(MICRON**3 PER CC)
155 m
19-152 m
0-9m
DATE = 022876
TIME = 085600 TO 092930
RANGE 3
UPLEG
PARTICLE RADIUS (MICRONS)

Figure A3-r

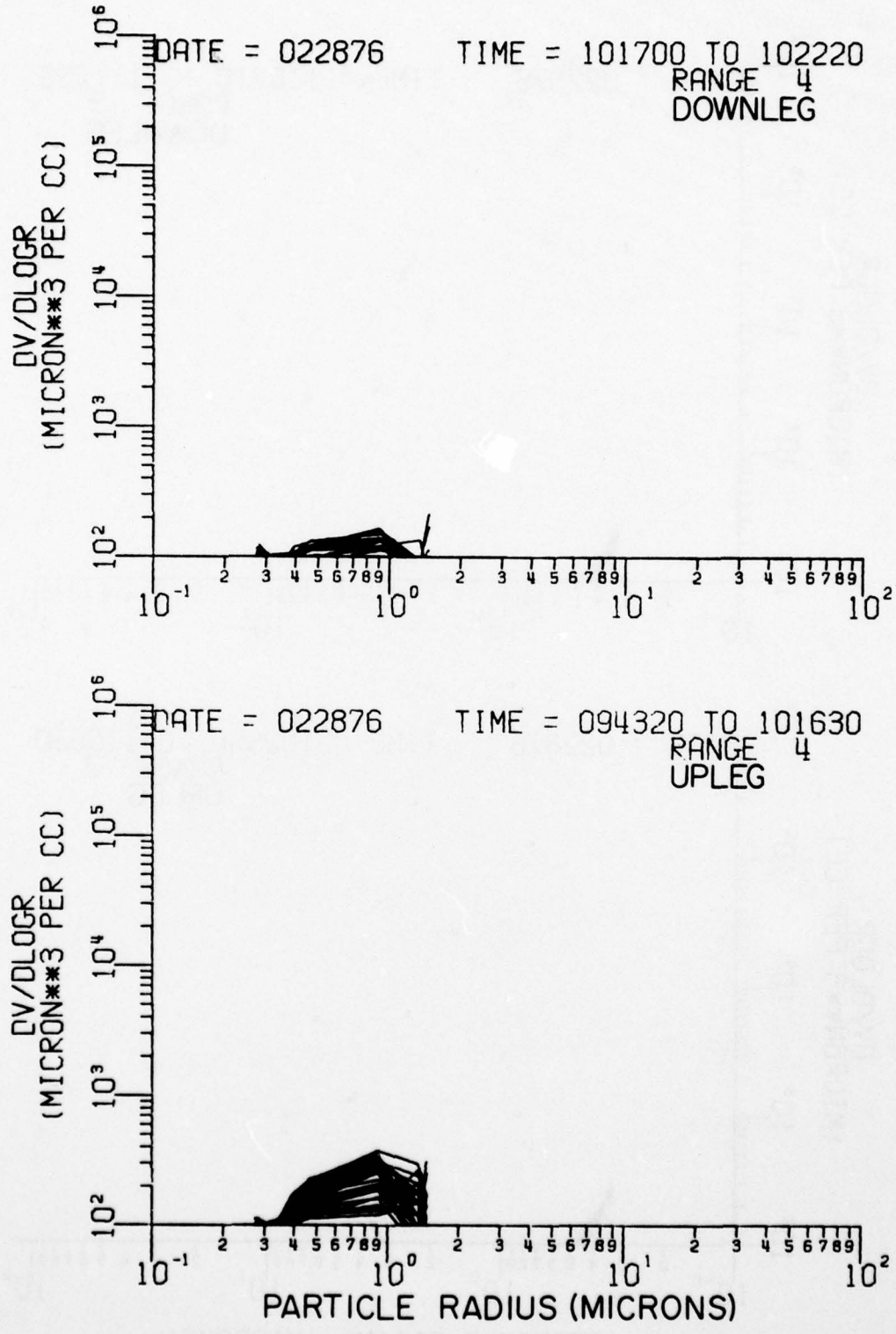
DATE = 022876
TIME = 101700 TO 102220
RANGE 4
DOWNLEG
DV/DLOGR
(MICRON**3 PER CC)
DATE = 022876
TIME = 094320 TO 101630
RANGE 4
UPLEG
DV/DLOGR
(MICRON**3 PER CC)
PARTICLE RADIUS (MICRONS)

Figure A3-e

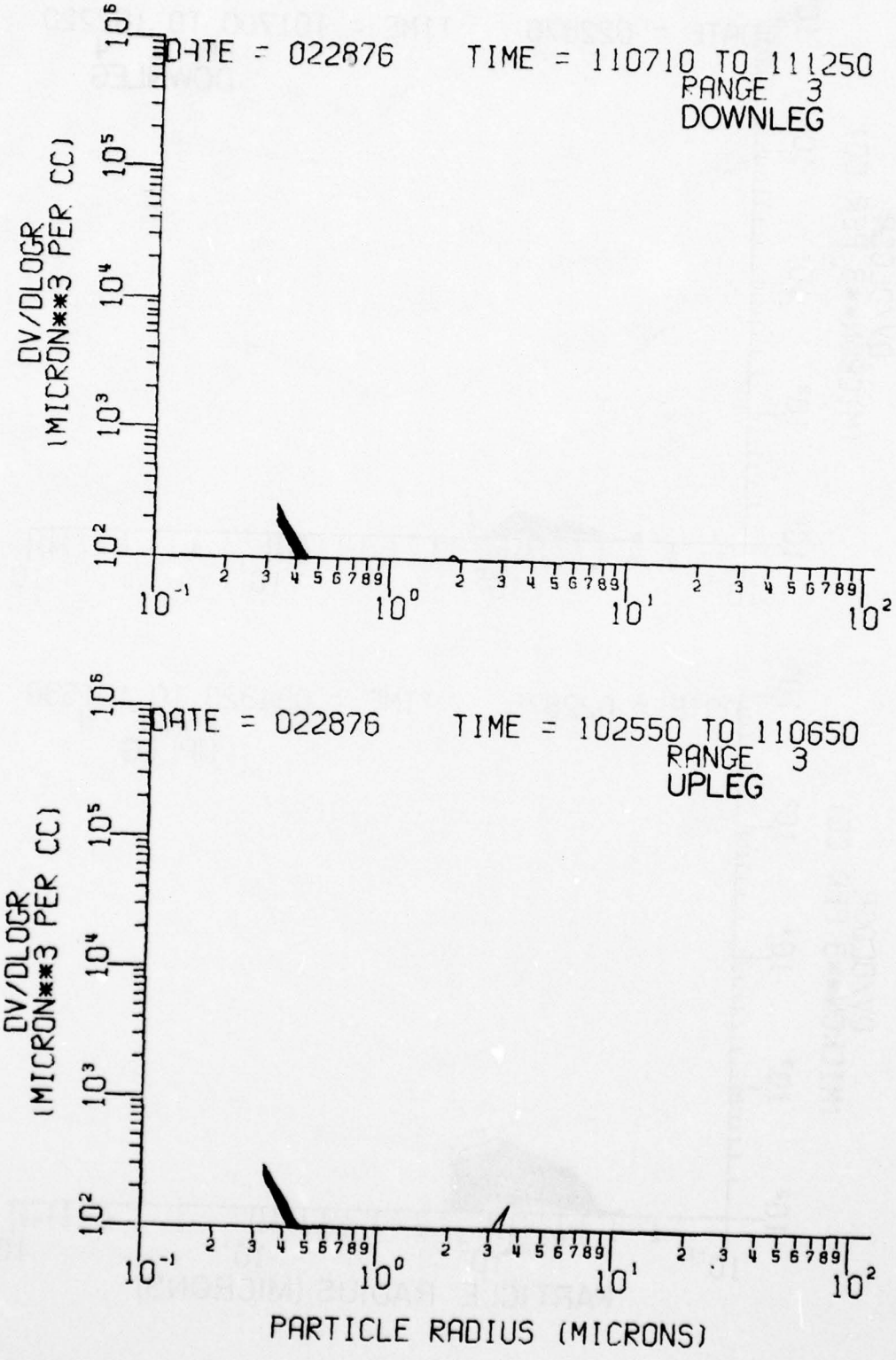
DATE = 022876
TIME = 110710 TO 111250
RANGE 3
DOWNLEG
DV/DLOGR
(MICRON**3 PER CC)
DATE = 022876
TIME = 102550 TO 110650
RANGE 3
UPLEG
PARTICLE RADIUS (MICRONS)

Figure A3-t

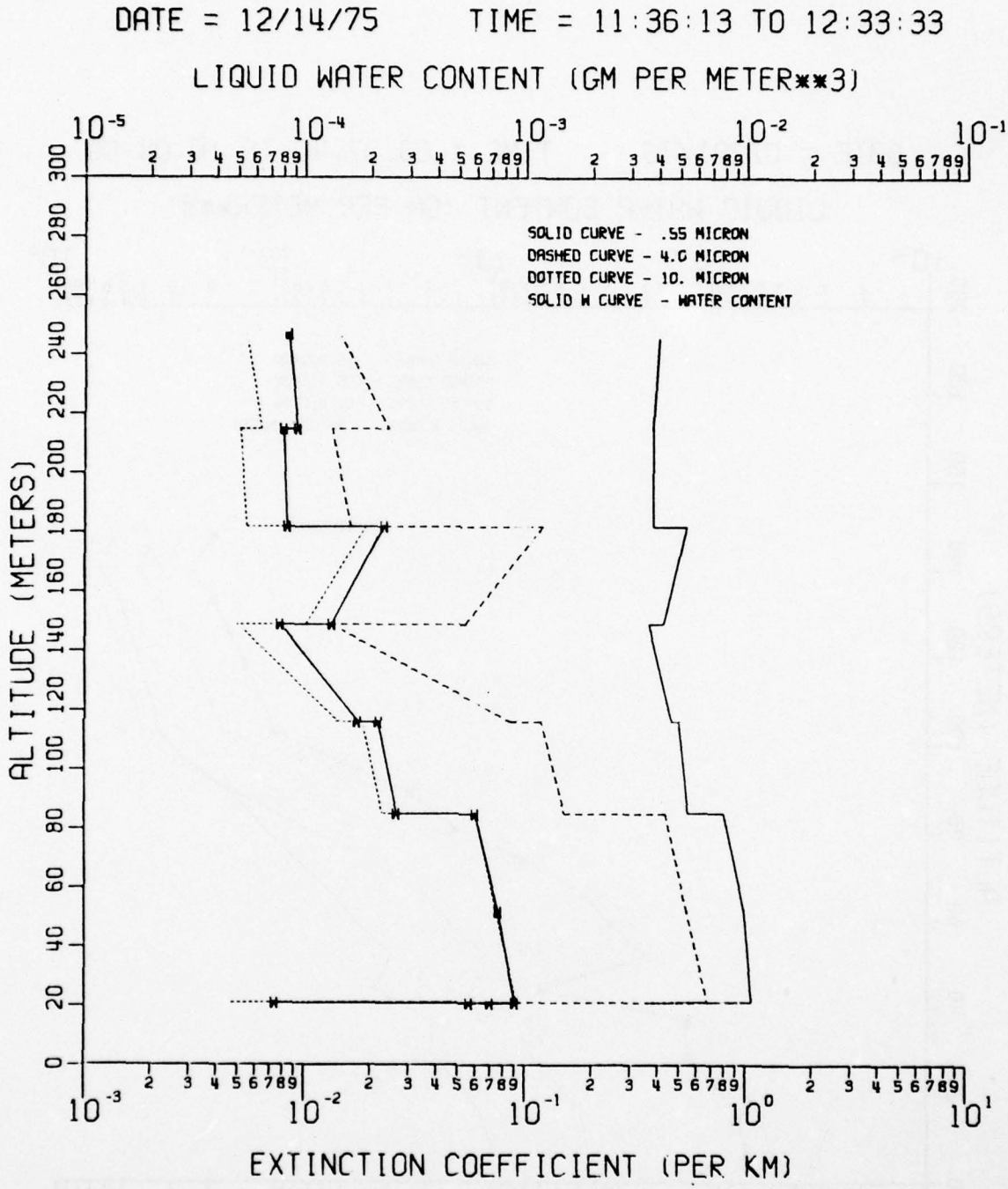

Figure A4-a. Profiles of particulate extinction and liquid water content inferred from particle size distribution measurements (shown in Fig. A1 made with a balloon-borne aerosol counter. Only the downleg portions of each traverse are presented. The solid "w" curve indicates liquid water content and the solid, dashed, and dotted curves indicate the inferred extinction at 0.55μm, 4μm, and 10μm wavelengths. The date, local time (hours, minutes, seconds) and time interval for the measurements are given.

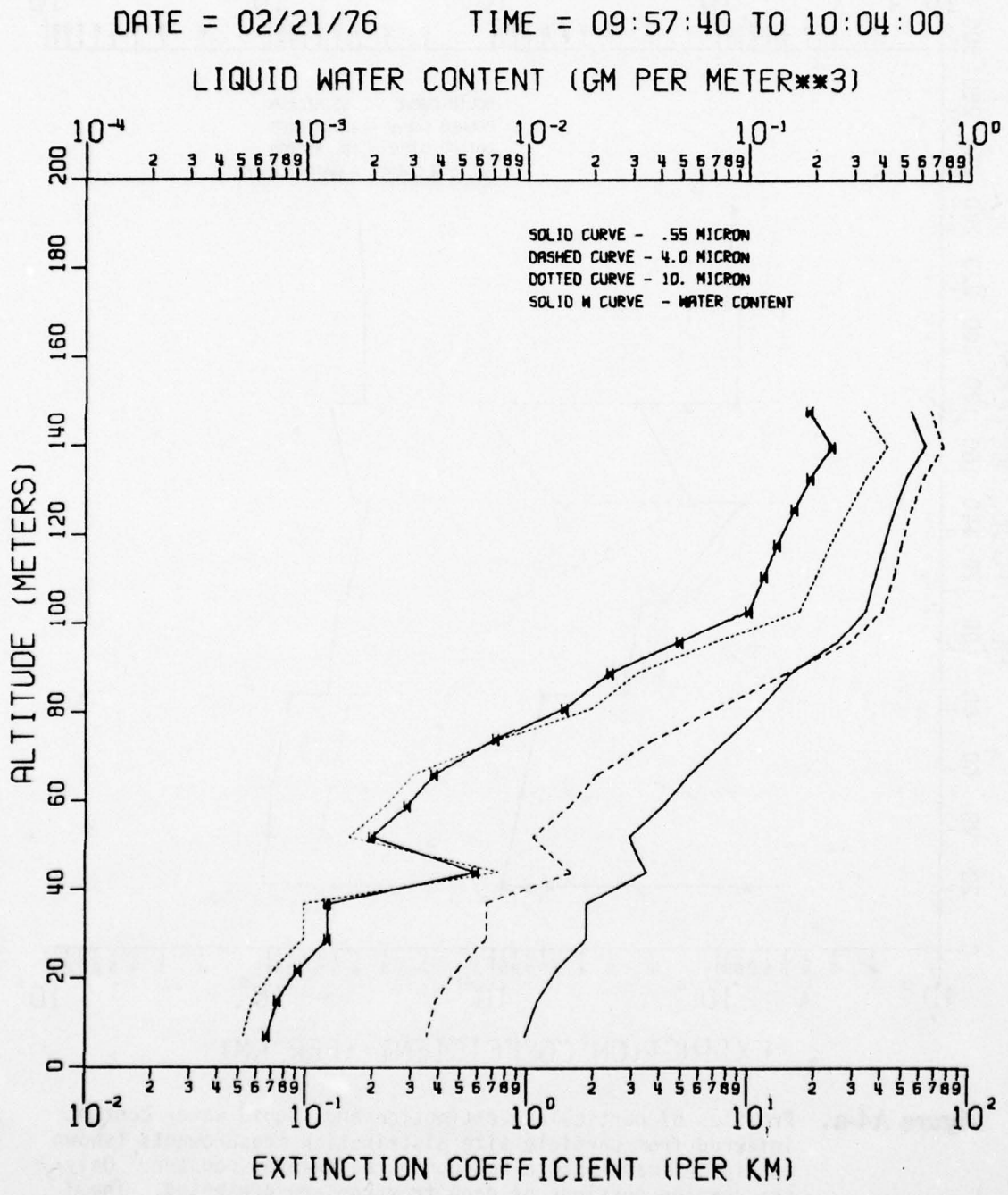
DATE = 02/21/76 TIME = 09:57:40 TO 10:04:00
LIQUID WATER CONTENT (GM PER METER**3)
SOLID CURVE - .55 MICRON
DASHED CURVE - 4.0 MICRON
DOTTED CURVE - 10. MICRON
SOLID W CURVE - WATER CONTENT
ALTITUDE (METERS)
EXTINCTION COEFFICIENT (PER KM)

Figure A4-b

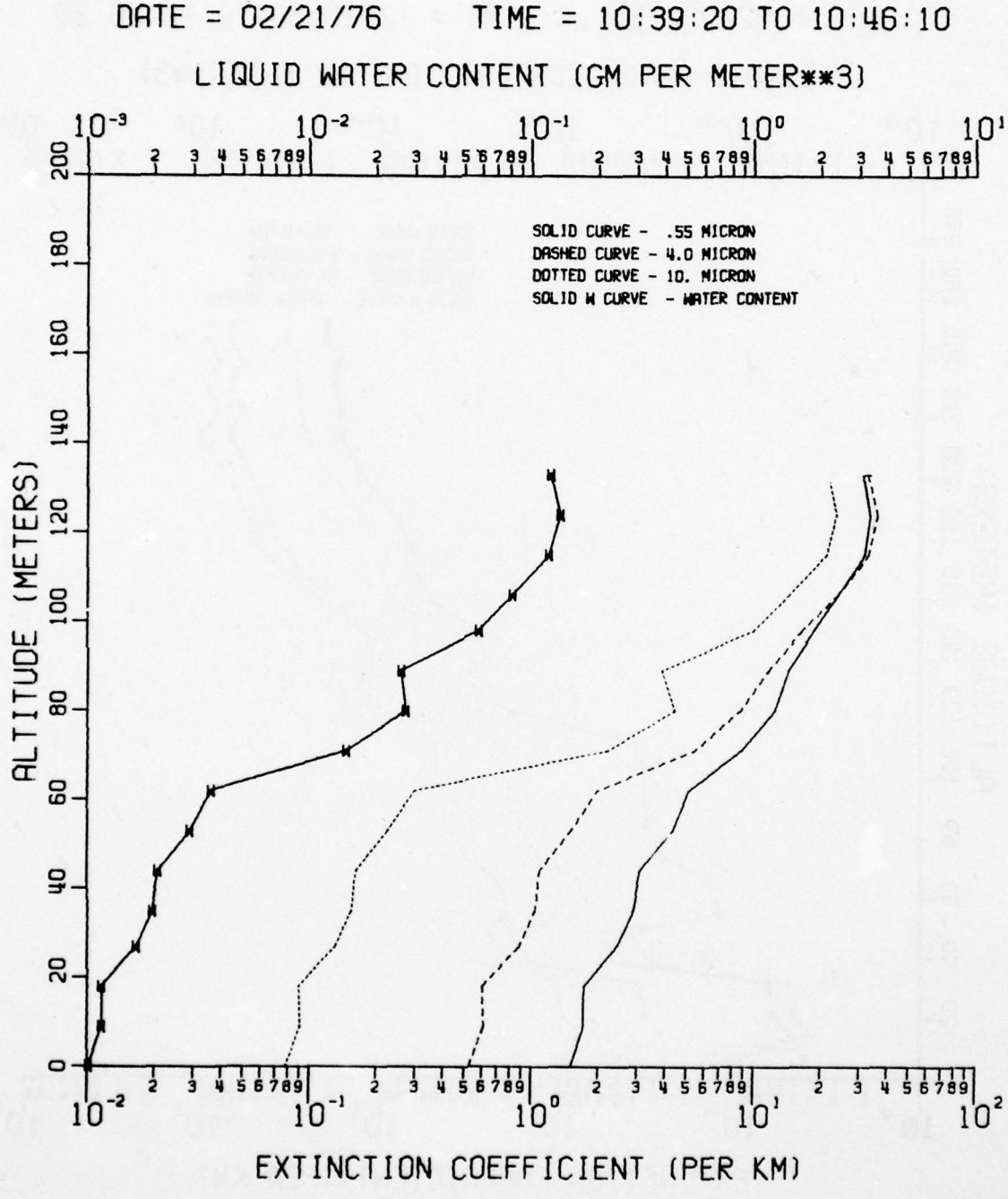
DATE = 02/21/76 TIME = 10:39:20 TO 10:46:10
LIQUID WATER CONTENT (GM PER METER**3)
SOLID CURVE - .55 MICRON
DASHED CURVE - 4.0 MICRON
DOTTED CURVE - 10. MICRON
SOLID W CURVE - WATER CONTENT
ALTITUDE (METERS)
EXTINCTION COEFFICIENT (PER KM)

Figure A4-c

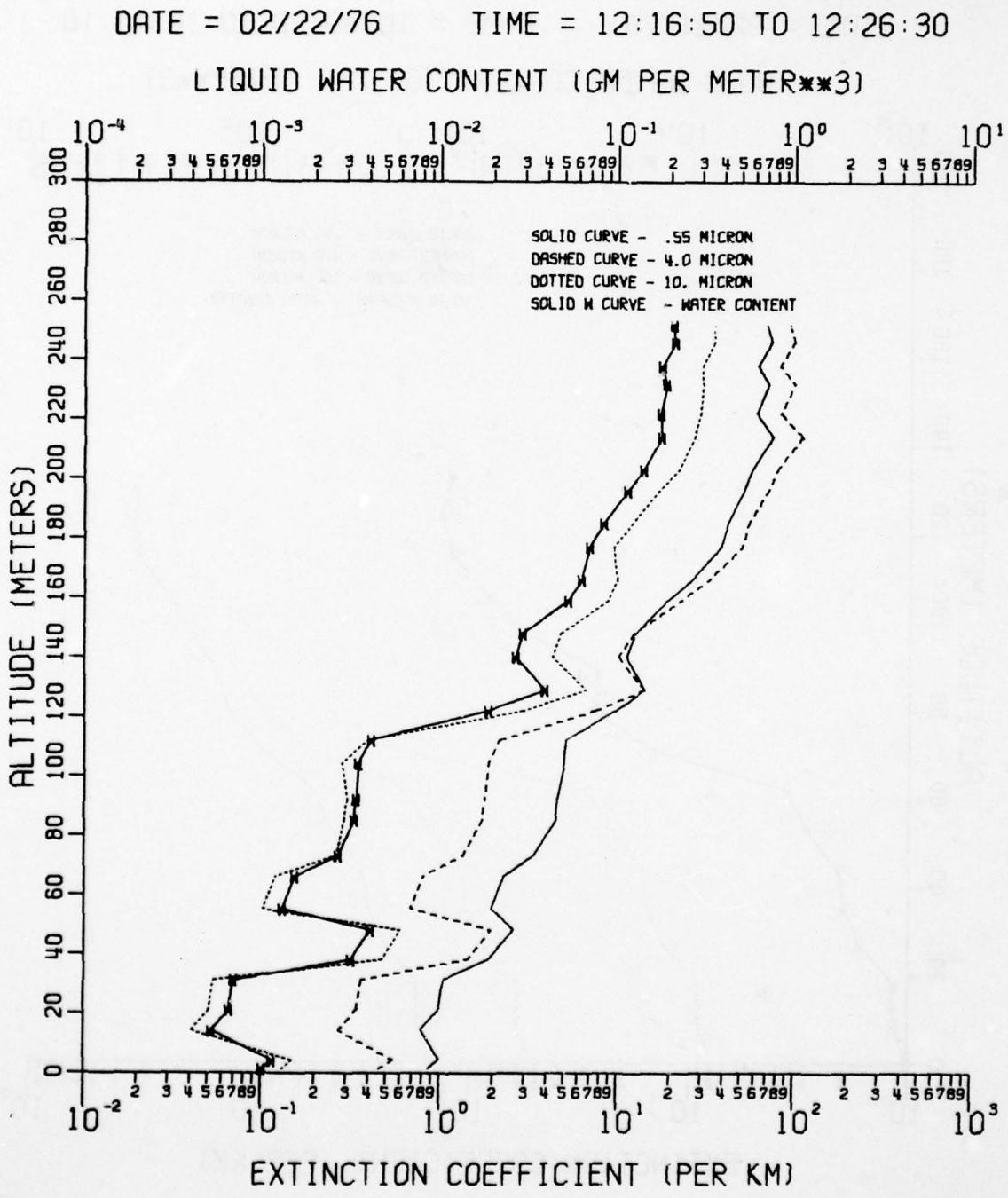
DATE = 02/22/76 TIME = 12:16:50 TO 12:26:30
LIQUID WATER CONTENT (GM PER METER**3)
SOLID CURVE - .55 MICRON
DASHED CURVE - 4.0 MICRON
DOTTED CURVE - 10. MICRON
SOLID W CURVE - WATER CONTENT
ALTITUDE (METERS)
EXTINCTION COEFFICIENT (PER KM)

Figure A4-d

AD-A058 127 ARMY ELECTRONICS RESEARCH AND DEVELOPMENT COMMAND WS--ETC F/G 4/2
VERTICAL STRUCTURE IN ATMOSPHERIC FOG AND HAZE AND ITS EFFECTS --ETC(U)
JUL 78 R G PINNICK, D L HOIHJELLE

UNCLASSIFIED ERADCOM/ASL-TR-0010 NL

2 OF 2
ADA
058127

END
DATE
FILMED
10 78
DDC

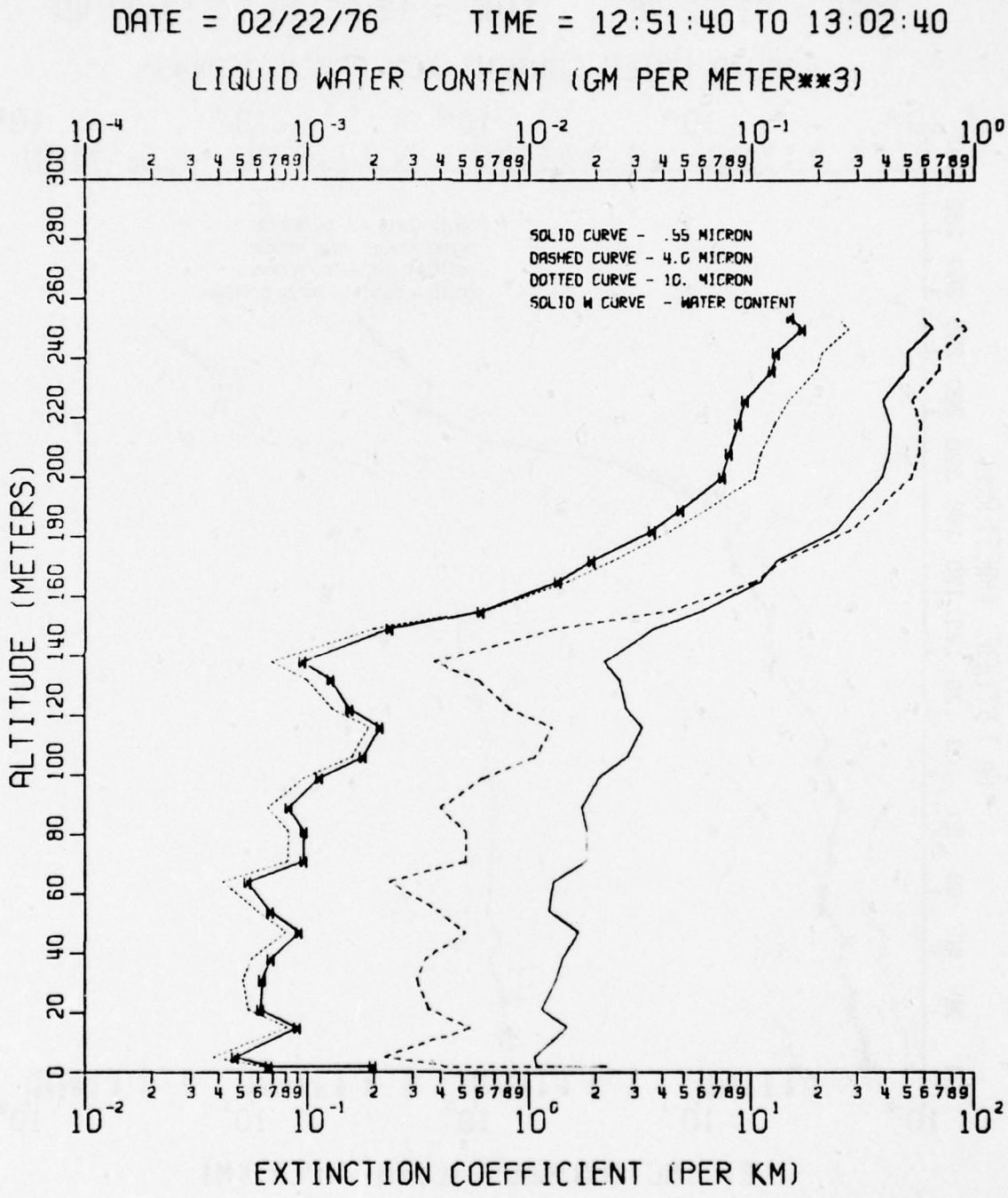
DATE = 02/22/76 TIME = 12:51:40 TO 13:02:40
LIQUID WATER CONTENT (GM PER METER**3)
SOLID CURVE - .55 MICRON
DASHED CURVE - 4.0 MICRON
DOTTED CURVE - 10. MICRON
SOLID W CURVE - WATER CONTENT
ALTITUDE (METERS)
EXTINCTION COEFFICIENT (PER KM)

Figure A4-e

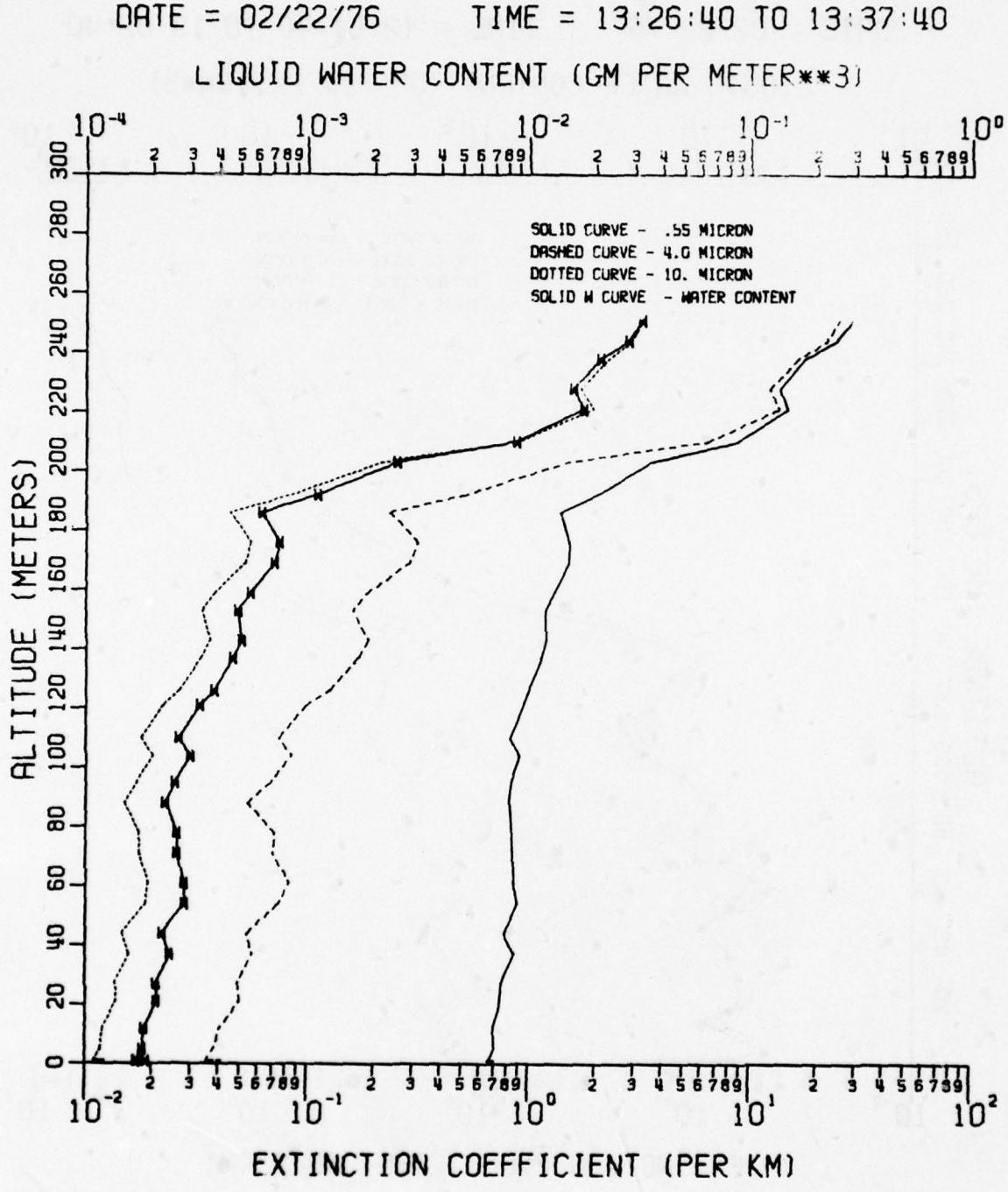
DATE = 02/22/76 TIME = 13:26:40 TO 13:37:40
LIQUID WATER CONTENT (GM PER METER**3)
SOLID CURVE - .55 MICRON
DASHED CURVE - 4.0 MICRON
DOTTED CURVE - 10. MICRON
SOLID W CURVE - WATER CONTENT
ALTITUDE (METERS)
EXTINCTION COEFFICIENT (PER KM)

Figure A4-f

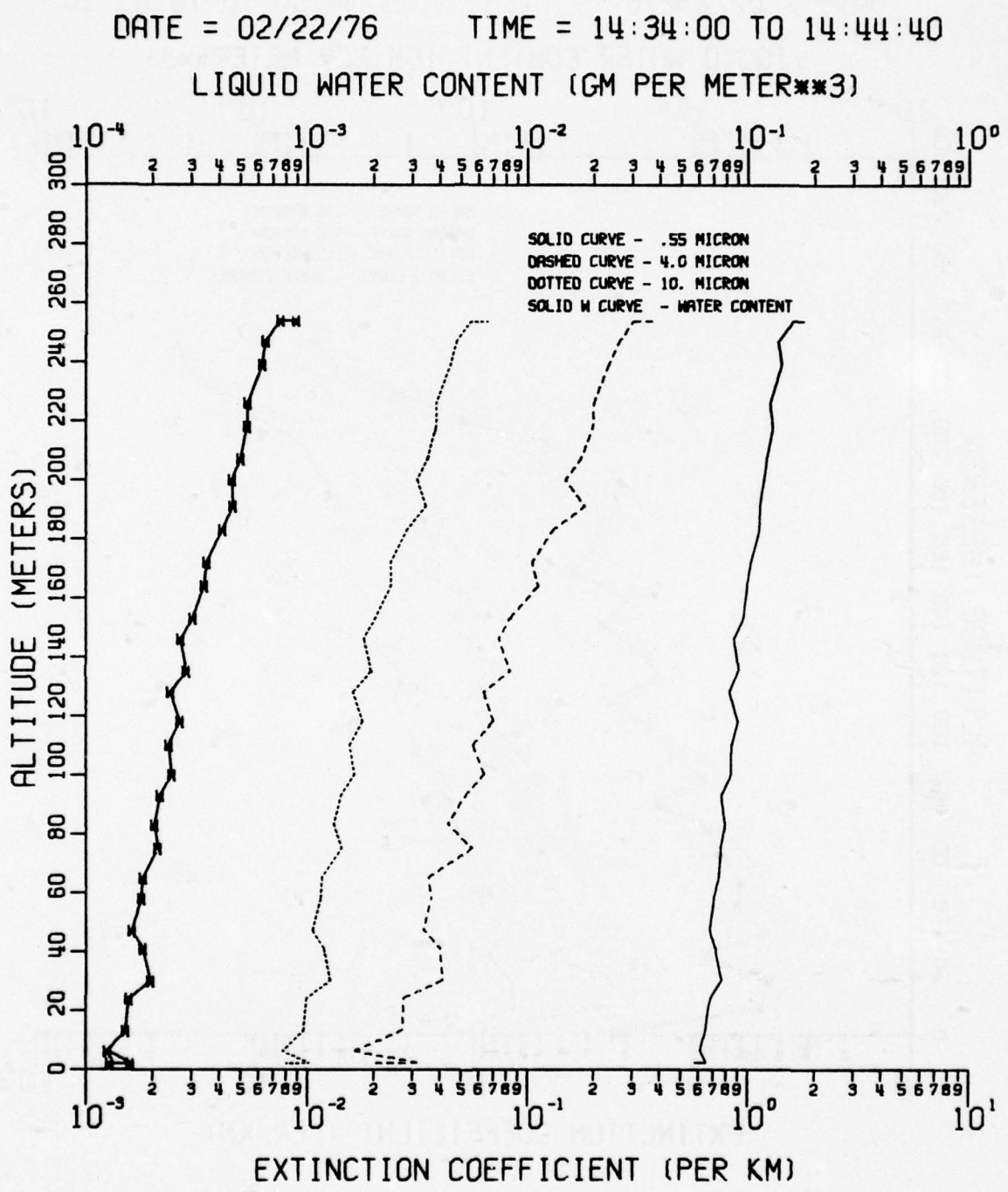
DATE = 02/22/76 TIME = 14:34:00 TO 14:44:40
LIQUID WATER CONTENT (GM PER METER**3)
SOLID CURVE - .55 MICRON
DASHED CURVE - 4.0 MICRON
DOTTED CURVE - 10. MICRON
SOLID W CURVE - WATER CONTENT
ALTITUDE (METERS)
EXTINCTION COEFFICIENT (PER KM)

Figure A4-g

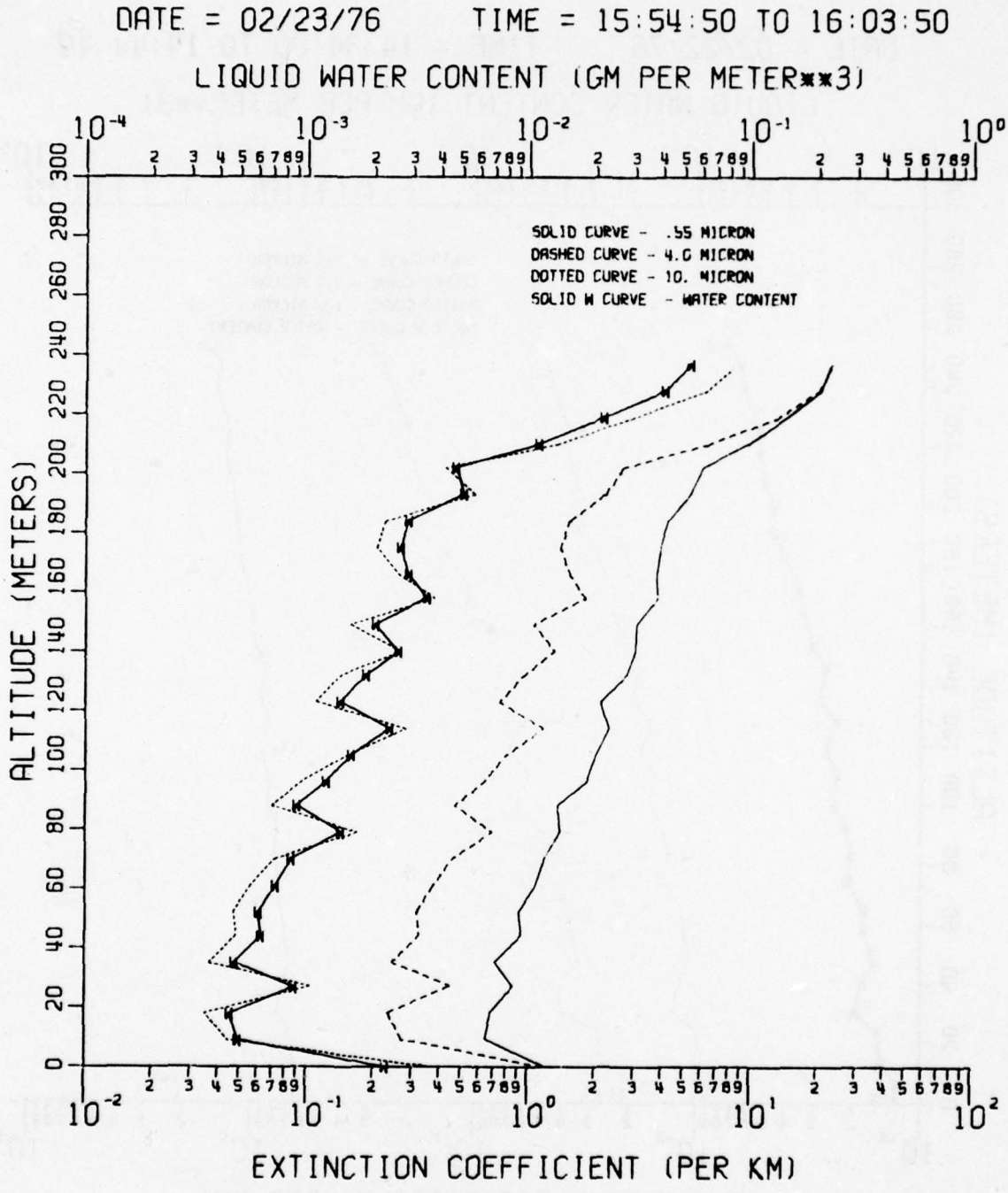
DATE = 02/23/76 TIME = 15:54:50 TO 16:03:50
LIQUID WATER CONTENT (GM PER METER**3)
SOLID CURVE - .55 MICRON
DASHED CURVE - 4.0 MICRON
DOTTED CURVE - 10. MICRON
SOLID W CURVE - WATER CONTENT
ALTITUDE (METERS)
EXTINCTION COEFFICIENT (PER KM)

Figure A4-h

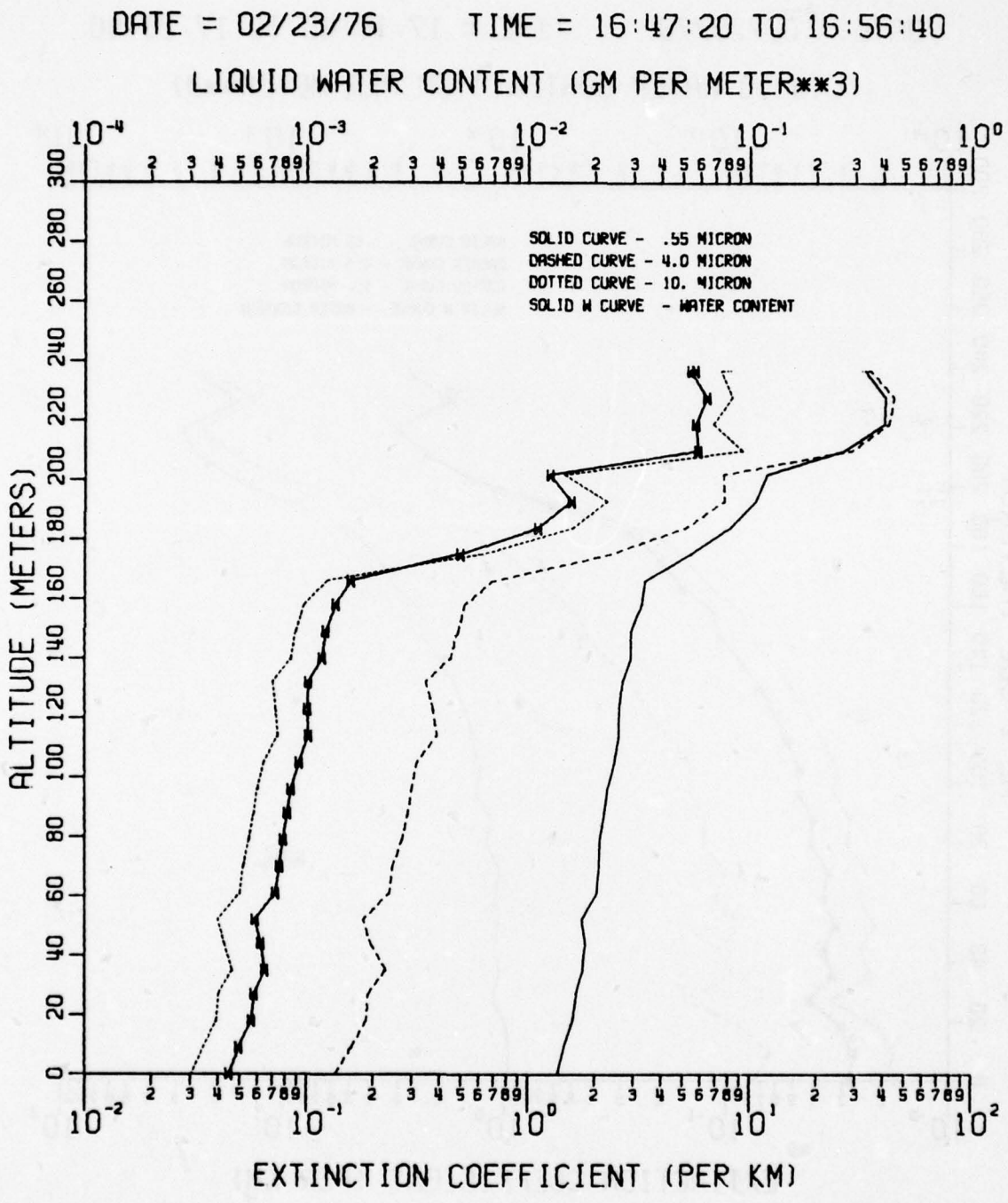
DATE = 02/23/76 TIME = 16:47:20 TO 16:56:40
LIQUID WATER CONTENT (GM PER METER**3)
SOLID CURVE - .55 MICRON
DASHED CURVE - 4.0 MICRON
DOTTED CURVE - 10. MICRON
SOLID W CURVE - WATER CONTENT
ALTITUDE (METERS)
EXTINCTION COEFFICIENT (PER KM)

Figure A4-i

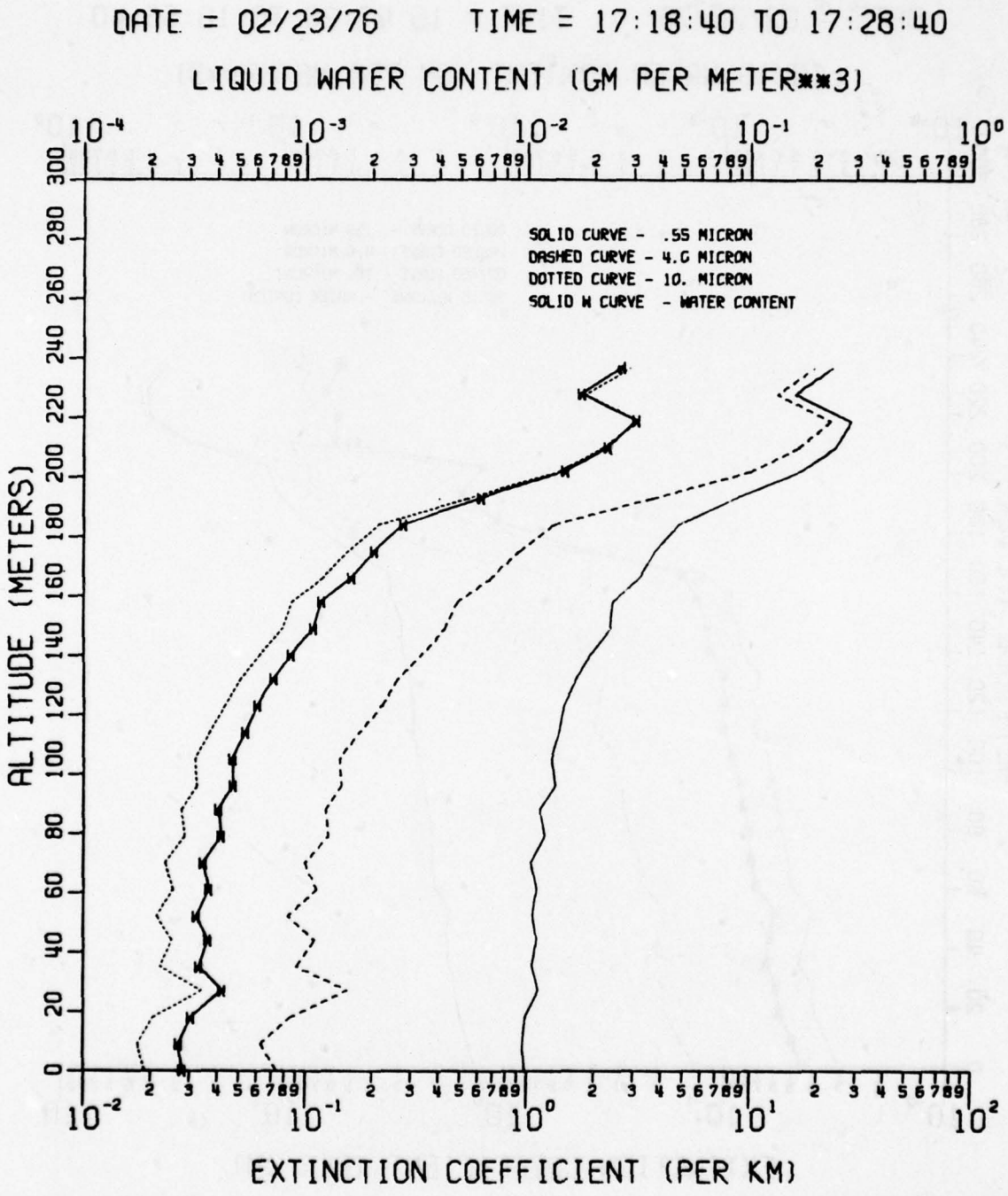
DATE = 02/23/76 TIME = 17:18:40 TO 17:28:40
LIQUID WATER CONTENT (GM PER METER**3)
SOLID CURVE - .55 MICRON
DASHED CURVE - 4.6 MICRON
DOTTED CURVE - 10. MICRON
SOLID W CURVE - WATER CONTENT
ALTITUDE (METERS)
EXTINCTION COEFFICIENT (PER KM)

Figure A4-j

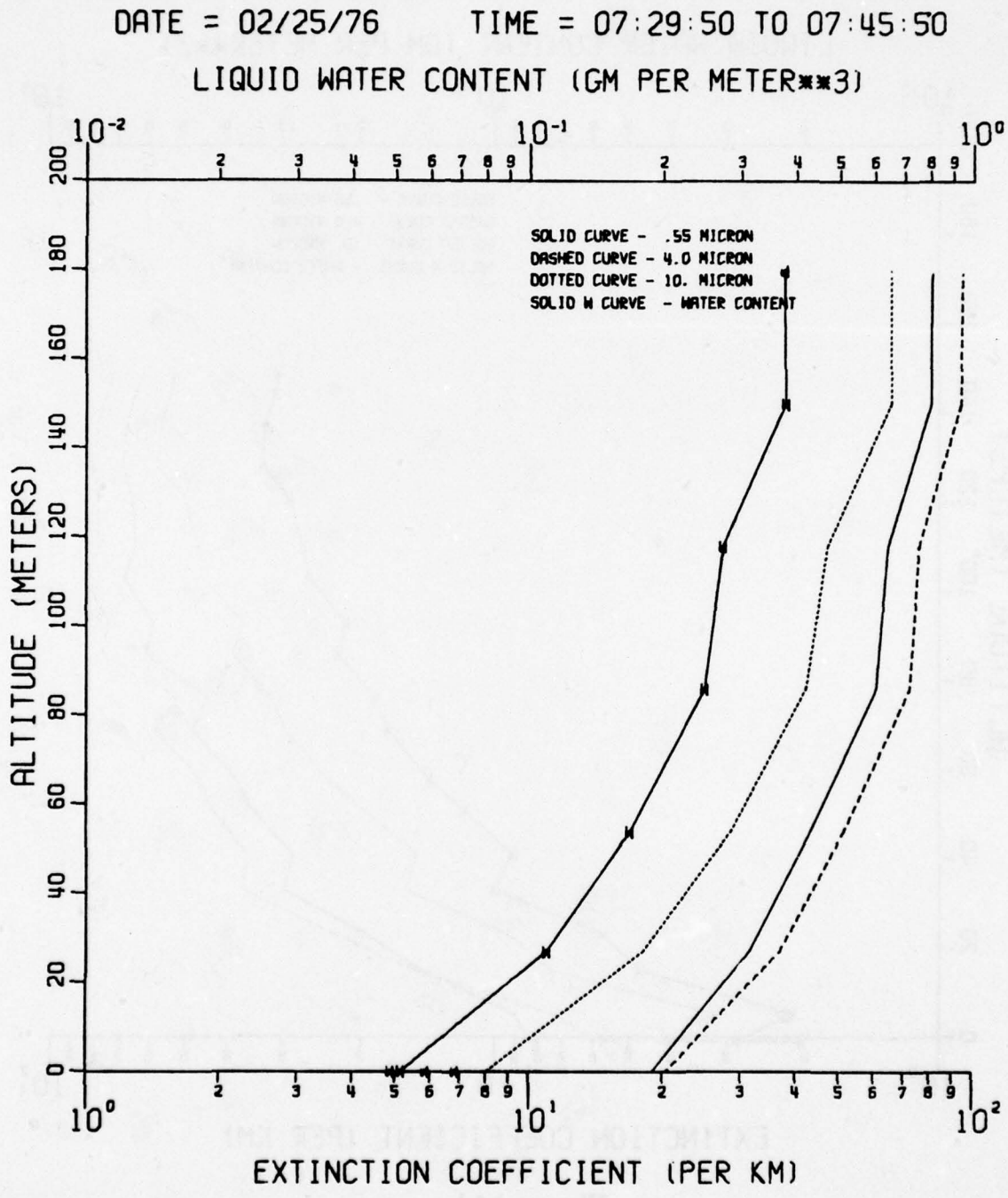
DATE = 02/25/76 TIME = 07:29:50 TO 07:45:50
LIQUID WATER CONTENT (GM PER METER**3)
SOLID CURVE - .55 MICRON
DASHED CURVE - 4.0 MICRON
DOTTED CURVE - 10. MICRON
SOLID W CURVE - WATER CONTENT
ALTITUDE (METERS)
EXTINCTION COEFFICIENT (PER KM)

Figure A4-k

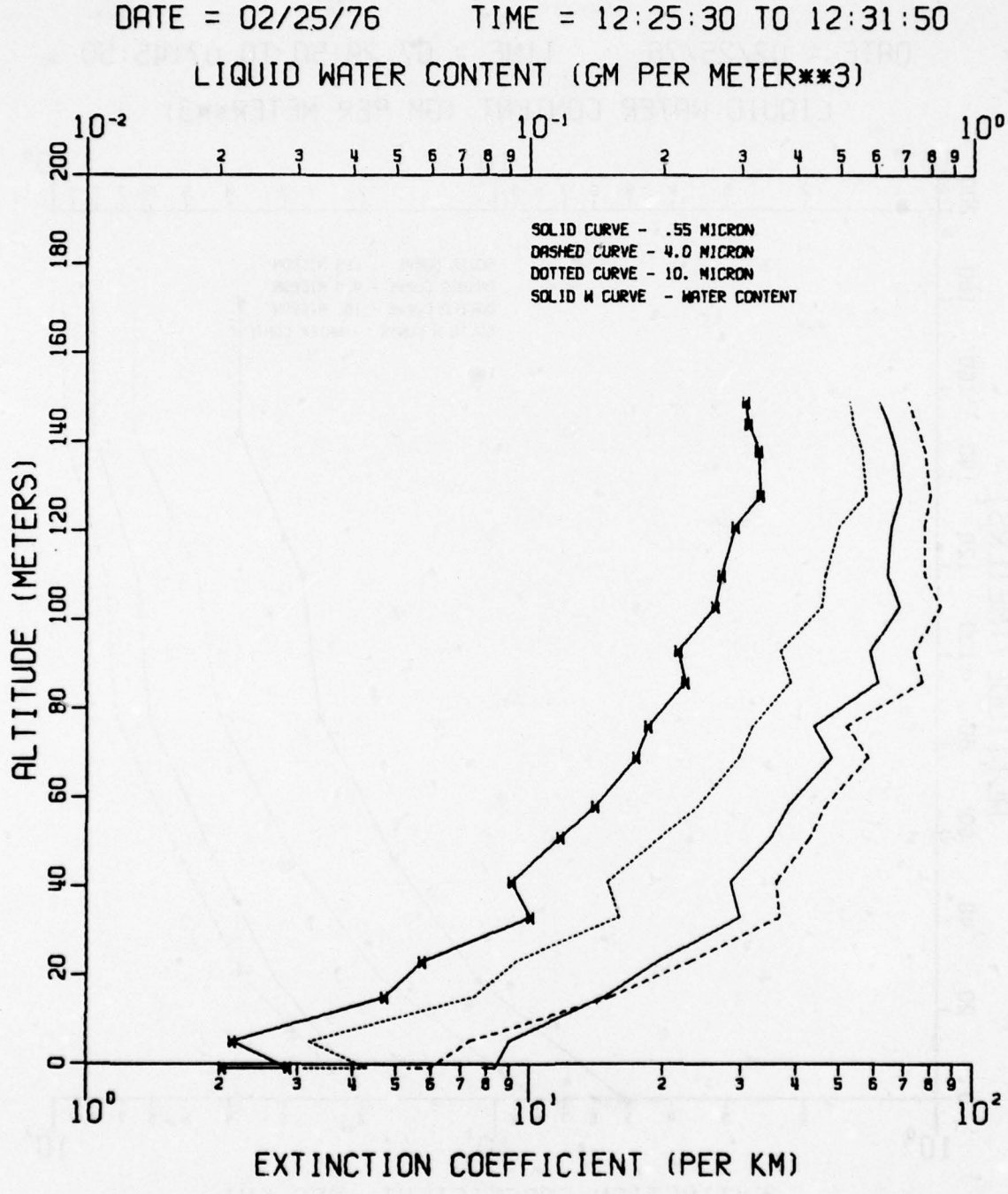
DATE = 02/25/76 TIME = 12:25:30 TO 12:31:50
LIQUID WATER CONTENT (GM PER METER**3)
SOLID CURVE - .55 MICRON
DASHED CURVE - 4.0 MICRON
DOTTED CURVE - 10. MICRON
SOLID W CURVE - WATER CONTENT
ALTITUDE (METERS)
EXTINCTION COEFFICIENT (PER KM)

Figure A4-1

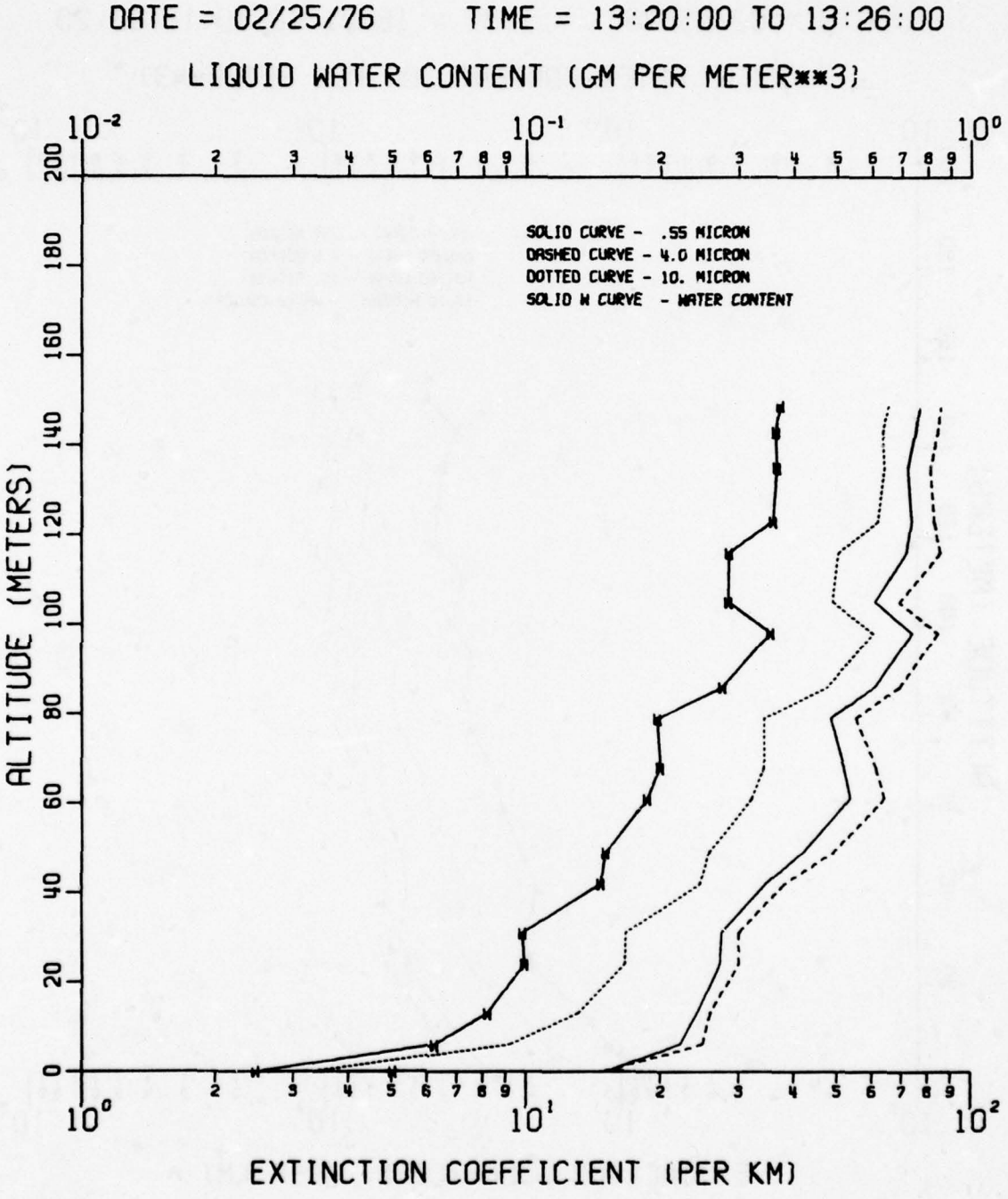
DATE = 02/25/76 TIME = 13:20:00 TO 13:26:00
LIQUID WATER CONTENT (GM PER METER**3)
SOLID CURVE - .55 MICRON
DASHED CURVE - 4.0 MICRON
DOTTED CURVE - 10. MICRON
SOLID W CURVE - WATER CONTENT
ALTITUDE (METERS)
EXTINCTION COEFFICIENT (PER KM)

Figure A4-m

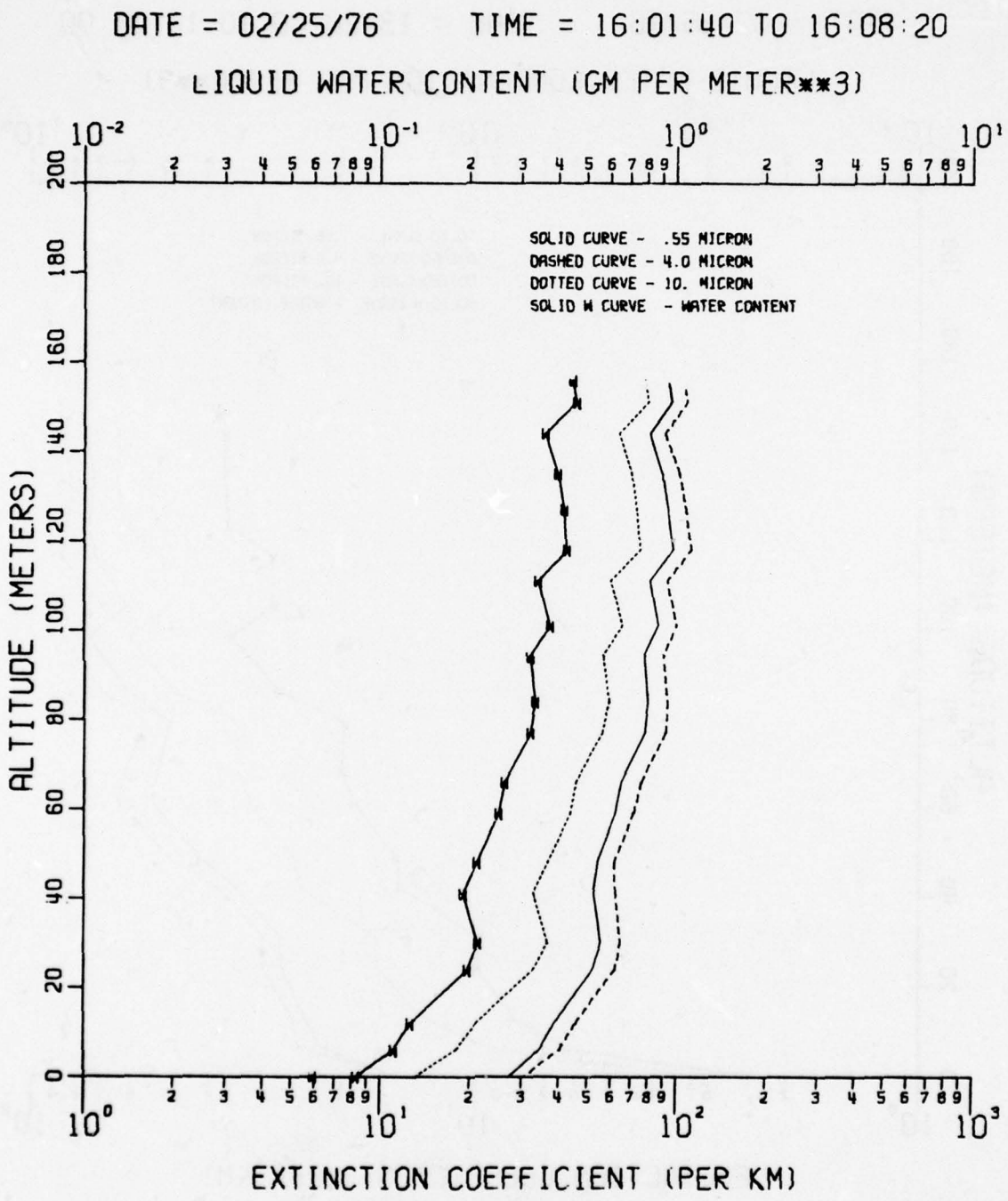
DATE = 02/25/76 TIME = 16:01:40 TO 16:08:20
LIQUID WATER CONTENT (GM PER METER**3)
SOLID CURVE - .55 MICRON
DASHED CURVE - 4.0 MICRON
DOTTED CURVE - 10. MICRON
SOLID W CURVE - WATER CONTENT
ALTITUDE (METERS)
EXTINCTION COEFFICIENT (PER KM)

Figure A4-n

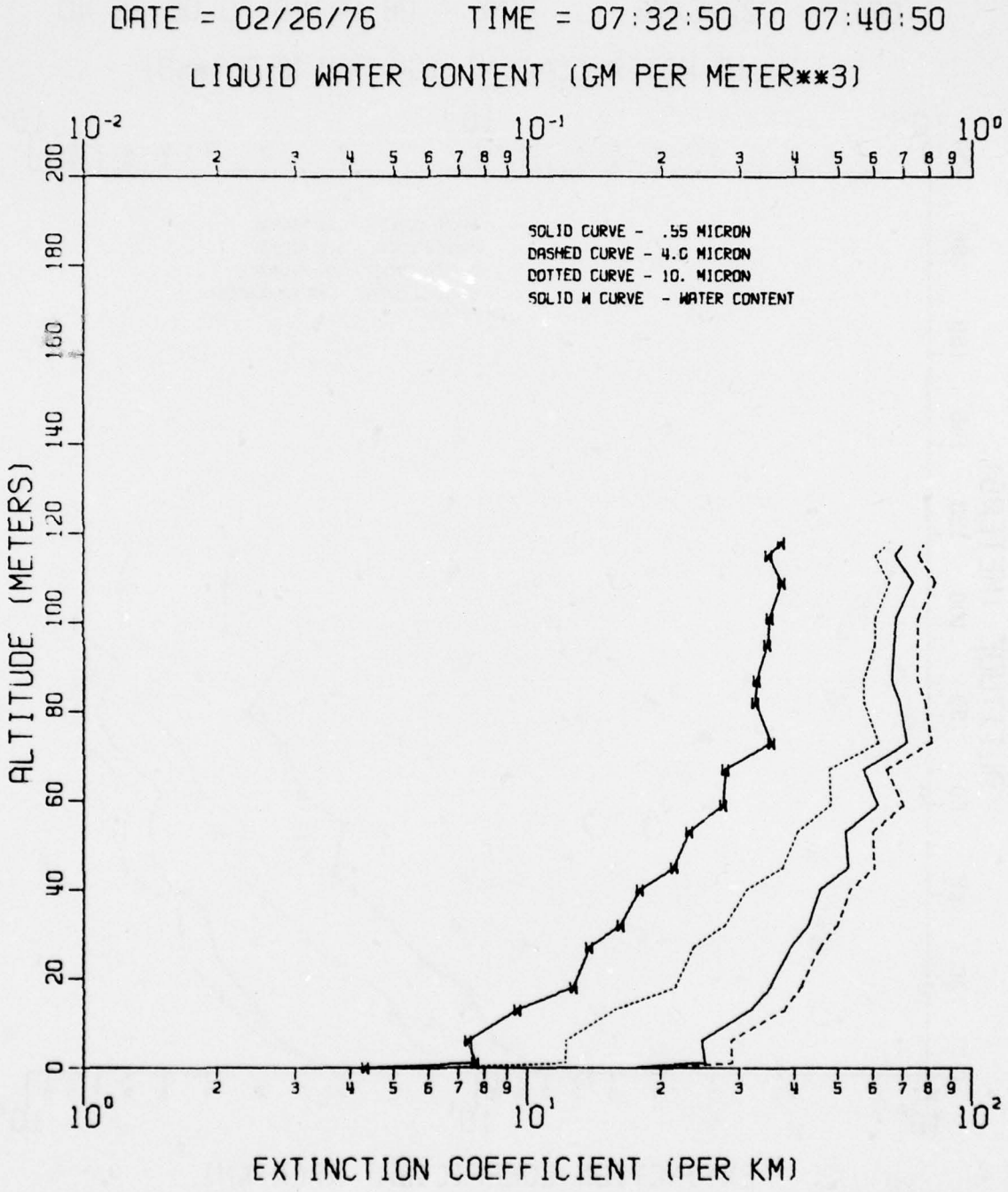
DATE = 02/26/76 TIME = 07:32:50 TO 07:40:50
LIQUID WATER CONTENT (GM PER METER**3)
SOLID CURVE - .55 MICRON
DASHED CURVE - 4.0 MICRON
DOTTED CURVE - 10. MICRON
SOLID W CURVE - WATER CONTENT
ALTITUDE (METERS)
EXTINCTION COEFFICIENT (PER KM)

Figure A4-o

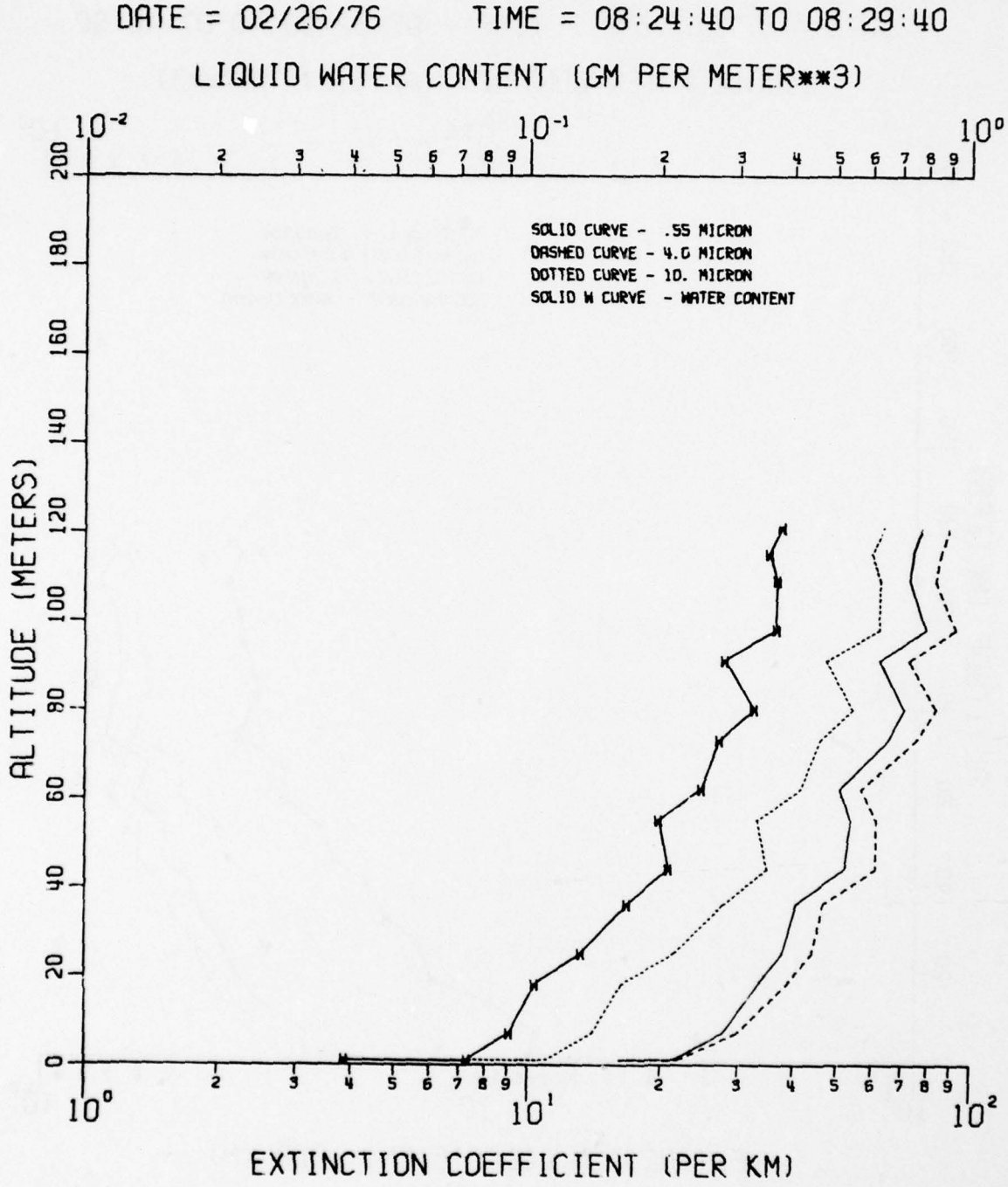
DATE = 02/26/76 TIME = 08:24:40 TO 08:29:40
LIQUID WATER CONTENT (GM PER METER**3)
SOLID CURVE - .55 MICRON
DASHED CURVE - 4.0 MICRON
DOTTED CURVE - 10. MICRON
SOLID W CURVE - WATER CONTENT
ALTITUDE (METERS)
EXTINCTION COEFFICIENT (PER KM)

Figure A4-p

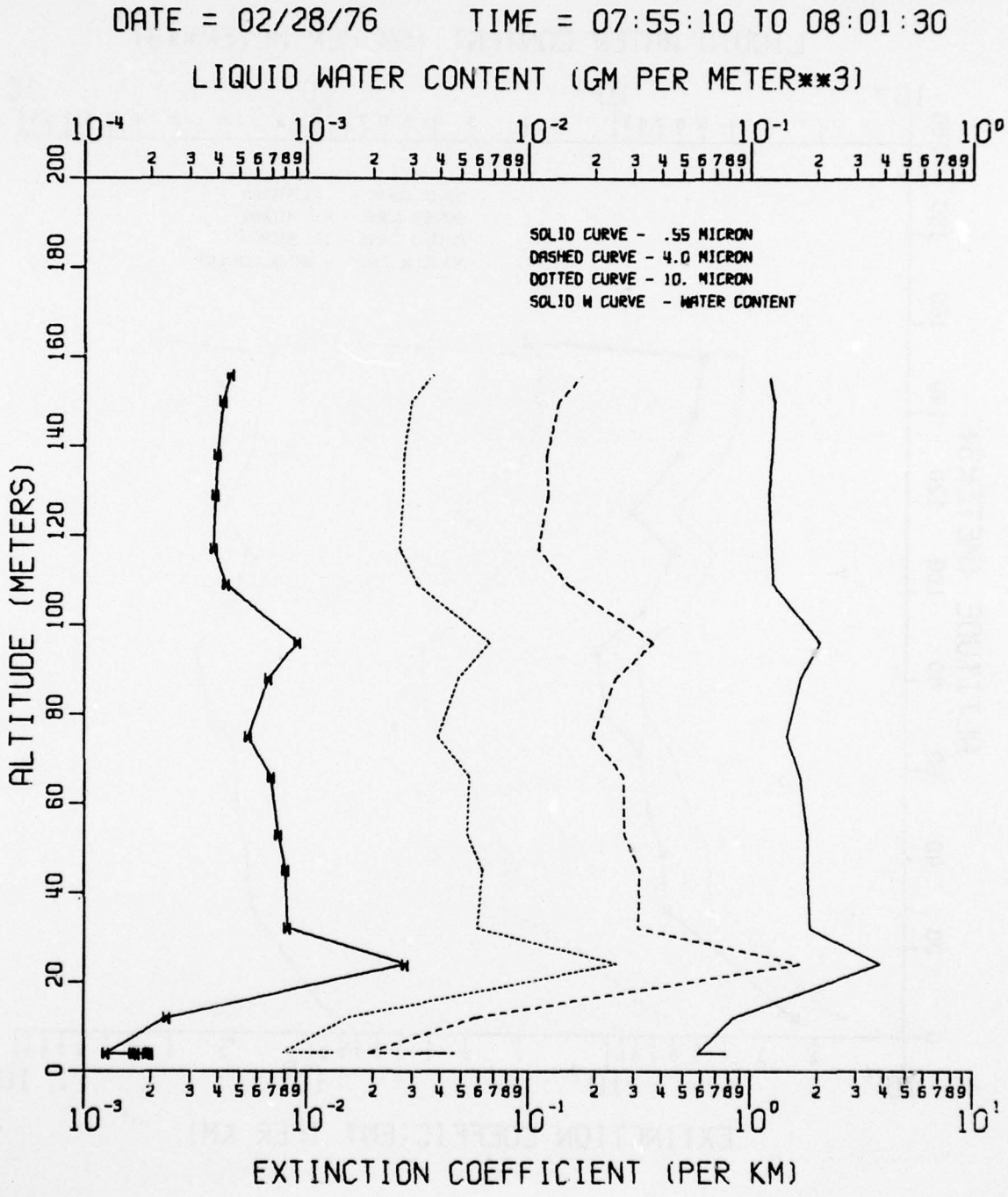
DATE = 02/28/76 TIME = 07:55:10 TO 08:01:30
LIQUID WATER CONTENT (GM PER METER**3)
SOLID CURVE - .55 MICRON
DASHED CURVE - 4.0 MICRON
DOTTED CURVE - 10. MICRON
SOLID W CURVE - WATER CONTENT
ALTITUDE (METERS)
EXTINCTION COEFFICIENT (PER KM)

Figure A4-q

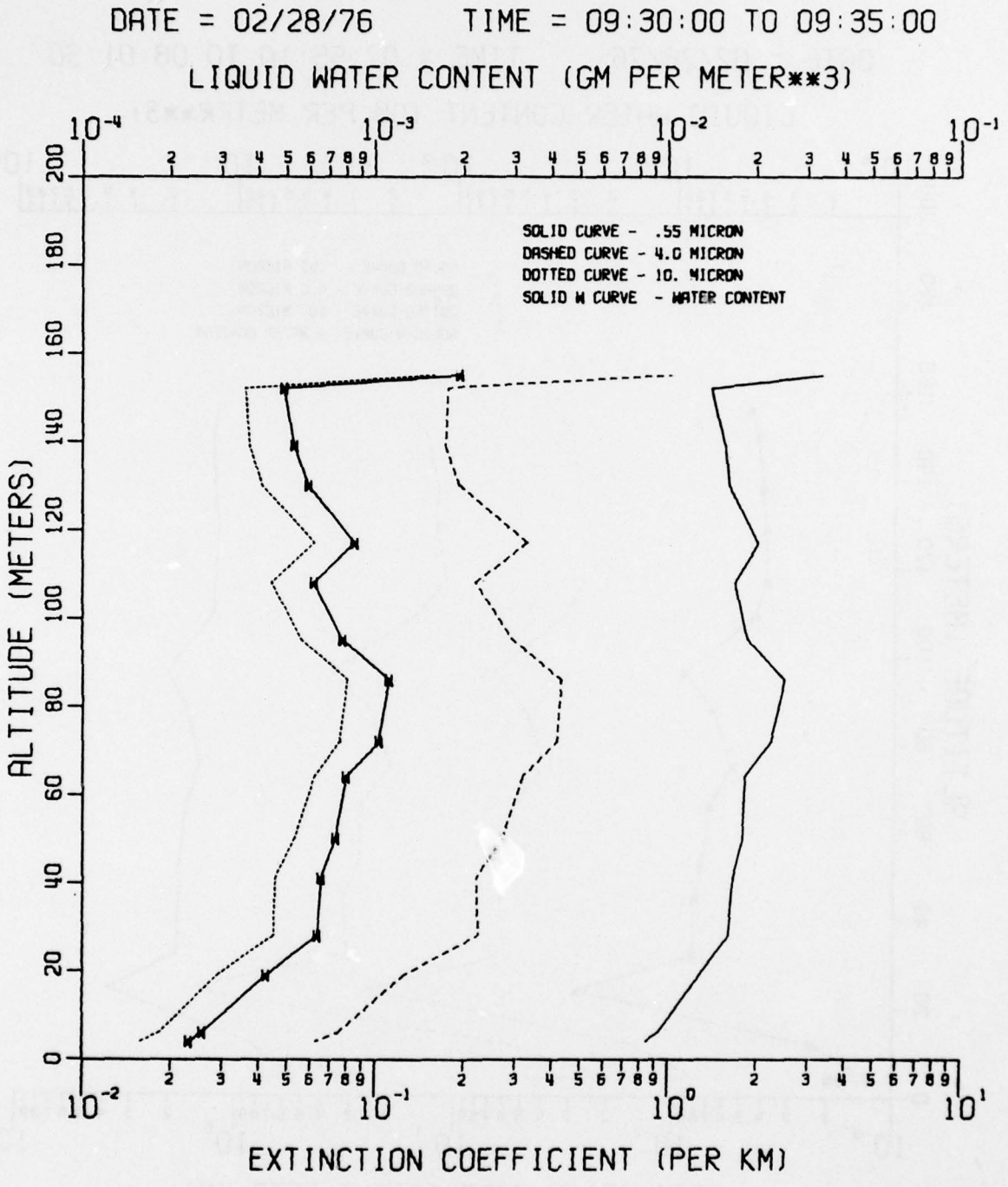
DATE = 02/28/76 TIME = 09:30:00 TO 09:35:00
LIQUID WATER CONTENT (GM PER METER**3)
SOLID CURVE - .55 MICRON
DASHED CURVE - 4.0 MICRON
DOTTED CURVE - 10. MICRON
SOLID W CURVE - WATER CONTENT
ALTITUDE (METERS)
EXTINCTION COEFFICIENT (PER KM)

Figure A4-r

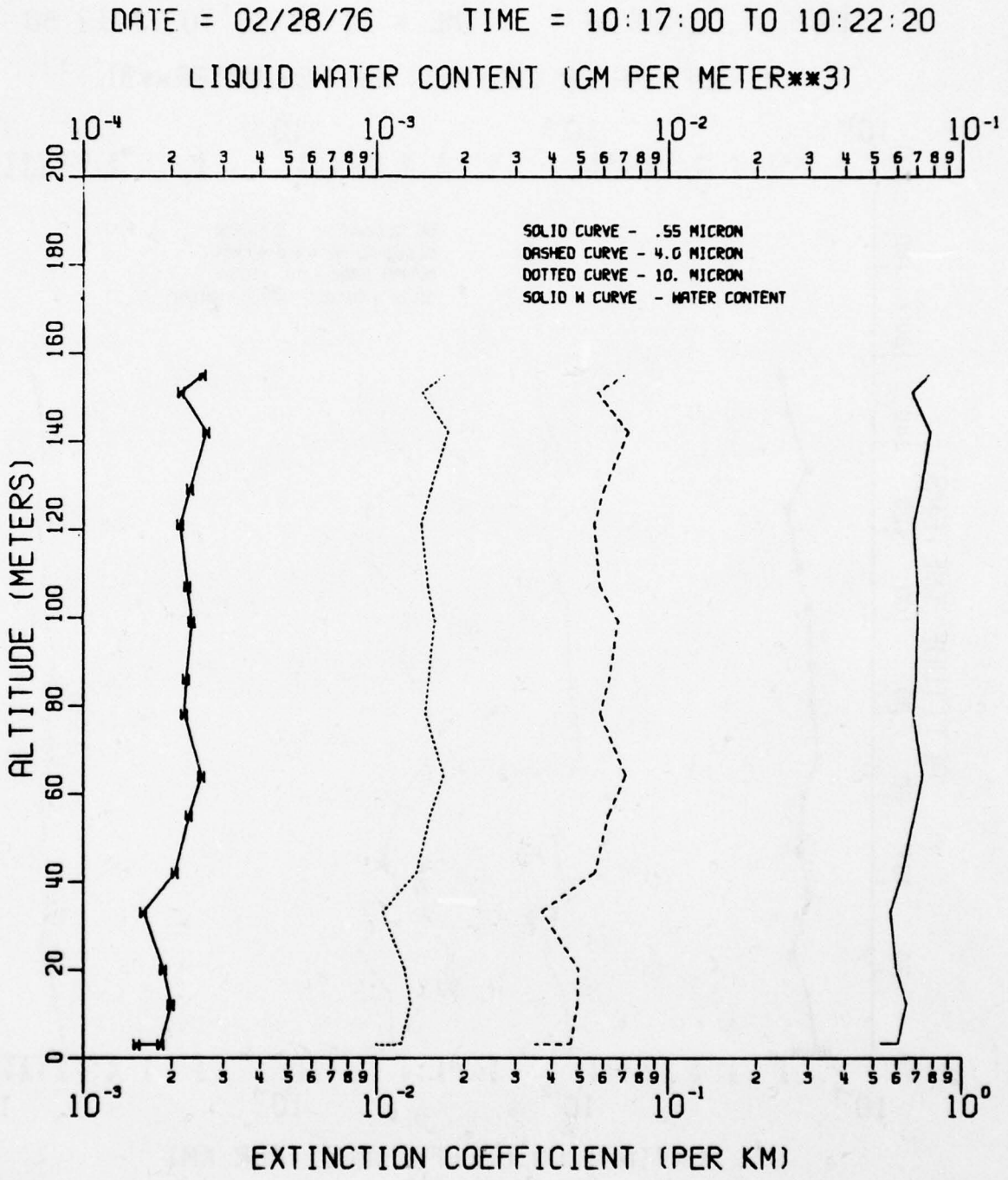
DATE = 02/28/76 TIME = 10:17:00 TO 10:22:20
LIQUID WATER CONTENT (GM PER METER**3)
SOLID CURVE - .55 MICRON
DASHED CURVE - 4.0 MICRON
DOTTED CURVE - 10. MICRON
SOLID W CURVE - WATER CONTENT
ALTITUDE (METERS)
EXTINCTION COEFFICIENT (PER KM)

Figure A4-s

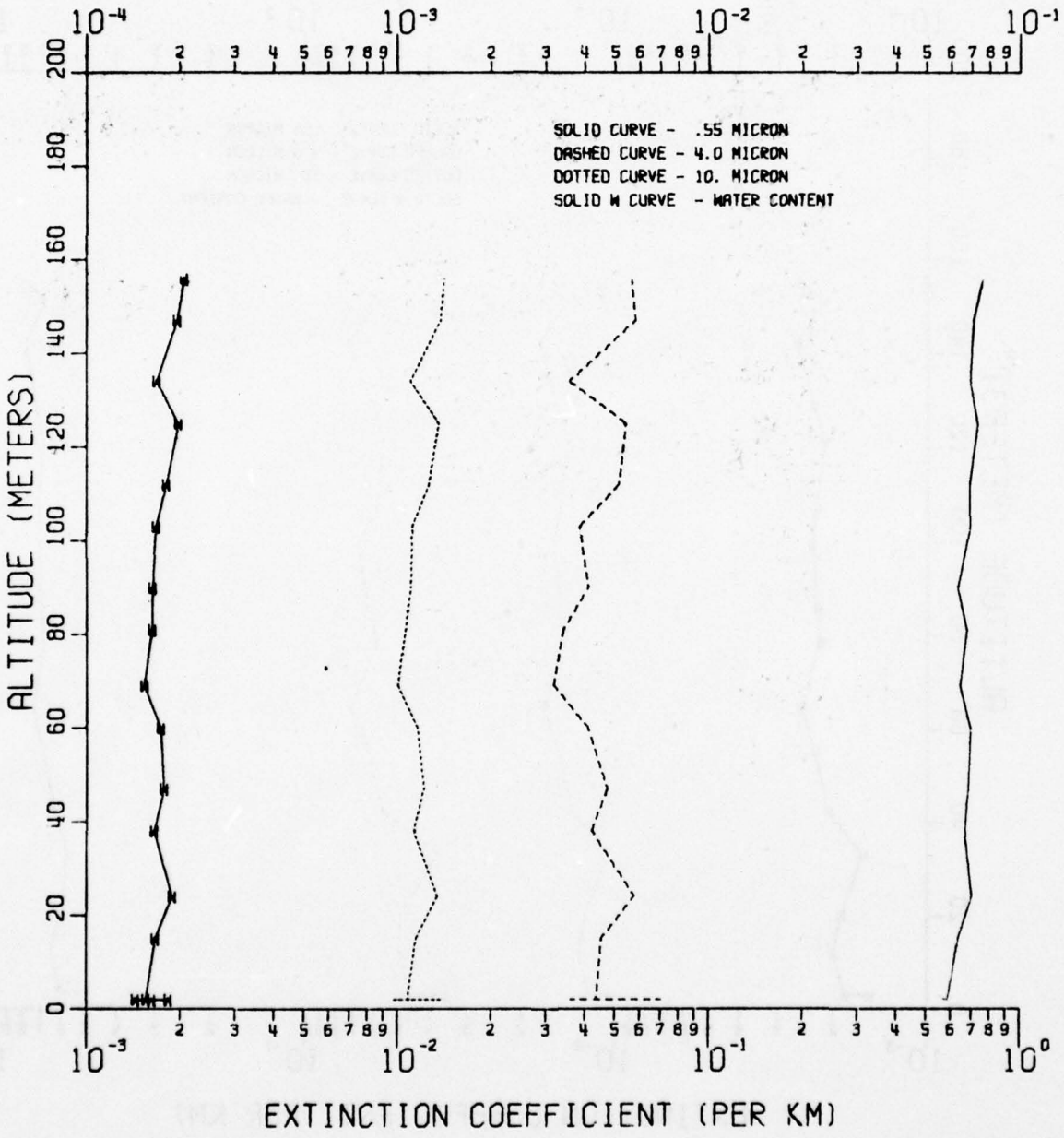
DATE = 02/28/76 TIME = 11:07:10 TO 11:12:50
LIQUID WATER CONTENT (GM PER METER**3)
SOLID CURVE - .55 MICRON
DASHED CURVE - 4.0 MICRON
DOTTED CURVE - 10. MICRON
SOLID W CURVE - WATER CONTENT
ALTITUDE (METERS)
EXTINCTION COEFFICIENT (PER KM)

Figure A4-t

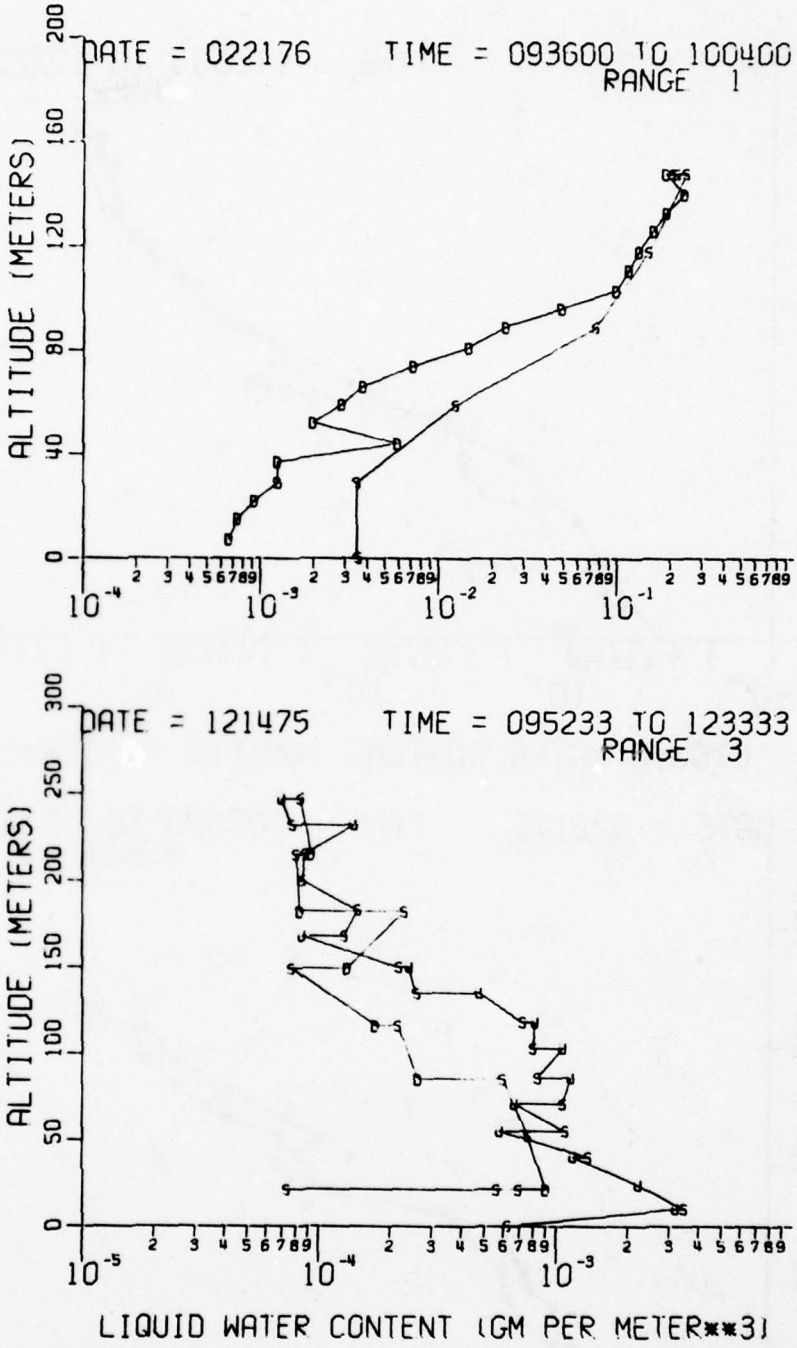

Figure A5-a. Profiles of liquid water content inferred from particle size distribution measurements (shown in Fig. A1) made with a balloon-borne aerosol counter. Both upleg and downleg portions of each traverse are presented. The u, s, and d symbols indicate the aerosol counter was moving upward, was stationary, or was moving downward during the measurement period. The date, local time (hours, minutes, seconds) and time interval for the measurements are given, along with the size range setting (see Fig. 4) of the aerosol counter.

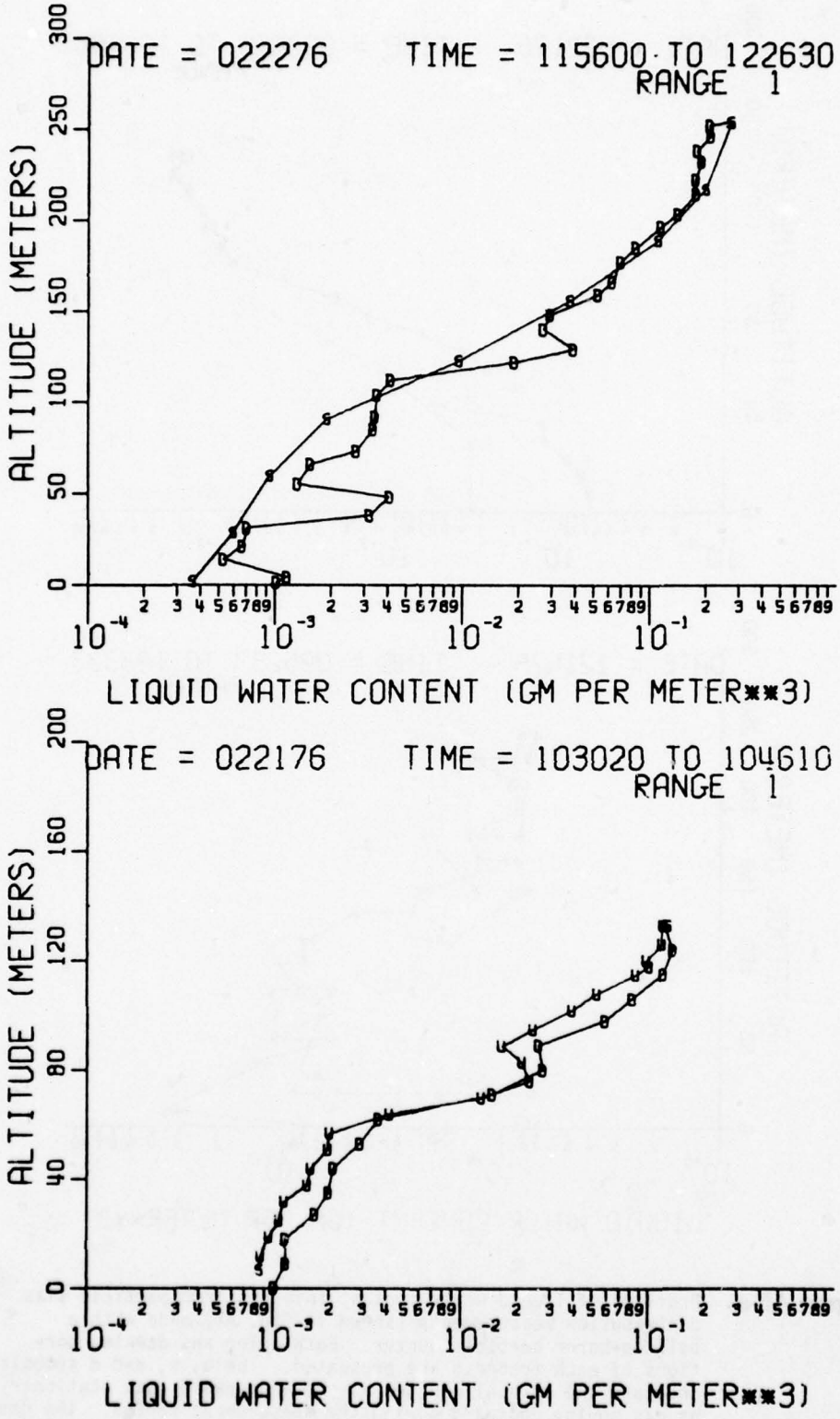
DATE = 022276 TIME = 115600 TO 122630
RANGE 1
ALTITUDE (METERS)
0
50
100
150
200
250
300
LIQUID WATER CONTENT (GM PER METER**3)
DATE = 022176 TIME = 103020 TO 104610
RANGE 1
ALTITUDE (METERS)
0
40
80
120
160
200
LIQUID WATER CONTENT (GM PER METER**3)

Figure A5-b

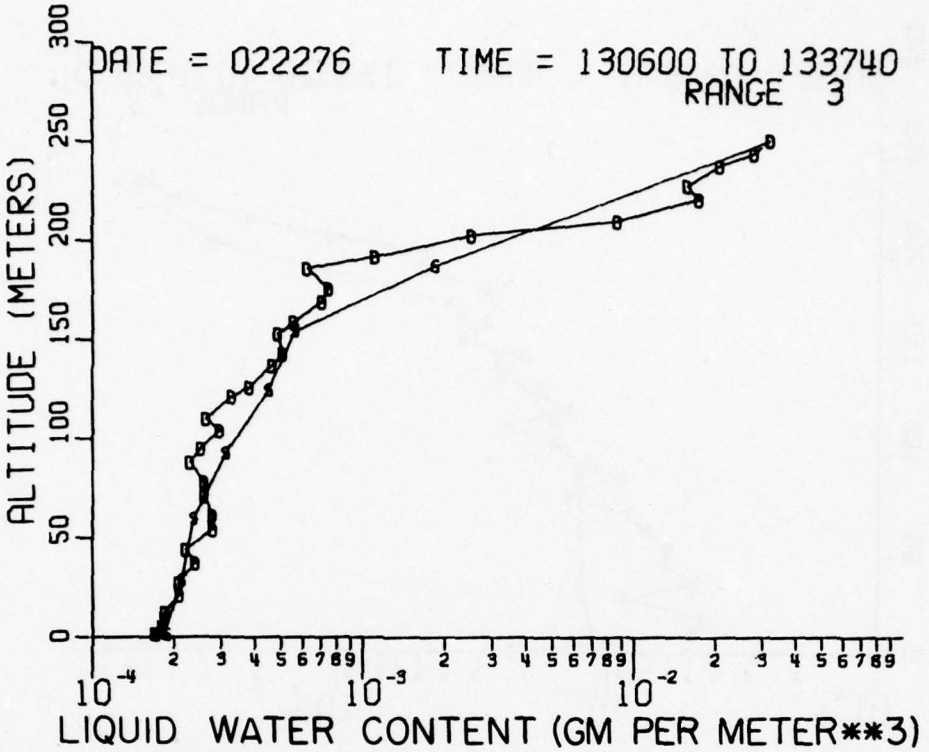
DATE = 022276
TIME = 130600 TO 133740
RANGE 3
ALTITUDE (METERS)
0
50
100
150
200
250
300
10^{-4}
10^{-3}
10^{-2}
LIQUID WATER CONTENT (GM PER METER**3)

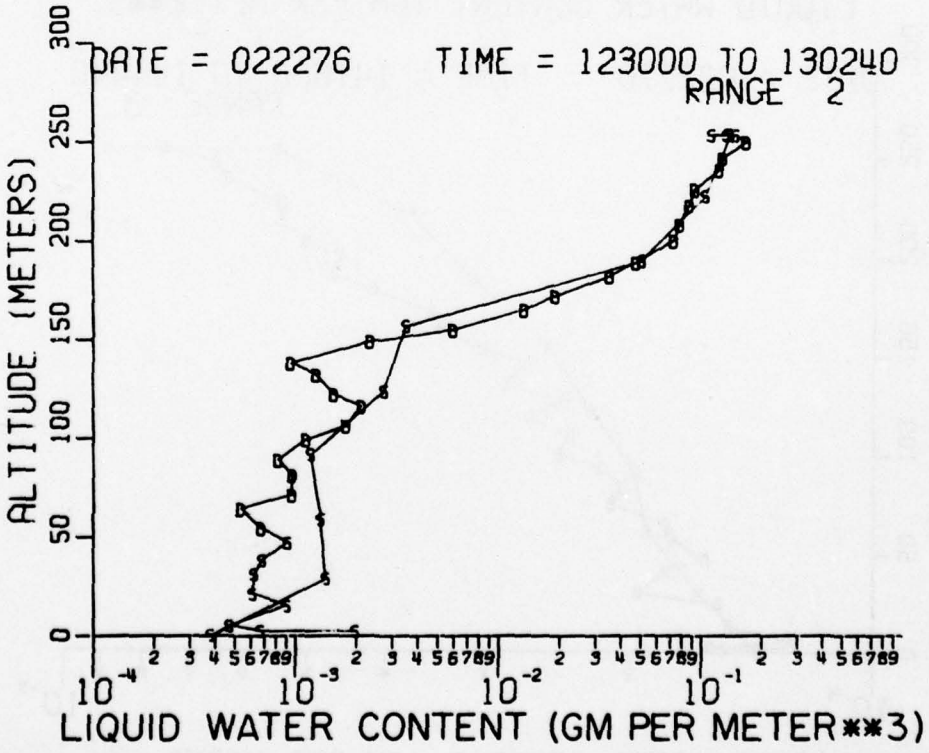
DATE = 022276
TIME = 123000 TO 130240
RANGE 2
ALTITUDE (METERS)
0
50
100
150
200
250
300
10^{-4}
10^{-3}
10^{-2}
10^{-1}
LIQUID WATER CONTENT (GM PER METER**3)

Figure A5-c

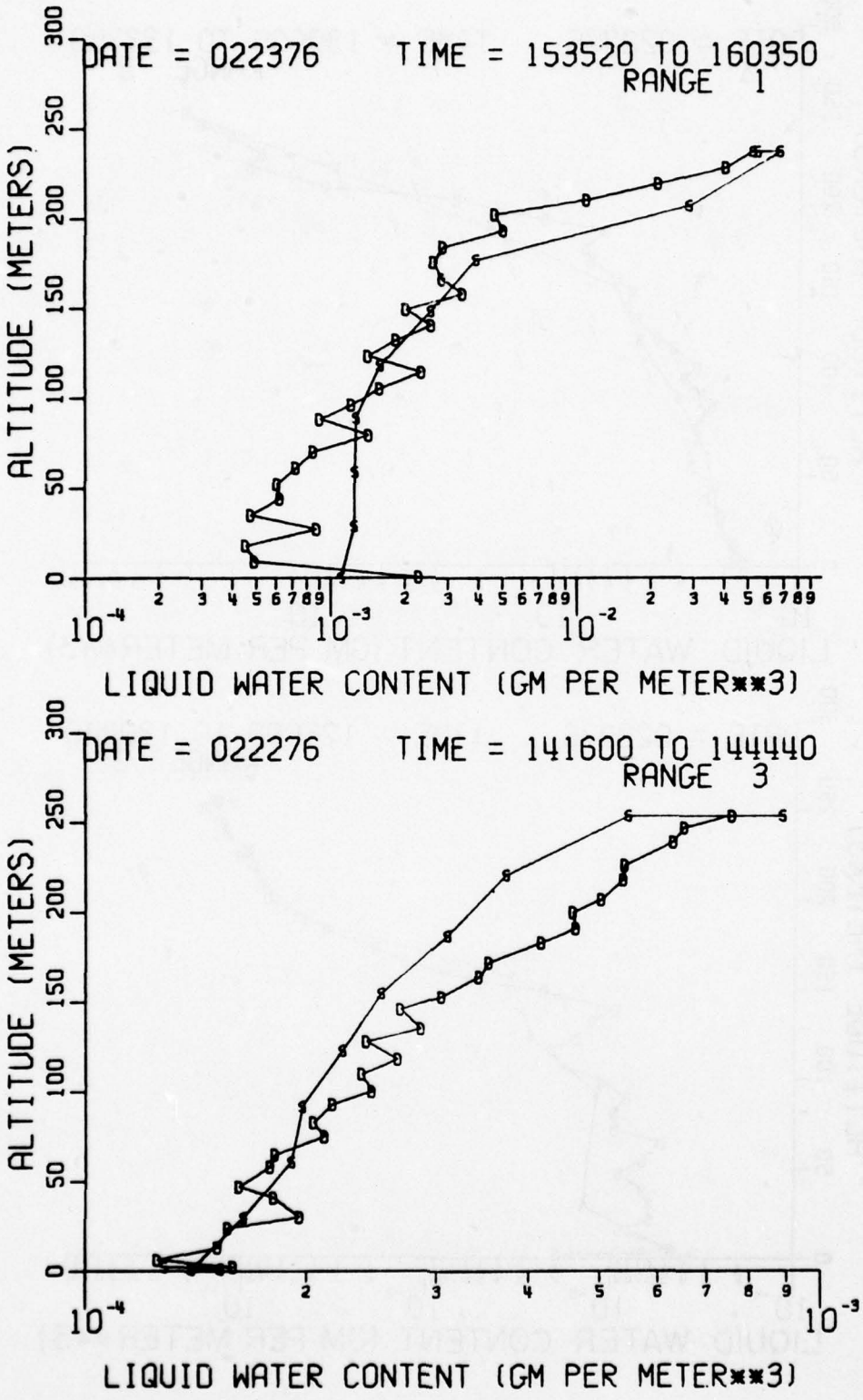
DATE = 022376 TIME = 153520 TO 160350
RANGE 1
ALTITUDE (METERS)
0
50
100
150
200
250
300
10^{-4}
10^{-3}
10^{-2}
LIQUID WATER CONTENT (GM PER METER**3)
DATE = 022276 TIME = 141600 TO 144440
RANGE 3
ALTITUDE (METERS)
10^{-4}
10^{-3}
LIQUID WATER CONTENT (GM PER METER**3)

Figure A5-d

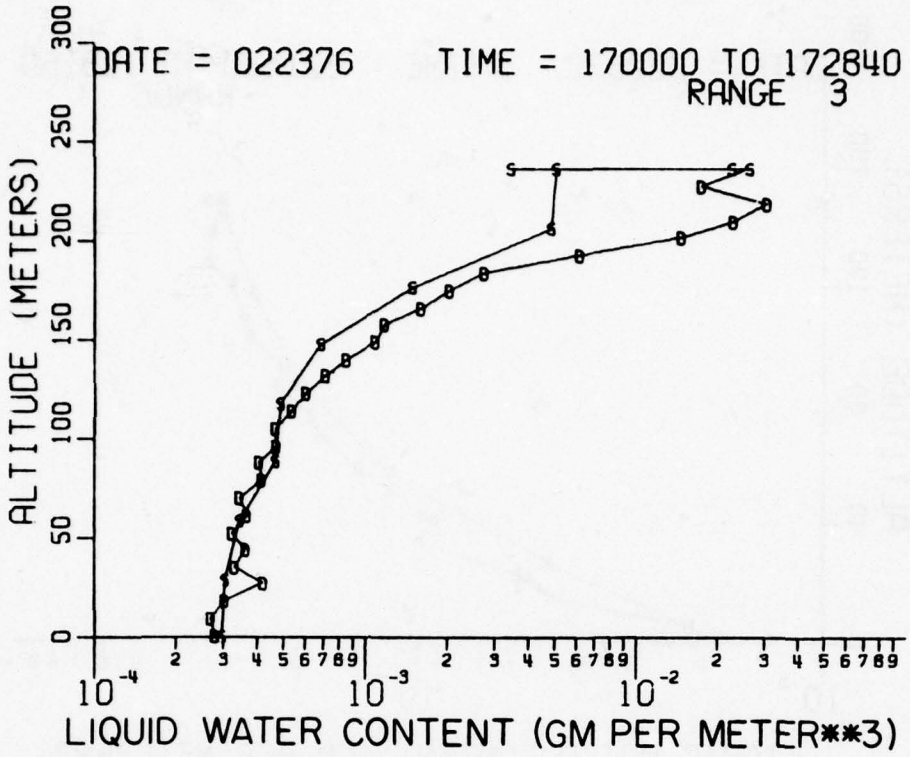
DATE = 022376 TIME = 170000 TO 172840
RANGE 3
ALTITUDE (METERS)
0
50
100
150
200
250
300
10^{-4}
10^{-3}
10^{-2}
LIQUID WATER CONTENT (GM PER METER**3)

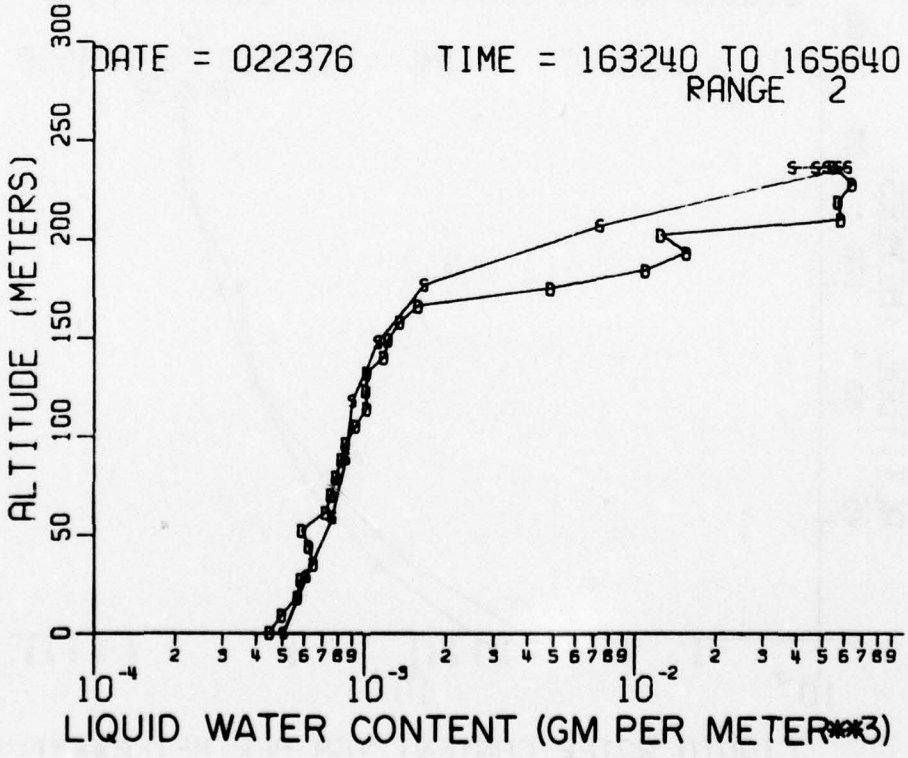
DATE = 022376 TIME = 163240 TO 165640
RANGE 2
ALTITUDE (METERS)
0
50
100
150
200
250
300
10^{-4}
10^{-3}
10^{-2}
LIQUID WATER CONTENT (GM PER METER**3)

Figure A5-e

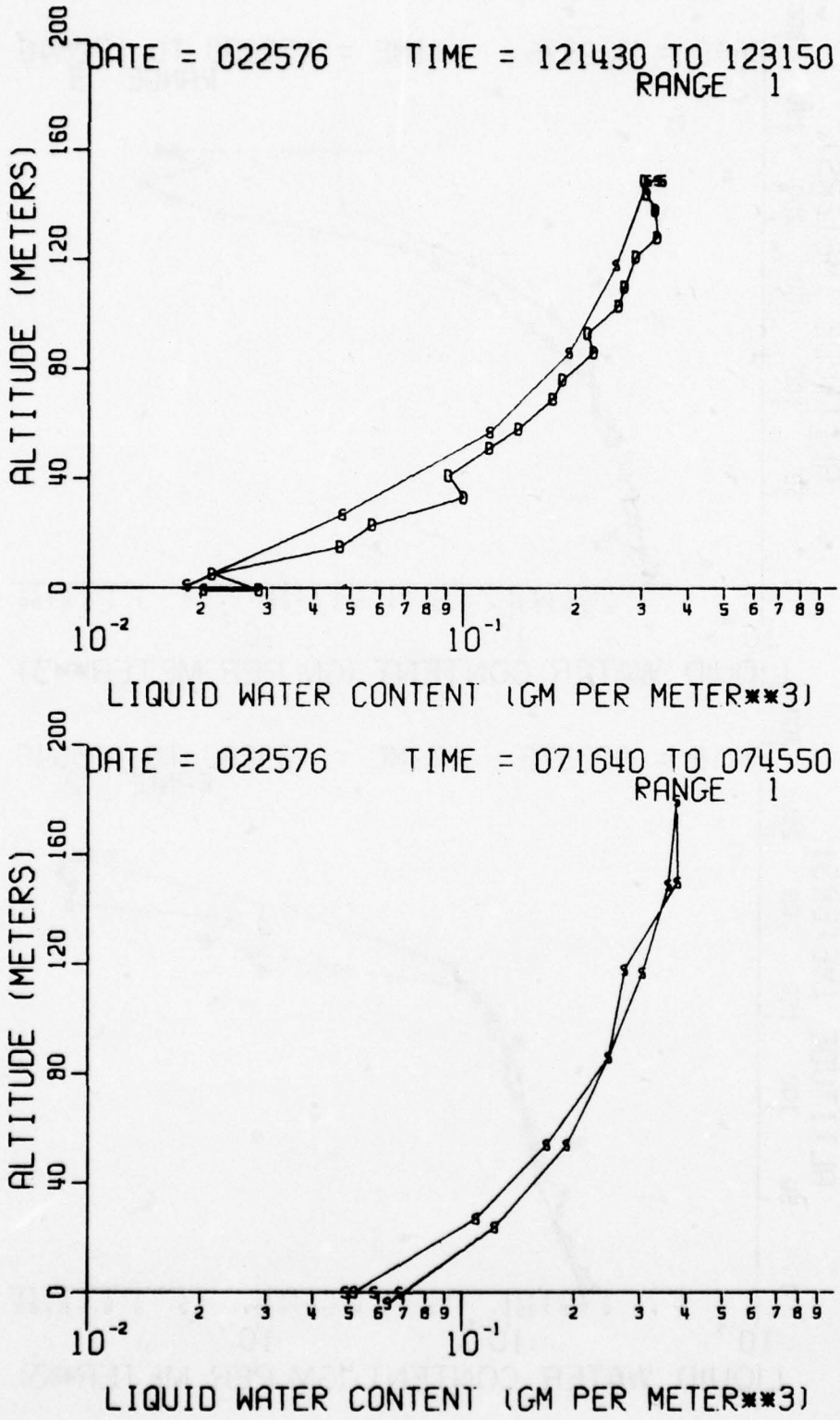
DATE = 022576 TIME = 121430 TO 123150
RANGE 1
ALTITUDE (METERS)
0
40
80
120
160
200
2 3 4 5 6 7 8 9
10^{-2}
10^{-1}
2 3 4 5 6 7 8 9
LIQUID WATER CONTENT (GM PER METER**3)
DATE = 022576 TIME = 071640 TO 074550
RANGE 1
ALTITUDE (METERS)
0
40
80
120
160
200
2 3 4 5 6 7 8 9
10^{-2}
10^{-1}
2 3 4 5 6 7 8 9
LIQUID WATER CONTENT (GM PER METER**3)

Figure A5-f

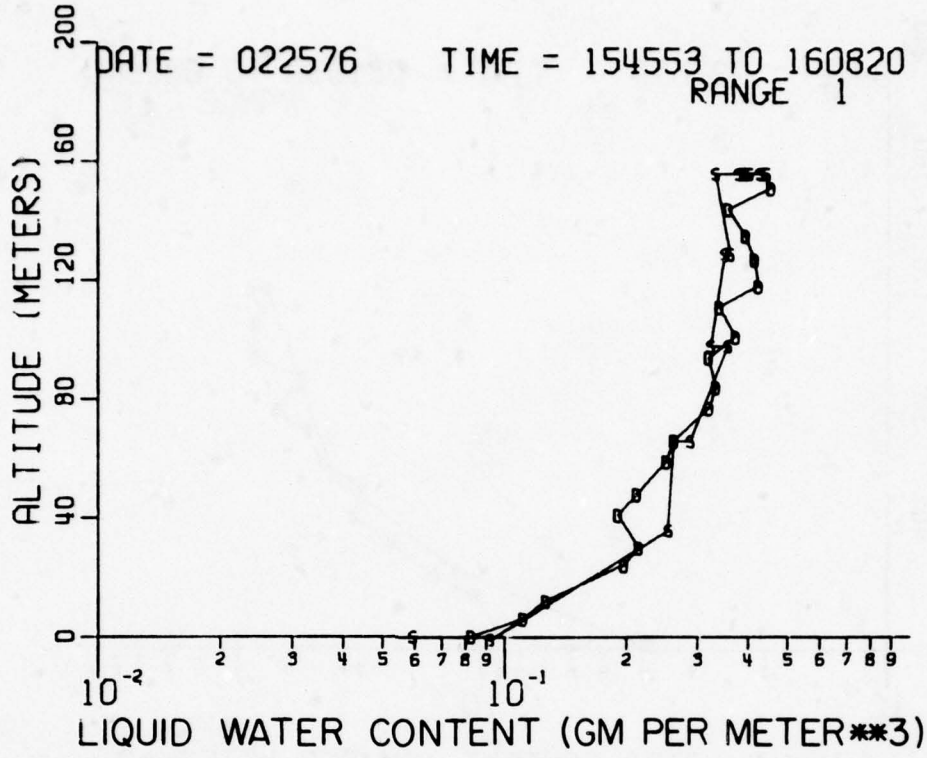
DATE = 022576
TIME = 154553 TO 160820
RANGE 1
ALTITUDE (METERS)
0
40
80
120
160
200
10^{-2}
10^{-1}
LIQUID WATER CONTENT (GM PER METER**3)

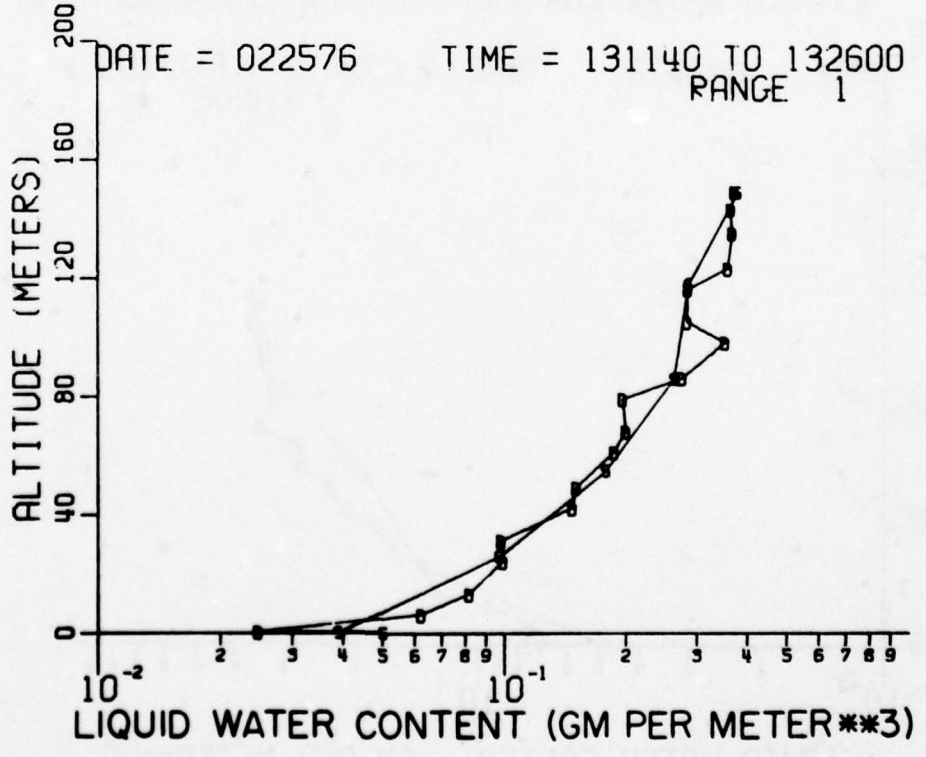
DATE = 022576
TIME = 131140 TO 132600
RANGE 1
ALTITUDE (METERS)
0
40
80
120
160
200
10^{-2}
10^{-1}
LIQUID WATER CONTENT (GM PER METER**3)

Figure A5-g

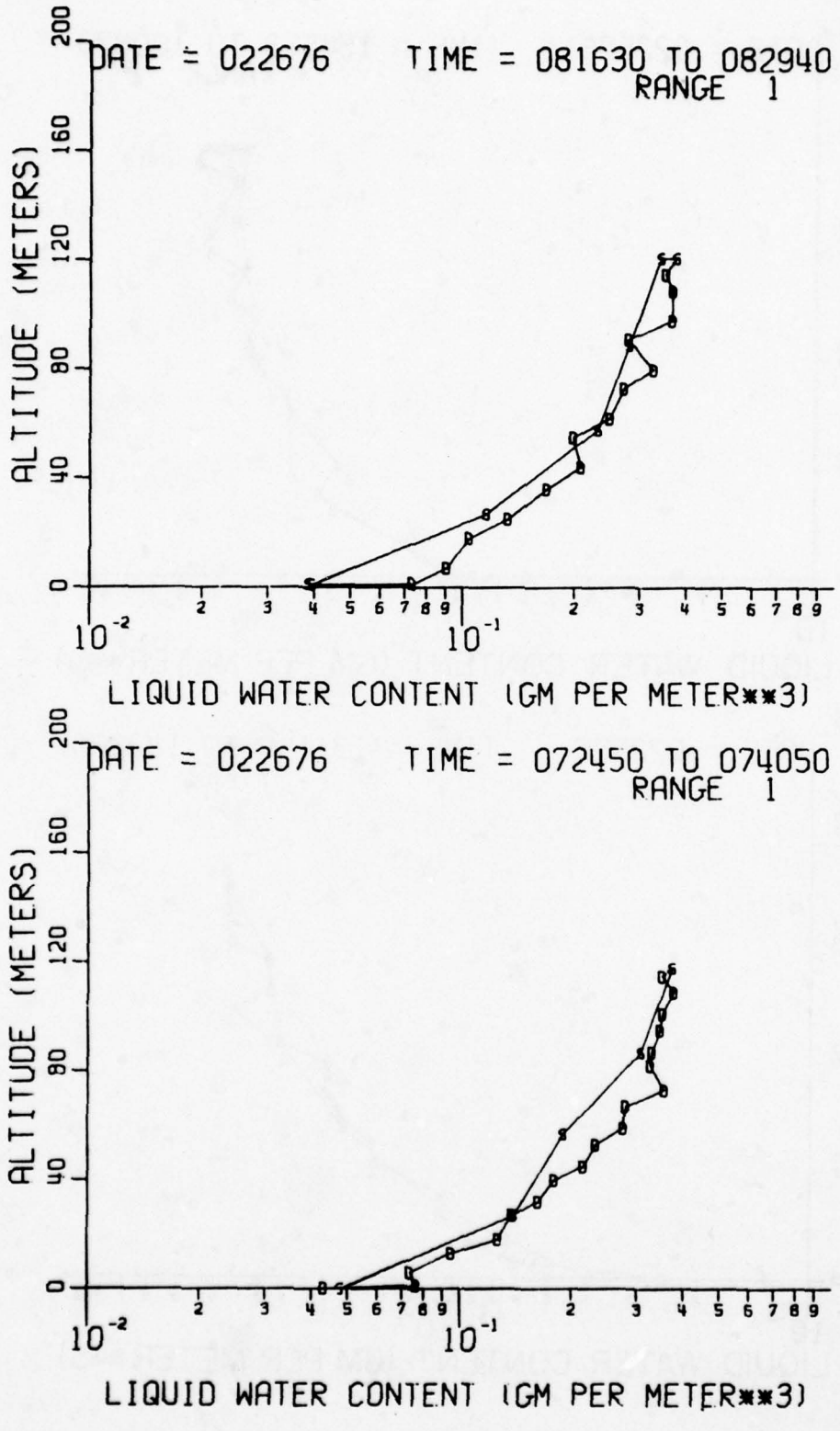
DATE = 022676 TIME = 081630 TO 082940
RANGE 1
ALTITUDE (METERS)
0
40
80
120
160
200
10^{-2}
10^{-1}
2 3 4 5 6 7 8 9
LIQUID WATER CONTENT (GM PER METER**3)
DATE = 022676 TIME = 072450 TO 074050
RANGE 1
ALTITUDE (METERS)
LIQUID WATER CONTENT (GM PER METER**3)

Figure A5-h

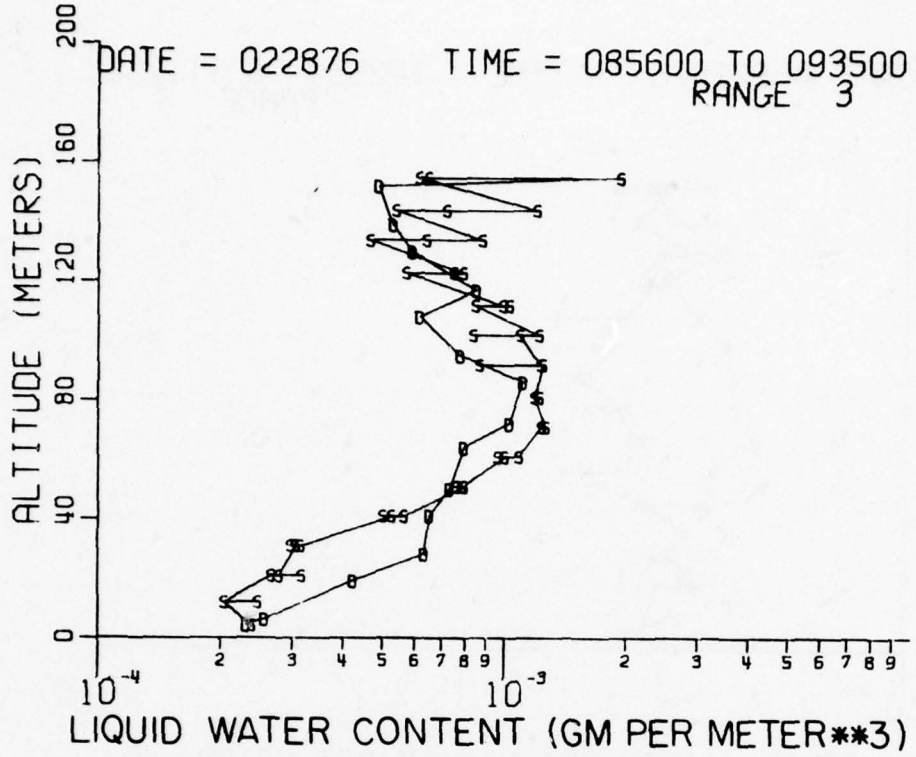
DATE = 022876 TIME = 085600 TO 093500
RANGE 3
ALTITUDE (METERS)
0
40
80
120
160
200
2 3 4 5 6 7 8 9
10^{-4}
10^{-3}
LIQUID WATER CONTENT (GM PER METER**3)

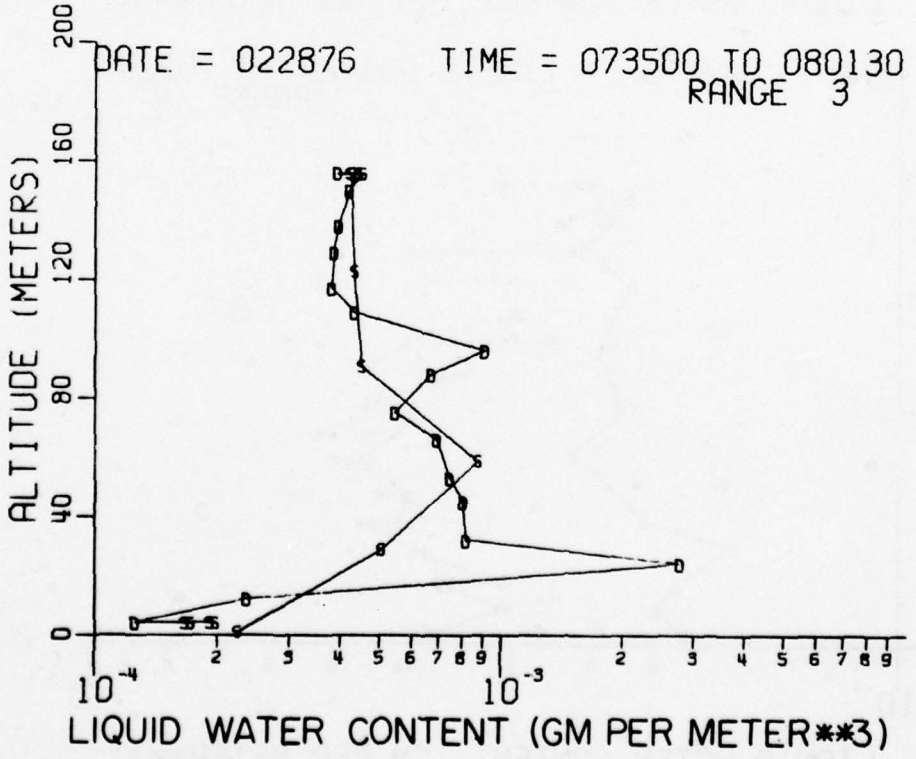
DATE = 022876 TIME = 073500 TO 080130
RANGE 3
ALTITUDE (METERS)
0
40
80
120
160
200
2 3 4 5 6 7 8 9
10^{-4}
10^{-3}
LIQUID WATER CONTENT (GM PER METER**3)

Figure A5-i

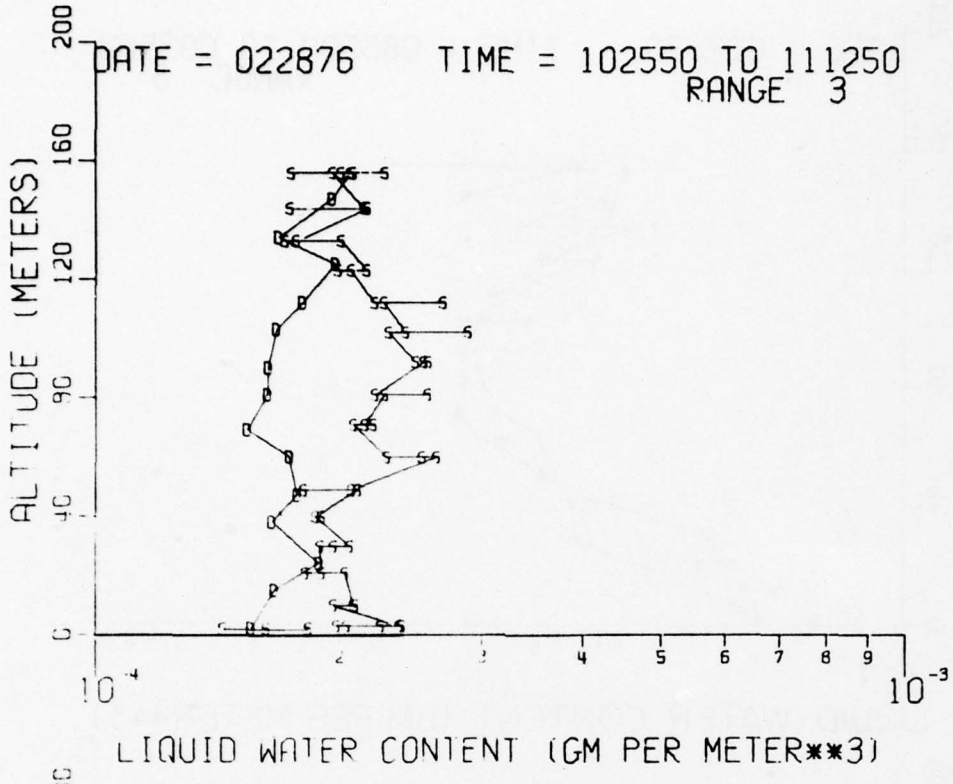
DATE = 022876 TIME = 102550 TO 111250
RANGE 3
ALTITUDE (METERS)
200
160
120
80
40
0
10^-4
10^-3
LIQUID WATER CONTENT (GM PER METER**3)

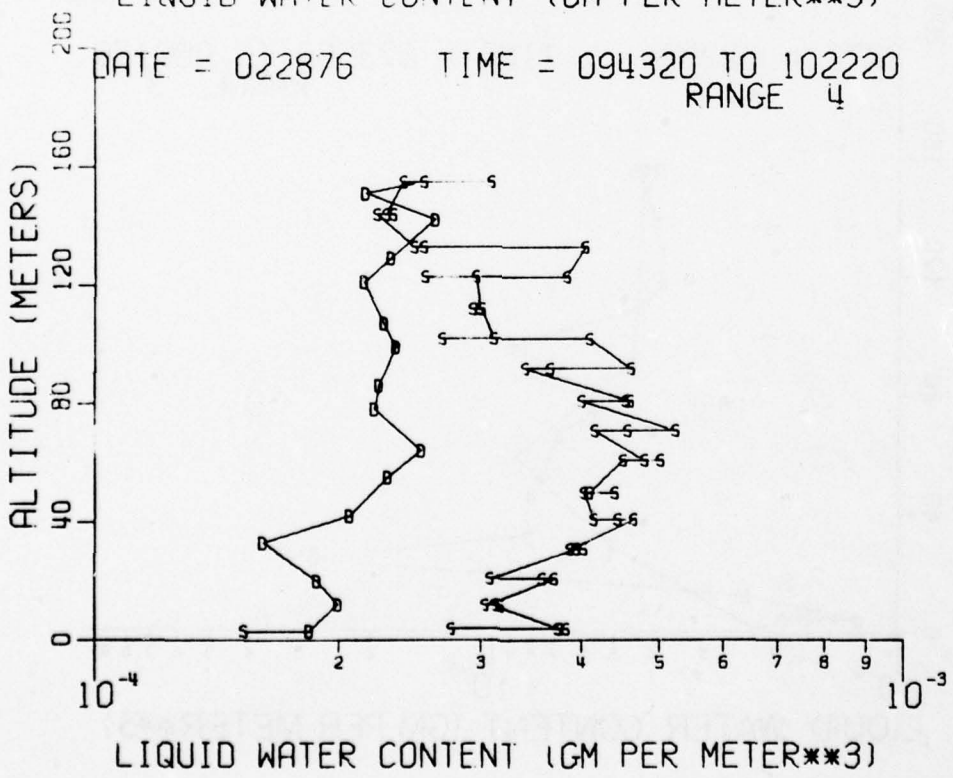
DATE = 022876 TIME = 094320 TO 102220
RANGE 4
ALTITUDE (METERS)
200
160
120
80
40
0
10^-4
10^-3
LIQUID WATER CONTENT (GM PER METER**3)

Figure A5-j

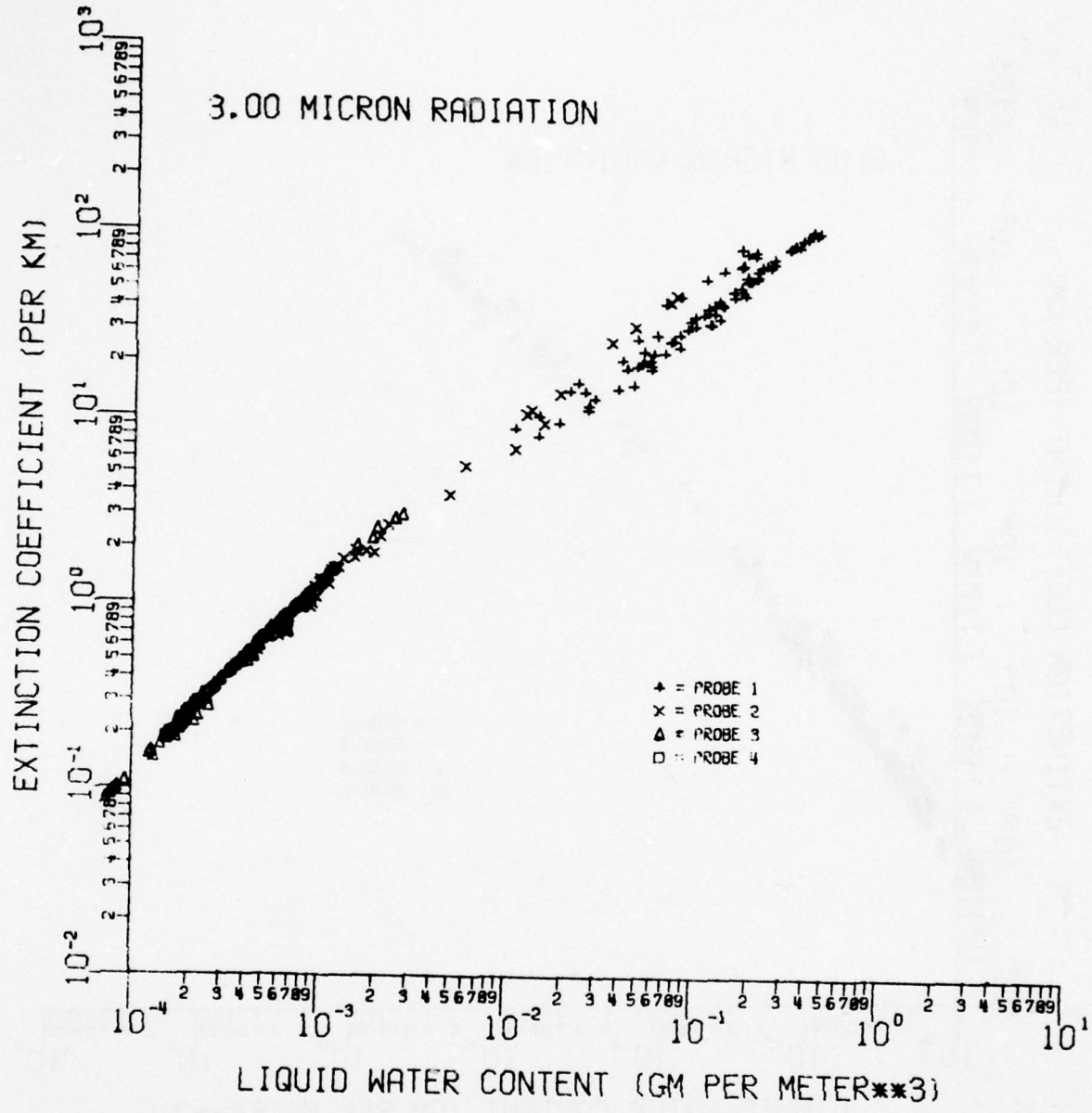

Figure A6-a. Values of the Mie theory calculated particulate extinction at 3μm, 5μm, 8μm, 11μm, and 12μm wavelengths versus liquid water content for a variety of particle size distributions of atmospheric fog and haze. The probe range setting 1-4 indicates the particle counter used to make the size distribution measurements on which this data is based was set on different size ranges of sensitivity (as per Fig. 4).

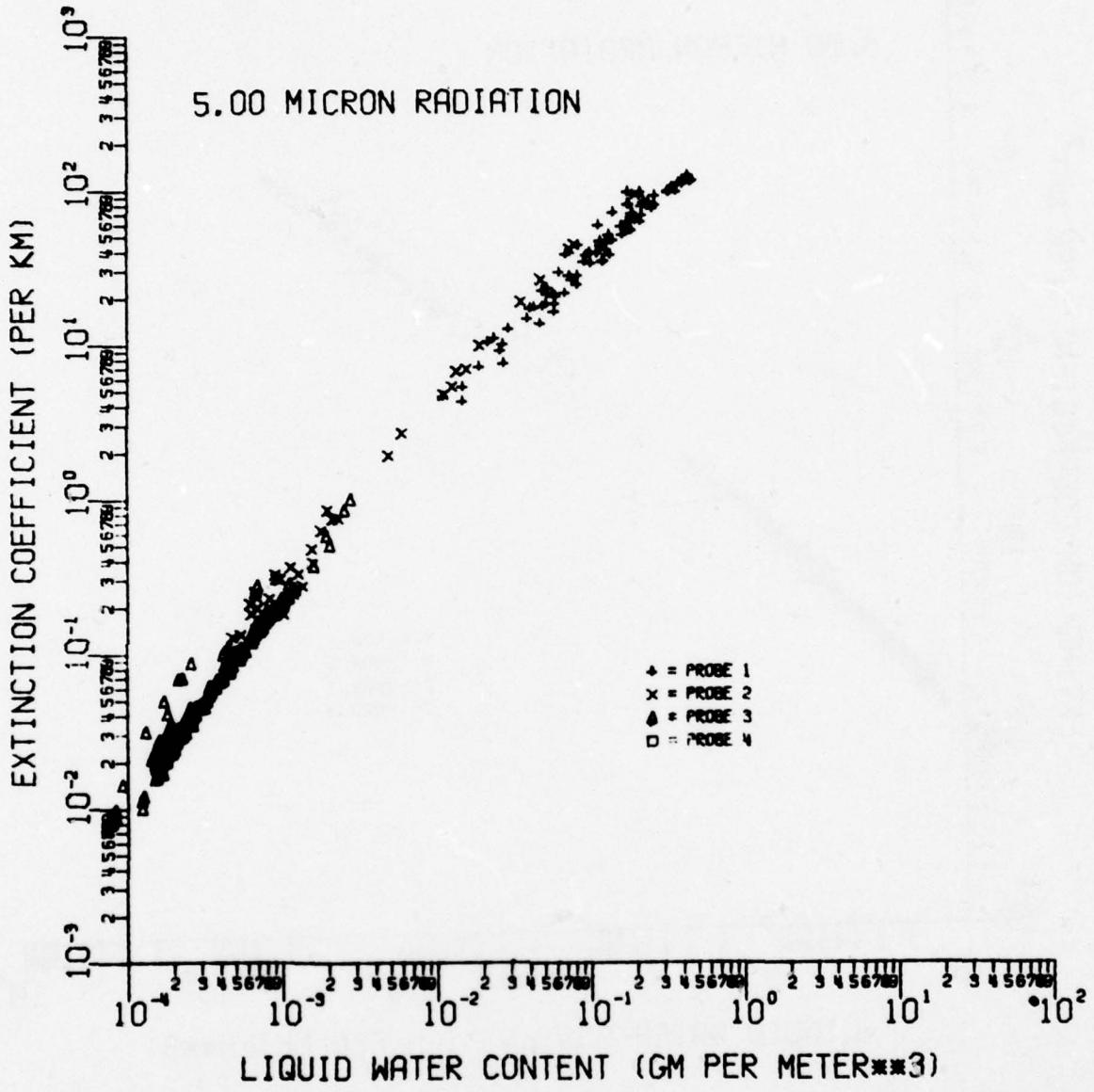
5.00 MICRON RADIATION
EXTINCTION COEFFICIENT (PER KM)
LIQUID WATER CONTENT (GM PER METER**3)
+ = PROBE 1
× = PROBE 2
▲ = PROBE 3
□ = PROBE 4

Figure A6-b

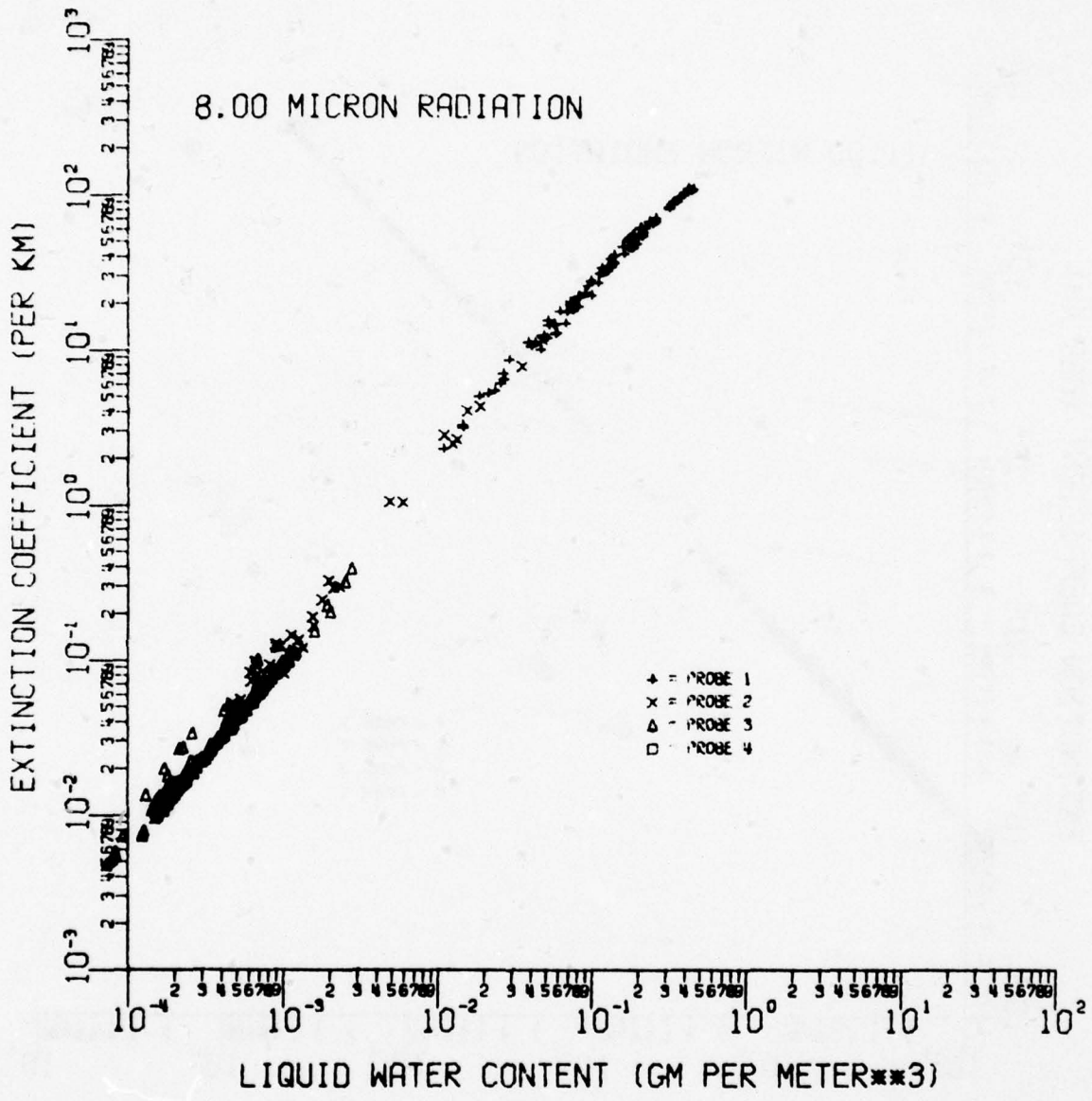
8.00 MICRON RADIATION
EXTINCTION COEFFICIENT (PER KM)
LIQUID WATER CONTENT (GM PER METER**3)
+ = PROBE 1
× = PROBE 2
Δ = PROBE 3
□ = PROBE 4

Figure A6-c

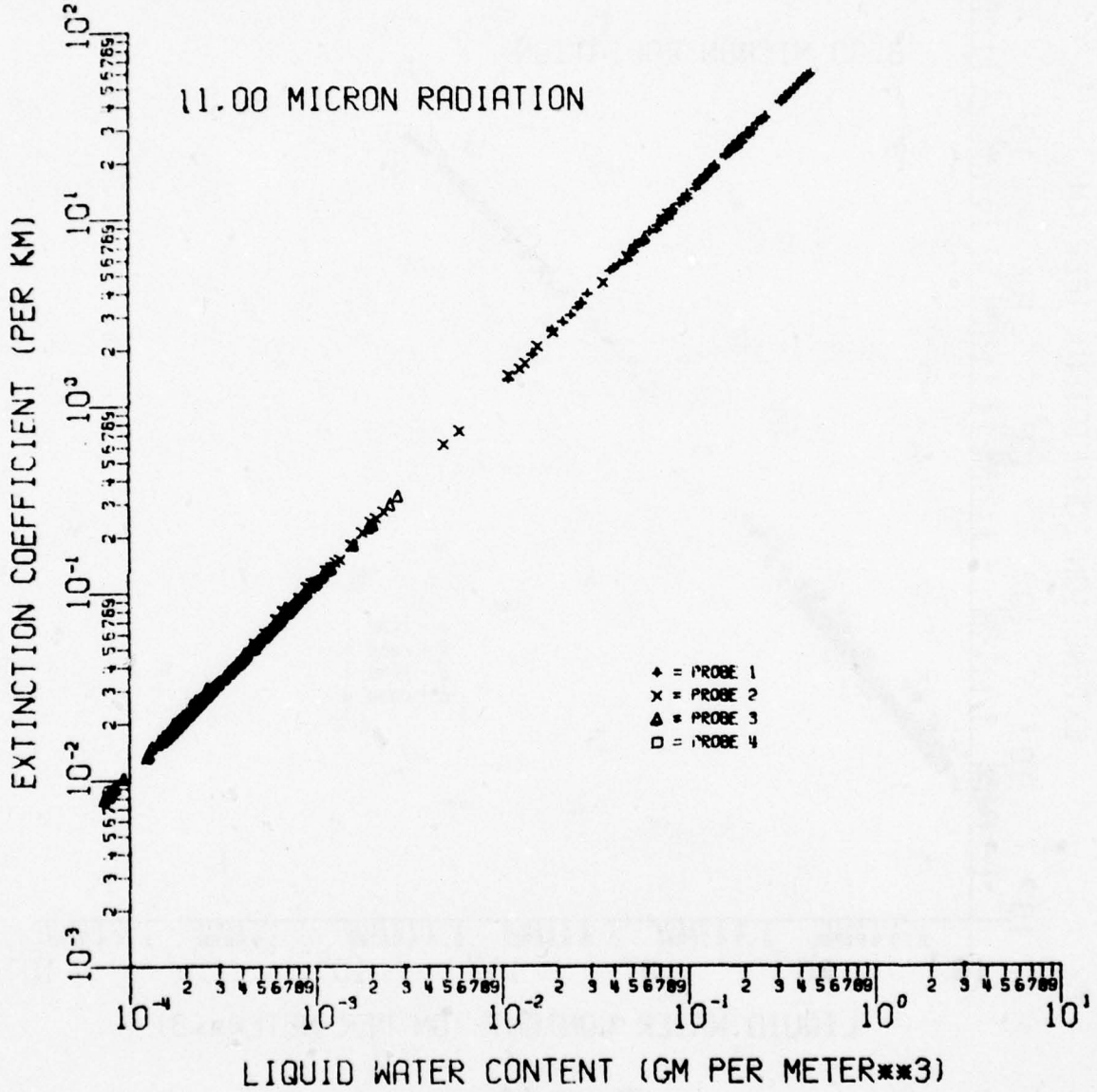
11.00 MICRON RADIATION
EXTINCTION COEFFICIENT (PER KM)
LIQUID WATER CONTENT (GM PER METER**3)
+ = PROBE 1
× = PROBE 2
Δ = PROBE 3
□ = PROBE 4

Figure A6-d

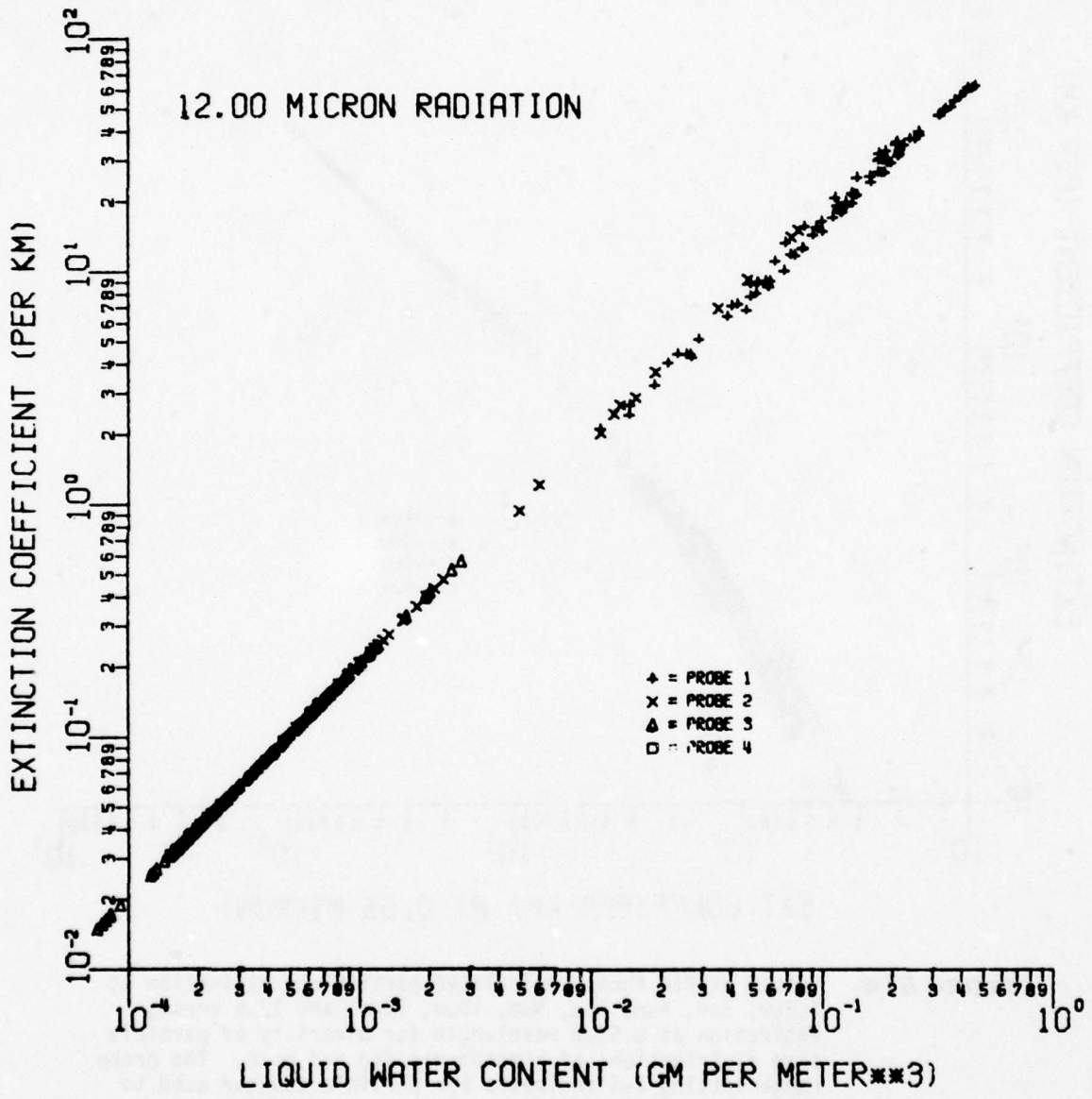
12.00 MICRON RADIATION
EXTINCTION COEFFICIENT (PER KM)
LIQUID WATER CONTENT (GM PER METER**3)
+ = PROBE 1
× = PROBE 2
Δ = PROBE 3
□ = PROBE 4

Figure A6-e

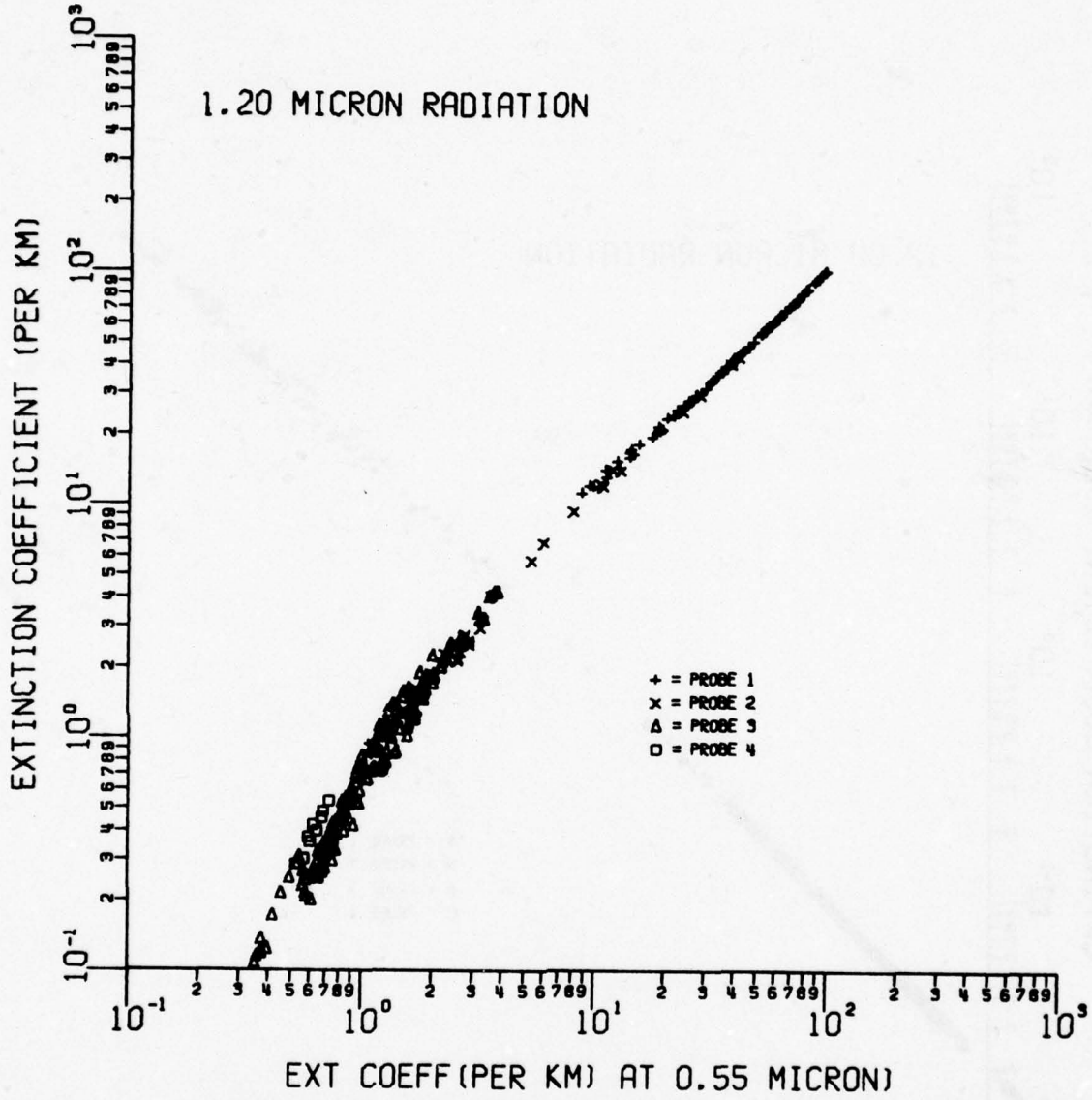

Figure A7-a. Values of Mie theory calculated particulate extinction at 1.2μm, 3μm, 4μm, 5μm, 8μm, 10μm, 11μm, and 12μm versus extinction at 0.55μm wavelength for a variety of particle size distributions of atmospheric fog and haze. The probe range setting 1-4 indicates the particle counter used to make the size distribution measurements on which this data is based was set on different size ranges of sensitivity (as per Fig. 4).

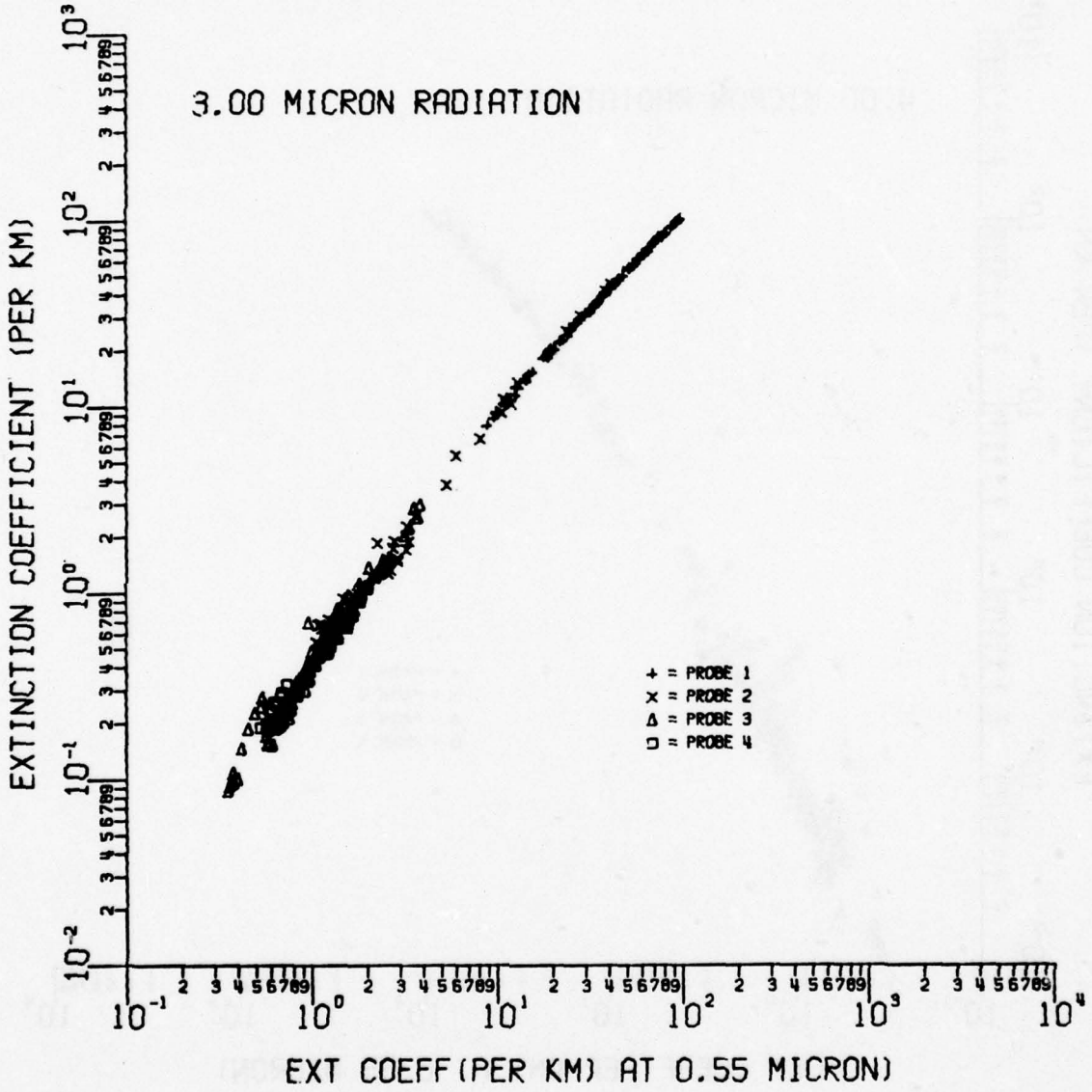
3.00 MICRON RADIATION
EXTINCTION COEFFICIENT (PER KM)
EXT COEFF(PER KM) AT 0.55 MICRON)
+ = PROBE 1
× = PROBE 2
Δ = PROBE 3
□ = PROBE 4

Figure A7-b

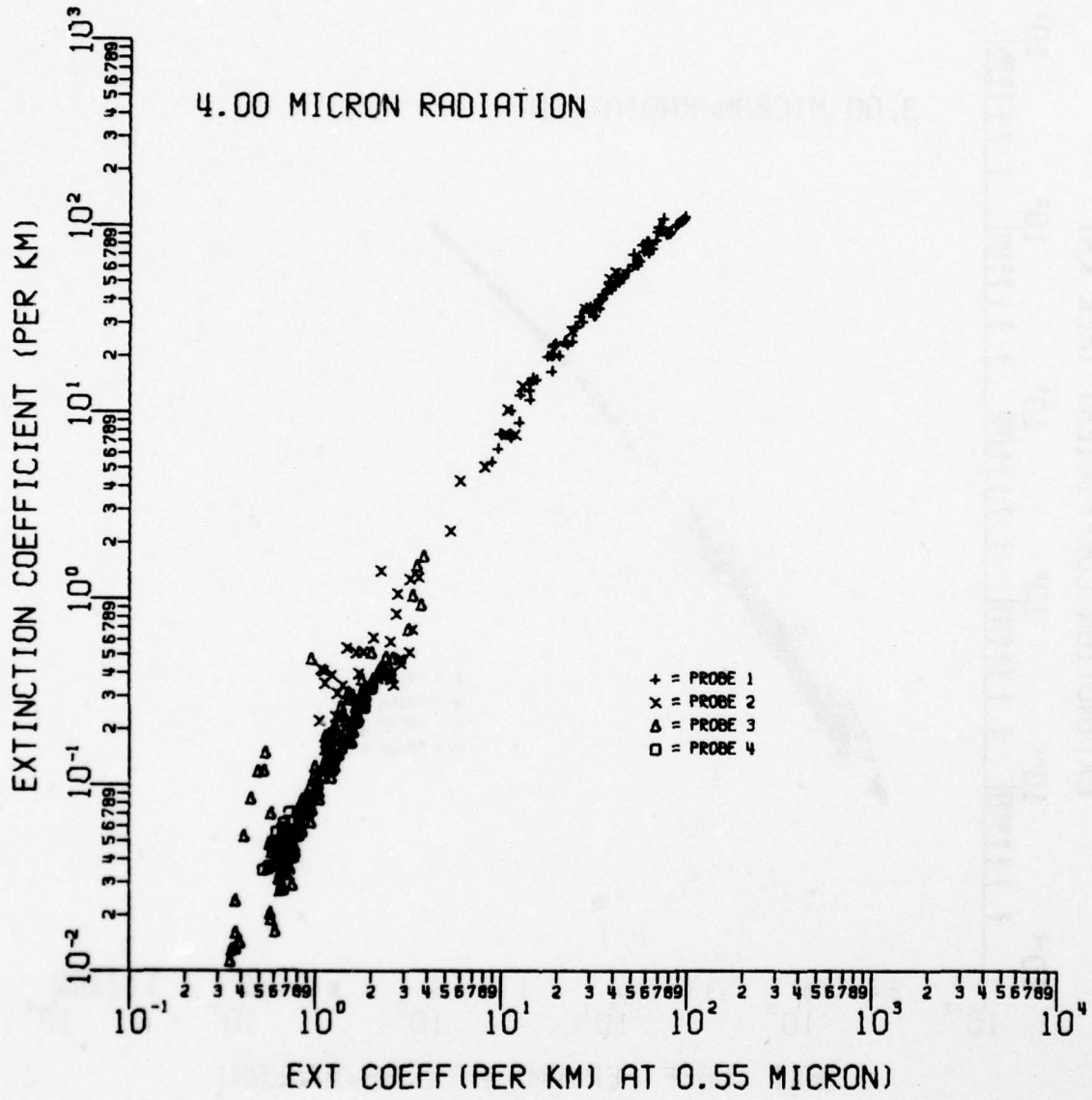
4.00 MICRON RADIATION
EXTINCTION COEFFICIENT (PER KM)
EXT COEFF(PER KM) AT 0.55 MICRON)
+ = PROBE 1
× = PROBE 2
Δ = PROBE 3
□ = PROBE 4

Figure A7-c

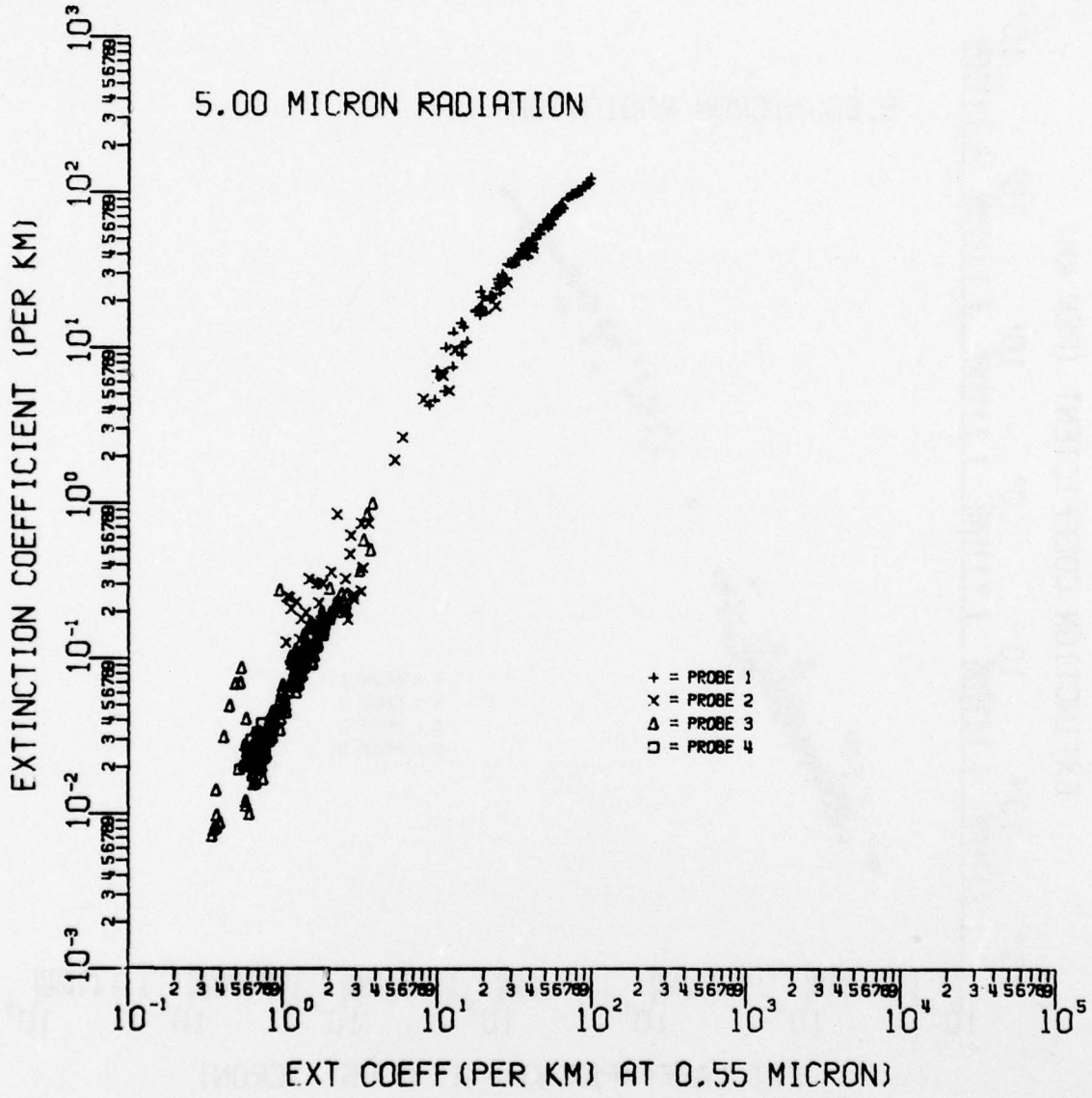
5.00 MICRON RADIATION
EXTINCTION COEFFICIENT (PER KM)
EXT COEFF(PER KM) AT 0.55 MICRON)
+ = PROBE 1
× = PROBE 2
Δ = PROBE 3
□ = PROBE 4

Figure A7-d

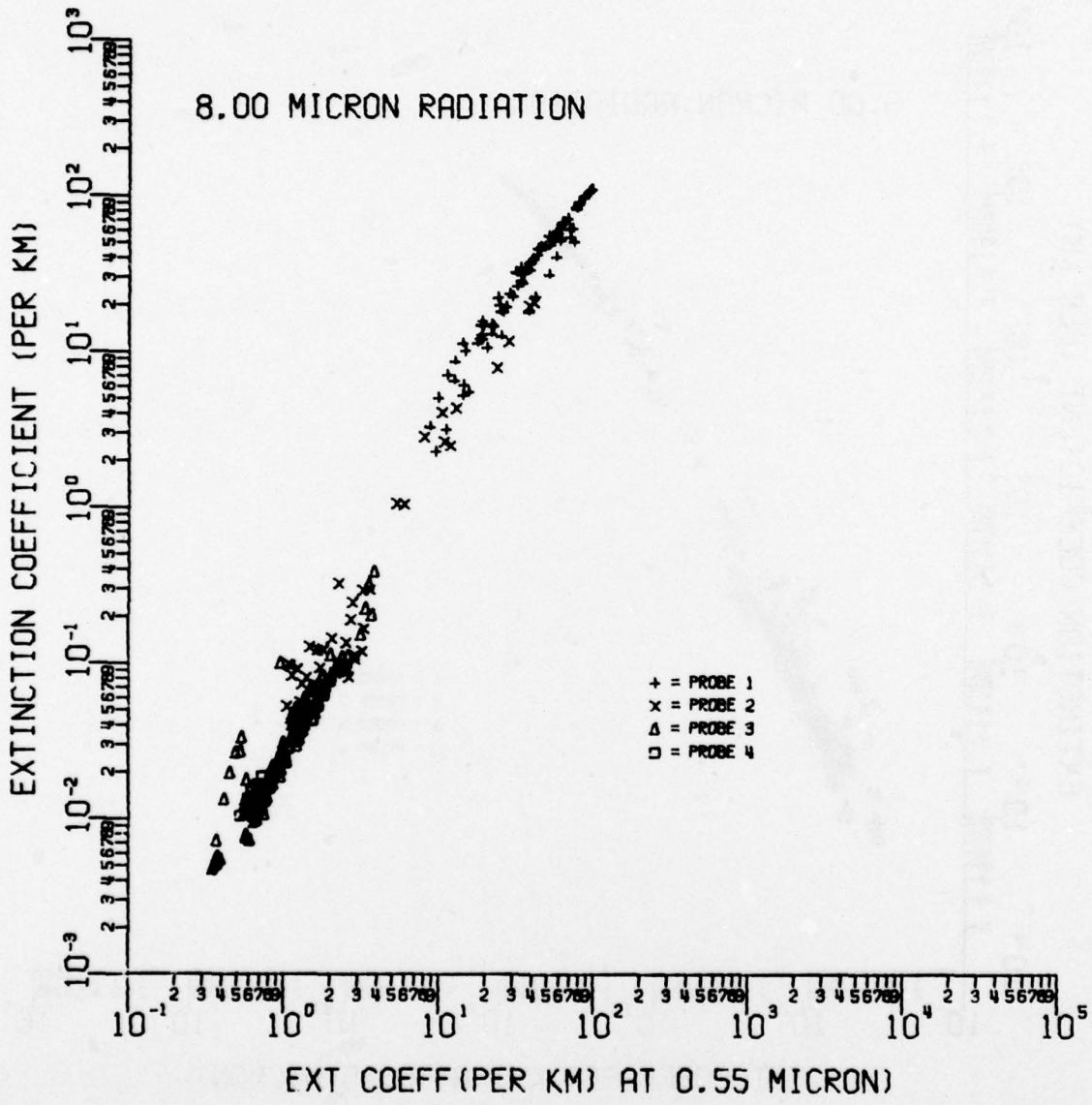
8.00 MICRON RADIATION
EXTINCTION COEFFICIENT (PER KM)
EXT COEFF(PER KM) AT 0.55 MICRON)
+ = PROBE 1
× = PROBE 2
Δ = PROBE 3
□ = PROBE 4

Figure A7-e

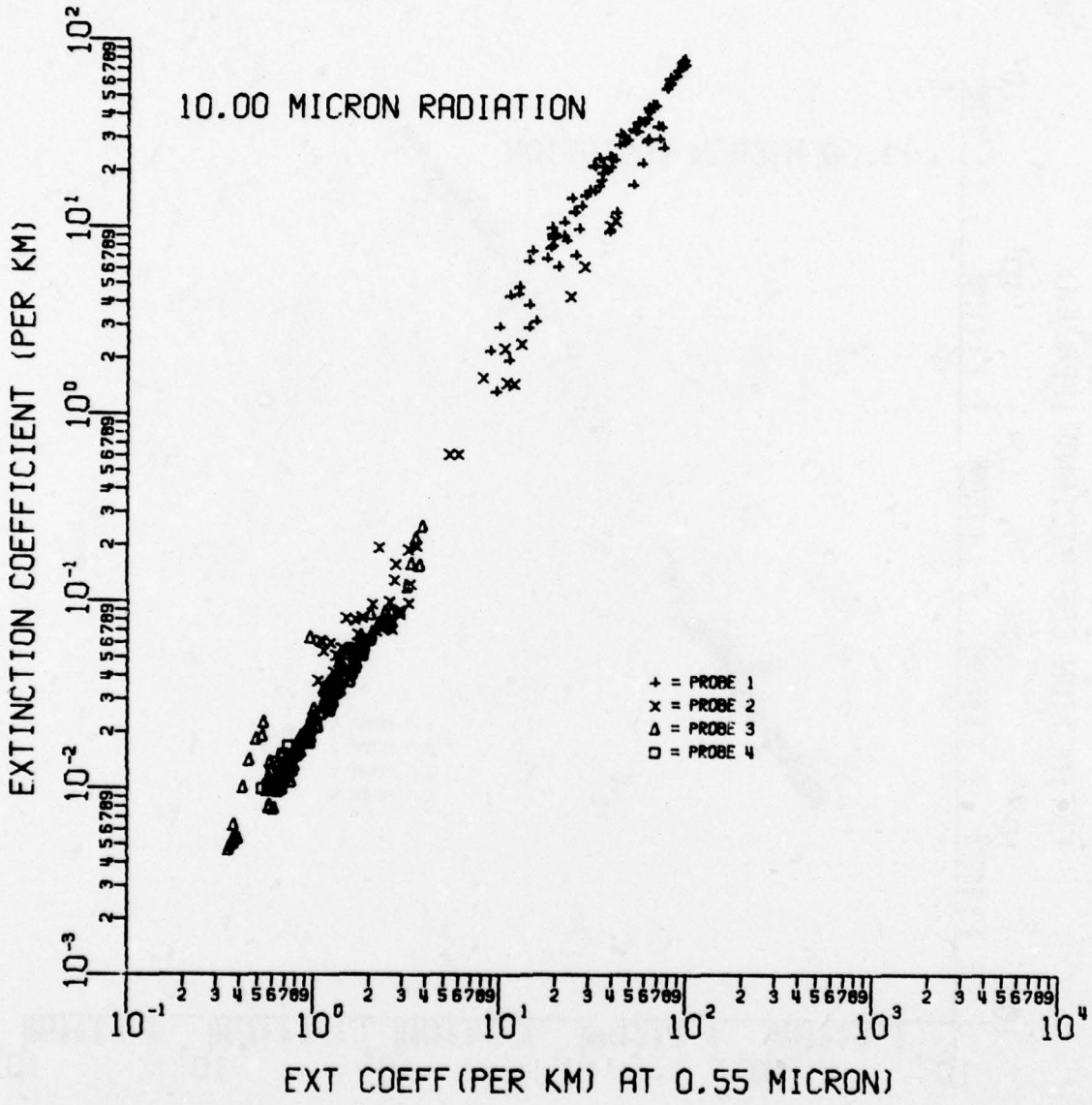
10.00 MICRON RADIATION
EXTINCTION COEFFICIENT (PER KM)
EXT COEFF(PER KM) AT 0.55 MICRON)
+ = PROBE 1
× = PROBE 2
Δ = PROBE 3
□ = PROBE 4

Figure A7-f

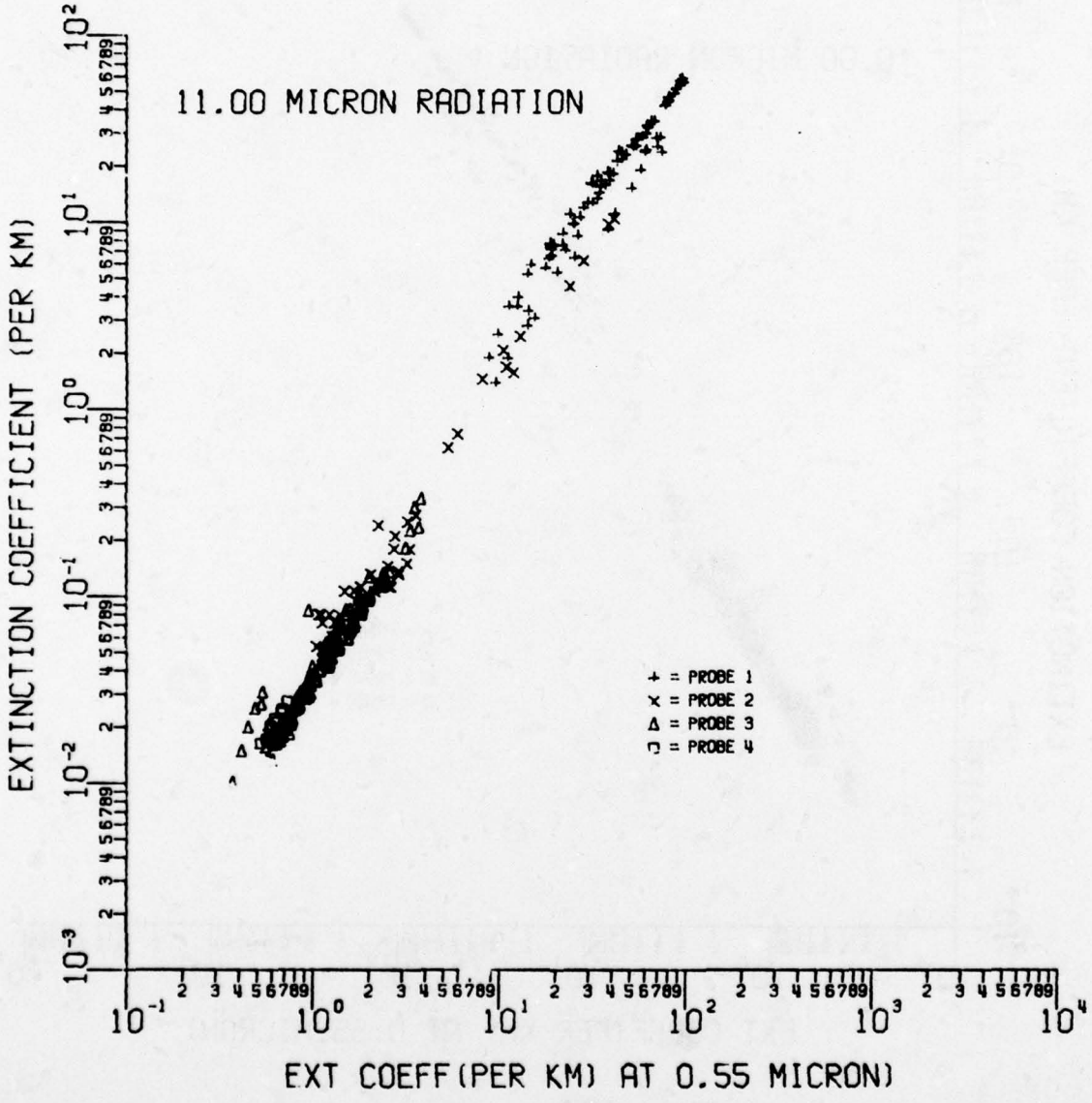
11.00 MICRON RADIATION
EXTINCTION COEFFICIENT (PER KM)
EXT COEFF(PER KM) AT 0.55 MICRON)
+ = PROBE 1
× = PROBE 2
Δ = PROBE 3
□ = PROBE 4

Figure A7-g

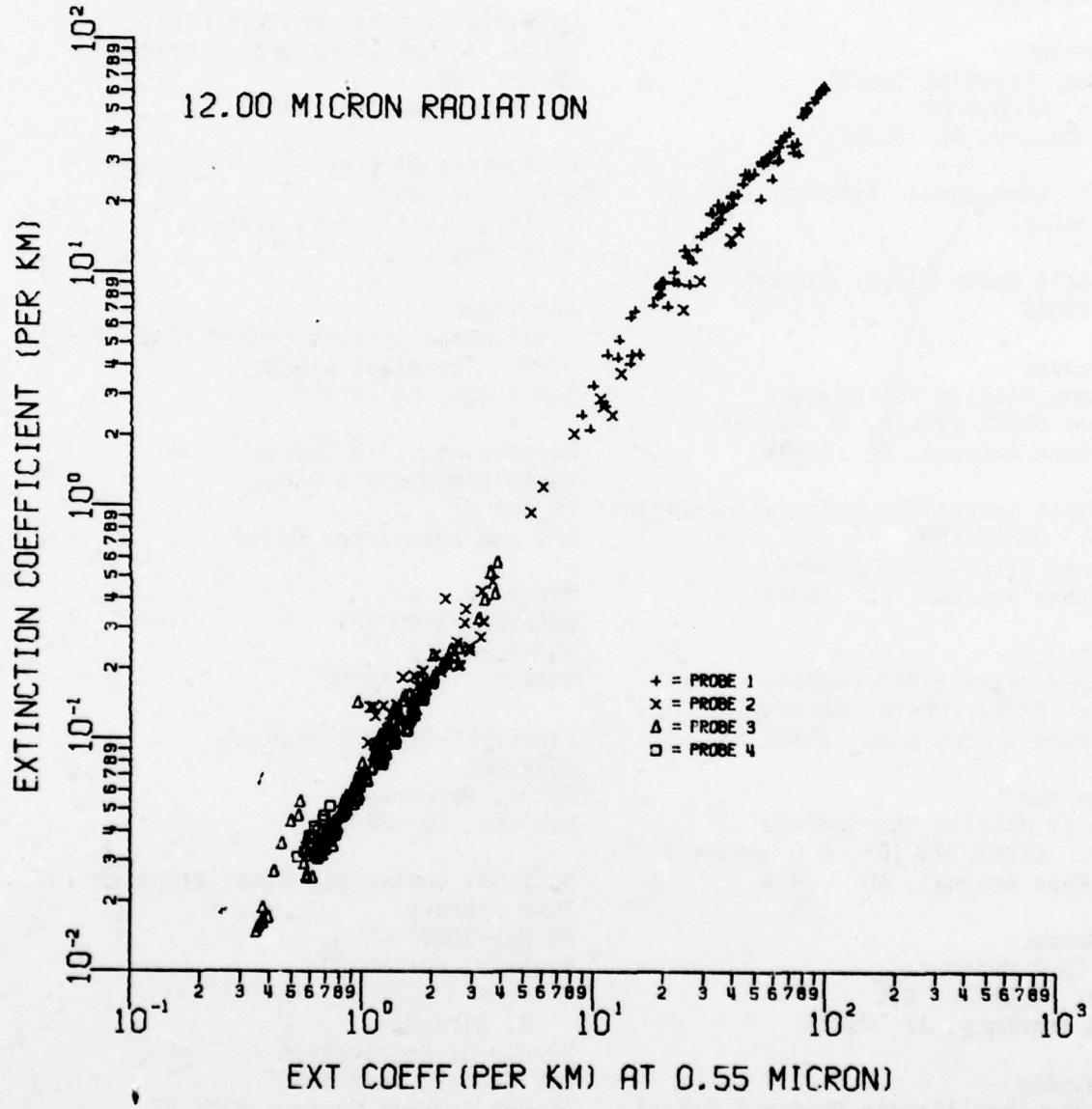
12.00 MICRON RADIATION
EXTINCTION COEFFICIENT (PER KM)
EXT COEFF(PER KM) AT 0.55 MICRON)
+ = PROBE 1
× = PROBE 2
Δ = PROBE 3
□ = PROBE 4

Figure A7-h

DISTRIBUTION LIST

Dr. Frank D. Eaton
Geophysical Institute
University of Alaska
Fairbanks, AK 99701

Commander
US Army Aviation Center
ATTN: ATZQ-D-MA
Fort Rucker, AL 36362

Chief, Atmospheric Sciences Div
Code ES-81
NASA
Marshall Space Flight Center,
AL 35812

Commander
US Army Missile R&D Command
ATTN: DRDMI-CGA (B. W. Fowler)
Redstone Arsenal, AL 35809

Redstone Scientific Information Center
ATTN: DRDMI-TBD
US Army Missile R&D Command
Redstone Arsenal, AL 35809

Commander
US Army Missile R&D Command
ATTN: DRDMI-TEM (R. Haraway)
Redstone Arsenal, AL 35809

Commander
US Army Missile R&D Command
ATTN: DRDMI-TRA (Dr. F[illegible]nwanger)
Redstone Arsenal, AL [illegible]9

Commander
HQ, Fort Huachuca
ATTN: Tech Ref Div
Fort Huachuca, AZ 85613

Commander
US Army Intelligence Center & School
ATTN: ATSI-CD-MD
Fort Huachuca, AZ 85613

Commander
US Army Yuma Proving Ground
ATTN: Technical Library
Bldg 2100
Yuma, AZ 85364

Naval Weapons Center (Code 3173)
ATTN: Dr. A. Shlanta
China Lake, CA 93555

Sylvania Elec Sys Western Div
ATTN: Technical Reports Library
PO Box 205
Mountain View, CA 94040

Geophysics Officer
PMTC Code 3250
Pacific Missile Test Center
Point Mugu, CA 93042

Commander
Naval Ocean Systems Center (Code 4473)
ATTN: Technical Library
San Diego, CA 92152

Meteorologist in Charge
Kwajalein Missile Range
PO Box 67
APO San Francisco, 96555

Director
NOAA/ERL/APCL R31
RB3-Room 567
Boulder, CO 80302

Library-R-51-Tech Reports
NOAA/ERL
320 S. Broadway
Boulder, CO 80302

National Center for Atmos Research
NCAR Library
PO Box 3000
Boulder, CO 80307

B. Girardo
Bureau of Reclamation
E&R Center, Code 1220
Denver Federal Center, Bldg 67
Denver, CO 80225

National Weather Service
National Meteorological Center
W321, WWB, Room 201
ATTN: Mr. Quiroz
Washington, DC 20233

Mil Assistant for Atmos Sciences
Ofc of the Undersecretary of Defense
for Rsch & Engr/E&LS - Room 3D129
The Pentagon
Washington, DC 20301

Defense Communications Agency
Technical Library Center
Code 205
Washington, DC 20305

Director
Defense Nuclear Agency
ATTN: Technical Library
Washington, DC 20305

HQDA (DAEN-RDM/Dr. de Percin)
Washington, DC 20314

Director
Naval Research Laboratory
Code 5530
Washington, DC 20375

Commanding Officer
Naval Research Laboratory
Code 2627
Washington, DC 20375

Dr. J. M. MacCallum
Naval Research Laboratory
Code 1409
Washington, DC 20375

The Library of Congress
ATTN: Exchange & Gift Div
Washington, DC 20540
2

Head, Atmos Rsch Section
Div Atmospheric Science
National Science Foundation
1800 G. Street, NW
Washington, DC 20550

CPT Hugh Albers, Exec Sec
Interdept Committee on Atmos Science
National Science Foundation
Washington, DC 20550

Director, Systems R&D Service
Federal Aviation Administration
ATTN: ARD-54
2100 Second Street, SW
Washington, DC 20590

ADTC/DLODL
Eglin AFB, FL 32542

Naval Training Equipment Center
ATTN: Technical Library
Orlando, FL 32813

Det 11, 2WS/OI
ATTN: Maj Orondorff
Patrick AFB, FL 32925

USAFETAC/CB
Scott AFB, IL 62225

HQ, ESD/TOSI/S-22
Hanscom AFB, MA 01731

Air Force Geophysics Laboratory
ATTN: LCB (A. S. Carten, Jr.)
Hanscom AFB, MA 01731

Air Force Geophysics Laboratory
ATTN: LYD
Hanscom AFB, MA 01731

Meteorology Division
AFGL/LY
Hanscom AFB, MA 01731

US Army Liaison Office
MIT-Lincoln Lab, Library A-082
PO Box 73
Lexington, MA 02173

Director
US Army Ballistic Rsch Lab
ATTN: DRDAR-BLB (Dr. G. E. Keller)
Aberdeen Proving Ground, MD 21005

Commander
US Army Ballistic Rsch Lab
ATTN: DRDAR-BLP
Aberdeen Proving Ground, MD 21005

Director
US Army Armament R&D Command
Chemical Systems Laboratory
ATTN: DRDAR-CLJ-I
Aberdeen Proving Ground, MD 21010

Chief CB Detection & Alarms Div
Chemical Systems Laboratory
ATTN: DRDAR-CLC-CR (H. Tannenbaum)
Aberdeen Proving Ground, MD 21010

Commander
Harry Diamond Laboratories
ATTN: DELHD-CO
2800 Powder Mill Road
Adelphi, MD 20783

Commander
ERADCOM
ATTN: DRDEL-AP
2800 Powder Mill Road
Adelphi, MD 20783
2

Commander
ERADCOM
ATTN: DRDEL-CG/DRDEL-DC/DRDEL-CS
2800 Powder Mill Road
Adelphi, MD 20783

Commander
ERADCOM
ATTN: DRDEL-CT
2800 Powder Mill Road
Adelphi, MD 20783

Commander
ERADCOM
ATTN: DRDEL-EA
2800 Powder Mill Road
Adelphi, MD 20783

Commander
ERADCOM
ATTN: DRDEL-PA/DRDEL-ILS/DRDEL-E
2800 Powder Mill Road
Adelphi, MD 20783

Commander
ERADCOM
ATTN: DRDEL-PAO (S. Kimmel)
2800 Powder Mill Road
Adelphi, MD 20783

Chief
Intelligence Materiel Dev & Support Ofc
ATTN: DELEW-WL-I
Bldg 4554
Fort George G. Meade, MD 20755

Acquisitions Section, IRDB-D823
Library & Info Service Div, NOAA
6009 Executive Blvd
Rockville, MD 20852

Naval Surface Weapons Center
White Oak Library
Silver Spring, MD 20910

The Environmental Research
Institute of MI
ATTN: IRIA Library
PO Box 8618
Ann Arbor, MI 48107

Mr. William A. Main
USDA Forest Service
1407 S. Harrison Road
East Lansing, MI 48823

Dr. A. D. Belmont
Research Division
PO Box 1249
Control Data Corp
Minneapolis, MN 55440

Director
Naval Oceanography & Meteorology
NSTL Station
Bay St Louis, MS 39529

Director
US Army Engr Waterways Experiment Sta
ATTN: Library
PO Box 631
Vicksburg, MS 39180

Environmental Protection Agency
Meteorology Laboratory
Research Triangle Park, NC 27711

US Army Research Office
ATTN: DRXRO-PP
PO Box 12211
Research Triangle Park, NC 27709

Commanding Officer
US Army Armament R&D Command
ATTN: DRDAR-TSS Bldg 59
Dover, NJ 07801

Commander
HQ, US Army Avionics R&D Activity
ATTN: DAVAA-O
Fort Monmouth, NJ 07703

Commander/Director
US Army Combat Surveillance & Target
Acquisition Laboratory
ATTN: DELCS-D
Fort Monmouth, NJ 07703

Commander
US Army Electronics R&D Command
ATTN: DELCS-S
Fort Monmouth, NJ 07703

Commander
US Army Electronics R&D Command
ATTN: DELCS-S (Dr. Swingle)
Fort Monmouth, NJ 07703
3

Director
US Army Electronics Technology &
Devices Laboratory
ATTN: DELET-D
Fort Monmouth, NJ 07703

Commander
US Army Electronic Warfare Laboratory
ATTN: DELEW-D
Fort Monmouth, NJ 07703

Commander
US Army Night Vision &
Electro-Optics Laboratory
ATTN: DELNV-L (Dr. Rudolf Buser)
Fort Monmouth, NJ 07703

Commander
ERADCOM Technical Support Activity
ATTN: DELSD-L
Fort Monmouth, NJ 07703

Project Manager, FIREFINDER
ATTN: DRCPM-FF
Fort Monmouth, NJ 07703

Project Manager, REMBASS
ATTN: DRCPM-RBS
Fort Monmouth, NJ 07703

Commander
US Army Satellite Comm Agency
ATTN: DRCPM-SC-3
Fort Monmouth, NJ 07703

Commander
ERADCOM Scientific Advisor
ATTN: DRDEL-SA
Fort Monmouth, NJ 07703

6585 TG/WE
Holloman AFB, NM 88330

AFWL/WE
Kirtland, AFB, NM 87117

AFWL/Technical Library (SUL)
Kirtland AFB, NM 87117

Commander
US Army Test & Evaluation Command
ATTN: STEWS-AD-L
White Sands Missile Range, NM 88002

Rome Air Development Center
ATTN: Documents Library
TSLD (Bette Smith)
Griffiss AFB, NY 13441

Commander
US Army Tropic Test Center
ATTN: STETC-TD (Info Center)
APO New York 09827

Commandant
US Army Field Artillery School
ATTN: ATSF-CD-R (Mr. Farmer)
Fort Sill, OK 73503

Commandant
US Army Field Artillery School
ATTN: ATSF-CF-R
Fort Sill, OK 73503

Director CFD
US Army Field Artillery School
ATTN: Met Division
Fort Sill, OK 73503

Commandant
US Army Field Artillery School
ATTN: Morris Swett Library
Fort Sill, OK 73503

Commander
US Army Dugway Proving Ground
ATTN: MT-DA-L
Dugway, UT 84022

William Peterson
Research Associates
Utah State University, UNC 48
Logan, UT 84322

Inge Dirmhirn, Professor
Utah State University, UNC 48
Logan, UT 84322

Defense Documentation Center
ATTN: DDC-TCA
Cameron Station, Bldg 5
Alexandria, VA 22314
12

Commanding Officer
US Army Foreign Sci & Tech Center
ATTN: DRXST-IS1
220 7th Street, NE
Charlottesville, VA 22901

Naval Surface Weapons Center
Code G65
Dahlgren, VA 22448

Commander
US Army Night Vision
& Electro-Optics Lab
ATTN: DELNV-D
Fort Belvoir, VA 22060

Commander and Director
US Army Engineer Topographic Lab
ETL-TD-MB
Fort Belvoir, VA 22060

Director
Applied Technology Lab
DAVDL-EU-TSD
ATTN: Technical Library
Fort Eustis, VA 23604

Department of the Air Force
OL-C, 5WW
Fort Monroe, VA 23651

Department of the Air Force
5WW/DN
Langley AFB, VA 23665

Director
Development Center MCDEC
ATTN: Firepower Division
Quantico, VA 22134

US Army Nuclear & Chemical Agency
ATTN: MONA-WE
Springfield, VA 22150

Director
US Army Signals Warfare Laboratory
ATTN: DELSW-OS (Dr. R. Burkhardt)
Vint Hill Farms Station
Warrenton, VA 22186

Commander
US Army Cold Regions Test Center
ATTN: STECR-OP-PM
APO Seattle, 98733

ATMOSPHERIC SCIENCES RESEARCH PAPERS

1. Lindberg, J.D., "An Improvement to a Method for Measuring the Absorption Coefficient of Atmospheric Dust and other Strongly Absorbing Powders, " ECOM-5565, July 1975.
2. Avara, Elton, P., "Mesoscale Wind Shears Derived from Thermal Winds," ECOM-5566, July 1975.
3. Gomez, Richard B., and Joseph H. Pierluissi, "Incomplete Gamma Function Approximation for King's Strong-Line Transmittance Model," ECOM-5567, July 1975.
4. Blanco, A.J., and B.F. Engebos, "Ballistic Wind Weighting Functions for Tank Projectiles," ECOM-5568, August 1975.
5. Taylor, Fredrick J., Jack Smith, and Thomas H. Pries, "Crosswind Measurements through Pattern Recognition Techniques," ECOM-5569, July 1975.
6. Walters, D.L., "Crosswind Weighting Functions for Direct-Fire Projectiles," ECOM-5570, August 1975.
7. Duncan, Louis D., "An Improved Algorithm for the Iterated Minimal Information Solution for Remote Sounding of Temperature," ECOM-5571, August 1975.
8. Robbiani, Raymond L., "Tactical Field Demonstration of Mobile Weather Radar Set AN/TPS-41 at Fort Rucker, Alabama," ECOM-5572, August 1975.
9. Miers, B., G. Blackman, D. Langer, and N. Lorimier, "Analysis of SMS/GOES Film Data," ECOM-5573, September 1975.
10. Manquero, Carlos, Louis Duncan, and Rufus Bruce, "An Indication from Satellite Measurements of Atmospheric CO2 Variability," ECOM-5574, September 1975.
11. Petracca, Carmine, and James D. Lindberg, "Installation and Operation of an Atmospheric Particulate Collector," ECOM-5575, September 1975.
12. Avara, Elton P., and George Alexander, "Empirical Investigation of Three Iterative Methods for Inverting the Radiative Transfer Equation," ECOM-5576, October 1975.
13. Alexander, George D., "A Digital Data Acquisition Interface for the SMS Direct Readout Ground Station — Concept and Preliminary Design," ECOM-5577, October 1975.
14. Cantor, Israel, "Enhancement of Point Source Thermal Radiation Under Clouds in a Nonattenuating Medium," ECOM-5578, October 1975.
15. Norton, Colburn, and Glenn Hoidale, "The Diurnal Variation of Mixing Height by Month over White Sands Missile Range, N.M," ECOM-5579, November 1975.
16. Avara, Elton P., "On the Spectrum Analysis of Binary Data," ECOM-5580, November 1975.
17. Taylor, Fredrick J., Thomas H. Pries, and Chao-Huan Huang, "Optimal Wind Velocity Estimation," ECOM-5581, December 1975.
18. Avara, Elton P., "Some Effects of Autocorrelated and Cross-Correlated Noise on the Analysis of Variance, " ECOM-5582, December 1975.
19. Gillespie, Patti S., R.L. Armstrong, and Kenneth O. White, "The Spectral Characteristics and Atmospheric CO2 Absorption of the Ho^{+3}:YLF Laser at 2.05μm," ECOM-5583, December 1975.
20. Novlan, David J. "An Empirical Method of Forecasting Thunderstorms for the White Sands Missile Range," ECOM-5584, February 1976.
21. Avara, Elton P., "Randomization Effects in Hypothesis Testing with Autocorrelated Noise," ECOM-5585, February 1976.
22. Watkins, Wendell R., "Improvements in Long Path Absorption Cell Measurement," ECOM-5586, March 1976.
23. Thomas, Joe, George D. Alexander, and Marvin Dubbin, "SATTEL — An Army Dedicated Meteorological Telemetry System," ECOM-5587. March 1976.
24. Kennedy, Bruce W., and Delbert Bynum, "Army User Test Program for the RDT&E-XM-75 Meteorological Rocket," ECOM-5588, April 1976.

25. Barnett, Kenneth M., "A Description of the Artillery Meteorological Comparisons at White Sands Missle Range, October 1974 - December 1974 ('PASS' - Prototype Artillery [Meteorological] Subsystem)," ECOM-5589, April 1976.
26. Miller, Walter B., "Preliminary Analysis of Fall-of-Shot From Project 'PASS'," ECOM-5590, April 1976.
27. Avara, Elton P., "Error Analysis of Minimum Information and Smith's Direct Methods for Inverting the Radiative Transfer Equation," ECOM-5591, April 1976.
28. Yee, Young P., James D. Horn, and George Alexander, "Synoptic Thermal Wind Calculations from Radiosonde Observations Over the Southwestern United States," ECOM-5592, May 1976.
29. Duncan, Louis D., and Mary Ann Seagraves, "Applications of Empirical Corrections to NOAA-4 VTPR Observations," ECOM-5593, May 1976.
30. Miers, Bruce T., and Steve Weaver, "Applications of Meterological Satellite Data to Weather Sensitive Army Operations,"ECOM-5594, May 1976.
31. Sharenow, Moses, "Redesign and Improvement of Balloon ML-566," ECOM-5595, June, 1976.
32. Hansen, Frank V., "The Depth of the Surface Boundary Layer," ECOM-5596, June 1976.
33. Pinnick, R.G., and E.B. Stenmark, "Response Calculations for a Commercial Light-Scattering Aerosol Counter," ECOM-5597, July 1976.
34. Mason, J., and G.B. Hoidale, "Visibility as an Estimator of Infrared Transmittance," ECOM-5598, July 1976.
35. Bruce, Rufus E., Louis D. Duncan, and Joseph H. Pierluissi, "Experimental Study of the Relationship Between Radiosonde Temperatures and Radiometric-Area Temperatures," ECOM-5599, August 1976.
36. Duncan, Louis D., "Stratospheric Wind Shear Computed from Satellite Thermal Sounder Measurements," ECOM-5800, September 1976.
37. Taylor, F., P. Mohan, P. Joseph and T. Pries, "An All Digital Automated Wind Measurement System," ECOM-5801, September 1976.
38. Bruce, Charles, "Development of Spectrophones for CW and Pulsed Radiation Sources," ECOM-5802, September 1976.
39. Duncan, Louis D., and Mary Ann Seagraves,"Another Method for Estimating Clear Column Radiances," ECOM-5803, October 1976.
40. Blanco, Abel J., and Larry E. Taylor, "Artillery Meteorological Analysis of Project Pass," ECOM-5804, October 1976.
41. Miller, Walter, and Bernard Engebos," A Mathematical Structure for Refinement of Sound Ranging Estimates," ECOM-5805, November, 1976.
42. Gillespie, James B., and James D. Lindberg, "A Method to Obtain Diffuse Reflectance Measurements from 1.0 to 3.0 μm Using a Cary 17I Spectrophotometer," ECOM-5806, November 1976.
43. Rubio, Roberto, and Robert O. Olsen,"A Study of the Effects of Temperature Variations on Radio Wave Absorption,"ECOM-5807, November 1976.
44. Ballard, Harold N., "Temperature Measurements in the Stratosphere from Balloon-Borne Instrument Platforms, 1968-1975," ECOM-5808, December 1976.
45. Monahan, H.H., "An Approach to the Short-Range Prediction of Early Morning Radiation Fog," ECOM-5809, January 1977.
46. Engebos, Bernard Francis, "Introduction to Multiple State Multiple Action Decision Theory and Its Relation to Mixing Structures," ECOM-5810, January 1977.
47. Low, Richard D.H.,"Effects of Cloud Particles on Remote Sensing from Space in the 10-Micrometer Infrared Region," ECOM-5811, January 1977.
48. Bonner, Robert S., and R. Newton, "Application of the AN/GVS-5 Laser Rangefinder to Cloud Base Height Measurements," ECOM-5812, February 1977.
49. Rubio, Roberto, "Lidar Detection of Subvisible Reentry Vehicle Erosive Atmospheric Material," ECOM-5813, March 1977.
50. Low, Richard D.H., and J.D. Horn, "Mesoscale Determination of Cloud-Top Height: Problems and Solutions," ECOM-5814, March 1977.

51. Duncan, Louis D., and Mary Ann Seagraves,"Evaluation of the NOAA-4 VTPR Thermal Winds for Nuclear Fallout Predictions," ECOM-5815, March 1977.
52. Randhawa, Jagir S., M. Izquierdo, Carlos McDonald and Zvi Salpeter, "Stratospheric Ozone Density as Measured by a Chemiluminescent Sensor During the Stratcom VI-A Flight," ECOM-5816, April 1977.
53. Rubio, Roberto, and Mike Izquierdo, "Measurements of Net Atmospheric Irradiance in the 0.7- to 2.8-Micrometer Infrared Region," ECOM-5817, May 1977.
54. Ballard, Harold N., Jose M. Serna, and Frank P. Hudson Consultant for Chemical Kinetics, "Calculation of Selected Atmospheric Composition Parameters for the Mid-Latitude, September Stratosphere," ECOM-5818, May 1977.
55. Mitchell, J.D., R.S. Sagar, and R.O. Olsen, "Positive Ions in the Middle Atmosphere During Sunrise Conditions," ECOM-5819, May 1977.
56. White, Kenneth O., Wendell R. Watkins, Stuart A. Schleusener, and Ronald L. Johnson, "Solid-State Laser Wavelength Identification Using a Reference Absorber," ECOM-5820, June 1977.
57. Watkins, Wendell R., and Richard G. Dixon, "Automation of Long-Path Absorption Cell Measurements," ECOM-5821, June 1977.
58. Taylor, S.E., J.M. Davis, and J.B. Mason, "Analysis of Observed Soil Skin Moisture Effects on Reflectance," ECOM-5822, June 1977.
59. Duncan, Louis D. and Mary Ann Seagraves, "Fallout Predictions Computed from Satellite Derived Winds," ECOM-5823. June 1977.
60. Snider, D.E., D.G. Murcray, F.H. Murcray, and W.J. Williams, "Investigation of High-Altitude Enhanced Infrared Backround Emissions" (U), SECRET, ECOM-5824, June 1977.
61. Dubbin, Marvin H. and Dennis Hall, "Synchronous Meteorlogical Satellite Direct Readout Ground System Digital Video Electronics," ECOM-5825, June 1977.
62. Miller, W., and B. Engebos, "A Preliminary Analysis of Two Sound Ranging Algorithms," ECOM-5826, July 1977.
63. Kennedy, Bruce W., and James K. Luers, "Ballistic Sphere Techniques for Measuring Atomspheric Parameters," ECOM-5827, July 1977.
64. Duncan, Louis D., "Zenith Angle Variation of Satellite Thermal Sounder Measurements," ECOM-5828, August 1977.
65. Hansen, Frank V., "The Critical Richardson Number," ECOM-5829, September 1977.
66. Ballard, Harold N., and Frank P. Hudson (Compilers), "Stratospheric Composition Balloon-Borne Experiment," ECOM-5830, October 1977.
67. Barr, William C., and Arnold C. Peterson, "Wind Measuring Accuracy Test of Meteorological Systems," ECOM-5831, November 1977.
68. Ethridge, G.A. and F.V. Hansen, "Atmospheric Diffusion: Similarity Theory and Empirical Derivations for Use in Boundary Layer Diffusion Problems," ECOM-5832, November 1977.
69. Low, Richard D.H., "The Internal Cloud Radiation Field and a Technique for Determining Cloud Blackness," ECOM-5833, December 1977.
70. Watkins, Wendell R., Kenneth O. White, Charles W. Bruce, Donald L. Walters, and James D. Lindberg, "Measurements Required for Prediction of High Energy Laser Transmission," ECOM-5834, December 1977.
71. Rubio, Robert, "Investigation of Abrupt Decreases in Atmospherically Backscattered Laser Energy," ECOM-5835. December 1977.
72. Monahan, H.H. and R.M. Cionco, "An Interpretative Review of Existing Capabilities for Measuring and Forecasting Selected Weather Variables (Emphasizing Remote Means)," ASL-TR-0001, January 1978.
73. Heaps, Melvin G., "The 1979 Solar Eclipse and Validation of D-Region Models," ASL-TR-0002. March 1978.

74. Jennings, S.G., and J.B. Gillespie, "M.I.E. Theory Sensitivity Studies - The Effects of Aerosol Complex Refractive Index and Size Distribution Variations on Extinction and Absorption Coefficients Part II: Analysis of the Computational Results," ASL-TR-0003, March 1978.
75. White, Kenneth O. et al, "Water Vapor Continuum Absorption in the 3.5μm to 4.0μm Region," ASL-TR-0004, March 1978.
76. Olsen, Robert O., and Bruce W. Kennedy, "ABRES Pretest Atmospheric Measurements," ASL-TR-0005, April 1978.
77. Ballard, Harold N., Jose M. Serna, and Frank P. Hudson, "Calculation of Atmospheric Composition in the High Latitude September Stratosphere," ASL-TR-0006, May 1978.
78. Watkins, Wendell R. et al, "Water Vapor Absorption Coefficients at HF Laser Wavelengths," ASL-TR-0007, May 1978.
79. Hansen, Frank V., "The Growth and Prediction of Nocturnal Inversions," ASL-TR-0008, May 1978.
80. Samuel, Christine, Charles Bruce, and Ralph Brewer, "Spectrophone Analysis of Gas Samples Obtained at Field Site," ASL-TR-0009, June 1978.
81. Pinnick, R.G. et al., "Vertical Structure in Atmospheric Fog and Haze and its Effects on IR Extinction," ASL-TR-0010, July 1978.

☆ U.S. GOVERNMENT PRINTING OFFICE: 1978 777-093/6